UNIVERSITY OF TRENTO

Doctoral School in Civil, Environmental and Mechanical Engineering

Curriculum 3. Modelling and Simulation

Shubhra Pande

# Development of constitutive models for thin thermoelastic interphase in composite materials

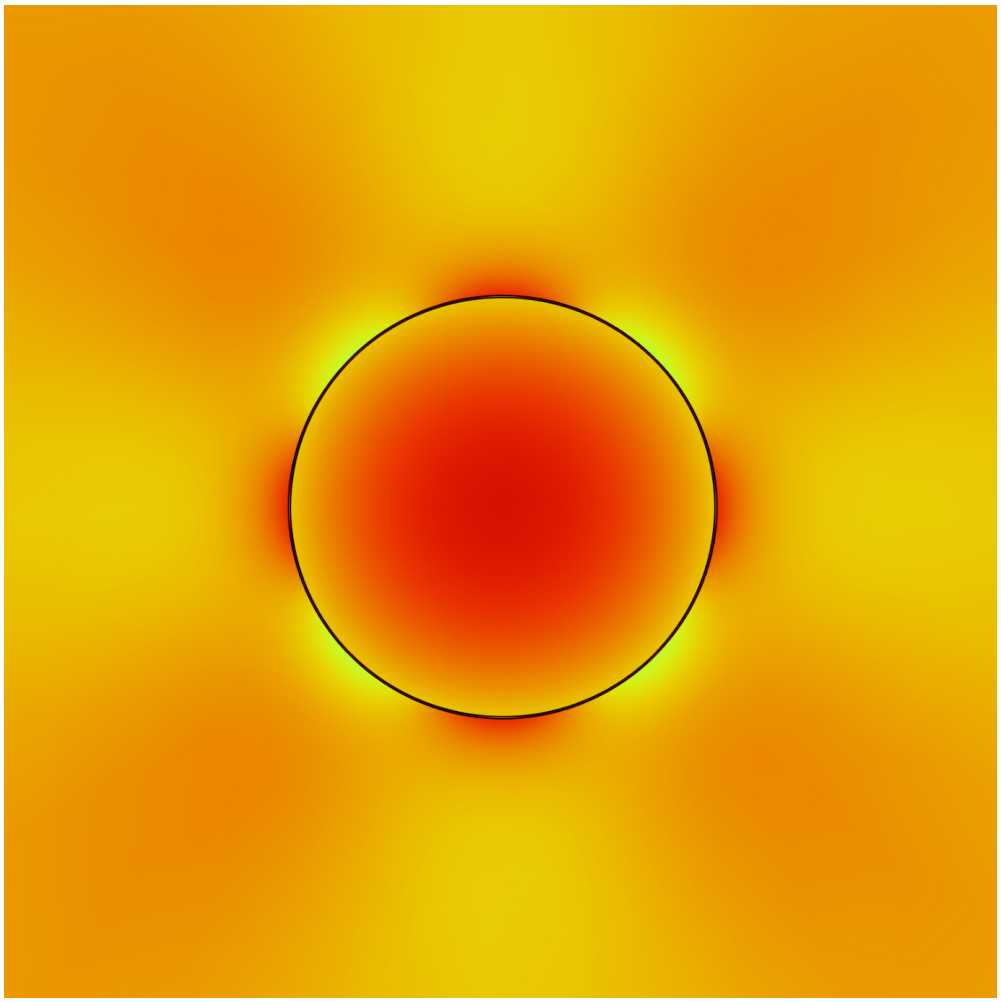

2026 - Doctoral thesis

UNIVERSITY OF TRENTO - Italy
Department of Civil, Environmental
and Mechanical Engineering

Doctoral School in Civil, Environmental and Mechanical Engineering
Topic 3. Modelling and Simulation - 37th cycle 2015/2017

Doctoral Thesis - May 2026

Shubhra Pande

# Development of constitutive models for thin thermoelastic interphase in composite materials

**Supervisor**
Prof. Andrea Piccolroaz, University of Trento



University of Trento
Doctoral School in Civil, Environmental and Mechanical Engineering
*http://web.unitn.it/en/dricam*
Via Mesiano 77, I-38123 Trento
Tel. +39 0461 282670 / 2611 - *dicamphd@unitn.it*

# Acknowledgment

I would like to express my sincere gratitude to my supervisor, prof. Andrea Piccolroaz, for his continuous support, guidance, and encouragement throughout this project. His insightful comments and constructive feedback have not only strengthened the results presented in this thesis but have also shaped my understanding of the values and ethics that underpin scientific research.

I am deeply grateful to Prof. Gennady Mishuris for his support and relentless guidance and many fruitful discussions that have helped me to fortify the results provided in this thesis. Without his support, this PhD thesis would not have been possible.

I also want to take this opportunity to offer my sincere thanks to prof. Vladimir Buljak, for giving me the opportunity to complete my secondment period in Serbia.

I also gratefully acknowledge the funding from the European Union's Horizon 2020 research and innovation program under the Marie Sklodowska-Curie grant agreement No 955944-REFRACTURE2.

I would like to thank my family and friends for their unwavering support and encouragement during this journey, even in moments that looked bleak to me. I am extremely grateful to you all for being my pillars of support. I express my heartfelt gratitude and thanks to my parents and my sister Somya, who have supported me in and encouraged me to follow my dreams. Thank you for my being my rock-solid foundation throughout this journey.

And most importantly, I wish to express my deepest gratitude to my husband, Divas. His steadfast support, gentle encouragement, patience, and constant motivation made this journey easier. I am eternally grateful to have him by my side. You are the wind beneath my wings!

# Abstract

Composite materials consist of two or more constituent phases with distinct geometries and physical properties. These materials incorporate reinforcements that enhance their overall thermo-mechanical performance. At the micro-mechanical scale, a distinct interphase forms between the constituent materials, characterized by its own unique set of properties. The thermo-mechanical behavior across this interphase is of critical importance, as gradients or discontinuities in these properties may lead to localized accumulations of thermal or mechanical energy and the corresponding surface fluxes. Such accumulations can serve as precursors to the initiation of micro-cracks within the composite. Under repeated cyclic loading, these micro-cracks can propagate throughout the domain, ultimately leading to structural failure. Therefore, a comprehensive understanding of the micro-mechanical behavior within the interphase is essential for optimizing the structural integrity of composite systems. However, due to the extremely small thickness of the interphase, accurately modeling its behavior and capturing variations across and within it presents a significant computational challenge. To address these difficulties, the physical interphase in the three-phase problem is replaced with an equivalent zero-thickness interface that represents the boundary between the two materials. Numerical models are then formulated across this interface to replicate the discontinuities (jumps) in thermo-mechanical fields, thereby substantially reducing the computational cost associated with direct modeling of the thin interphase domain. This research proposes two novel models that provide an effective framework for addressing the aforementioned challenges. The models are derived through asymptotic expansion with respect to the interphase thickness parameter $\epsilon$, while the state variables within the interphase are expressed using Taylor series expansions about boundary points. The proposed formulations extend and refine the classical models developed by Benveniste, offering new insights into the influence of various parameters governing property variations along the normal direction. The robustness of the proposed models is examined for thermally conductive interphases of different geometries—specifically, flat, circular, and wavy configurations, as well as for circular interphases in the settings of linear elasticity and thermo-elasticity. Their accuracy and efficiency are evaluated across a broad range of thermal and mechanical properties and curvature values. Additionally, the influence of volumetric heat sources, positioned within the interphase, is analyzed to assess its effect on model performance. The predictive capability of the proposed models is further validated by comparing with established models from the literature, and the numerical model developed in this work is found to have better approximation than the benchmark solutions.

# Contents


**1 Introduction** **1**

**2 Curvilinear Coordinates** **7**
2.1 Preliminaries . . . 7
2.1.1 Unit Base Vectors . . . 8
2.1.2 Metric Tensor . . . 9
2.1.3 Scale Factors . . . 10
2.1.4 Arc-length . . . 11
2.1.5 Volume element . . . 13
2.1.6 Physical components of a vector . . . 13
2.1.7 Derivatives of base vectors: Christoffel Symbols . . . 13
2.2 Gradients in Orthogonal Curvilinear Coordinates . . . 15
2.2.1 Gradient of a scalar . . . 15
2.2.2 Gradient of a vector . . . 16
2.2.3 Gradient of a tensor . . . 16
2.3 Divergence in Orthogonal Curvilinear Coordinates . . . 16
2.3.1 Divergence of a vector . . . 17
2.3.2 Divergence of a tensor . . . 17
2.4 Laplacian Operator in Orthogonal Curvilinear Coordinates . . . 19
2.5 Theory of Parallel Coordinates . . . 19
2.5.1 Curvature . . . 19
2.5.2 Parallel Surfaces . . . 21
2.5.3 Parametric Curves: Wavy Interphase . . . 21
2.5.4 Numerical Implementation of the Parametric Curves . . . 22
2.6 Problem Setup . . . 23

**3 Thermo-mechanics of Continuum Media** **25**
3.1 Part 1: Thermodynamics . . . 26
3.1.1 Basic terminology . . . 26
3.1.2 Laws of Thermodynamics . . . 27
3.1.3 Thermodynamics and Heat Transfer . . . 28
3.1.4 Thermal Conduction . . . 28
3.1.5 Balance Law: Heat Equation . . . 30
3.2 Part II: Continuum Mechanics . . . 31
3.2.1 Eulerian and Lagrangian Description . . . 31
3.2.2 Kinematics: Introducing Deformation Gradient . . . 32
3.2.3 Strain Measures . . . 34
3.2.4 Infinitesimal Strain Tensor . . . 34
3.2.5 Gradient of displacement . . . 34

3.2.6 Strains . . . 35
3.2.7 Stress . . . 37
3.2.8 Hooke's Law . . . 37
3.2.9 Balance Equations . . . 39
3.3 Part III : Thermoelasticity . . . 41
3.3.1 First law of Thermomechanical: Conservation of Energy . . . 42
3.3.2 Second Law of Thermodynamics . . . 43
3.3.3 Clausius-Duhem Inequality . . . 44
3.3.4 Energy Equation for an Elastic Solid . . . 46
3.3.5 Isotropic Linear Thermoelasticity . . . 47
3.3.6 Weak Form of Thermoelasticity . . . 50

**4 Transmission Conditions across a thin conductive interface 53**
4.1 Motivation . . . 53
4.2 Development of Transmission Conditions . . . 57
4.2.1 Transmission conditions for the first integration scheme . . . 59
4.2.2 Transmission conditions for the second integration scheme . . . 61
4.2.3 Comparison of the transmission conditions . . . 63
4.3 Overview of models in literature. . . . 65
4.4 Results and Discussion . . . 68
4.4.1 Parallel Interphase . . . 72
4.4.2 Circular And Non-circular Interphase . . . 78
4.4.3 Wavy Interphase . . . 87
4.5 Appendix . . . 105

**5 Transmission conditions across a thin, spring-type elastic interface 109**
5.1 Introduction . . . 109
5.2 Governing Equations in Curvilinear Coordinates . . . 109
5.3 Motivation . . . 110
5.4 Modified Transmission Conditions . . . 116
5.5 Development of Transmission conditions for a thin interphase. . . . 118
5.5.1 First Integration Scheme . . . 118
5.5.2 Second Integration Scheme . . . 122
5.5.3 Comparison of the transmission conditions . . . 124
5.6 Overview of models in literature. . . . 125
5.7 Results and Discussion . . . 126

**6 Transmission conditions across a thin thermoelastic interface 135**
6.1 Introduction . . . 135
6.2 Motivation . . . 135
6.3 Problem Statement . . . 138
6.4 Development of Transmission Conditions . . . 139
6.5 First Integration Scheme . . . 141
6.5.1 Two points Integration scheme . . . 141
6.5.2 Three points Integration scheme . . . 142
6.6 Second Integration Scheme . . . 147
6.6.1 Two points Integration scheme . . . 147
6.6.2 Three points Integration scheme . . . 148
6.7 Numerical Verification . . . 150
6.8 Results and Discussion . . . 152

**7 Conclusions** **165**

# List of Figures


1.1 *Right:*A representation of the inclusion embedded inside the interphase. *Left:* zoomed-in view of the interphase (marked by red boundaries and its interaction with the surrounding materials. . . . . 2

2.1 Curvilinear Coordinates . . . . . 8
2.2 Arc length $ds$ is the distance between two points $P(\alpha_1, \alpha_2, \alpha_3)$ and $Q(\alpha_1, \alpha_2, \alpha_3)$. 12
2.3 Improving the accuracy of spline. . . . . 22
2.4 (a) Perfect interphase conditions representing thin interphase between materials 1 and 2. (b) Imperfect transmission condition: zero-thickness interface $\Gamma$ between material 1 and 2. . . . . 23

4.1 Example of an interphase between two materials with non-uniform heat sources inside the interphase. . . . . 55
4.2 Illustrative examples:0 Constant heat source, linear heat source, quadratic heat source and cubic heat source distribution. Also here we assume $t_1 = t_2 = t/2 = h$ and we take $\zeta = h/2$, while the heat source $Q_0 = 1.0 \times 10^{-}4(W/m^3)$ . . . . . 56
4.3 Comparison of jumps conditions given by Benveniste-Miloh and Andreeva et al, for three increasing heat source magnitude $Q_0$: (4.3a, 4.3b) shows $[\![T]\!]$ and $[\![q_n]\!]$ for limiting case of $Q_0 = 0$, ie, no heat source inside the interphase (original formulation), (4.3c, 4.3d) shows $[\![T]\!]$ and $[\![q_n]\!]$ for the case of low heat source magnitude $Q_0 = 1$, and (4.3e, 4.3f and 4.3g, 4.3h) shows $[\![T]\!]$ and $[\![q_n]\!]$ for higher heat source consideration inside the interphase $Q_0 = 100$. *HC* stands for High conductive and *LC* stands for Low Conductive interphase and the thickness of the interphase is depicted by $\epsilon$. . . . . 70
4.4 Perfect and Imperfect flat interphase between two materials with different thermal conductivity. . . . . 72
4.5 Normalized $[\![T]\!]$ and $[\![q_x]\!]$ for a flat interphase of thickness, $\epsilon = 0.05$ and heat source $Q_0 = 1.0$. The red curve with square markers represent the proposed two points scheme (Eqns,(4.23),(4.22)), and blue curve with filled circles represents the proposed three-points scheme (Eqns,(4.35),(4.34)). . . 77
4.6 Normalized $[\![T]\!]$ and $[\![q_x]\!]$ for a flat interphase of thickness, $t = 0.001$ and heat source $Q_0 = 100.0$. The red curve with square markers represent the proposed two points scheme (Eqns.(4.23),(4.22)), and blue curve with filled circles represents the proposed three-points scheme (Eqns,(4.35),(4.34)). . . 78
4.7 Geometric representation of the problem. . . . . 79
4.8 Plots of normalized temperature jumps and normal component of heat flux jumps, with their corresponding relative errors for circular interphase of thickness $\epsilon = 0.05$ having heat source of magnitude $Q_0 = 1.0\ W/m^3$. . . . . 86

4.9 Plots of normalized $[\![T]\!]$ and $[\![q_n]\!]$, with their corresponding relative errors for circular interphase of thickness $\epsilon = 0.001$ having heat source of magnitude $Q_0 = 100.0\ W/m^3$. . . . . 87
4.10 Circular and non-circular geometries with varying curvature. . . . . 88
4.11 Geometric representation of the wavy interphase. . . . . 88
4.12 Verification of the numerical solutions by comparison with known analytical solution, for a perfect circular inclusion, having low heat source value, $Q_0 = 1W/m^3$ of volumetric heat source. The results illustrated in this graph are the $[\![T]\!]$ and $[\![q_n]\!]$ computed across the boundaries of the perfect interphase setting. . . . . 90
4.13 Variation of parameters $g, \beta, \gamma$ computed from the Eqns.(4.20) (for the First Integration Scheme) and (2.118), (2.119) for the Second Integration Scheme respectively. . . . . 91
4.14 Values of LHS and RHS of Eqn.(4.33), along with corresponding relative error, $\delta$ for a low conductive (LC) interphase, $k^{(i)} = 0.01\,W/m.K$ and $\epsilon = 0.01$. 91
4.15 Values of LHS and RHS of Eqn.(4.33), along with corresponding relative error, $\delta$ for a high conductive (HC) interphase, $k^{(i)} = 100\,W/m.K$ and $\epsilon = 0.01$. . . . . 92
4.16 Normalized heat flux values at point $A_3$ taken as: exact value from numerical simulation, represented by blue dashed line, green curve with star markers represents values computed from the Eqns.(4.37) for FIS (First Integration Scheme) and magenta curve with filled circle markers represents values computed from (4.50) for SIS (Second Integration Scheme), for a low conductive (LC) type interphase having thickness $\epsilon = 0.01$. . . . . 93
4.17 Normalized heat flux values at point $A_3$ taken as: exact value from numerical simulation, represented by blue dashed line, green curve with star markers represents values computed from the Eqns.(4.37) for FIS (First Integration Scheme) and magenta curve with filled circle markers represents values computed from (4.50) for SIS (Second Integration Scheme), for a high conductive (HC) type interphase having thickness $\epsilon = 0.01$. . . . . 94
4.18 Normalized jumps of temperature and heat flux across a perfect interphase (three-phase solution) setting, with respect to increasing curvature for a wavy interphase of thickness $\epsilon = 0.01$, having a low conductive ($k_i = 0.01W/m.K$ Figs.4.18a,4.18b) and high conductive ($k_i = 100W/m.K$ Figs.4.18c,4.18d) interphase. . . . . 95
4.19 $[\![T]\!]$ and $[\![q_n]\!]$ for a wavy interphase of thickness $\epsilon = 0.01$, with heat source of $Q_0 = 1.0$. Fig.4.19a and 4.19b show the temperature jumps and relative errors, respectively, and Figs.4.19c,4.19d represent jumps in normal component of heat flux for low conductive interphase ($k^{(i)}/k^{(2)} = 0.01$), against increasing curvature values, $N$. . . . . 97
4.20 $[\![T]\!]$ and $[\![q_n]\!]$ for a wavy interphase of thickness $\epsilon = 0.01$, with heat source of $Q_0 = 1.0$. Fig.4.20a and 4.20b show the temperature jumps and relative errors, respectively, and Figs.4.20c,4.20d represent jumps in normal component of heat flux for high conductive interphase ($k^{(i)}/k^{(2)} = 100$), against increasing curvature values, $N$. . . . . 98
4.21 Variation of temperature and heat flux at the inner and outer boundaries of the interphase, for different values of oscillations, $N$, for an interphase of thickness $\epsilon = 0.01$, and thermal conductivity $k^{(i)}/k^{(2)} = 0.01$, having an internal heat source of magnitude $Q_0 = 1\,W/m^3$. . . . . 99

4.22 Variation of temperature and heat flux at the inner and outer boundaries of the interphase, for different values of oscillations, $N$, for an interphase of thickness $\epsilon = 0.01$, and thermal conductivity $k^{(i)}/k^{(2)} = 100$, having an internal heat source of magnitude $Q_0 = 1\,W/m^3$. . . . . 100
4.23 $[\![T]\!]$ and $[\![q_n]\!]$ for a wavy interphase of thickness $\epsilon = 0.01$, with heat source of $Q_0 = 100.0$. Fig.4.23a and 4.23b show the temperature jumps and relative errors, respectively, and Figs.4.23c,4.23d represent jumps in normal component of heat flux for low conductive interphase ($k^{(i)}/k^{(2)} = 0.01$), against increasing curvature values, $N$. . . . . 101
4.24 $[\![T]\!]$ and $[\![q_n]\!]$ for a wavy interphase of thickness $\epsilon = 0.01$, with heat source of $Q_0 = 100.0\,W/m^3$. Fig.4.24a and 4.24b show $[\![T]\!]$ and relative errors, respectively, and Figs.4.24c,4.24d represent $[\![q_n]\!]$ for high conductive interphase ($k^{(i)}/k^{(2)} = 100$), against increasing curvature values, $N$. . . . . 102
4.25 Variation of parameters $g, \beta, \gamma$ for a wavy interphase of amplitude $A = 0.08m$ computed from the Eqns.(4.20) (for the First Integration Scheme) and (2.118), (2.119) for the Second Integration Scheme respectively. . . . . 103
4.26 Values of LHS and RHS of Eqn.(4.33), along with corresponding relative error, $\delta$ for an interphase of thickness $\epsilon = 0.01$, and amplitude $A = 0.08$. . . 103
4.27 Normalized heat flux values at point $A_3$ taken as: exact value from numerical simulation, represented by blue dashed line, green curve with star markers represents values computed from the Eqns.(4.37) for FIS (First Integration Scheme) and magenta curve with filled circle markers represents values computed from (4.50) for SIS (Second Integration Scheme), for an interphase having thickness $\epsilon = 0.01$ and amplitude of $A = 0.08m$. . . . . 104
4.28 Zoomed in view of temperatures (4.28a-4.28d) and heat fluxes (4.28e-4.28h) at $\theta = 0\,\text{deg}$, for increasing values of N. The volumetric heat source is small $Q_0 = 1$. The plot shows the effect of curvature geometry on the temperature contours for a low conductive interphase ($k_i/k_2 = 0.01, \epsilon = 0.01$). . . . . 105
4.29 Zoomed in view of temperatures (4.29a-4.29d) and heat fluxes (4.29e-4.29h) at $\theta = 0\,\text{deg}$, for increasing values of N. The volumetric heat source is high $Q_0 = 100$. The plot shows the effect of curvature geometry on the temperature contours for a low conductive interphase ($k_i/k_2 = 0.01, \epsilon = 0.01$). 105
4.30 Zoomed in view of temperatures (4.30a-4.30d) and heat fluxes (4.30e-4.30h) at $\theta = 0$ rad, for increasing values of N. The volumetric heat source is small $Q_0 = 1$. The plot shows the effect of curvature geometry on the temperature contours for a high conductive interphase ($k_i/k_2 = 100, \epsilon = 0.01$). . . . . 106
4.31 Zoomed in view of temperatures (4.31a-4.31d) and heat fluxes (4.31e-4.31h) at $\theta = 0\,\text{deg}$, for increasing values of N. The volumetric heat source is high $Q_0 = 100$. The plot shows the effect of curvature geometry on the temperature contours for a high conductive interphase ($k_i/k_2 = 100, \epsilon = 0.01$). 106

5.1 Example of an interphase between two materials with uniformly distributed body forces inside the interphase. . . . . 114
5.2 Illustrative example for a constant, linear, quadratic and cubic body force distributed uniformly inside the interphase. Here we have assumed $t_1 = t_2 = t/2 = h$ and $\zeta = h/2$, while the body force $Q_0 = 1.0 \times 10^{-}4(N/m^2)$ . . 115
5.3 Geometric representation of the problem. . . . . 126
5.4 Plots of normalized displacement jumps with their corresponding absolute errors for circular interphase of thickness $\epsilon = 0.01$. . . . . 130

5.5 Plots of normalized displacement jumps with their corresponding absolute errors for circular interphase of thickness $\epsilon = 0.01$. . . . . 132

6.1 Mesh distribution across a thermoelastic circular interphase of thickness $\epsilon = 0.01$. . . . . 151
6.2 Convergence plots for the temperature $T$ and displacement fields,$\boldsymbol{u}$, for both cases of: 6.2a represents thermally resistive $k^{(i)}/k^{(2)} = 0.001$, soft interphase $G^{(i)}/G^{(2)} = 0.001$. 6.2b represents convergence plots for highly conductive $k^{(i)}/k^{(2)} = 1000$ and rigid interphase $G^{(i)}/G^{(2)} = 1000$, for an interphase of thickness $\epsilon = 0.01$ and volumetric heat source of magnitude $Q_0 = 100\,W/m^3$ and shear load of $\sigma^*_{xy} = 2\,G^{(2)}\,\beta_{el}$. . . . . 152
6.3 Distribution of temperature $\Theta = T - T_{ref}$ (volume reference temperature) and heat flux magnitude $q$ across a thermoelastic circular interphase of thickness $\epsilon = 0.01$, with volumetric heat source $Q_0 = 100\,W/m^3$ and tensile loads of $\sigma^* = 1\,MPa/$. Figs.6.3a and 6.3b illustrate $\Theta$ and $q$ for insulating, soft interphase while Figs.6.3c and 6.3d illustrate $\Theta$ and $q$ for conductive, rigid interphase. . . . . 154
6.4 Distribution of displacement magnitude $U$ across a thermoelastic circular interphase of thickness $\epsilon = 0.01$. . . . . 155
6.5 Distribution of normal component of stresses $\sigma_{xx}, \sigma_{yy}$ and the shear stress $\sigma_{xy}$ in MPa across a thermoelastic circular interphase of thickness $\epsilon = 0.01$. 156
6.6 Distribution of stress along x-direction $\sigma_{xx}$ in GPa across a thermoelastic circular interphase with three different coefficients of thermal expansions $(\alpha^{(i)}/\alpha^{(2)}$ of thickness $\epsilon = 0.01$, with volumetric heat source $Q_0 = 1\,W/m^3$ and remote shear stress of $\sigma^*_{xy} = 2\,GPa$ for conductive $k^{(i)}/k^{(2)} = 1000$ and rigid interphase $G^{(i)}/G^{(2)} = 1000$. . . . . 157
6.7 Distribution of stress along y-direction $\sigma_{yy}$ in GPa across a thermoelastic circular interphase with three different coefficients of thermal expansions $(\alpha^{(i)}/\alpha^{(2)}$ of thickness $\epsilon = 0.01$, with volumetric heat source $Q_0 = 1\,W/m^3$ and remote shear stress of $\sigma^*_{xy} = 2\,GPa$ for conductive $k^{(i)}/k^{(2)} = 1000$ and rigid interphase $G^{(i)}/G^{(2)} = 1000$. . . . . 158
6.8 Distribution of shear stresses $\sigma_{xy}$ in GPa across a thermoelastic circular interphase with three different coefficients of thermal expansions $(\alpha^{(i)}/\alpha^{(2)}$ of thickness $\epsilon = 0.01$, with volumetric heat source $Q_0 = 1\,W/m^3$ and remote shear load of $\sigma^*_{xy} = 2\,GPa$ for conductive $k^{(i)}/k^{(2)} = 1000$ and rigid interphase $G^{(i)}/G^{(2)} = 1000$. . . . . 159
6.9 Heat flux values $q_n$ at point $A_3$ inside the interphase, computed for First Integration and Second Integration Scheme and compared with the exact solution, for a thermoelastic circular interphase of thickness $\epsilon = 0.01$ for low conductive $k^{(i)}/k^{(2)} = 0.001$ and a soft interphase $G^{(i)}/G^{(2)} = 0.001$. . . . . 161
6.10 Radial stress values $q_n$ at point $A_3$ inside the interphase, computed for First Integration and Second Integration Scheme and compared with the exact solution, for a thermoelastic circular interphase of thickness $\epsilon = 0.01$ for low conductive $k^{(i)}/k^{(2)} = 0.001$ and a soft interphase $G^{(i)}/G^{(2)} = 0.001$. . . . . 161
6.11 Tangential stress values $q_n$ at point $A_3$ inside the interphase, computed for First Integration and Second Integration Scheme and compared with the exact solution, for a thermoelastic circular interphase of thickness $\epsilon = 0.01$ for low conductive $k^{(i)}/k^{(2)} = 0.001$ and a soft interphase $G^{(i)}/G^{(2)} = 0.001$. 162

# List of Tables


2.1 Values of Christoffel symbols based on $m, n, r$. . . . . 14

3.1 Thermal conductivities in $W/m.K$ of some common materials in increasing order of conductivity. . . . . 29
3.2 Relations between different elastic moduli. $R = \sqrt{E^2 + 9\lambda^2 + 2E\lambda}$ . . . . . 39

5.1 Elastic properties of the material in perfect interphase setting. . . . . 129
5.2 Relative errors ($\delta$) values computed for displacement vectors from all models for a soft ($G^{(i)}/G^{(2)} = 10^{-3}$) and rigid interphase ($G^{(i)}/G^{(2)} = 10^{3}$). Here, FIS refers to the proposed methods in First Integration Scheme and SIS stands for Second Integration scheme. . . . . 131
5.3 Relative errors ($\delta$) values computed for displacement vectors from all models for a soft ($G^{(i)}/G^{(2)} = 10^{-5}$) and rigid interphase ($G^{(i)}/G^{(2)} = 10^{5}$). Here, FIS refers to the proposed methods in First Integration Scheme and SIS stands for Second Integration scheme. . . . . 132

6.1 Thermoelastic properties of the material in perfect interphase setting. . . . 151
6.2 $[\![\Theta]\!]$ for an uncoupled quasistatic thermoelastic interphase of thickness $\epsilon = 0.01$. with volumetric heat source $Q_0 = 1.0\,W/m^3$, computed for three different value of interphase CTE: $\alpha^{(i)}/\alpha^{(2)} = \{0.1, 5.0, 25.0\}$ . Here, Case A refers to thermally resistive and soft interphase: $k^{(i)}/k^{(2)} = 0.001$ and $G^{(i)}/G^{(2)} = 0.001$ while Case B represents thermally conductive and elastically rigid interphase $k^{(i)}/k^{(2)} = 1000$ and $G^{(i)}/G^{(2)} = 1000$. . . . . 160
6.3 $[\![q_n]\!]$ for an uncoupled quasistatic thermoelastic interphase of thickness $\epsilon = 0.01$. with volumetric heat source $Q_0 = 1.0\,W/m^3$, computed for three different value of interphase CTE: $\alpha^{(i)}/\alpha^{(2)} = \{0.1, 5.0, 25.0\}$ . Here, Case A refers to thermally resistive and soft interphase: $k^{(i)}/k^{(2)} = 0.001$ and $G^{(i)}/G^{(2)} = 0.001$ while Case B represents thermally conductive and elastically rigid interphase $k^{(i)}/k^{(2)} = 1000$ and $G^{(i)}/G^{(2)} = 1000$. . . . . 160

# Chapter 1

# Introduction

Thin layers arise naturally in a wide range of physical systems, including thermal barriers in composite materials, adhesive films, biological membranes, and interfacial coatings in micro- and nanoscale devices. These interfaces—often manifested as thin interphases—are regions of intense mechanical and physical interaction where load transfer, stress localization, and damage initiation occur. Although these layers are often orders of magnitude thinner than the surrounding domains, they can exert a disproportionate influence on overall system behavior due to sharp gradients in physical fields such as temperature, concentration, or mechanical stress. Accurate modeling of such layers is essential for predicting system performance, but their small thickness poses significant challenges for direct numerical simulation and classical continuum modeling approaches. Interface theories have therefore emerged as essential tools for understanding and modeling the complex mechanisms that control the overall response of composite systems. By providing a rigorous link between microscale interfacial behavior and macroscale structural performance, such theories form the foundation for reliable analysis, design, and optimization of advanced composite materials.

The interphase can be thought of as a distinct region having its own properties and/or chemical composition, or in terms of Reifsnider, 1994, "the region that is formed as a result of the bonding between fibre and matrix which has significantly distinct morphology or chemical composition compared with the bulk fibre or bulk matrix material", explaining its origin as "a diffusion zone, a nucleation zone, a chemical reaction zone, and so forth, or any combination of the above." For example, it can exist as a thin layer of glue between the fiber and the matrix, or formed by the chemical result of two materials brought into contact, slightly altering their properties near the contact zone with a diagrammatic scheme presented in Fig.1.1.

From early investigations in the field of Linear Elastic Fracture Mechanics (LEFM), it was observed that there was "rapid oscillations" in the behaviour of displacements and stress fields within the interphase, suggesting interpenetration. In order to resolve this, two models were proposed, Comninou, 1990:

- First model was proposed by Atkinson, where he "recognizes that the interface between two materials is almost never sharp" thus providing a gradual transition from material 1 to material 2, avoiding the oscillatory behaviour.
- Second by Comninou, which accepts the presence of inequalities, allowing for "partial closure at the tips"

Since Atkinson's model provided a more simplified solution to analyze the mechanical fields with ease, it is therefore more widely used in the studies of interfaces replacing a

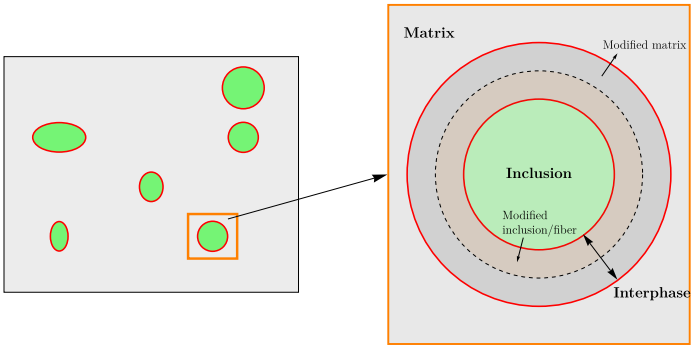


**Fig. 1.1.** *Right:*A representation of the inclusion embedded inside the interphase. *Left:* zoomed-in view of the interphase (marked by red boundaries and its interaction with the surrounding materials.

non-homogeneous interphase with a homogeneous or graded non-homogeneous interface, providing an insight into the stress concentration near the surfaces, as well as the behaviour inside the interphase domain.

Since the interphase is very thin, the challenge arose of accurately capturing the effects at the boundary of this interphase as well as the evolution of thermal and mechanical fields within the layer. Several numerical techniques such as *asymptotic modeling* provided an effective approach for addressing this challenge. The asymptotic techniques serves as the powerful tool which is used to "simplify complex interphase behaviours by considering small parameters, such as adhesive thickness, to derive effective macroscopic laws from detailed microscopic phenomena"Research, 2024. By systematically exploiting the small thickness of the layer as a perturbation parameter, asymptotic methods enable the derivation of simplified models that capture the leading-order effects of the layer without fully resolving its detailed structure. These reduced models often replace the thin region (perfect interphase or the three-phase problem) with effective transmission or interface conditions, preserving the accuracy of the original problem while greatly enhancing analytical and computational efficiency. These asymptotic models treat the thin layer as a perturbation in the governing equations. This approach, allows for the derivation of effective interface or transmission conditions that encapsulate the leading-order behavior of the layer without the need to resolve its full internal structure. A very common feature of asymptotic models is the appearance of jump conditions across the layer, capturing discontinuities or rapid transitions in field variables like temperature or heat flux. These effective conditions simplify complex boundary-value problems and offer significant computational savings, particularly in multiscale simulations. In addition, they provide information on how the material and geometric properties of the layer influence the surrounding domains. The development of transmission conditions across an imperfect interface implies isolating a single inclusion (also known as dilute approximation)(Miloh and Y.Benveniste, 1999a) and study its perturbative effect on the thermo-mechanical properties across the boundary of the interface. These perturbative method assume that the inclusion, and the interphase are completely isolated from any neighbouring inclusions, and the remote boundaries are extremely far away so as to not exert any effect on the behaviour of the transmission conditions. This allowed to understand the thermal and elastic stress concentrations that occurred near the boundaries of the interface which would decay as one moved away from the interphase. Using this technique, Hashin, 2001 derived transmission conditions in the context of potential problems (thermal or electrical, etc) using Taylor series expansion of the potential term (eg, temperature) and fluxes (eg, heat flux) at a point in the boundary. The unique feature of his work involved derivation of a simple model that worked perfectly

across a wide range of interphases. This served as a benchmark for many later works, such as Benveniste, 2006a.

In case of interphase formations involving temperatures, these thin layers accumulate temperature or heat flux, thereby creating small regions of thermal barriers or conductive layers. Thermal conductivity is the key player here, as the lower conductive values create thermal barriers, known as *Interfacial Thermal Resistance* or the Kapitza resistance model (Kapitza, 1965,Benveniste and Miloh, 1986), named after Pyotr Kapitza who first observed this effect in liquid helium and solids at extremely low temperatures. It was observed through experiments that at the nano-scale, two materials kept in contact showed some finite jumps in temperature across the interphase boundaries, even though the temperature flow was continuous, leading the way to recognize thermal resistance $R_k$ at the interface, given as

$$R_k = \frac{\Delta T}{q} \tag{1.1}$$

The Kapitza model defining interfacial thermal resistance is standard model for low conductive interphases, and can be found in numerous studies, for example, in the development of solid electrolyte interface (SEI) during lower working temperatures in Lithium ion metal batteries Weng, 2023, or in the application of silica coated gold nano-particles for use in cancer thermo-therapy Hatam-Lee et al., 2022. On the other hand, if the interphase has a high conductivity, then it allows the heat to pass through it without any resistance. Such materials serve as excellent mediums for heat sinks and heat transfers, especially in high power electronics, where heat accumulation could lead to component damage. The most common examples include thermal pastes and thermal pads, more commonly referred to as Thermal Interface Materials (TIM) that are commonly employed in CPUs, 5G transmission etc to rapidly cool the electronic systems. Further and more detailed information on the different types of TIMs can be found in Kaur, 2026 wherein a detailed study on different thermal interface materials for use in electronics field has been made.

Several earlier models in the literature primarily rely on the use of Taylor series expansions around the points on the interphase boundaries to approximate field variables in the normal direction, in the vicinity of the interphase. Miloh and Y.Benveniste, 1999a derived separate conditions for the low and high conductive interphase, where the continuity of heat flux in case of low conductive interphase and continuity of temperature in case of high conductive interphase were maintained. For the high conductive interphase conditions, the resulting model for jumps in heat flux did not account for the curvature of the boundary. This was addressed in the later work of Hashin, 2001, wherein he devised a simple model that held true across a wide range of thermal conductivities. Later, different models were developed by taking into account the expanded thermal and/or mechanical fields from both sides of the interphase. This greatly improved the accuracy of the models.

Another fundamental parameter in the analysis of thermally conductive interphases is the *volumetric heat source*, which, within the scope of this study, is assumed to be distributed throughout the interphase. In general, the heat source can be assumed to be energy that is given off from the system during any chemical or mechanical process. The chemical process can include the formation of the interphase layer, SOFC cells, etc. while the mechanical processes can include the plastic deformation, frictional dissipation the debonding taking place. In heterogeneous composites, the interphase often exhibits distinct mechanical and thermal properties. Heat can be generated due to thermo-mechanical coupling, micro-slip at the interface or due to debonding or cohesive zone dissipation. These effects are particularly relevant in fiber-reinforced composites and layered materials. While the accuracy of the benchmark solutions of Hashin (Hashin, 2001,Hashin, 2002),

Benveniste (Miloh and Y.Benveniste, 1999a,Benveniste, 2006aBenveniste, 2006b) methods have already been proved with appropriate examples, it is clearly seen that the models' accuracy declines when a heat source is assumed inside the interphase.

An interphase can not only have thermal properties but also mechanical properties that defines its overall strength and structure, and the ability to transfer loads between the adjoining materials. Benveniste and Miloh, 2001 identified seven types of interphases, including the more widely identified spring-type interphase. A spring-type interphase is one where the interphase behaves like an elastic spring, and the jumps in mechanical fields (displacements and stress vectors) are proportional to the "spring constants", where the traction forces are

$$\boldsymbol{t}_n = D_n[\![\boldsymbol{u}]\!] \qquad ; \qquad \boldsymbol{t}_t = D_t[\![\boldsymbol{u}]\!]$$

where $D_n, D_t$ are the spring constants along the normal and tangential directions, $\boldsymbol{t}$ is the traction vector, and $[\![\boldsymbol{u}]\!]$ is the jump of the displacement vector. The $D_n, D_t$ are mentioned in Hashin, 2002 as:

$$D_n = \frac{t}{\lambda_i + 2\,G_i} \qquad ; \qquad D_t = \frac{t}{G_i}$$

where $t$ is the thickness of the interphase, and $\lambda_i, G_i$ are the Lame's parameters of the interphase. The capability of the interphase to absorb or transmit loads effectively depends on its material properties and strength: whether the interphase is soft or stiff. If the interphase is extremely soft or compliant, it would mean that is has low Young's modulus, and/or shear modulus. This allows the interphase to absorb the loads and to deform greatly or slide-along the tangential direction, without any resistance. Thus, the interphase deforms easily and exhibits significant displacement changes.

On the contrast, if the materials have a high rigidity, characterized by high Young's modulus or shear modulus, the interphase transmits the loads to the neighbouring material without undergoing any deformation. However, rigid interphases are more prone to cracking, as they accumulate more stress without any change in their displacement.

This work is presented as follows: In general case, the shape of the inclusion is arbitrary, and hence to generalize the form of transmission conditions developed within this framework, use of orthogonal curvilinear coordinates has been made. Chapter 2 throws light on the basic fundamentals involving the curvilinear coordinates, as well as on *parallel coordinates* which are a special case of curvilinear coordinates. Chapter 3 sheds light on the theoretical background serving as the foundation of the models proposed in this work. Chapter 4 deals with the development of transmission conditions for a thermally conductive interphase, while Chapter 5 focuses on the development of transmission conditions for a spring-types elastic interphase. And finally Chapter 6 combines the understand from the previous two cases to arrive at the interface model for a thin thermoelastic interphase within the realm of linear thermoelasticity. The final chapter 7 concludes the entire work presented in this research.

# Chapter 2

# Curvilinear Coordinates

In many physical problems, the geometry of the system plays a central role in simplifying analysis and interpretation. While Cartesian coordinates (x,y,z) are convenient for describing flat, rectangular geometries, they are often inefficient for systems involving curved boundaries or symmetry, such as circular motion, spherical bodies, or flow around curved surfaces.

To handle such situations more naturally, curvilinear coordinate systems are used. In these systems, the coordinate lines and surfaces are generally curved, and the coordinates are defined in terms of smoothly varying scalar functions of position. Examples include cylindrical and spherical coordinates, which are particularly useful in problems with axial or radial symmetry.

Curvilinear coordinates allow physical laws to be expressed in a form that reflects the underlying geometry of the problem. However, this convenience comes at the cost of additional mathematical structure: the basis vectors are no longer constant, and quantities such as gradients, divergences, and curls require careful treatment using scale factors and position-dependent unit vectors.

In this chapter, we develop the general theory of curvilinear coordinates, introduce the associated base vectors and scale factors, and derive expressions for common vector operators. These tools provide a powerful framework for analyzing a wide range of problems in physics, engineering, and applied mathematics. The equations for gradient of scalar, vectors, and tensors, as well the those representing divergence of vector and tensor terms in curvilinear coordinates, is utilized in developing the appropriate transmission conditions for thermal, elastic and thermoelastic case in general curvilinear coordinates. Thus, it is important to establish a sound theory that explains the terminology involved in the orthogonal curvilinear coordinates.

## 2.1 Preliminaries

Consider a Cartesian system of coordinates $(x, y, z)$, having its origin at point $O$, as shown in the figure. At any point $P$, there are three curves intersecting at that point. These curves are $(\alpha_1, \alpha_2, \alpha_3)$. Consider three surfaces defined as $\alpha_1 = c_1, \alpha_2 = c_2, \alpha_3 = c_3$. The three surfaces intersect each other at the three curves. The curve of intersection of the surface $\alpha_2 = c_2$ and $\alpha_3 = c_3$ is $\alpha_1$ curve; similarly, the curve of intersection of the surface $\alpha_3 = c_3$ and $\alpha_1 = c_1$ is $\alpha_2$ curve and for the surface $\alpha_1 = c_1$ and $\alpha_2 = c_2$, $\alpha_3$ curve is the curve of intersection. Here, $c_1, c_2, c_3$ are constants, while $\alpha_1, \alpha_2, \alpha_3$ are the single valued functions of positions. The surfaces intersecting at point P are known as **"coordinate surfaces"**, and $\alpha_1, \alpha_2, \alpha_3$ are known as **"coordinate lines"**. The lines tangential to the coordinate

lines are known as **"coordinate axes"**. If the relative position of the coordinate axis $(\hat{\boldsymbol{e}}_1, \hat{\boldsymbol{e}}_2, \hat{\boldsymbol{e}}_3)$ change from point to point within the coordinate system, then it is known as **"general curvilinear coordinates"**. However, if any two surfaces intersect at 90°, then it is known as **"orthogonal curvilinear coordinates"**, ie, all the coordinates axes are mututally perpendicular to each other.

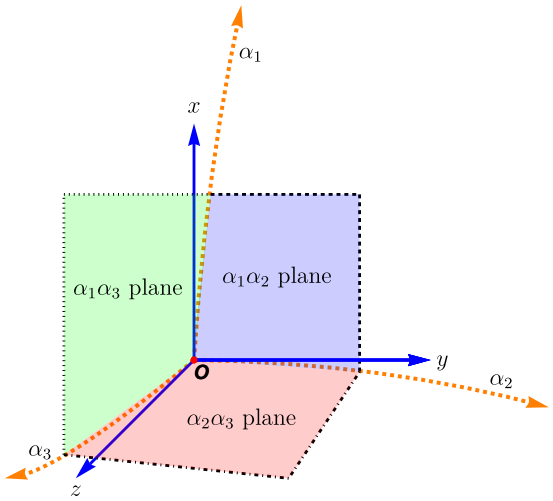


**Fig. 2.1.** Curvilinear Coordinates

It is assumed that at any given point (for example, point $P$ as considered here), there exists the following set of transformation equations:

$$x = x_1 = f_1(\alpha_1, \alpha_2, \alpha_3) \tag{2.1}$$
$$y = x_2 = f_2(\alpha_1, \alpha_2, \alpha_3) \tag{2.2}$$
$$z = x_3 = f_3(\alpha_1, \alpha_2, \alpha_3) \tag{2.3}$$

Then, in such a case, the inverse of these functions also exists:

$$\alpha_1 = F_1(x_1, x_2, x_3) \tag{2.4}$$
$$\alpha_2 = F_2(x_1, x_2, x_3) \tag{2.5}$$
$$\alpha_3 = F_3(x_1, x_2, x_3) \tag{2.6}$$

where $(\alpha_1, \alpha_2, \alpha_3)$ are the general curvilinear coordinates and $(x_1, x_2, x_3)$ or $(x, y, z)$ are the Cartesian coordinates of any point P. The functions $f_1, f_2, f_3$ and $F_1, F_2, F_3$ are the **transformation functions** which will be defined later.

### 2.1.1 Unit Base Vectors

For a orthogonal curvilinear coordinates, the tangents to these $\alpha_i$ curves through the intersection point $P$ are known as *unit basis vectors* or the *unit tangent vectors* given as $\hat{\boldsymbol{e}}_i = (\hat{\boldsymbol{e}}_1, \hat{\boldsymbol{e}}_2, \hat{\boldsymbol{e}}_3)$ These unit vectors are in general not orthogonal, and change their direction at each point in the space. Let the position vector between point $P$ and $A$ in terms of curvilinear coordinates is given as:

$$\boldsymbol{r} = \boldsymbol{r}(\alpha_1, \alpha_2, \alpha_3) \tag{2.7}$$

Thus, the base vector, or the tangent vector is:

$$\boldsymbol{e}_i = \frac{\partial \boldsymbol{r}}{\partial \alpha_i} \tag{2.8}$$

and the unit vector is simply:

$$\hat{\boldsymbol{e}}_i = \frac{\boldsymbol{e}_i}{|\boldsymbol{e}_i|} = \frac{1}{\left|\frac{\partial \boldsymbol{r}}{\partial \alpha_i}\right|}\frac{\partial \boldsymbol{r}}{\partial \alpha_i} \tag{2.9}$$

The curvilinear coordinates , in their general form, are defined in terms of Cartesian coordinates as:

$$\alpha_i = \alpha_i(x, y, z) \quad ; \quad x_i = x_i(\alpha_1, \alpha_2, \alpha_3) \tag{2.10}$$

It is assumed that the three functions of $\alpha_i$ and $x_i$ have continuous $\mathcal{C}^1$ derivatives:

$$|\boldsymbol{x}/\boldsymbol{\alpha}| \equiv \left|\frac{\partial x_i}{\partial \alpha_i}\right| \neq 0 \tag{2.11}$$

There maybe a singularity at a single point on the curve, but never throughout the entire volume.

Therefore, a unit vector $\hat{E}_1$, normal to the surface $\alpha_1\alpha_2$ is defined as:

$$\hat{E}_1 = \frac{\nabla \boldsymbol{\alpha}_1}{|\nabla \boldsymbol{\alpha}_1|} \tag{2.12}$$

$$\hat{E}_2 = \frac{\nabla \boldsymbol{\alpha}_2}{|\nabla \boldsymbol{\alpha}_2|} \tag{2.13}$$

$$\hat{E}_3 = \frac{\nabla \boldsymbol{\alpha}_3}{|\nabla \boldsymbol{\alpha}_3|} \tag{2.14}$$

$$\tag{2.15}$$

The tangential vectors $\frac{\partial \boldsymbol{r}}{\partial \alpha_1}, \frac{\partial \boldsymbol{r}}{\partial \alpha_2}, \frac{\partial \boldsymbol{r}}{\partial \alpha_3}$ and the normal vectors $\nabla \boldsymbol{\alpha}_1, \nabla \boldsymbol{\alpha}_2, \nabla \boldsymbol{\alpha}_3$ form a reciprocal system.

$$\implies \quad \frac{\partial \boldsymbol{r}}{\partial \alpha_1} \cdot \nabla \alpha_1 = \frac{\partial \boldsymbol{r}}{\partial \alpha_2} \cdot \nabla \alpha_2 = \frac{\partial \boldsymbol{r}}{\partial \alpha_3} \cdot \nabla \alpha_3 = 1 \tag{2.16}$$

and

$$\frac{\partial \boldsymbol{r}}{\partial \alpha_1} \cdot \nabla \alpha_2 = \frac{\partial \boldsymbol{r}}{\partial \alpha_2} \cdot \nabla \alpha_1 = \frac{\partial \boldsymbol{r}}{\partial \alpha_2} \cdot \nabla \alpha_3 = \frac{\partial \boldsymbol{r}}{\partial \alpha_3} \cdot \nabla \alpha_2 = \frac{\partial \boldsymbol{r}}{\partial \alpha_3} \cdot \nabla \alpha_1 = \frac{\partial \boldsymbol{r}}{\partial \alpha_1} \cdot \nabla \alpha_3 = 0 \tag{2.17}$$

$\{\frac{\partial \boldsymbol{r}}{\partial \alpha_1}, \frac{\partial \boldsymbol{r}}{\partial \alpha_2}, \frac{\partial \boldsymbol{r}}{\partial \alpha_3}\}$ and $\{\nabla \boldsymbol{\alpha}_1, \nabla \boldsymbol{\alpha}_2, \nabla \boldsymbol{\alpha}_3\}$ are known as the **Unitary Base Vectors**, i.e, basis from which we can find unit vectors.

Any vector in space can be expressed in terms of its components. Similarly, any component in general curvilinear coordinates can be expressed in two ways: Consider a vector $\boldsymbol{F}$. If $F_1, F_2, F_3$ are the components of $\boldsymbol{F}$ in direction of $\hat{e}_1, \hat{e}_2, \hat{e}_3$, then $\boldsymbol{F}$ can be written as:

$$\boldsymbol{F} = F_1\hat{e}_1 + F_2\hat{e}_2 + F_3\hat{e}_3 \tag{2.18}$$

If $f_1, f_2, f_3$ be the component of $\boldsymbol{F}$ along $\hat{E}_1, \hat{E}_2, \hat{E}_3$, then:

$$\boldsymbol{F} = f_1\hat{E}_1 + f_2\hat{E}_2 + f_3\hat{E}_3 \tag{2.19}$$

### 2.1.2 Metric Tensor

In simple words, as stated in Ville Hirvonen, 2025, "the metric tensor is a mathematical object that describes the geometry of a coordinate system or manifold. The components of the metric describe lengths and angles between the basis vectors". The metric tensors are used to:

- define dot product for any space
- convert coordinates spaces to distances.

The components of a metric tensor $\boldsymbol{g}$ or $g_{ij}$ are defined as the dot product of any two unit basis vectors $\hat{\boldsymbol{e}}_i$ and $\hat{\boldsymbol{e}}_j$. Thus,

$$g_{ij} = \hat{\boldsymbol{e}}_i \cdot \hat{\boldsymbol{e}}_j \tag{2.20}$$

In order to exemplify the first point, let us consider two vectors $\boldsymbol{u}$ and $\boldsymbol{v}$ where each component of the vector is given as:

$$\boldsymbol{u} = u_i \hat{e}_i \qquad \text{and} \qquad \boldsymbol{v} = v_j \hat{e}_j \tag{2.21}$$

Then the dot product of the two vectors is given as:

$$\boldsymbol{u} \cdot \boldsymbol{v} = (u_i \hat{e}_i) \cdot (v_j \hat{e}_j) = u_i v_j \hat{e}_i \cdot \hat{e}_j = u_i \, v_j \, g_{ij} \tag{2.22}$$

If the tensor $g_{ij} = 0$ then it means that the two basis vectors represent an orthogonal coordinate system. In other words, the coefficients of the metric tensor characterize the relative nature of the coordinate orientation in space. In case of orthogonal coordinates,

$$g_{11} = {h_1}^2 \quad ; \quad g_{22} = {h_2}^2 \quad ; \quad g_{33} = {h_3}^2 \tag{2.23}$$

### 2.1.3 Scale Factors

The scale factors are the non-negative functions (as the unit base vector $\hat{\boldsymbol{e}}_i$ always points in the positive or the increasing direction of the coordinate) of the position of a point in a curvilinear coordinate system. While the unit base vectors define the "position" of the point in the curvilinear geometry, the scale factors define how the coordinates "stretch" to reach that point.

$$\hat{\boldsymbol{e}}_i = \frac{1}{\left| \frac{\partial \boldsymbol{r}}{\partial \alpha_1} \right|} \frac{\partial \boldsymbol{r}}{\partial \alpha_1} \tag{2.24}$$

$$= \frac{1}{h_i} \frac{\partial \boldsymbol{r}}{\partial \alpha_1} \tag{2.25}$$

where $h_i = \left| \frac{\partial \boldsymbol{r}}{\partial \alpha_i} \right|$ is the *scale factor* (or *scale velocity*) , which is equal to length of the unit base vector. Thus,

$$\implies \qquad \hat{e}_1 = \frac{1}{h_1} \frac{\partial \boldsymbol{r}}{\partial \alpha_1} \tag{2.26}$$

$$\hat{e}_2 = \frac{1}{h_2} \frac{\partial \boldsymbol{r}}{\partial \alpha_2} \tag{2.27}$$

$$\hat{e}_3 = \frac{1}{h_3} \frac{\partial \boldsymbol{r}}{\partial \alpha_3} \tag{2.28}$$

To simplify, we can say that the scale factors are the measure of the actual distance moved by any arbitrary point along the curvilinear coordinate $\alpha_i$. For example, i case of Polar coordinates $(r, \theta)$, since the radial coordinate is straight, $dr = d\alpha_1$, thus, to move a unit distance along the radial coordinate, the point moves the same distance in curvilinear coordinate, thus, $h_1 = h_r = 1$. But when it moves along the $\theta-$direction, it covers the distance (arc-length) which is $r \, d\alpha_2$ in curvilinear coordinates, and hence the scale factor

becomes $h_2 = h_\theta = r$. In terms of metric tensor, they are the square root of the diagonal terms of the tensor, which means,

$$h_k = \sqrt{g_{kk}} \tag{2.29}$$

The concept of scale factors will become more clear with the introduction of the next segment, the arc-length.

### 2.1.4 Arc-length

The concept of arc-length and volume element is useful when transforming equations of cartesian, polar and spherical coordinates. Simply defined, arc-length is the measure of the distance traversed by a point along a curve.

In terms of Cartesian coordinates, the position vector from the origin $O$ to the point $P$ is expressed as:

$$\boldsymbol{r} = x_1\hat{i} + x_2\hat{j} + x_3\hat{k} \tag{2.30}$$

So, from the transformation equations above, we can rewrite the position vector as:

$$\boldsymbol{r} = \boldsymbol{r}(\alpha_1, \alpha_2, \alpha_3) \tag{2.31}$$

Now, any element of displacement is given by :

$$d\boldsymbol{r} = \frac{\partial \boldsymbol{r}}{\partial \alpha_1} d\alpha_1 + \frac{\partial \boldsymbol{r}}{\partial \alpha_2} d\alpha_2 + \frac{\partial \boldsymbol{r}}{\partial \alpha_3} d\alpha_3 \tag{2.32}$$

$$\implies d\boldsymbol{r} = \sum_{i=1}^{3} \frac{\partial \boldsymbol{r}}{\partial \alpha_i} d\alpha_i = d\boldsymbol{s} \tag{2.33}$$

where $d\boldsymbol{s}$ is the **arc-length** of the curve.

According to Fig.2.2, the arc-length $ds$ is the distance between the points $P(\alpha_1, \alpha_2, \alpha_3)$ and $Q(\alpha_1, \alpha_2, \alpha_3)$, given as:

$$(ds)^2 = (ds_1)^2 + (ds_2)^2 + (ds_3)^2 \tag{2.34}$$

where $ds_i$ is the distance moved by the point only along the corresponding coordinate curve $\alpha_i$, given as:

$$ds_1 = h_1\, d\alpha_1 \text{ for } d\alpha_1 \geq 0 \quad ; \quad d\alpha_2 = d\alpha_3 = 0, \tag{2.35}$$

$$ds_2 = h_2\, d\alpha_2 \text{ for } d\alpha_2 \geq 0 \quad ; \quad d\alpha_1 = d\alpha_3 = 0, \tag{2.36}$$

$$ds_3 = h_3\, d\alpha_3 \text{ for } d\alpha_3 \geq 0 \quad ; \quad d\alpha_1 = d\alpha_2 = 0, \tag{2.37}$$

So, the arc-length can be re-written as:

$$(ds)^2 = (h_1\, d\alpha_1)^2 + (h_2\, d\alpha_2)^2 + (h_3\, d\alpha_3)^2 = (h_i\, d\alpha_i)^2 = g_{ij} dx_i dx_j \tag{2.38}$$

Thus, the arc-length is the sum of the distance traveled by the point along the coordinate curve. In Eqn.(2.38), $h_i$ is the scale factor that provides information on magnitude of the distance moved as $\alpha_i$ changes. The scale factor $h_i$ relates a coordinate change $d\alpha_i$ to the true physical distance $ds$ (arc length) along the corresponding coordinate curve via the relation described in (2.35). The direction of the displacement is given by the associated unit basis vector $\hat{\boldsymbol{e}}_i$

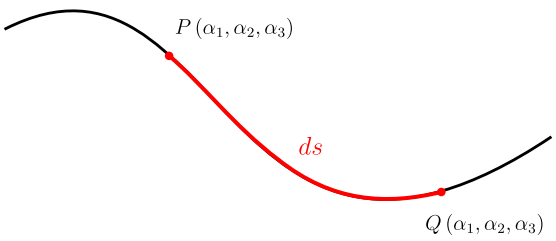


**Fig. 2.2.** Arc length $ds$ is the distance between two points $P(\alpha_1, \alpha_2, \alpha_3)$ and $Q(\alpha_1, \alpha_2, \alpha_3)$.

Alternatively, in terms of unit base vectors,

$$\frac{\partial \boldsymbol{r}}{\partial \alpha_i} = h_i \hat{e}_i \tag{2.39}$$

The arc-length of a differential element in orthogonal curvilinear coordinate system is then given as:

$$ds^2 = \partial \boldsymbol{r} \cdot \partial \boldsymbol{r} = (h_1 d\alpha_1)^2 \cdot (\hat{e}_1 \cdot \hat{e}_1) + (h_2 d\alpha_2)^2 \cdot (\hat{e}_2 \cdot \hat{e}_2) + (h_3 d\alpha_3)^2 \cdot (\hat{e}_3 \cdot \hat{e}_3) \tag{2.40}$$

$$\implies \quad ds^2 = {h_1}^2 {d\alpha_1}^2 + {h_2}^2 {d\alpha_2}^2 + {h_3}^2 {d\alpha_3}^2 \tag{2.41}$$

which is equivalent to Eqn.2.38.

Another important aspect is to understand how the unit base vectors of the curvilinear system can be expressed in terms of the unit basis vectors $\hat{\boldsymbol{\imath}}_k$ of the Cartesian system. This relation is significant because the unit vectors $\hat{\boldsymbol{e}}_r$ of the curvilinear system depend on the *curvature* of the coordinate system, and while their magnitude remains the same, their direction changes as the point moves along the coordinate axes, much like jogging along a circular track - while your speed remains the same, you keep changing directions at each point on the track. But the unit basis of the Cartesian system are naturally orthonormal, fixed in direction and have a constant length of unit vectors. Establishing a relation between the base vectors of the curvilinear systems to that of the Cartesian systems provides a simplified path to :

- perform calculations in the curvilinear system.
- easily perform vector calculus with consistency.
- convert seamlessly between coordinate systems.

Thus, it is important to define the $\hat{\boldsymbol{e}}_r$ with respect to $\hat{\boldsymbol{\imath}}_k$ via:

$$\hat{\boldsymbol{e}}_r = \frac{dx_k}{ds_r}\,\hat{\boldsymbol{\imath}}_k = \frac{\partial x_k}{\partial \alpha_r}\frac{d\alpha_r}{ds_r}\,\hat{\boldsymbol{\imath}}_k = \frac{1}{h_r}\frac{\partial \boldsymbol{r}}{\partial \alpha_r} = \frac{1}{h_r}\frac{\partial x_k}{\partial \alpha_r}\,\hat{\boldsymbol{\imath}}_k \tag{2.42}$$

where $dx_k/ds_r$ is the rectangular component of the unit vector $\hat{\boldsymbol{e}}_r$, meaning it is the directional derivative of Cartesian coordinate $x_k$ along the curvilinear coordinate $\alpha_r$ and $\boldsymbol{r} = x_k\,\hat{\boldsymbol{\imath}}_k$ is the position vector in Cartesian coordinate, defined in (2.30).

### 2.1.5 Volume element

In orthogonal curvilinear coordinate system, the volume element is given as:

$$\begin{aligned} dV &= x\, y\, z \\ &= [(h_1\, d\alpha_1\, \hat{e}_1) \times (h_2\, d\alpha_2\, \hat{e}_2)] \cdot (h_3\, d\alpha_3\, \hat{e}_3) \\ &= [h_1\, h_2\, d\alpha_1\, d\alpha_2\, (\hat{e}_1 \times \hat{e}_2)] \cdot (h_3\, d\alpha_3\, \hat{e}_3) \\ &= h_1\, h_2\, d\alpha_1\, d\alpha_2\, \hat{e}_3 \cdot h_3\, d\alpha_3\, \hat{e}_3 \\ &= h_1\, h_2\, h_3\, d\alpha_1\, d\alpha_2\, d\alpha_3 \end{aligned} \tag{2.43}$$

### 2.1.6 Physical components of a vector

The components of a vector $\boldsymbol{u}$ or a tensor $\boldsymbol{T}$ can be expressed from Cartesian components in local coordinate system (given by $v_k$) in terms of curvilinear coordinates, At any given point in the curvilinear space, the local Cartesian coordinate axes, given as $x_k$, are tangent to the coordinates curves of the curvilinear coordinate system, such that the unit base vector of the two systems are equivalent, ($\hat{\boldsymbol{i}}_r \equiv \hat{\boldsymbol{e}}_r$), and thus:

$$v_r = e_r^k v_k \tag{2.44}$$

where

$$e_n^m = \frac{1}{h_n} \frac{\partial x_m}{\partial \alpha_n} \tag{2.45}$$

is the *transformation coefficient* that defines the relation between orthonormal curvilinear basis $\hat{\boldsymbol{e}}_r$ to the orthonormal Cartesian basis $\hat{\boldsymbol{i}}_k$. Similarly, for the second-order tensor $\boldsymbol{T}$, the components are obtained as:

$$T_{ij} = \boldsymbol{e}_i^m\, \boldsymbol{e}_j^n\, T_{mn} \tag{2.46}$$

Any vectorial or tensorial equation that does not involve the spatial derivative of the vector $\boldsymbol{v}$ or the tensor $\boldsymbol{T}$, is invariant of the coordinate system. Consider, for example, the Hooke's law in elasticity, given as:

$$\boldsymbol{\sigma} = \mathbb{C}\, \boldsymbol{\epsilon} \tag{2.47}$$

Since there are no derivatives with respect to coordinates in this equation and has only tensor values at each point, the physical components of the stress tensor will have the same form in orthogonal curvilinear coordinates, as it does in orthonormal Cartesian coordinates.

### 2.1.7 Derivatives of base vectors: Christoffel Symbols

However, when the strains are computed as gradients of the displacement vector:

$$\boldsymbol{\epsilon} = \operatorname{grad} \boldsymbol{u} + (\operatorname{grad} \boldsymbol{u})^T \tag{2.48}$$

or Fourier's law in thermodynamics, which relates the heat flux to the gradient of temperature:

$$\boldsymbol{q} = -k_i\, (\operatorname{grad} \boldsymbol{T}) \tag{2.49}$$

In both these equations, the resulting vector is dependent on the gradient of the vector (displacement) or the scalar (temperature). In such a scenario, the orthogonal Cartesian coordinate system is transformed into a curvilinear coordinate system, in which the basis vectors vary in direction from point to point while retaining unit magnitude. As a result, the derivatives of these unit base vectors with respect to the curvilinear coordinate is not

zero, and represents how the coordinate system changes from one point in the space to another.

$$\frac{\partial(h_r\,\hat{\boldsymbol{e}}_r)}{\partial\alpha_n} = h_r\,\frac{\partial\hat{\boldsymbol{e}}_r}{\partial\alpha_n} + \hat{\boldsymbol{e}}_r\,\frac{\partial h_r}{\partial\alpha_n} = \frac{\partial^2 x_k}{\partial\alpha_n\,\partial\alpha_r}\,\hat{\boldsymbol{i}}_k \tag{2.50}$$

This term is known as **Christoffel Symbol**, denoted as $\Gamma^k_{mn}$. In other words,

$$\Gamma^k_{mn} = \frac{\partial\hat{\boldsymbol{e}_m}}{\partial\alpha_n}\cdot\hat{\boldsymbol{e}_k} \tag{2.51}$$

This implies that Christoffel symbols measure how the unit basis vector $\hat{\boldsymbol{e}_m}$ moving along the coordinate $\alpha_n$ changes in the direction of $\hat{\boldsymbol{e}_k}$. When summation is introduced, the Christoffel symbols simply illustrate how the basis vectors change throughout a Riemannian geometry, given as

$$\Gamma^k_{mn} = \sum_k \frac{\partial^2 x_k}{\partial\alpha_n\,\partial\alpha_r}\,\frac{\partial x^k}{\partial\alpha_r} = \frac{1}{2}\left[\frac{\partial g_{nr}}{\partial\alpha_m} + \frac{\partial g_{rm}}{\partial\alpha_n} - \frac{\partial g_{mn}}{\partial\alpha_r}\right] \tag{2.52}$$

where $g_{ij} = h_i\,h_j\,\delta_{ij}$ is the metric tensor defined in Sec.2.1.2. An important property of the Christoffel symbols is the symmetry of their lower indices, that is, $\Gamma^k_{mn} = \Gamma^k_{nm}$, since by definition, Riemannian geometry does not include torsion effects. Based on the values of $m, n, r$ the Christoffel symbols can take the following form given in Table 2.1.

| | |
|---|---|
| $m, n, r$ are all different | 0 |
| $m = n \neq r$ (no sum) | $-h_m\frac{\partial h_m}{\partial\alpha_r}$ |
| $m = r = n$ (no sum) | $h_m\frac{\partial h_m}{\partial\alpha_m}$ |
| $n = r \neq m$ (no sum) | $h_r\frac{\partial h_r}{\partial\alpha_m}$ |
| $m = r \neq n$ (no sum) | $h_r\frac{\partial h_r}{\partial\alpha_n}$ |

**Table 2.1.** Values of Christoffel symbols based on $m, n, r$.

For orthogonal curvilinear coordinates, the derivates of the unit base vectors simply boil down to the following compact rule

$$\frac{\partial\hat{\boldsymbol{e}}_m}{\partial\alpha_n} = \begin{cases} \dfrac{1}{h_m}\dfrac{\partial h_n}{\partial\alpha_m}\,\hat{\boldsymbol{e}}_n, & m \neq n \\ -\left(\dfrac{1}{h_r}\dfrac{\partial h_m}{\partial\alpha_r}\,\hat{\boldsymbol{e}}_r + \dfrac{1}{h_s}\dfrac{\partial h_m}{\partial\alpha_s}\,\hat{\boldsymbol{e}}_s\right), & m = n \end{cases} \tag{2.53}$$

Thus, using the Christoffel symbols the derivatives of the unit basis vectors can be represented in the orthogonal curvilinear form with no explicit reference to the Cartesian system. This is extremely important when representing the gradient or the divergence of any vector or tensor in curvilinear coordinates. For example, the partial derivatives of a vector $\boldsymbol{v} = \sum_m v_{<m>}\hat{\boldsymbol{e}_m}$ can be written as

$$\frac{\partial\boldsymbol{v}}{\partial\alpha_n} = \sum_m\left(\frac{\partial v_{<m>}}{\partial\alpha_n}\hat{\boldsymbol{e}}_m + v_{<m>}\frac{\partial\hat{\boldsymbol{e}}_m}{\partial\alpha_n}\right) \tag{2.54}$$

$$\frac{\partial\boldsymbol{v}}{\partial\alpha_n} = \sum_m\frac{\partial v_{<m>}}{\partial\alpha_n}\hat{\boldsymbol{e}}_m + v_{<r>}\frac{1}{h_r}\frac{\partial h_n}{\partial\alpha_r}\hat{\boldsymbol{e}}_n + v_{<s>}\frac{1}{h_s}\frac{\partial h_n}{\partial\alpha_s}\hat{\boldsymbol{e}}_n - \left(\frac{v_{<n>}}{h_r}\frac{\partial h_n}{\partial\alpha_r}\hat{\boldsymbol{e}}_r + \frac{v_{<n>}}{h_s}\frac{\partial h_n}{\partial\alpha_s}\hat{\boldsymbol{e}}_s\right) \tag{2.55}$$

where $n, s, r$ are all different.

## 2.2 Gradients in Orthogonal Curvilinear Coordinates

The gradient of any function (scalar, vector, or tensor) provides an idea of how the given function changes in space and in which direction it changes fastest. In terms of vectors and higher order tensors, it represents how each term of the vector (or tensor) field changes in space, that is, with respect to each coordinate. For example, the gradient of a scalar field like temperature only shows the variation of temperature along that particular coordinate, but the gradient of a vector field like displacement also sheds light on the behaviour of each term of the displacement field components in every direction, which is why we have shearing strains, along with normal strains. In the following subsections, we have a look at the general form of gradient of each type of field (scalar, vector, tensor) in the settings of orthogonal curvilinear coordinates. These equations would be utilized in areas of thermal and elastic equations, and thus, it is important to have a good understanding of these equations.

### 2.2.1 Gradient of a scalar

Let $\phi(\alpha_1, \alpha_2, \alpha_3)$ be a scalar point function in an orthogonal curvilinear coordinate system. The resultant is a vector such that for the unit vector $\hat{\boldsymbol{e}}$, the directional derivative $d\phi/ds$ along the direction of the unit base vector is given by:

$$\frac{d\phi}{ds} = \nabla\phi \cdot \hat{\boldsymbol{a}} \tag{2.56}$$

Eqn.(2.56) is invariant of the coordinate system. To identify the components of the gradient vector in any orthogonal coordinate system, we revoke the definition of the unit vector $\hat{\boldsymbol{e}}$:

$$\hat{\boldsymbol{a}} = \frac{d\boldsymbol{r}}{ds} = \frac{\partial \boldsymbol{r}}{\partial \alpha_r}\frac{d\alpha_r}{ds} = h_r \frac{d\alpha_r}{ds}\hat{\boldsymbol{e}}_r \tag{2.57}$$

Applying the chain rule to the LHS of (2.56),

$$\frac{d\phi}{ds} = \sum \frac{\partial \phi}{\partial \alpha_r}\frac{d\alpha_r}{ds} \tag{2.58}$$

Next, for the RHS of (2.56):

$$\nabla\phi \cdot \hat{\boldsymbol{a}} = \sum_r (\nabla\phi)_r\, \hat{\boldsymbol{e}}_r \cdot \sum_p h_p \frac{d\alpha_p}{ds}\hat{\boldsymbol{e}}_p \tag{2.59}$$

For $(r = p), \hat{\boldsymbol{e}}_r \cdot \hat{\boldsymbol{e}}_p = 1$. Thus,

$$\nabla\phi \cdot \hat{\boldsymbol{a}} = \sum_r (\nabla\phi)_r h_r \frac{d\alpha_r}{ds} \tag{2.60}$$

Substituting both sides of the equation gives:

$$\sum_r \left[ h_r (\nabla\phi)_r - \frac{\partial \phi}{\partial \alpha_r} \right] \frac{d\alpha_r}{ds} = 0 \tag{2.61}$$

Thus,

$$(\nabla\phi)_{<r>} = \frac{1}{h_r}\frac{\partial \phi}{\partial \alpha_r} \quad \text{or} \quad \nabla\phi = \sum_r \frac{1}{h_r}\frac{\partial \phi}{\partial \alpha_r}\hat{\boldsymbol{e}}_r \tag{2.62}$$

$$\nabla = \sum_r \frac{1}{h_r}\frac{\partial}{\partial \alpha_r}\hat{\boldsymbol{e}}_r \tag{2.63}$$

### 2.2.2 Gradient of a vector

The gradient of a vector $\boldsymbol{v}$ results in a second-order tensor:

$$\frac{d\boldsymbol{v}}{ds} = (\boldsymbol{v}\nabla)\cdot\hat{\boldsymbol{a}} = \hat{\boldsymbol{a}}\cdot(\nabla\boldsymbol{v}) \tag{2.64}$$

where $(\boldsymbol{v}\nabla)$ is the second-order tensor in Cartesian components, $\hat{\boldsymbol{a}}$ is the unit base vector, and $\boldsymbol{v}\nabla = (\nabla\boldsymbol{v})^T$. In index notation:

$$\frac{d\boldsymbol{v}}{ds} = \sum_r \frac{\partial\boldsymbol{v}}{\partial\alpha_r}\frac{d\alpha_r}{ds} \tag{2.65}$$

$$= \sum_r \left(h_r\frac{d\alpha_r}{ds}\right)\left(\frac{1}{h_r}\frac{\partial\boldsymbol{v}}{\partial\alpha_r}\right) \tag{2.66}$$

$$= \left(\sum_m h_m\frac{d\alpha_m}{ds}\,\hat{\boldsymbol{e}}_m\right)\cdot\left(\sum_n \frac{1}{h_n}\frac{\partial\boldsymbol{v}}{\partial\alpha_n}\,\hat{\boldsymbol{e}}_n\right) \tag{2.67}$$

where $\hat{\boldsymbol{e}}_m\cdot\hat{\boldsymbol{e}}_n = g_{mn}$. In the definition above, the derivative term $\frac{\partial\boldsymbol{v}}{\partial\alpha_n}$ is given by (2.1.6).

### 2.2.3 Gradient of a tensor

The gradient of a second order tensor $\boldsymbol{T}$ is given as:

$$\frac{d\boldsymbol{T}}{ds} = (\nabla\boldsymbol{T})\cdot\hat{\boldsymbol{a}} = \hat{\boldsymbol{a}}\cdot(\boldsymbol{T}\nabla) \tag{2.68}$$

Following the similar procedure as above:

$$\frac{d\boldsymbol{T}}{ds} = \sum_r \frac{\partial\boldsymbol{T}}{\partial\alpha_r}\frac{d\alpha_r}{ds} \tag{2.69}$$

$$= \sum_r \left(\frac{1}{h_r}\frac{\partial\boldsymbol{T}}{\partial\alpha_r}\right)\left(h_r\frac{d\alpha_r}{ds}\right) \tag{2.70}$$

$$= \left(\sum_m \frac{1}{h_m}\frac{\partial\boldsymbol{T}}{\partial\alpha_m}\hat{\boldsymbol{e}}_m\right)\cdot\left(\sum_n h_n\frac{d\alpha_n}{ds}\hat{\boldsymbol{e}}_n\right) \tag{2.71}$$

$$= \left(\sum_m h_m\frac{d\alpha_m}{ds}\hat{\boldsymbol{e}}_m\right)\cdot\left(\sum_n \frac{1}{h_n}\frac{\partial\boldsymbol{T}}{\partial\alpha_n}\hat{\boldsymbol{e}}_n\right) \tag{2.72}$$

where the precise form of $\partial\boldsymbol{T}/\partial\alpha_r$ is replaced by (2.1.7). From the above equations, a concise form of the gradient of a tensor is obtained as:

$$\boldsymbol{T}\nabla = \boldsymbol{T}\left(\frac{\partial}{\partial\alpha_r}\frac{1}{h_r}\hat{\boldsymbol{e}}_r\right) \quad \text{and} \quad \nabla\boldsymbol{T} = \left(\hat{\boldsymbol{e}}_r\frac{1}{h_r}\frac{\partial}{\partial\alpha_r}\right)\boldsymbol{T} \tag{2.73}$$

## 2.3 Divergence in Orthogonal Curvilinear Coordinates

Physically, the divergence of a vector or tensor field illustrates how much the field spreads out or converges at a point in space. However, the resulting term for a vector and a tensor field represent different physics occurring at the surface. The divergence of a vector field, for example, a heat flux through a surface generally results in a scalar quantity that measures the net outflow at a point, that is, it measures the "strength" or the magnitude

of the vector field at that point. The divergence of a tensor field, on the other hand, measures how much a vector field changes across a surface, that is the magnitude, as well as the direction in which it changes. Thus, the divergence of a tensor field gives a vector output. The divergence of stress, appearing in balance equation, shows how the stress vector changes in each direction, and across the surface. In the forthcoming subsections, we understand the general form of these equations in curvilinear space.

### 2.3.1 Divergence of a vector

The divergence of a vector $\boldsymbol{v}$ results in a scalar function, acting at a point in the coordinate space. It is defined in the orthogonal curvilinear coordinate system as:

$$\operatorname{div} \boldsymbol{v} = \nabla \cdot \boldsymbol{v} = \boldsymbol{v} \cdot \nabla \tag{2.74}$$

The components in any orthogonal coordinate system can be obtained by substituting the definition of $\nabla$ operator from defined previously.

$$\nabla \cdot \boldsymbol{v} = \left( \sum_r \hat{\boldsymbol{e}}_r \frac{1}{h_r} \frac{\partial}{\partial \alpha_r} \right) \cdot \boldsymbol{v} \tag{2.75}$$

$$= \sum_m \hat{\boldsymbol{e}}_m \frac{1}{h_m} \frac{\partial}{\partial \alpha_m} \left( \sum_n v_{<n>} \hat{\boldsymbol{e}}_n \right) \tag{2.76}$$

$$= \sum_m \sum_n \left( \frac{1}{h_m} \frac{\partial v_{<n>}}{\partial \alpha_m} \hat{\boldsymbol{e}}_m \cdot \hat{\boldsymbol{e}}_n + \frac{1}{h_m} v_{<n>} \hat{\boldsymbol{e}}_m \cdot \frac{\partial \hat{\boldsymbol{e}}_n}{\partial \alpha_m} \right) \tag{2.77}$$

where $v_{<n>}$ is the component of the vector $\boldsymbol{v}$ in curvilinear coordinates. Since $\hat{\boldsymbol{e}}_n \cdot \hat{\boldsymbol{e}}_m = \delta_{mn}$, this simplifies:

$$\nabla \cdot \boldsymbol{v} = \sum_n \frac{1}{h_n} \frac{\partial v_{<n>}}{\partial \alpha_n} + \sum_n \left( \sum_m \frac{v_{<m>}}{h_m h_n} \frac{\partial h_n}{\partial \alpha_m} \right) \tag{2.78}$$

which can be further simplified to the following well-known form of the divergence of a vector:

$$\operatorname{div} \boldsymbol{v} = \frac{1}{h_1 h_2 h_3} \left[ \frac{\partial}{\partial \alpha_1} (h_2 h_3 v_{<1>}) + \frac{\partial}{\partial \alpha_2} (h_3 h_1 v_{<2>}) + \frac{\partial}{\partial \alpha_3} (h_1 h_2 v_{<3>}) \right] \tag{2.79}$$

or

$$\operatorname{div} \boldsymbol{v} = \frac{1}{\sqrt{g}} \sum_n \frac{\partial}{\partial \alpha_n} \left( \frac{\sqrt{g}}{h_n} v_{<n>} \right) \tag{2.80}$$

where $\sqrt{g} = h_1 h_2 h_3 = \det|g_{ij}|$.

### 2.3.2 Divergence of a tensor

Divergence of a second order tensor $\boldsymbol{T}$ results in a vector, whose invariant form is:

$$\operatorname{div} \boldsymbol{T} = \nabla \cdot \boldsymbol{T} \neq \boldsymbol{T} \cdot \nabla \tag{2.81}$$

The components of this divergence vector can be obtained in terms of curvilinear coordinates by substituting the values of $\nabla$ in the equation.

$$(\operatorname{div}\boldsymbol{T})_i = \sum_j \frac{\partial T_{ij}}{\partial \alpha_j} \tag{2.82}$$

$$= \sum_{m,n,r} \left(T_{<mn>}\hat{\boldsymbol{e}}_m \otimes \hat{\boldsymbol{e}}_n\right)\left(\nabla_{<r>}\hat{\boldsymbol{e}}_r\right) \tag{2.83}$$

$$= \sum_{m,n} \frac{1}{h_r}\frac{\partial T_{<mr>}}{\partial \alpha_r}\hat{\boldsymbol{e}}_m + \sum_{m,r} T_{<mr>}\frac{1}{h_r}\frac{\partial \hat{\boldsymbol{e}}_m}{\partial \alpha_r} + \sum_{m,n,r} T_{<mn>}\frac{1}{h_r}\left(\frac{\partial \hat{\boldsymbol{e}}_n}{\partial \alpha_r}\cdot\hat{\boldsymbol{e}}_r\right)\hat{\boldsymbol{e}}_m \tag{2.84}$$

where the definition of $\nabla = 1/h_r\partial/\partial\alpha_r$ has been implemented. From 2.1.7, we substitute the values for the spatial derivatives of the unit base vectors:

$$\frac{\partial \hat{\boldsymbol{e}}_n}{\partial \alpha_n}\cdot\hat{\boldsymbol{e}}_r = \begin{cases} 0, & n = r \\ \dfrac{1}{h_n}\dfrac{\partial h_r}{\partial \alpha_r}, & n \neq r \end{cases} \tag{2.85}$$

Thus, the last term in (2.82) can be written as:

$$\sum_{m,n,r} T_{<mn>}\frac{1}{h_r}\left(\frac{\partial \hat{\boldsymbol{e}}_n}{\partial \alpha_r}\cdot\hat{\boldsymbol{e}}_r\right)\hat{\boldsymbol{e}}_m = \sum_{m,r}\frac{1}{h_r}\left(\sum_{n\neq r} T_{<mn>}\frac{1}{h_n}\frac{\partial h_r}{\partial \alpha_n}\right)\hat{\boldsymbol{e}}_m \tag{2.86}$$

and

$$\sum_{m,n} T_{<mn>}\frac{1}{h_r}\left(\frac{\partial \hat{\boldsymbol{e}}_m}{\partial \alpha_r}\right) = \sum_r \left\{\frac{1}{h_r}\left(\sum_{m\neq r} T_{<mr>}\frac{1}{h_m}\frac{\partial h_r}{\partial \alpha_m}\right)\hat{\boldsymbol{e}}_r + \frac{1}{h_r}T_{<rr>}\left(-\frac{1}{h_p}\frac{\partial h_r}{\partial \alpha_p}\hat{\boldsymbol{e}}_p - \frac{1}{h_q}\frac{\partial h_r}{\partial \alpha_q}\hat{\boldsymbol{e}}_q\right)\right\} \tag{2.87}$$

Substituting (2.86) and (2.87) back into (2.82) gives:

$$\begin{aligned}\operatorname{div}\boldsymbol{T} = \sum_m \left[\sum_r \left(\frac{1}{h_r}\frac{\partial T_{<mr>}}{\partial \alpha_r} + \sum_{n\neq r}\frac{T_{<mn>}}{h_r h_n}\frac{\partial h_r}{\partial \alpha_n}\right)\right]\hat{\boldsymbol{e}}_m + \sum_r\left[\sum_{m\neq r}\frac{T_{<mr>}}{h_r h_m}\frac{\partial h_r}{\partial \alpha_m}\right]\hat{\boldsymbol{e}}_r \\ - \frac{T_{<11>}}{h_1}\left(\frac{1}{h_2}\frac{\partial h_1}{\partial \alpha_2}\hat{\boldsymbol{e}}_2 + \frac{1}{h_3}\frac{\partial h_1}{\partial \alpha_3}\hat{\boldsymbol{e}}_3\right) - \frac{T_{<22>}}{h_2}\left(\frac{1}{h_1}\frac{\partial h_2}{\partial \alpha_1}\hat{\boldsymbol{e}}_1 + \frac{1}{h_3}\frac{\partial h_2}{\partial \alpha_3}\hat{\boldsymbol{e}}_3\right) \\ - \frac{T_{<33>}}{h_3}\left(\frac{1}{h_2}\frac{\partial h_3}{\partial \alpha_2}\hat{\boldsymbol{e}}_2 + \frac{1}{h_1}\frac{\partial h_3}{\partial \alpha_1}\hat{\boldsymbol{e}}_1\right)\end{aligned} \tag{2.88}$$

Eqn.(2.88) represents the general form of divergence of a tensor in orthogonal curvilinear coordinate space. It can be used to write, for example, the balance equation in solid mechanics, defined in 3.76, where stress is the tensor.

$$\boldsymbol{T} = \sum_{m,n} T_{\langle mn\rangle}\,\hat{\boldsymbol{e}}_m \otimes \hat{\boldsymbol{e}}_n,$$

the divergence is expressed as

$$\nabla \cdot \boldsymbol{T} = \sum_{r} \frac{1}{h_r} \frac{\partial}{\partial \alpha_r} \left( \sum_{m,n} T_{\langle mn \rangle} \hat{\boldsymbol{e}}_m \otimes \hat{\boldsymbol{e}}_n \right) \cdot \hat{\boldsymbol{e}}_r \tag{2.89}$$

$$= \sum_{m,r} \frac{1}{h_r} \frac{\partial T_{\langle mr \rangle}}{\partial \alpha_r} \hat{\boldsymbol{e}}_m + \sum_{m,r} T_{\langle mr \rangle} \frac{1}{h_r} \frac{\partial \hat{\boldsymbol{e}}_m}{\partial \alpha_r} \tag{2.90}$$

$$+ \sum_{m,n,r} T_{\langle mn \rangle} \frac{1}{h_r} \left( \frac{\partial \hat{\boldsymbol{e}}_n}{\partial \alpha_r} \cdot \hat{\boldsymbol{e}}_r \right) \hat{\boldsymbol{e}}_m. \tag{2.91}$$

## 2.4 Laplacian Operator in Orthogonal Curvilinear Coordinates

Consider a scalar function $\phi$, which in orthogonal curvilinear coordinates can be expressed as $\phi = \phi(\alpha_1, \alpha_2, \alpha_3)$.

$$\nabla^2 \phi = \nabla \cdot \nabla \phi \tag{2.92}$$

$$= \left\{ \frac{\hat{e}_1}{h_1} \frac{\partial}{\partial \alpha_1} + \frac{\hat{e}_2}{h_2} \frac{\partial}{\partial \alpha_2} + \frac{\hat{e}_3}{h_3} \frac{\partial}{\partial \alpha_3} \right\} \cdot \left\{ \frac{\hat{e}_1}{h_1} \frac{\partial \phi}{\partial \alpha_1} + \frac{\hat{e}_2}{h_2} \frac{\partial \phi}{\partial \alpha_2} + \frac{\hat{e}_3}{h_3} \frac{\partial \phi}{\partial \alpha_3} \right\} \tag{2.93}$$

Thus the Laplacian operator in terms of orthogonal curvilinear coordinates can be defined as:

$$\nabla^2 = \frac{1}{h_1 h_2 h_3} \left\{ \frac{\partial}{\partial \alpha_1} \left( \frac{h_2 h_3}{h_1} \frac{\partial}{\partial \alpha_1} \right) + \frac{\partial}{\partial \alpha_2} \left( \frac{h_1 h_3}{h_2} \frac{\partial}{\partial \alpha_2} \right) + \frac{\partial}{\partial \alpha_3} \left( \frac{h_1 h_2}{h_3} \frac{\partial}{\partial \alpha_3} \right) \right\} \tag{2.94}$$

If the curvilinear coordinate $\alpha_1$ is taken to be aligned with the normal, then $h_1 = 1$ and the surface Laplacian can be simplified to:

$$\nabla_s^2 = \frac{1}{h_2 h_3} \left\{ \frac{\partial}{\partial \alpha_2} \left( \frac{h_3}{h_2} \frac{\partial}{\partial \alpha_2} \right) + \frac{\partial}{\partial \alpha_3} \left( \frac{h_2}{h_3} \frac{\partial}{\partial \alpha_3} \right) \right\} \tag{2.95}$$

which, simply represents the diffusion of the thermo-mechanical properties along the surface of the curve, ie, along the tangential directions.

## 2.5 Theory of Parallel Coordinates

Upto this point, the mathematical mapping of the curvilinear geometry has been achieved. In this section and the preceding subsections, a brief introduction to the underlying principals of the "shape" of the curvilinear geometry is presented. This include the curvature and the related terms, and the parallelism of two surfaces. The mathematical development in this section paves the way to write the definition of curvatures and surface differentials of the parametric curves used an example geometry in this work.

### 2.5.1 Curvature

The first and the foremost concept of the the curvilinear geometry is the idea of curvature. As the name suggests, curvature is simply the deviation of the geometry (line or a surface) from the flat one.

The emergence of calculus in the seventeenth century, most notably through the work of Newton and Leibniz, enabled the systematic evaluation of curvature for planar curves. This analytical framework was subsequently extended by Euler to the study of surfaces, and later fundamentally transformed by Gauss through the introduction of intrinsic curvature—an invariant independent of the manner in which a surface is embedded in Euclidean space. Riemann further generalized these concepts to spaces of arbitrary dimension. In the modern differential-geometric formulation, the curvature of a smooth curve is defined via its osculating circle. Within this framework, Augustin-Louis Cauchy demonstrated that the center of curvature corresponds to the intersection point of two infinitesimally neighboring normal lines to the curve (Borovik A, 2012).

Curvature is a measures of how fast the direction of the curve changes over a small unit of distance. Faster the changes, "tighter" is the curve. The direction of the curve is measured by its tangent vector $\hat{\boldsymbol{t}}$. A small section of the curve is called an "arc", and its length between any two points is known as "arc-length" $ds$ described for a curvilinear system in 2.1.4. In planar geometry, curvature describes the relationship between arc length and the evolution of the curve's tangent vector (HYDE et al., 1997).

Consider a parameterized curve in Cartesian coordinates whose position vector is given as

$$\boldsymbol{r}(t) = \{x(t), y(t), z(t)\} \tag{2.96}$$

The tangent vector (also known as the velocity vector) to this curve becomes

$$\boldsymbol{r}'(t) = \{x'(t), y'(t), z'(t)\} \tag{2.97}$$

For each value of the parameter $t \in \mathcal{I}$, where $\boldsymbol{r}'(t) \neq 0$, there exists a well defined straight line called the **tangent line** to $\boldsymbol{r}$ at $t$. The study of differential geometry ensures that such a line exists at every point in the curve. If at any point $\boldsymbol{r}'(t) = 0$, then it is known as the *singular point* of the curve $\boldsymbol{r}(t)$. The arc-length $ds$ of this parameterized curve is the length of the curve between any two points $t_0$ and $t$:

$$s(t) = \int_{t_0}^{t} |\boldsymbol{r}'(t)|\, dt \qquad ; |\boldsymbol{r}'(t)| = \sqrt{(x'(t))^2 + (y'(t))^2 + (z'(t))^2} \tag{2.98}$$

or

$$|\boldsymbol{r}'(t)| = \frac{ds}{dt} \tag{2.99}$$

the curvature $\kappa$ of the curve is given as

$$\kappa(t) = \frac{x'(t)\, y''(t) - x''(t)\, y'(t)}{(p)^3} \qquad ; \qquad p = \sqrt{x'(t)^2 + y'(t)^2} \tag{2.100}$$

The radius of curvature is equal to the reciprocal of the curvature, that is,

$$R = \frac{1}{\kappa} \tag{2.101}$$

The intersection of the plane curve with a surface along the normal direction $\hat{\boldsymbol{n}}$ results in planar curve, whose curvature can be computed as defined above. In terms of surface curves, this is known as *normal curvature,* $\kappa_n$, and the sign of the curvature is determined by the orientation of the plane $P$. The set of normal curvatures having the same tangent vector on the curve gives the values of maximum and minimum curvatures, known as *principal curvatures,* $\kappa_1$ and $\kappa_2$ of the surface at point P, and their directions are called

as *principal directions.* These principal curvatures are used to determine the *Gaussian curvature* ($K$) and *mean curvature* $H$ to measure the curvature of the surface.

$$K = \kappa_1\,\kappa_2 \qquad ; \qquad H = \frac{\kappa_1 + \kappa_2}{2} \tag{2.102}$$

These definitions of the curvatures (for both curves and surfaces) allows us to define the parallel surfaces.

### 2.5.2 Parallel Surfaces

In differential geometry, parallel surfaces are any two surfaces that are maintained at constant distance from each other, sharing a common normal vector. In other words, two surfaces are parallel if the normal vector of one surface is the normal vector to the other surface. Thus, a set of parallel surfaces can be obtained by translating any surface along its normal direction (Rouse and Appel, 1965, HYDE et al., 1997).

### 2.5.3 Parametric Curves: Wavy Interphase

To ensure the verification of the transmission conditions developed in this work, they are tested in the setting of parametric curves representing a "wavy" interphase with $N$ oscillations. The geometry of the parametric curve is given by

$$R(\theta) = r_i = a + A\cos\left(N\theta\right) \tag{2.103}$$

where $a$ is the base radius of the curve (or the inclusion) and $A$ is the amplitude of the wavelength. The position vector of the curve is given by $\boldsymbol{r}(\theta) = R(\theta)\,\hat{\boldsymbol{e}}_i$ or equivalently in Cartesian coordinates:

$$x(\theta) = R(\theta)\,\cos\theta \qquad ; \qquad y(\theta) = R(\theta)\,\sin\theta$$

The parallel curve at a distance of $\xi$ given as

$$R_\xi = R(\theta) + \xi\cdot\hat{\boldsymbol{n}} \tag{2.104}$$

where $\xi$ is the offset or thickness of the parallel curves in the outward unit normal direction $\hat{\boldsymbol{n}}$.

The scale factors (metric coefficients) of the parametric curve are computed as:

$$h_1 = h_\xi = 1, \qquad h_\theta = \frac{\partial \boldsymbol{r}(\theta)}{\partial\theta} = \sqrt{R^2(\theta) + (R'(\theta))^2} \tag{2.105}$$

The unit tangent vector $\hat{\boldsymbol{t}}$ is evaluated following the discussion above as

$$\hat{\boldsymbol{t}} = \left\{\hat{t}_x, \hat{t}_y\right\} = \frac{\frac{\partial \boldsymbol{r}}{\partial\theta}}{|\frac{\partial \boldsymbol{r}}{\partial\theta}|} = \frac{1}{|\frac{\partial \boldsymbol{r}}{\partial\theta}|}\left\{x'(\theta),\, y'(\theta)\right\} = \left\{\begin{array}{c} \frac{R'(\theta)\cos(\theta) - R(\theta)\sin(\theta)}{\sqrt{R'(\theta)^2 + R^2(\theta)}} \\ \frac{R'(\theta)\sin(\theta) + R(\theta)\cos(\theta)}{\sqrt{R'(\theta)^2 + R^2(\theta)}} \end{array}\right\} \tag{2.106}$$

and the unit normal vector $\hat{\boldsymbol{n}}$ is 90 deg counterclockwise to the unit tangent vector

$$\hat{\boldsymbol{n}} = \{\hat{n}_x, \hat{n}_y\} = \left\{-\hat{t}_y, \hat{t}_x\right\} = \frac{\frac{\partial \boldsymbol{r}}{\partial\theta}}{|\frac{\partial \boldsymbol{r}}{\partial\theta}|} = \left\{\begin{array}{c} \frac{R'(\theta)\sin(\theta) + R(\theta)\cos(\theta)}{\sqrt{R'(\theta)^2 + R^2(\theta)}} \\ \frac{R(\theta)\sin(\theta) - R'(\theta)\cos(\theta)}{\sqrt{R'(\theta)^2 + R^2(\theta)}} \end{array}\right\} \tag{2.107}$$

The curvature of this parametrized curve, using (2.100) is

$$\kappa(\theta) = \frac{R^2(\theta) + 2(R'(\theta))^2 - R(\theta)R'(\theta)}{(R^2(\theta) + (R'(\theta))^2)^{3/2}} \tag{2.108}$$

Therefore, the value of function $g$ (defined later in Chapters 4, 5 and in 6) can be written as

$$g = \frac{1}{h_1 h_2}\frac{\partial h_1 h_2}{\partial n} = \nabla \cdot \boldsymbol{n} = \kappa(\theta) \qquad \text{(local curvature term)} \tag{2.109}$$

The angular derivative of temperature is the projection of gradient of temperature in the tangent direction $\boldsymbol{t}$:

$$\frac{\partial}{\partial\theta}\left(T^{(i)}(R(\theta),\theta)\right) = \|\frac{\partial \boldsymbol{r}(\theta)}{\partial\theta}\| \nabla T \cdot \boldsymbol{t} \tag{2.110}$$

and thus $\mathcal{D}_s\boldsymbol{q}$ (surface Laplacian term) is computed as

$$\mathcal{D}_s\boldsymbol{q} = \frac{-k_i}{h_\theta}\left\{\frac{\partial}{\partial\theta}\left(\frac{1}{h_\theta}\frac{\partial}{\partial\theta}\left(T^{(i)}(R(\theta),\theta)\right)\right)\right\} \tag{2.111}$$

$$= \frac{-k_i}{h_\theta}\left\{\frac{1}{h_\theta}\frac{\partial^2}{\partial\theta^2}T(R(\theta),\theta) - \left(\frac{h'_\theta}{h_\theta^2}\right)\frac{\partial}{\partial\theta}T^{(i)}(R(\theta),\theta)\right\} \tag{2.112}$$

where

$$h'_\theta = \frac{\partial h_\theta}{\partial\theta} = \frac{R'(\theta)\Big(R(\theta) + R''(\theta)\Big)}{\sqrt{R^2(\theta) + (R'(\theta))^2}} \tag{2.113}$$

represents the change in angular scale factor when moving along the tangential direction.

The computations of the first and second order gradients of temperature depends on the smoothness of the curve, which in turn is dependent on the curve approximation and the density of mesh in the interphase.

### 2.5.4 Numerical Implementation of the Parametric Curves

The parametric curves are created B-spline, which is computed to approximate the mathematical curve defined by the form in $(x, y)$ (in 2D). The accuracy of the computed solution depends on the accuracy of the curve, which is improved by introducing more control points in the curve. This can be understood more easily from the graph below, where the black curve shows the B-spline, and blue points represent the control points, and red line joining those points, shows the actual shape of the curve. It can be seen that by including more points (Fig.2.3b and 2.3c) the curve becomes more accurate in shape.

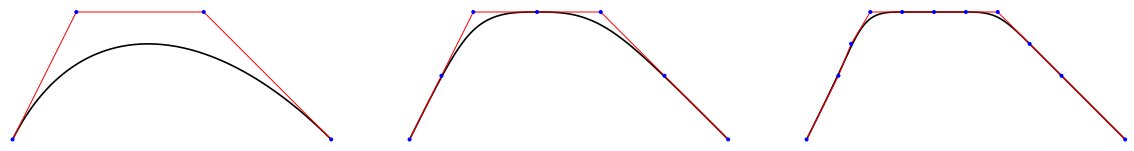

(a) (b) (c)

**Fig. 2.3.** Improving the accuracy of spline.

The effect of this approximation is felt more strongly when computing the second-order gradient terms, like the surface Laplacian terms (defined above in (2.95)) where accuracy is lost if the parametric curve has insufficient control points.

## 2.6 Problem Setup

Throughout the developement of transmission conditions presented in this work, use of orthognal curvilinear coordinates has been made extensively. Therefore, it is assumed that the curvilinear coordinate axis $\alpha_1$ coincides with the normal unit vector, and thus the scale factor $h_1 = 1$. Therefore, the jumps in the properties of the material are taken along the normal direction as

$$[\![f]\!] = \frac{\partial f}{\partial \alpha_1} = \frac{\partial f}{\partial n} \tag{2.114}$$

and $\alpha_2, \alpha_3$ serve as tangential directions.

Consider a parallel curvilinear coordinate system , within which lies an arbitrarily shaped interphase, of thickness $t$, situated between two media, "1" and "2". The sandwiched interphase is a distinct region having its own thermal and/or mechanical properties which are different from those of the surrounding material.

The curvilinear system is defined using coordinates $(\alpha_1, \alpha_2, \alpha_3)$. The boundaries $S_1$ and $S_2$ can be thought of as surfaces composed of parametric curves $\alpha_2$ and $\alpha_3$, which define the parallel surfaces, and the coordinate $\alpha_1$ is chosen to coincide with the common normal to the surfaces. The domain enclosed by the boundaries $S_1$ and $S_2$ is known as the interphase. The thickness of this interphase, $t$, is the distance between these two boundaries, Consider three points $A_1, A_2, A_3$ lying within the interphase. The point $A_1$ lies on the boundary between medium "1" and the interphase, and similarly, point $A_2$ lies on the boundary between medium "2" and the interphase. The point $A_3$ lies inside the interphase, such that the distance between points $A_3$ and points $A_1$ and $A_2$ is $t_1$ and $t_2$ respectively. For the sake of simplicity, we assume that $t_1 = t_2 = t/2$, i.e., the point $A_3$ lies exactly in the middle of the interphase, but this is not the only case, and the interphase can be assumed to be positioned at any arbitrary location $\xi \in [-t/2, t/2]$.

The corresponding metric coefficients or the scale factors of this orthogonal curvilinear coordinate system are $(h_1, h_2, h_3)$ with $h_1 = 1$, as it is along the normal direction. The unit vectors in the tangential direction of the curvilinear coordinate system are denoted by $(\hat{\boldsymbol{e}}_2, \hat{\boldsymbol{e}}_3)$ and $\hat{\boldsymbol{e}}_1$ is the unit normal.

Fig.2.4a gives the graphical representation of a perfect 3 phase system, with three distinct regions marked as material 1, material 2, and the thin interphase in between. The thermomechanical properties are continuous across the boundaries of the interface.

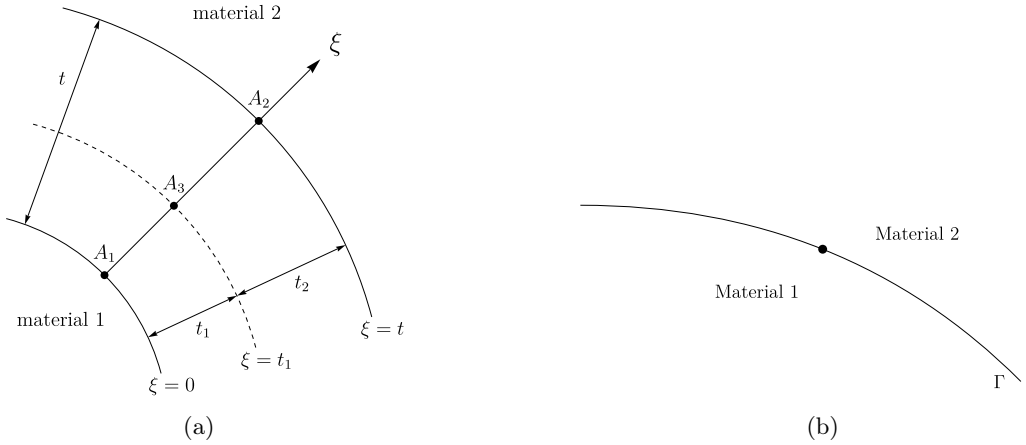


**Fig. 2.4.** (a) Perfect interphase conditions representing thin interphase between materials 1 and 2. (b) Imperfect transmission condition: zero-thickness interface $\Gamma$ between material 1 and 2.

If the thickness of this interphase is taken to be zero ($\lim t \to 0$), then the domain is replaced by a surface of "zero-thickness", known as the "interface" ($\Gamma$) that separates the two materials, as depicted in Fig. 2.4b. The thermal and/or mechanical properties are no longer continuous across this surface, and there is an accumulation of temperature/ displacement or surfaces fluxes at the boundary, known as "jump" of the property, and is denoted as:

$$[\![f]\!] = f|_{A_2} - f|_{A_1} \tag{2.115}$$

while the average of the thermomechanical properties across the interphase boundaries is taken as:

$$\langle f \rangle = \frac{f|_{A_1} + f|_{A_2}}{2} \tag{2.116}$$

where $f$ represents the thermal fields (temperature or heat flux) or the mechanical fields (displacements or stress). The aim of the present work is to derive the model for the jumps in thermomechanical field variables (displacements or temperature) and surface fluxes across the thin interface that mimics the variation within the interphase along the normal direction, while also reducing the modeling complexities involved when solving the complete domain having a thin layer.

Lastly, in the development of the transmission conditions across an imperfect interface in the background of thermal, elastic, and thermoelastic settings, the following identities have been used extensively. Consider $a$ and $b$ to be any arbitrary functions, then the jumps and average of the product of these functions can be expressed as follows:

$$[\![ab]\!] = \langle a \rangle [\![b]\!] + [\![a]\!] \langle b \rangle, \quad \langle ab \rangle = \langle a \rangle \langle b \rangle + \frac{1}{4} [\![a]\!] [\![b]\!], \tag{2.117}$$

and the parameter $\beta$

$$\beta(t, \alpha_1, \alpha_2) = \frac{[\![h_2 h_3]\!]}{\langle h_2 h_3 \rangle}, \quad -2 \leq \beta \leq 2. \tag{2.118}$$

paramater $\gamma$

$$\gamma(t, \alpha_1, \alpha_2) = \frac{h_2 h_3|_{A_3}}{\langle h_2 h_3 \rangle} \tag{2.119}$$

are the two parameters defined in the proposed schemes that are developed within the framework of this thesis.

# Chapter 3

# Thermo-mechanics of Continuum Media

The thermomechanics of solids provides a unified theoretical framework for describing the interaction between thermal and mechanical phenomena in deformable bodies. Many engineering and physical systems operate under conditions where temperature variations and mechanical deformations occur simultaneously, giving rise to thermal stresses, thermally induced deformations, and energy exchange between mechanical work and heat. A consistent treatment of such problems requires the integration of thermodynamic principles with the kinematics and balance laws of continuum mechanics.

This chapter presents the fundamental concepts underlying the thermomechanical behavior of solids and establishes the theoretical foundation required for the development of transmission conditions outlined in the subsequent chapters. Emphasis is placed on formulating governing equations that are both mechanically and thermodynamically consistent, ensuring adherence to the first and second laws of thermodynamics.

The chapter is organized into three parts. In Part I, the essential principles of thermodynamics are reviewed, including the laws of thermodynamics, entropy production, and thermodynamic potentials. Particular attention is given to the Clausius–Duhem inequality and the role of free energy functions in constraining admissible material behavior. These concepts provide the thermodynamic framework necessary for constitutive modeling.

Part II introduces the fundamentals of continuum mechanics required for thermomechanical analysis. This part covers the kinematics of deformation, measures of strain, stress tensors, and the balance laws of mass, momentum, and energy. The formulation is presented in a general continuum setting, forming the mechanical backbone of the theory.

Building on the thermodynamic and mechanical foundations established in the first two parts, Part III focuses on thermoelasticity. Constitutive relations for thermoelastic solids are derived in a thermodynamically consistent manner using appropriate free energy functions. Both coupled and uncoupled thermoelastic theories are discussed, with particular emphasis on linear isotropic thermoelasticity and its governing equations. This part illustrates how temperature and deformation interact in elastic solids and provides the basis for analyzing thermal stresses and thermomechanical coupling effects.

Together, these three parts form a coherent and systematic presentation of the thermomechanics of solids, progressing from fundamental principles to applied constitutive theories.

## 3.1 Part 1: Thermodynamics

Thermo-mechanics of continuum media is concerned with the deformation of continuum media (solids or fluids) subjected to thermal loads. It combines the principals of thermodynamics and solid (or fluid) mechanics, focusing on thermal and mechanical balance laws - balance of mass, momentum, angular momentum and energy - to describe governing equations that capture the thermal effects on the solid deformation. A general strain field is produced due to thermo-mechanical effects (Sadd, 2009,Barber, 2002, Boley and Weiner, 2012).

Thermodynamics is the physics of power generated by heat. It defines the relationship between the system and its surroundings. The subject of thermodynamics is based on four laws, which are summarized in the sections below. A quick recap of the basic thermal terminology is presented in the next section.

### 3.1.1 Basic terminology

Before we proceed to understand the basic laws of thermodynamics, let us have a quick look at some of the terminology and their meanings, as used in thermodynamics. We begin by the concept of *thermodynamic system*, which is the defined domain under study. Within this system, we have a thermodynamic *system*, which is separated from its *surroundings* by a boundary. When a system is at equilibrium under a given set of conditions, it is said to be in a *definite thermodynamic state*. The state of the system can be described by a number of *state quantities* that does not depend on the process by which the system arrived at its state. The properties of the system can be described by an equation of state which specifies the relationship between these variables. A state may be thought of as the instantaneous quantitative description of a system with a set number of variables held constant. If a system has $(m+n)$ state variable, given as $B_a$, where $a = (1, 2, ....., n+m)$ and $B_a$ can be $n$ state variables, which may be $(B_1, B_2, ...., B_n)$, then the equation:

$$B_a = f_a(B_1, B_2, ...., B_n) \tag{3.1}$$

is called *equation of state*.

#### Empirical Temperature

The empirical temperature is the value or the temperature at which two or more systems exist in thermal equilibrium. As per the zeroth law of thermodynamics (3.1.2), two thermal systems $A$ and $B$, when brought into perfect contact with each other, can exist in thermal equilibrium. If another system $C$ is brought into thermal contact, then if $A = B$ and $B = C$, then $A = C$. At thermal equilibrium, these systems have the same value, which is the empirical temperature, and is given by $\theta$.

#### Work

In thermodynamics, work performed by a system is the energy transferred by the system to its surroundings. Kinetic energy, potential energy and internal energy are forms of energy that are properties of a system. Work is a form of energy, but it is energy in transit. A system contains no work, work is a process done by or on a system. In general, work is defined for mechanical systems as the action of a force on an object through a distance.

#### Internal Energy

The system's internal energy is called the total energy that a system contains. This energy can be modified by exerting work on it or by the transfer of energy. The system's energy can change by transferring heat or work (or both) between the system and its surroundings. If positive work is applied, the system gains energy. The first law of thermodynamics postulates that the increase in internal energy is equal to the total heat added plus the work done by the environment. If it is an isolated system, it remains constant. Internal energy is a *state function*. Its value depends only on the current state of the system. It is also an extensive property. The unit of measurement, according to the International System, is the joule (J).

### 3.1.2 Laws of Thermodynamics

The laws governing the thermodynamics are the fundamental principals that outline the most basic identity of thermal flow: the concept of equilibrium stated in *Zeroth Law*, the conservation of energy from *First Law*, the *Second Law* illuminates the concept of increasing entropy and irreversibility of thermal processes, stating the direction in which the processes take place while the *Third Law* describes the behaviour of thermal systems near absolute zero (minimum entropy).

#### Zeroth Law: Thermal Equilibrium

The Zeroth law of thermodynamics simply highlights the tendency of the thermal bodies to stay in equilibrium. If two bodies $A$ and $B$ (which are at different temperatures $T_A$ and $T_B$) are in thermal equilibrium with a third body $C$, then the bodies $A$ and $B$ are said to be in thermal equilibrium with each other, $T_A = T_B$. It can be stated as:

> If two systems are in equilibrium with a third system, then they are in thermal equilibrium with each other.

#### First Law: Law of Conservation of Energy

The zeroth law provided a basic idea that bodies, or a system that reaches thermal equilibrium with its surroundings, continues to stay in that state unless acted upon by an external force or loadings. This is in agreement with Newton's first law of motion.

> In a closed or isolated system, the change in internal energy $U$ of the system is the difference between the heat provided to the system $Q$ and the thermodynamic work done by the system $W$.

$$\Delta U = Q + W \tag{3.2}$$

#### Second Law: law of irreversibility

The second law of thermodynamics introduces the concept of *entropy* as physical property of the thermal system that quantifies *disorder, energy dispersion and irreversibility* of the system. For an isolated system in thermal equilibrium, the entropy ($S$) reaches it maximum value. Entropy is a measure of how energy is dispersed in a system and determines the direction and irreversibility of physical processes.

> The state of entropy of the entire universe, as an isolated system (no energy or matter transfer with its surrounding), will always increase in any natural and spontaneous process.

For a reversible process, the entropy change $dS$ is given as:

$$dS = \frac{\delta Q_{rev}}{T} \tag{3.3}$$

where $\delta Q_{rev}$ is the infinitesimal portion of heat transfer between the system and its surroundings when the system is at temperature $T$. Thus, for any cyclic reversible process,

$$\oint \frac{\delta Q_{rev}}{T} \leq 0 \tag{3.4}$$

Because of the tendency of all thermodynamics system to reach thermal equilibrium, at which point the entropy is maximum, any process that evolves on a time scale insufficient to maintain thermal equilibrium is intrinsically irreversible. This irreversibility manifests as positive entropy production and entails a loss in the maximum work that can be extracted from the process.

#### Third Law: Law of Absolute Zero

The third law of thermodynamics defines the *minimum* value of the entropy of the system. Since entropy is dependent on the state of the system at a current time, then there exists one state, known as *ground state* where the energy of the system (or the entropy) is at its minimum value.

> As the temperature of a system approaches absolute zero, all processes cease and the entropy of the system approaches a minimum value.

### 3.1.3 Thermodynamics and Heat Transfer

Heat transfer in a continuous media can take place through *heat conduction, convection* or *through radiation.* Convection is the process of heat transfer between a solid and a fluid medium, while radiation occurs from solid to gaseous medium or between two solids that are not in contact. Convection and Radiation are the main modes of heat transfer in fluids, and thus are excluded from the present discussion.

For a thin interphase, the heat transfer takes place through the mechanism of heat conduction, which is defined in the following section. Since the convection and radiation are out of the scope of the present work, their detailed explanation has been omitted from this discussion.

### 3.1.4 Thermal Conduction

Thermal conduction is the mechanism of heat transfer through adjacent molecule having higher kinetic energy than its neighbour. Conduction takes place in fluids (liquids and gases) via the heat transfer by the *collision* and *diffusion* of highly energetic molecules in random motion. It is most commonly and easily observed in solids, where the heat transfer takes place due to *vibration of the molecules in a lattice and the energy transported by the free electrons* Cengel, 2017.

The rate of heat conduction through any solid medium depends on the *geometry* of the medium, and the temperature difference ($\Delta T$) that drives the heat conduction process, as per second law of thermodynamics, from a region of higher temperature to the region of cold temperature. In the most basic example of one-dimensional heat transfer through a plane wall, the rate of heat conduction is given as

$$\text{Rate of heat conduction} \propto \frac{(\text{Area} \times \text{Temperature Difference})}{\text{Thickness}}$$

or

$$\dot{Q}_{cond} = -kA\frac{\Delta T}{L}$$

where $k$ is the *Thermal conductivity of the medium.*

### Thermal Conductivity, $k$

The thermal conductivity of the material is the physical property that "measures the ability of a material to conduct heat" (Cengel, 2017), measured in $W/(m.K)$ Materials with higher thermal conductivity are known as *good conductors* of heat (eg, metals like copper, gold, platinum, etc), as they allow heat to pass through because of the presence of free-moving electrons in their lattice structure. The most commonly used in heat sinks in electronics, where rapid heat transfer is required to efficiently cool the system. Conversely, materials that have low conductivity are known as *insulators* (eg, rubber, styrofoam, etc), and as the name suggests, they are commonly employed in areas that require thermal insulation, to effectively trap the heat. The thermal conductivities of some common materials at atmospheric pressure and room temperature is provided in the Table 3.1 as taken from Cengel, 2017.

| Rigid Foam | Air | Rubber | Wood | Iron | Aluminum | Gold | Copper | Silver | Diamond |
|---|---|---|---|---|---|---|---|---|---|
| 0.026 | 0.026 | 0.13 | 0.17 | 80.2 | 237 | 317 | 401 | 429 | 2300 |

**Table 3.1.** Thermal conductivities in $W/m.K$ of some common materials in increasing order of conductivity.

In interphases, the thermal conductivity of the material plays a key role. As the interphase lies between the two materials, the mismatch of the thermal conductivity at the boundaries of the interphase determine whether the temperature (in case of lower thermal conductivity) or the heat flux (in case of higher thermal conductivity) is accumulated at the boundaries.

### Heat Flux, $q$

The heat flux $\boldsymbol{q}$, $(W/m^2)$ is the rate of heat transfer through a surface area or boundary of a system which is perpendicular to the heat flow. It can also be defined as the rate of energy flow per unit area per unit time. Since it defines the *direction* of the flow of heat (from higher to lower temperatures) as well as the *magnitude* of heat, it is a vector quantity. At any point in space, the heat flux passing through the point is defined by taking the area of the surface to be infinitesimally small $\Delta x \to 0$. The **Law of Heat Conduction** or **Fourier's Law** states that

> the rate of heat transfer through a material is proportional to the negative gradient of the temperature and to the area, at right angles to that gradient, through which the heat flows.

The gradient of a temperature field $T = T(\alpha_1, \alpha_2, \alpha_3)$, given as $\nabla T$ is the vector quantity (following the discussion in 2.2.1) that describes the magnitude as well as the direction in which heat flows rapidly at a point in space. The negative gradient signifies the heat transfer from a region at higher temperature to the region at lower temperatures. In terms of Cartesian coordinates, the temperature gradient is given as

$$\nabla T = \left(\frac{\partial T}{\partial x}, \frac{\partial T}{\partial y}, \frac{\partial T}{\partial z}\right) \tag{3.5}$$

In terms of orthogonal curvilinear coordinates, the gradient is defined in (2.63)

$$\nabla T = \frac{1}{h_1}\frac{\partial T}{\partial \alpha_1} + \frac{1}{h_2}\frac{\partial T}{\partial \alpha_2} + \frac{1}{h_3}\frac{\partial T}{\partial \alpha_3} \tag{3.6}$$

where $\{\alpha_1, \alpha_2, \alpha_3\}$ are the curvilinear coordinates, and $h_r$ is the scale factor of each coordinate curve.

A higher temperature gradient indicates accumulation of temperature at a point, along a particular axes, which is usually seen in the case of low conductive interphases (Hashin, 2001, Benveniste and Miloh, 2001, etc).

The **Fourier's law** for a homogeneous, isotropic material can now be defined as

$$\boldsymbol{q} = -k\nabla T \quad \text{or} \quad \int_S \boldsymbol{q} \cdot d\boldsymbol{S} = -k \int_S \nabla T \cdot d\boldsymbol{S} \tag{3.7}$$

If the material is non-homogeneous or anisotropic, the thermal conductivity $k$ becomes symmetric, second-rank tensor known as **thermal conductivity tensor**, $\boldsymbol{\kappa}$.

### 3.1.5 Balance Law: Heat Equation

The heat equation is a parabolic partial differential equation that describes the evolution of temperature in space and time due to heat conduction.

From the First law of thermodynamics, we know that energy is conserved within a volume (law of energy conservation - 3.1.2). Thus, for any control volume element $V$, the energy that the rate of change of internal energy $U$ in a volume $V$ is equal to the rate of heat generation (heat source/sinks) and flux $\boldsymbol{q}$ across the boundary $dS$ of the volume with outward unit normal $\hat{\boldsymbol{n}}$ (Cengel, 2017.)

$$\frac{\partial e}{\partial t} = E_{cond} + E_{gen} \tag{3.8}$$

In the integral form, it is expressed as:

$$\int_V \frac{\partial(\rho e)}{\partial t}\, dV = \int_V E_{cond}\, dV + \int_V E_{gen}\, dV \tag{3.9}$$

The change in internal energy of the system is

$$\int_V \frac{\partial e}{\partial t} dV = \int_V \frac{\partial(\rho\, c_E\, T)}{\partial t} dV = \int_V \rho\, c_E\, \frac{\partial T}{\partial t} dV \tag{3.10}$$

The change in internal energy of the system is

$$\int_V \frac{\partial E_{cond}}{\partial t} dV = \int_S \boldsymbol{q} \cdot \hat{\boldsymbol{n}} dS \tag{3.11}$$

Applying divergence theorem, we get

$$-\int_S \boldsymbol{q} \cdot \hat{\boldsymbol{n}} dS = -\int_V \nabla \cdot \boldsymbol{q} dV \tag{3.12}$$

And finally, the volumetric heat source term is

$$\int_V E_{gen} dV = \int_V Q dV \tag{3.13}$$

Substituting all these values in the balance equation

$$\int_V \rho c \frac{\partial T}{\partial t} dV = -\int_V \nabla \cdot \boldsymbol{q} dV + \int_V Q dV \tag{3.14}$$

or, rearranging the terms, we get

$$\int_V \left( \rho \, c_E \, \frac{\partial T}{\partial t} + \nabla \cdot \boldsymbol{q} - Q \right) dV = 0 \tag{3.15}$$

which is the integral form of the thermal balance equation. From the Fourier's law of heat conduction (3.7),

$$\int_V \left( \rho c \frac{\partial T}{\partial t} - k \nabla^2 T - Q \right) dV = 0 \tag{3.16}$$

$$\rho \, c_E \, \frac{\partial T}{\partial t} - k \nabla^2 T - Q = 0 \tag{3.17}$$

$$\implies \rho \, c_E \, \frac{\partial T}{\partial t} = k \nabla^2 T + Q \tag{3.18}$$

where $\nabla^2 T$ is the Laplacian operator (defined in 2.4 for orthogonal curvilinear coordinates). Eqn (3.18) is the classical form of heat equation for any homogeneous, isotropic material.

For *steady-state* heat transfer, then the time derivative terms $\partial T/\partial t$ becomes zero, which implies that the heat transfer takes place only along the spatial coordinates, and is independent of time ($T = T(x, y, z)$), whereas in *transient* conduction, temperature field is a function of space *and* time, and thus, the heat equation describes that the conduction occurs at a point in space at a particular instance in time.

Eqns.(3.7) and (3.18) form the governing equations for heat transfer through conduction mechanism across any arbitrary, homogeneous, isotropic material.

## 3.2 Part II: Continuum Mechanics

Continuum mechanics refers to the study of deformation of a materials, which can be a solid or a fluid, under the action of an applied force. It key principle lies in the fact that the material is considered to be a continuous media, rather than a collection of discrete points. Thus, the forces transmitted through this media are continuous at each point in the volume. It is the branch of physics that deals with the deformation of the solid or fluid element by mapping the reference and current configurations, and through the application of constitutive laws, kinematics and equilibrium equations. It treats the physical properties of the material as independent property, that is, invariant of the coordinate system. This provides efficiency in defining the properties at each point within the domain. The concept of a continuum lies in the mathematical framework that assumes the bulk material, ignoring the microscopic cracks or the defects, is continuous at each point within a volume $V$, and at any local point or infinitesimal volume $dV$ within this volume, the same constitutive laws can be applied as that to the bulk materials. This is basis of theories of solid and fluid mechanics. In the oncoming sections, we will cover the basics of the solid mechanics, starting with the description of the motion of the particle.

### 3.2.1 Eulerian and Lagrangian Description

A central feature of continuum mechanics is the use of Eulerian (spatial) and Lagrangian (material) descriptions to characterize motion. These descriptions differ in whether physical fields are tracked with material particles or observed at fixed spatial locations, and they form the basis for kinematic, kinetic, and constitutive formulations.

In Lagrangian description, an individual particle is tracked over a period of time, thus providing a history of motion in space and time. This means that you fix a particle and move along with it through each reference frame. In contrast, the Eulerian approach fixes a point (or a control volume) in space rather than a particle and captures the behaviour of particles as they pass through that point or control volume. To better understand the concept, think of two cyclists in a race. If we fix our observation on one cyclist and track its motion, that is, displacement, velocity, etc throughout the duration of the race, then it is the Lagrangian approach. However, if we instead focus on the finishing line (which becomes a fixed reference frame) and observe the cyclist who reaches the finishing mark first, then it becomes a Eulerian approach. The Lagrangian description naturally lends itself to solid mechanics, where material identity, reference configurations, and deformation history play a central role, whereas the Eulerian description is more commonly adopted in fluid mechanics and problems involving large transport or flow. Nevertheless, both descriptions coexist within the general framework of continuum mechanics and are connected through appropriate mappings between reference and current configurations.

### 3.2.2 Kinematics: Introducing Deformation Gradient

Any change between the reference and current configuration of a continuum body results in displacement. It has two parts: a rigid body displacement and the deformation. A rigid body translates and/or rotates without undergoing any change in its original shape or volume, which means it only changes its position or orientation. A deformed body on the other hand, refers to a series of changes in shape and volume of a body at each instance of time.

Let $B_0$ be the initial state of the undeformed body. This state is also know as *reference state* or the *material state* of the undeformed body. Each point in this body can be collectively identified by a vector $\boldsymbol{X}$. When a motion $\boldsymbol{\chi}$ acts on this body, it deforms the body to its *current state* or the *spatial state* $B$, where each point in the deformed body is denoted by the vector $\boldsymbol{x}$. The orthonormal basis vector $\hat{\boldsymbol{e}}_i = \{\hat{\boldsymbol{e}}_1, \hat{\boldsymbol{e}}_2, \hat{\boldsymbol{e}}_3\}$ is fixed with respect to both configurations of the body. Thus, each points in the material and spatial state can be given as $X_i\hat{\boldsymbol{e}}_i$ and $x_i\hat{\boldsymbol{e}}_i$ respectively. The motion $\boldsymbol{\chi}$ is the vector function that transforms each point in the material state to its final position in the spatial state. Thus,

$$\boldsymbol{x} = \boldsymbol{\chi}(\boldsymbol{X}) \quad \text{or} \quad \boldsymbol{X} = \boldsymbol{\chi}^{-1}(\boldsymbol{x}) \tag{3.19}$$

In the equation above, $\boldsymbol{\chi}$ represents transformation of the points from the material state ($B_0$) to the spatial state ($B$), and $\boldsymbol{\chi}^{-1}$ represents transformation from the spatial state to the material state.

Now, consider a point $P_0$ in the body $B_0$, occupying a position $\boldsymbol{x}_0$, and another point $Q_0$ in its neighbourhood, at position $\boldsymbol{x}_0 + d\boldsymbol{x}_0$. The motion $\boldsymbol{\chi}$ applied on this line element $PQ$ in material state is transformed to $PQ$ in the spatial state, such that:

$$\boldsymbol{x}(P) = \boldsymbol{x}_0 = \boldsymbol{\chi}(\boldsymbol{X}) \quad \text{and} \quad \boldsymbol{x}(Q) = \boldsymbol{x}_0 + d\boldsymbol{x}_0 = \boldsymbol{\chi}(\boldsymbol{X} + d\boldsymbol{X}) \tag{3.20}$$

In the spatial state, we use Taylor series expansion about point $Q$ to expand $\boldsymbol{\chi}$ about $\boldsymbol{X}$:

$$\boldsymbol{\chi}(\boldsymbol{X} + d\boldsymbol{X}) = \boldsymbol{\chi}(\boldsymbol{X}) + \frac{\partial \boldsymbol{\chi}}{\partial \boldsymbol{X}} d\boldsymbol{X} + \mathcal{O}(d\boldsymbol{X}^2) \tag{3.21}$$

Since $d\boldsymbol{X}$ is infinitesimal, higher order can be neglected.

The infinitesimal change $d\boldsymbol{x}_0$ in the positions of the two points in the reference state is given as:

$$\begin{aligned} d\boldsymbol{x}_0 &= d\boldsymbol{x}_0 + \boldsymbol{x}_0 - \boldsymbol{x}_0 && (3.22)\\ &= \boldsymbol{x}(Q) - \boldsymbol{x}(P) && (3.23)\\ &= \boldsymbol{\chi}(\boldsymbol{X} + d\boldsymbol{X}) - \boldsymbol{\chi}(\boldsymbol{X}) && (3.24)\\ &= \frac{\partial \boldsymbol{\chi}}{\partial \boldsymbol{X}} d\boldsymbol{X} && (3.25)\\ &= \boldsymbol{F}\, d\boldsymbol{X} && (3.26) \end{aligned}$$

where $\boldsymbol{F} = F_{ij}$ is the deformation gradient, a two-point tensor that acts as a linear map containing information of local deformation (such as stretch, shear, rotation or volume change) of the transformation of a point from a reference tangent space to the spatial tangent space. In other words, the deformation gradient arises naturally as the first derivative of the motion mapping, providing the best linear approximation that maps infinitesimal material line elements from the reference configuration to the current configuration. Thus,

$$\boldsymbol{F} = \frac{\partial \boldsymbol{x}_0(\boldsymbol{X})}{\partial \boldsymbol{X}} \tag{3.27}$$

where $\boldsymbol{x}_0(\boldsymbol{X}) = \boldsymbol{\chi}(\boldsymbol{X})$.

Let us now return to the reference and spatial states of an arbitrary body. In solid mechanics, the difference between the reference state of the body ($\boldsymbol{x}_0$) and the current state of the deformed body ($\boldsymbol{X}$) is known as *displacement field* of a body.

$$\boldsymbol{u}(\boldsymbol{x}) = \boldsymbol{X}_0(\boldsymbol{x}) - \boldsymbol{x}_0 \quad \text{or} \quad \boldsymbol{X}_0(\boldsymbol{X}) = \boldsymbol{u}(\boldsymbol{X}) + \boldsymbol{X} \tag{3.28}$$

From the definition of the displacement gradient in (3.27), we get:

$$\begin{aligned} \boldsymbol{F} &= \frac{\partial \boldsymbol{x}_0(\boldsymbol{X})}{\partial \boldsymbol{X}} && (3.29)\\ &= \frac{\partial \boldsymbol{u}(\boldsymbol{X}) + \boldsymbol{X}}{\partial \boldsymbol{X}} && (3.30)\\ &= \frac{\partial \boldsymbol{u}(\boldsymbol{X})}{\partial \boldsymbol{X}} + \boldsymbol{I} && (3.31)\\ &= \nabla_{\boldsymbol{X}} \boldsymbol{u} + \boldsymbol{I} && (3.32) \end{aligned}$$

where $\boldsymbol{I}$ is the identity matrix and $\nabla_{\boldsymbol{X}} \boldsymbol{u}$ is the *material gradient of the displacement vector.*

### Polar Decomposition of the Deformation Gradient

The displacement gradient can be decomposed into products of its symmetric tensor and rotation tensor, given as

$$\boldsymbol{F} = \boldsymbol{V}\boldsymbol{R} = \boldsymbol{R}\boldsymbol{U} \tag{3.33}$$

The decomposition is particularly useful in the analysis of material deformation by separating the stretch and rotation effects. $R$ is the orthogonal tensor representing Rotation matrix - transformation matrix that is used for rotation in Euclidean matrix - and $R^{-1} = R^T$. The tensors $U$ and $V$ are the left and right stretch tensors. From the orthogonality of the rotation matrix

$$\boldsymbol{V} = \boldsymbol{R}\boldsymbol{U}\boldsymbol{R}^{-1} \tag{3.34}$$

This gives a very important result of the polar decomposition of the rotation matrix - the left and right stretch vectors have the same eigenvalues or the principal stretches, but different eigenvectors or principal directions.

### 3.2.3 Strain Measures

Strain measures are different ways to evaluate the difference between the displacements in a body from the rigid body deformations locally. A body under pure rotations does not induce strains in the body. Thus, the following strain measures are commonly employed in the field of continuum mechanics to quantify the local deformations that occur in the body.

- **Cauchy strain tensor:** Also known as *right Cauchy-Green deformation tensor* is given as:
$$\boldsymbol{C} = \boldsymbol{F}^T \boldsymbol{F} = \boldsymbol{U}^2 \tag{3.35}$$
- **Green strain tensor:** Also known as *left Cauchy-Green deformation tensor* is given as:
$$\boldsymbol{B} = \boldsymbol{F}\boldsymbol{F}^T = \boldsymbol{V}^2 \tag{3.36}$$
In physical terms, both represents the local stretch of a length of a body or a line segment.

Using these definitions of local stretching, the concept of strain can be put to use to measure the local deformations in the body. The most commonly used finite strain tensors is the *Lagrangian strain tensor* or the *Green-Lagrangian strain tensor*, given as:

$$\boldsymbol{E} = \frac{1}{2}\left(\boldsymbol{C} - \boldsymbol{I}\right) \tag{3.37}$$

In terms of displacement gradients, it is written as:

$$\boldsymbol{E} = \frac{1}{2}\left\{(\nabla_{\boldsymbol{X}}\boldsymbol{u})^T + \nabla_{\boldsymbol{X}}\boldsymbol{u}) + \nabla_{\boldsymbol{X}}\boldsymbol{u})^T \cdot \nabla_{\boldsymbol{X}}\boldsymbol{u})\right\} \tag{3.38}$$

### 3.2.4 Infinitesimal Strain Tensor

For an elastic body, or any material in the elastic zone, the displacement gradient $\nabla_{\boldsymbol{X}}\boldsymbol{u}$ is the local deformation occurring in the continuum body. These deformations are assumed to be infinitesimal, that is, less than unity, and for such small deformations, the Lagrangian (material) and Eulerian (spatial) approaches are indistinguishable. This is also the case in interphase theories, where the jumps in displacements are usually of the order of $10^{-3}$ units. Thus, if $\nabla_{\boldsymbol{X}}\boldsymbol{u} \ll 1$, them from (3.32), $\boldsymbol{F} = \boldsymbol{I}$ and $\nabla\boldsymbol{u}^T\nabla\boldsymbol{u}$ becomes negligible. Thus, the strain tensor is reduced to the linearized form of the Cauchy-Lagrangian strain tensor:

$$\boldsymbol{\varepsilon} = \frac{1}{2}\left(\nabla\boldsymbol{u} + \nabla\boldsymbol{u}^T\right) \tag{3.39}$$

This forms the basis of the classical linearized theory of elasticity.

### 3.2.5 Gradient of displacement

In general, the displacement gradient tensor $\nabla\boldsymbol{u}$ can be further decomposed into its symmetric and antisymmetric parts:

$$\nabla\boldsymbol{u} = \boldsymbol{\varepsilon} + \boldsymbol{\omega} \tag{3.40}$$

where

$$\varepsilon_{ij} = \frac{1}{2}\left(u_{i,j} + u_{j,i}\right) \tag{3.41}$$

is the symmetric strain tensor $\varepsilon_{ij} = \varepsilon_{ji}$, representing the stretching and shearing of the material and

$$\omega_{ij} = \frac{1}{2}\left(u_{i,j} - u_{j,i}\right) \tag{3.42}$$

is the skew-symmeteric rotation tensor $\omega_{ij} = -\omega_{ji}$ representing the rigid-body rotations of the body.

For infinitesimal strain theory, $\boldsymbol{\omega}$ is neglected, as the deformation is purely dependent on stretching and shearing, and rigid body rotations produce no strains.

### 3.2.6 Strains

Strain is the ratio of deformed length to the original length. In terms of orthogonal curvilinear coordinates, the strain is defined the ration of displacement (or stretch) of the body along each direction. The most simple and commonly used example to understand strain is the deformation of 1D bar or a thin string. If the bar is pulled (or compressed) along its length, then we observed a small amount of displacement or the stretch along its length. This produces the *normal strain or engineering strain* in the bar, occurring along its length, given by

$$\varepsilon = \frac{\nabla l}{l_0} \tag{3.43}$$

This is also known as *tensile or longitudinal strain.*

If the bottom of the bar is fixed, and the force is applied along its top surface, producing a change in its shape, then this produces a *shear strain* in the tangential direction. The deformation occurs due to lateral displacement along the force applied. It is basically the angular distortion of two initially orthogonal line elements, under the application of force. Also know an the *engineering shear strain*, it is defined as:

$$\gamma_{ij} = \frac{\partial u_i}{\partial x_j} + \frac{\partial u_j}{\partial x_i} \tag{3.44}$$

Thus, shear strain measures angular distortion between material lines and is given by the off-diagonal components of the symmetric part of the displacement gradient.

From these definitions, a simple relation between the displacement gradients and the resulting strains develops, which is an important governing equations in elasticity, known as **Strain-Displacement relation** given as:

$$\boldsymbol{\varepsilon} = \frac{1}{2}\left(\nabla \boldsymbol{u} + \nabla \boldsymbol{u}^T\right) \tag{3.45}$$

where $\varepsilon$ is a symmetric rank 2 tensor. In terms of curvilinear coordinates, using the definition of gradient of vectors defined in 2.2.2, the strain is defined as:

$$\boldsymbol{\varepsilon} = \frac{1}{2}\sum_{k,m}\left(\frac{1}{h_m}\frac{\partial}{\partial \alpha_m}(u_k\,\hat{e}_k)\otimes\hat{e}_m + \frac{1}{h_k}\frac{\partial}{\partial \alpha_k}(u_m\,\hat{e}_m)\otimes\hat{e}_k\right) \tag{3.46}$$

or

$$\varepsilon^{(i)}_{km} = \frac{1}{2}\left[\frac{1}{h_k}\frac{\partial u^{(i)}_m}{\partial \alpha_k} + \frac{1}{h_m}\frac{\partial u^{(i)}_k}{\partial \alpha_m} - \left(\frac{u^{(i)}_k}{h_m\,h_k}\frac{\partial h_k}{\partial \alpha_m} + \frac{u^{(i)}_m}{h_m\,h_k}\frac{\partial h_m}{\partial \alpha_k}\right)\right] \tag{3.47}$$

The equations for all six strains-displacement relations in curvilinear coordinates is given as:

1. Strain Displacement Equations:

$$\varepsilon_{11} = \frac{1}{h_1}\frac{\partial u_1}{\partial \alpha_1} + \frac{u_2}{h_1 h_2}\frac{\partial h_1}{\partial \alpha_2} + \frac{u_3}{h_1 h_3}\frac{\partial h_1}{\partial \alpha_3} \tag{3.48}$$

$$\varepsilon_{22} = \frac{1}{h_2}\frac{\partial u_2}{\partial \alpha_2} + \frac{u_1}{h_1 h_2}\frac{\partial h_2}{\partial \alpha_1} + \frac{u_3}{h_2 h_3}\frac{\partial h_2}{\partial \alpha_3} \tag{3.49}$$

$$\varepsilon_{33} = \frac{1}{h_3}\frac{\partial u_3}{\partial \alpha_3} + \frac{u_1}{h_1 h_3}\frac{\partial h_3}{\partial \alpha_1} + \frac{u_2}{h_2 h_3}\frac{\partial h_3}{\partial \alpha_2} \tag{3.50}$$

$$\varepsilon_{12} = \frac{1}{2}\left\{\frac{1}{h_2}\frac{\partial u_1}{\partial \alpha_2} + \frac{1}{h_1}\frac{\partial u_2}{\partial \alpha_1} - \frac{1}{h_1 h_2}\left(u_1\frac{\partial h_1}{\partial \alpha_2} + u_2\frac{\partial h_2}{\partial \alpha_1}\right)\right\} \tag{3.51}$$

$$\varepsilon_{13} = \frac{1}{2}\left\{\frac{1}{h_3}\frac{\partial u_1}{\partial \alpha_3} + \frac{1}{h_1}\frac{\partial u_3}{\partial \alpha_1} - \frac{1}{h_1 h_3}\left(u_1\frac{\partial h_1}{\partial \alpha_3} + u_3\frac{\partial h_3}{\partial \alpha_1}\right)\right\} \tag{3.52}$$

$$\varepsilon_{23} = \frac{1}{2}\left\{\frac{1}{h_2}\frac{\partial u_3}{\partial \alpha_2} + \frac{1}{h_3}\frac{\partial u_2}{\partial \alpha_3} - \frac{1}{h_2 h_3}\left(u_2\frac{\partial h_2}{\partial \alpha_3} + u_3\frac{\partial h_3}{\partial \alpha_2}\right)\right\} \tag{3.53}$$

For a composite material, the displacements are continuous at each point and across the interphase boundaries. However, the strain is generally considered to be inhomogeneous within the interphase. This is because at each point in the interphase undergoes stretching and shearing at a different rate than its neighbours.

### Strain Compatibility

For a linear infinitesimal deformation, the strain displacement relation (3.45) gives six equations from which strains can be evaluated if the displacement $\boldsymbol{u}(\alpha_1, \alpha_2, \alpha_3)$ is known. However, if the strain fields are known, then the integration of these strain fields must ensure the continuity of the displacement function at all points in the body. This is known as the Compatibility conditions. However, the integration of the six strain equations overdetermine the three unknown displacement fields. Thus, in order to ensure the continuity and single-value functions of displacement, obeying the rules of continuous media, compatibility equations also known as *Saint Venant compatibility equations* are required. The procedure involves eliminating the displacement functions from (3.45). The strain-displacement function (3.45) is differentiated twice to eliminate the displacement field, giving the following relation

$$\varepsilon_{ij,kl} = \frac{1}{2}\left(u_{i,jkl} + u_{j,ikl}\right) \tag{3.54}$$

giving the compatibility equation (Malvern, 1969)

$$\nabla \times \boldsymbol{\varepsilon} \times \nabla = 0 \tag{3.55}$$

or (Sadd, 2009)

$$\varepsilon_{ij,kl} + \varepsilon_{kl,ij} - \varepsilon_{ik,jl} - \varepsilon_{jl,ik} = 0 \tag{3.56}$$

This provides 81 individual equations, however, from the symmetric nature of the strain tensor $\varepsilon_{ij} = \varepsilon_{ji}$, (3.55) becomes

$$(\nabla \times \boldsymbol{\varepsilon}) \times \nabla = \nabla \times (\boldsymbol{\varepsilon} \times \nabla) \tag{3.57}$$

and the system of 81 equations reduces to only six equations. In Cartesian coordinates, the compatibility equations are given as

$$\frac{\partial \varepsilon_{xx}}{\partial y} 2 + \frac{\partial \varepsilon_{yy}}{\partial x} 2 = 2 \frac{\partial^2 \varepsilon_{xy}}{\partial x \, \partial y} \tag{3.58}$$

$$\frac{\partial \varepsilon_{yy}}{\partial z} 2 + \frac{\partial \varepsilon_{zz}}{\partial y} 2 = 2 \frac{\partial^2 \varepsilon_{yz}}{\partial y \, \partial z} \tag{3.59}$$

$$\frac{\partial \varepsilon_{xx}}{\partial z} 2 + \frac{\partial \varepsilon_{zz}}{\partial x} 2 = 2 \frac{\partial^2 \varepsilon_{xz}}{\partial x \, \partial z} \tag{3.60}$$

$$\frac{\partial^2 \varepsilon_{xx}}{\partial y \, \partial z} = \frac{\partial}{\partial x} \left( -\frac{\partial \varepsilon_{yz}}{\partial x} + \frac{\partial \varepsilon_{xz}}{\partial y} + \frac{\partial \varepsilon_{xy}}{\partial z} \right) \tag{3.61}$$

$$\frac{\partial^2 \varepsilon_{yy}}{\partial x \, \partial z} = \frac{\partial}{\partial y} \left( -\frac{\partial \varepsilon_{xz}}{\partial y} + \frac{\partial \varepsilon_{xy}}{\partial z} + \frac{\partial \varepsilon_{yz}}{\partial x} \right) \tag{3.62}$$

$$\frac{\partial^2 \varepsilon_{zz}}{\partial x \, \partial y} = \frac{\partial}{\partial z} \left( -\frac{\partial \varepsilon_{xy}}{\partial z} + \frac{\partial \varepsilon_{yz}}{\partial x} + \frac{\partial \varepsilon_{xz}}{\partial y} \right) \tag{3.63}$$

Thus, the eqn.(3.55) is the necessary condition and (3.56) is the sufficient condition for continuous, single-valued displacement field in simply connected domains.

### 3.2.7 Stress

Up to this point in our discussion, we have investigated only the kinematics of the deformation of the body. Stresses are a result of forces acting on a body. Forces can be classified into two categories - body forces that act on the entire volume of the body, for example, gravitational forces. In most of the cases, the body forces are either taken to be negligible or assumed to be distributed uniformly within the body. The second type are the surface forces that are subjected to a particular area of a body, for example, traction.

When an elastic material undergoes deformation, the body produces internal forces to counteract those deformations and restore its original configuration.

Stresses can be further divided into normal and shear stresses that act on a surface in all directions. In case of surface forces, following Newton's third law, a force that is equal and opposite to the surface forces acts on the neighbouring surface. This creates a shearing stress between the two layers of the material, like a frictional force.

### 3.2.8 Hooke's Law

Hooke's law states that force $\boldsymbol{F}$ applied to stretch or compress a spring is proportional to the distance $\boldsymbol{x}$ by which is deforms (stretches or compresses).

$$\boldsymbol{F} = -k\boldsymbol{x} \tag{3.64}$$

The law is generalized in the theory of linear elasticity to establish the constitutive relation between the strains and stresses. It states that the strain (deformation) induced in the elastic body is proportional to the stress (forces) applied to it. The stress $\boldsymbol{\sigma}$ and the strains $\boldsymbol{\varepsilon}$ are second-order tensors, containing information regarding the stress and strain at a point in each direction. Thus, the proportionality factor between these two quantities is a fourth order tensor that acts as a linear map between the two tensors, known as *stiffness tensor* or more commonly as the *elasticity tensor.*

$$\boldsymbol{\sigma} = \mathbb{C}\boldsymbol{\varepsilon} \quad \text{or} \quad \sigma_{ij} = C_{ijkl}\varepsilon_{kl} \tag{3.65}$$

where $\sigma_{ij}$ is the Cauchy stress tensor defined above, and $\varepsilon_{kl}$ is the infinitesimal strain tensor, also defined previously.

In general, $\mathbb{C}$ has a total of 81 independent components, but due to its symmetric nature (following from the symmetry of strain and stress tensors):

$$C_{ijkl} = C_{jikl} = C_{klij} = C_{lkij}$$

This reduces the number of independent components to 21. For an isotropic elastic material, where the materials properties remain same in all directions, the independent components reduce to 2, which can be a pair of any two *elastic moduli.* The most commonly encountered form of Hooke's law for a homogeneous, linearly isotropic elastic material is given as:

$$\boldsymbol{\sigma} = 2\,\mu\,\boldsymbol{\varepsilon} + \lambda\ \mathrm{tr}\,\boldsymbol{\varepsilon}\,\boldsymbol{I} \tag{3.66}$$

where $\boldsymbol{\sigma}$ is the second-order stress tensor, $\lambda, \mu$ are the Lame's parameters, and $\boldsymbol{\varepsilon}$ is the second order strain tensor. Here, $\boldsymbol{I}$ is the $2\times2$ identity materix, and tr is the trace function, representing the sum of the diagonal elements of the strain tensor. Comparing (3.65) and (3.66), the fourth order elasticity tensor for a linear, isotropic material is given as Malvern, 1969:

$$\mathbb{C} = C_{ijkl} = \lambda\delta_{ij}\delta_{kl} + \mu\,(\delta_{ik}\delta_{jl} + \delta_{il}\delta_{jk}) \tag{3.67}$$

where $\delta_{mn}$ denote the Kronecker delta. Inversely, the Hooke's law can be inverted to obtain strain from the stress terms:

$$\boldsymbol{\varepsilon} = \frac{1+\nu}{E}\boldsymbol{\sigma} - \frac{\nu}{E}\,\mathrm{tr}\,\boldsymbol{\sigma}\boldsymbol{I} \tag{3.68}$$

where $E$ is the Young's modulus and $\nu$ is the Poisson's ratio. These two elastic moduli, along with others are defined in the next section.

### Elastic moduli

An elastic modulus is a quantity that provides a measure of the body's resistance to elastic deformation under the application of stress. It is a dimensionless quantity defined as the slope of the stress-strain curve of a material in its elastic deformation zone. Stiffer the material, higher the elastic modulus. All elastic moduli are the measure or a ratio of stress to strain.

- Young's Modulus, $E$: also known as *elastic modulus,* it is the measure of an body to deform (stretch or compress) when a tensile load is applied along its length. It has the units of stress, $N/m^2$ or $Pa$.
- Shear Modulus $(G, \mu)$: also known as *modulus of rigidity,* this is the measure of shear stiffness or the deformation along the surface perpendicular to the applied force. It is simply the ratio of shear stress to shear strain in elastic material. It is also refered to as *Lame's second parameter* and must be positive for all materials. It has the units of stress, $N/m^2$ or $Pa$.
- Bulk Modulus, $K$: as the name suggests, it is the measure of the deformation of the bulk of the body, that is, the volume of the body in all directions under uniform loading. It has the units of stress, $N/m^2$ or $Pa$.
- Poisson's ratio $\nu$: it is simply the measure of Poisson effect, which is the tendency of the elastic material to expand (or contract) in the transverse direction of the applied force. It is the ratio of transverse strain to the axial strain, and is a dimensionless quantity. Most common materials have Poisson ratio in the range of 0.0 t 0.5, with rubber having Poisson ratio of 0.5 and is called incompressible.

- Lame's First Parameter, $\lambda$: Together with the shear modulus $\mu$, it forms a pair of parameters that are most commonly seen in Hooke's law for the linear isotropic material. They can be used or derived from the other elastic moduli as shown in the table below.

Elastic moduli define the material properties and play a key role in composite materials and interface theory. The mismatch of the these properties at the interface boundary leads to jumps in displacements or stresses. The relations between the different elastic moduli is presented in the table 3.2, taken from Sadd, 2009.

| | $E$ | $\nu$ | $K$ | $\mu$ | $\lambda$ |
|---|---|---|---|---|---|
| $E, \nu$ | $E$ | $\nu$ | $\frac{E}{3(1-2\nu)}$ | $\frac{E}{2(1+\nu)}$ | $\frac{E\nu}{(1+\nu)(1-2\nu)}$ |
| $E, K$ | $E$ | $\frac{3K-E}{6K}$ | $K$ | $\frac{3KE}{9K-E}$ | $\frac{3K(3K-E)}{9K-E}$ |
| $E, \mu$ | $E$ | $\frac{E-2\mu}{2\mu}$ | $\frac{E\mu}{3(3\mu-E)}$ | $\mu$ | $\frac{\mu(E-2\mu)}{(3\mu-E)}$ |
| $E, \lambda$ | $E$ | $\frac{2\lambda}{E+\lambda+R}$ | $\frac{E+3\lambda+R}{6}$ | $\frac{E-3\lambda+R}{4}$ | $\lambda$ |
| $\nu, K$ | $3K(1-2\nu)$ | $\nu$ | $K$ | $\frac{3K(1-2\nu)}{2(1+\nu)}$ | $\frac{3K\nu}{1+\nu}$ |
| $\nu, \mu$ | $2\mu(1+\nu)$ | $\nu$ | $\frac{2\mu(1+\nu)}{3(1-2\nu)}$ | $\mu$ | $\frac{2\mu\nu}{1-2\nu}$ |
| $\nu, \lambda$ | $\frac{\lambda(1+\nu)(1-2\nu)}{\nu}$ | $\nu$ | $\frac{\lambda(1+\nu)}{3\nu}$ | $\frac{\lambda(a-2\nu)}{2\nu}$ | $\lambda$ |
| $K, \mu$ | $\frac{9K\mu}{6K+\mu}$ | $\frac{3K-2\mu}{6K+2\mu}$ | $K$ | $\mu$ | $K-\frac{2}{3}\mu$ |
| $K, \lambda$ | $\frac{9K(K-\lambda)}{3K-\lambda}$ | $\frac{\lambda}{3K-\lambda}$ | $K$ | $\frac{3}{2}(K-\lambda)$ | $\lambda$ |
| $\mu, \lambda$ | $\frac{\mu(3\lambda+2\mu)}{\lambda+\mu}$ | $\frac{\lambda}{2(\lambda+\mu)}$ | $\frac{3\lambda+2\mu}{3}$ | $\mu$ | $\lambda$ |

**Table 3.2.** Relations between different elastic moduli. $R = \sqrt{E^2 + 9\lambda^2 + 2E\lambda}$

### 3.2.9 Balance Equations

All forces, whether internal or acting on a surface, must be balanced within a volume, which is the basic fundamental ideology of the conservation of momentum.

Consider a volume $V$ with boundary $S$ and outward unit normal $\hat{\boldsymbol{n}}$. Let $\rho$ be the mass density ($kg/m^3$), $\boldsymbol{v}$ is the velocity ($m/s$), $\boldsymbol{F}$ is body force per unit mass (e.g., gravity) and $\boldsymbol{t}(\boldsymbol{n})$ be traction on the surface.

From Newton's law of conservation of linear momentum, stated as "the change of motion of an object is proportional to the force impressed; and is made in the direction of the straight line in which the force is impressed."

$$\frac{d}{dt}\int_V \rho \boldsymbol{v} dV = \int_V \rho \boldsymbol{F} dV + \int_S \boldsymbol{t}(\hat{\boldsymbol{n}}) dA \tag{3.69}$$

The LHS of the equation can be expressed in terms of displacement vector $\boldsymbol{u}$ as

$$\frac{d}{dt}\rho \boldsymbol{v} = \rho \frac{d^2 \boldsymbol{u}}{dt^2} = \rho \ddot{\boldsymbol{u}} \tag{3.70}$$

From Cauchy's stress vector, the traction vector is related to stress tensor $\boldsymbol{\sigma}$ as:

$$\boldsymbol{t}(\hat{\boldsymbol{n}}) = \boldsymbol{\sigma}\hat{\boldsymbol{n}} \tag{3.71}$$

Next, we apply the divergence theorem to the Cauchy stress vector

$$\int_S \boldsymbol{\sigma}\hat{\boldsymbol{n}} dA = \int_V \nabla \cdot \boldsymbol{\sigma} dV \tag{3.72}$$

Substituting all these values in the balance of momentum equation gives the integral form of the balance equation:

$$\int_V \rho\ddot{\boldsymbol{u}} dV = \int_V \left(\rho \boldsymbol{F} dV + \nabla \cdot \boldsymbol{\sigma}\right) dV \tag{3.73}$$

Rearranging the equation we get

$$\int_V \rho\ddot{\boldsymbol{u}} dV = \int_V \left(\rho \boldsymbol{F} + \nabla \cdot \boldsymbol{\sigma}\right) dV \tag{3.74}$$

$$\implies \rho\ddot{\boldsymbol{u}} = \rho \boldsymbol{F} + \nabla \cdot \boldsymbol{\sigma} \tag{3.75}$$

where $\nabla \cdot \boldsymbol{\sigma}$ is the div $\boldsymbol{\sigma}$

Eqn.(3.75) is the **elasticity balance equation.**

For static equilibrium, conservation of linear momentum implies that the forces acting on this region are balanced and thus the resultant force must vanish (Sadd, 2009).

$$\text{div}\, \boldsymbol{\sigma} + \rho \boldsymbol{F} = 0 \tag{3.76}$$

This is the **equilibrium equation of elasticity** for a continuous medium.

In terms of curvilinear coordinates, the balance equations can be written in their complete form as

$$\frac{1}{h_1 h_2 h_3}\left[\frac{\partial h_1 h_2 \sigma_{11}}{\partial \alpha_1} + \frac{\partial h_1 h_3 \sigma_{21}}{\partial \alpha_2} + \frac{\partial h_2 h_3 \sigma_{31}}{\partial \alpha_3}\right] + \frac{\sigma_{12}}{h_1 h_2}\frac{\partial h_1}{\partial \alpha_2} + \frac{\sigma_{13}}{h_1 h_3}\frac{\partial h_1}{\partial \alpha_3} - \frac{\sigma_{22}}{h_1 h_2}\frac{\partial h_2}{\partial \alpha_1} - \frac{\sigma_{33}}{h_1 h_3}\frac{\partial h_3}{\partial \alpha_1} + \rho F_1 = 0 \tag{3.77}$$

$$\frac{1}{h_1 h_2 h_3}\left[\frac{\partial h_1 h_3 \sigma_{22}}{\partial \alpha_2} + \frac{\partial h_2 h_3 \sigma_{12}}{\partial \alpha_1} + \frac{\partial h_2 h_1 \sigma_{32}}{\partial \alpha_3}\right] + \frac{\sigma_{21}}{h_1 h_2}\frac{\partial h_2}{\partial \alpha_1} + \frac{\sigma_{23}}{h_2 h_3}\frac{\partial h_2}{\partial \alpha_3} - \frac{\sigma_{11}}{h_1 h_2}\frac{\partial h_1}{\partial \alpha_2} - \frac{\sigma_{33}}{h_1 h_3}\frac{\partial h_3}{\partial \alpha_2} + \rho F_2 = 0 \tag{3.78}$$

$$\frac{1}{h_1 h_2 h_3}\left[\frac{\partial h_1 h_2 \sigma_{33}}{\partial \alpha_3} + \frac{\partial h_2 h_3 \sigma_{13}}{\partial \alpha_1} + \frac{\partial h_3 h_1 \sigma_{23}}{\partial \alpha_2}\right] + \frac{\sigma_{31}}{h_1 h_3}\frac{\partial h_3}{\partial \alpha_1} + \frac{\sigma_{32}}{h_2 h_3}\frac{\partial h_3}{\partial \alpha_2} - \frac{\sigma_{11}}{h_1 h_3}\frac{\partial h_1}{\partial \alpha_3} - \frac{\sigma_{22}}{h_2 h_3}\frac{\partial h_2}{\partial \alpha_3} + \rho F_3 = 0 \tag{3.79}$$

**Balance of Angular Momentum**

In the eqn above, no information is provided on the symmetric nature of the stress tensor. The balance of angular momentum acting on an elastic body is derived to establish that the Cauchy stress tensor must be symmetric.

The angular momentum of a body about its origin is given as

$$\int_V \boldsymbol{x} \times (\rho \boldsymbol{v}) dV \tag{3.80}$$

The rate of change of angular momentum equals the total moment of external forces:

$$\frac{d}{dt} \int_V \boldsymbol{x} \times (\rho \boldsymbol{v}) dV = \int_V \boldsymbol{x} \times (\rho \boldsymbol{F}) dV + \int_S \boldsymbol{x} \times \boldsymbol{t}(\hat{\boldsymbol{n}}) dA \tag{3.81}$$

Applying the divergence theorem to the surface integral,

$$\int_S \boldsymbol{x} \times \boldsymbol{t}(\hat{\boldsymbol{n}}) dA = \int_S \boldsymbol{x} \times (\boldsymbol{\sigma} \hat{\boldsymbol{n}}) dA = \int_S (\boldsymbol{x} \times \boldsymbol{\sigma}) \hat{\boldsymbol{n}} dA = \int_V \nabla \cdot (\boldsymbol{x} \times \boldsymbol{\sigma}) dV \tag{3.82}$$

Employing the tensor identity:

$$\nabla \cdot (\boldsymbol{x} \times \boldsymbol{\sigma}) = \boldsymbol{x} \times (\nabla . \boldsymbol{\sigma}) + \boldsymbol{\sigma}^T - \boldsymbol{\sigma} \tag{3.83}$$

and substituting into the angular momentum equation gives:

$$\int_V \left[ \boldsymbol{x} \times (\rho \dot{\boldsymbol{v}} - \rho \boldsymbol{F} - \nabla \cdot \boldsymbol{\sigma}) \right] dV = \int_V \left[ \boldsymbol{x} \times (\rho \dot{\boldsymbol{v}} - \rho \boldsymbol{F} - \nabla \cdot \boldsymbol{\sigma}) + (\boldsymbol{\sigma}^T - \boldsymbol{\sigma}) \right] dV = 0 \tag{3.84}$$

From the linear momentum equation (3.76) we know that the first term goes to zero, thus,

$$\int_V (\boldsymbol{\sigma}^T - \boldsymbol{\sigma}) dV = 0 \tag{3.85}$$

From the localization principle, the equation must hold at each point in the arbitrary volume $V$, therefore

$$\boldsymbol{\sigma}^T = \boldsymbol{\sigma} \quad \text{implying that} \quad \sigma_{ij} = \sigma_{ji} \tag{3.86}$$

This is the balance of angular momentum in local form. It highlights that the internal forces cannot generate a net torque.

**Therefore, together with the six strain-displacement functions given in (3.45), and the six compatibility equations given in (3.58) and the three equilibrium equations (3.76) form a system of 15 equations to solve for 12 unknown functions (six independent stresses and six independent strains) in a boundary-value problem involving classical linear elasticity.**

## 3.3 Part III : Thermoelasticity

Thermoelasticity is a fundamental theory within continuum mechanics that addresses the coupling between thermal and mechanical responses in elastic solids. It provides a rigorous framework for describing how temperature variations generate elastic strains and stresses through thermal expansion, and how mechanical deformation may interact with the thermal field. Assuming reversible material behavior and the absence of dissipation due to plasticity or damage, thermoelasticity enables a consistent formulation based on the principles of energy conservation and thermodynamics. This theory is essential for the

analysis of thermal stresses and deformation in structures exposed to non-uniform or time-dependent temperature fields and forms the basis for more advanced thermo-mechanical models.

The starting point for the development of theory of thermoelasticity is the basic laws of thermodynamics that are now combined with the elastic balance equations to arrive at a slightly different form that is known as the balance equation for thermoelastic materials.

### 3.3.1 First law of Thermomechanical: Conservation of Energy

The first law of thermodynamics stated in 3.1.2 and the Newton's law of conservation of momentum, both states that energy, whether it is thermal or mechanical must be conserved at each point in the volume $V$. The next part derives this theorem, amalgamating the thermal (3.18) and the mechanical balance laws (3.75) to arrive at the thermo-mechanical equilibrium equation.

Consider a Euclidean body $B$, wherein a portion of the body is exposed to heat flux $q$, taken positive outward from the surface of the body $\partial B_q$. Similarly, we assume surface traction forces $\boldsymbol{t}_n$, positive outwards, acting on the surface $\partial B_t$, internal heat source $Q$, body forces $\boldsymbol{b}$. The Energy balance equation is given as:

$$\frac{\partial t}{\partial n}\int_{\partial B_t}\boldsymbol{t}_n\cdot\boldsymbol{v}\,dA+\int_B\boldsymbol{b}\cdot\boldsymbol{v}\,dV-\int_{\partial B_t}\boldsymbol{q}_n\,dA+\int_B Q\,dV=\frac{\partial}{\partial t}\left(\frac{1}{2}\int_B\rho\boldsymbol{v}\cdot\boldsymbol{v}\,dV+\int_B\rho e\,dV\right) \tag{3.87}$$

This is the first law of thermodynamics in integral form, where the first and the second term on the LHS combined represent work done by the external forces on the body, while the third term is the heat flux across $\partial B_q$, and the fourth term is the total internal heat. The first term on the RHS is the total kinetic energy, $\mathcal{K}$, and the second term represents the total internal energy, $U$. The term $\rho$ is the internal energy density. We now proceed to apply the Gauss-divergence theorem, i.e, transforming all the surface integrals into volume integrals :

$$\int_{\partial B_t}\boldsymbol{t}_n\cdot\boldsymbol{v}=\int_{\partial B_t}(\boldsymbol{\sigma}\cdot\boldsymbol{n})\cdot\boldsymbol{v}\,dA=\int_{\partial B_t}\boldsymbol{\sigma}\boldsymbol{v}\cdot\boldsymbol{n}\,dA=\int_B\operatorname{div}(\boldsymbol{\sigma}\cdot\boldsymbol{v})\,dV \tag{3.88}$$

Using Leibniz formula:

$$\operatorname{div}(\boldsymbol{\sigma}\cdot\boldsymbol{v})\,dA=\nabla\boldsymbol{\sigma}\cdot\boldsymbol{v}+\boldsymbol{\sigma}\cdot\nabla\boldsymbol{v} \tag{3.89}$$

Substituting this value back in (3.88) transforms the surface integral into volume integral as:

$$\int_{\partial B_t}\boldsymbol{t}_n\cdot\boldsymbol{v}\,dA=\int_B\nabla\boldsymbol{\sigma}\cdot\boldsymbol{v}\,dV+\boldsymbol{\sigma}\cdot\nabla\boldsymbol{v}\,dV \tag{3.90}$$

Similarly, we can convert the third term of (3.87) surface integrals form into volume integral form as:

$$\int_{\partial B_t}\boldsymbol{q}_n\,dA=\int_{\partial B_t}(\boldsymbol{q}\cdot\boldsymbol{n})\,dA=\int_B\nabla\boldsymbol{q}\,dV \tag{3.91}$$

The time derivatives of (3.87) can be re-written as:

$$\frac{\partial}{\partial t}\left(\frac{1}{2}\int_B\rho\boldsymbol{v}\cdot\boldsymbol{v}\,dV+\int_B\rho e\,dV\right)=\frac{1}{2}\int_B\rho\dot{\boldsymbol{v}}\cdot\boldsymbol{v}\,dV+\int_B\rho\dot{e}\,dV \tag{3.92}$$

Substituting all these values in (3.87), and rearranging all the terms, we get the following form of equation:

$$\implies \int_B (\operatorname{div} \boldsymbol{\sigma} + \boldsymbol{b} - \rho \dot{\boldsymbol{v}}) \cdot \boldsymbol{v} \, dV + \int_B (\boldsymbol{\sigma} \cdot \nabla \boldsymbol{v} - \operatorname{div} \boldsymbol{q} + Q - \rho \dot{e}) \, dV = 0 \tag{3.93}$$

In the above equation, the first term denotes the *equation of motion*, i.e, the linear momentum equation (3.75) and is null at each point in the body, while the second term of the equation represents *energy balance*. At equilibrium, for all points inside B, the sum of energies is zero, that means,

$$\boldsymbol{\sigma} \cdot \nabla \boldsymbol{v} - \operatorname{div} \boldsymbol{q} + Q - \rho \dot{e} = 0 \tag{3.94}$$

The $\boldsymbol{\sigma}$ is a symmetric tensor, defined in (3.86) From the equation of compatibility, we have seen that the velocity field (which is the time derivative of the displacement field) can be decomposed into a symmetric and a skew-symmetric part, as follows:

$$\nabla \boldsymbol{v} = \dot{\boldsymbol{\varepsilon}} + \dot{\boldsymbol{\omega}} \tag{3.95}$$

where

$$\dot{\boldsymbol{\epsilon}} = \frac{1}{2} \left( \nabla \dot{\boldsymbol{u}} + \nabla \dot{\boldsymbol{u}}^T \right) \tag{3.96}$$

and $\dot{\boldsymbol{\omega}}$ is the *Rate of rigid body motion*, which for a linear, isotropic thermoelastic material is considered to be zero. Substituting all the terms in (3.94)

$$\implies \quad \boldsymbol{\sigma} \cdot \dot{\boldsymbol{\varepsilon}} - \operatorname{div} \boldsymbol{q} + Q - \rho \dot{e} = 0 \tag{3.97}$$

This is the the **First Law of Thermodynamics** in the differential form with the thermal and mechanical terms. It emphasizes on the effect of rate of mechanical work done on the rate of change of internal energy due to heating.

### 3.3.2 Second Law of Thermodynamics

The second law of thermodynamics establishes the concept of **entropy**, as a physical attribute of the thermodynamic system. In the integral form, the law is given as:

$$\frac{\partial}{\partial t} \int_B \rho \eta \, dV \geq - \int_{\partial B} \frac{\boldsymbol{q} \cdot \hat{\boldsymbol{n}}}{T} \, dA + \int_B \frac{Q}{T} \, dV \tag{3.98}$$

where $\eta$ is the *specific entropy* (per unit mass) of the system, and $T = T(\boldsymbol{x}, T)$ is the *Absolute Temperature* of the system and $\hat{\boldsymbol{n}}$ is the outward unit normal. Applying the divergence theorem, as above:

$$\frac{\partial}{\partial t} \int_B \rho \eta \, dV = \rho \dot{\eta} \qquad ; \qquad \int_{\partial B} \frac{\boldsymbol{q} \cdot \boldsymbol{n}}{T} \, dA = \int_B \operatorname{div} \left( \frac{\boldsymbol{q}}{T} \right) \, dV \tag{3.99}$$

Substituting these values in (3.98) and applying the localization theorem we get the local entropy inequality:

$$\rho \dot{\eta} \geq - \operatorname{div} \left( \frac{\boldsymbol{q}}{T} \right) + \frac{Q}{T} \tag{3.100}$$

Rewriting $\operatorname{div} \left( \frac{\boldsymbol{q}}{T} \right)$ by applying product rule of differentiation:

$$\operatorname{div} \left( \frac{\boldsymbol{q}}{T} \right) = \frac{\nabla \boldsymbol{q}}{T} - \boldsymbol{q} \cdot \frac{\nabla T}{T^2} \tag{3.101}$$

Substituting these values:

$$\implies \rho\dot{\eta} \geq -\frac{\nabla \boldsymbol{q}}{T} - \boldsymbol{q} \cdot \frac{\nabla T}{T^2} + \frac{Q}{T} \tag{3.102}$$

This is the differential form of the **Second Law of Thermodynamics for a thermoelastic body**. It states that the entropy of the system is always increasing and states the irreversibility of the thermodynamic process.

### 3.3.3 Clausius-Duhem Inequality

The Clausius–Duhem inequality is the local (point-wise) expression of the second law of thermodynamics in continuum mechanics, imposing a non-negative entropy production constraint that governs the admissibility of constitutive relations.

If we look at the entropy inequality defined above, in (3.102)

$$\rho\dot{\eta} \geq -\frac{\nabla \boldsymbol{q}}{T} - \boldsymbol{q} \cdot \frac{\nabla T}{T^2} + \frac{Q}{T} \tag{3.103}$$

and substitute the value of $\operatorname{div} \boldsymbol{q}$ from the energy balance equation (3.97) (divided by $T$), we get the following form:

$$\rho\dot{\eta} \geq \frac{1}{T}\left(\rho\dot{e} - \boldsymbol{\sigma} \cdot \dot{\boldsymbol{\varepsilon}}\right) - \boldsymbol{q} \cdot \frac{\nabla T}{T^2} \tag{3.104}$$

This is **Clausius-Duhem Inequality** in terms of specific entropy $\eta$ and internal energy $(e)$of the system.

Since entropy of a system is not a convenient quantity to work with in thermodynamic systems, we re-parameterize the entire equation in terms of temperature.

We now introduce the term *Free energy function*, $\varphi$, also known as *Hemholtz Potential*, a thermodynamic state function which is a measure of how the systems change, and how much useful work they can produce, if the temperature is kept constant. Mathematically, it is expressed as the Legendre transformation of the internal energy $(e)$ which replaces entropy $(\eta)$. From thermodynamics definition, temperature $T$ is given as:

$$T = \frac{\partial e}{\partial \eta} \tag{3.105}$$

This allows us to define a new potential function

$$\varphi(\boldsymbol{\varepsilon}, T) = e(\boldsymbol{\varepsilon}, \eta) - T\eta \tag{3.106}$$

Dividing (3.106) with respect to time, to obtain the rate of change of free energy:

$$\dot{\varphi} = \dot{e} - \dot{T}\eta - T\dot{\eta} \quad \implies \quad \dot{e} = \dot{\varphi} + \dot{T}\eta + T\dot{\eta} \tag{3.107}$$

Substituting (3.107) into (3.104):

$$\rho\left(T\dot{\eta} - \dot{\varphi} + \dot{T}\eta + T\dot{\eta}\right) + \boldsymbol{\sigma} \cdot \dot{\boldsymbol{\varepsilon}} - \boldsymbol{q} \cdot \frac{\nabla T}{T} \geq 0 \tag{3.108}$$

Rearranging the equation gives

$$\boldsymbol{\sigma} \cdot \dot{\boldsymbol{\varepsilon}} - \rho\left(\dot{\varphi} + \dot{T}\eta\right) - \boldsymbol{q} \cdot \frac{\nabla T}{T} \geq 0 \tag{3.109}$$

This is the **free energy form of Clausius-Duhem inequality**, which states that the energy dissipation (which is rate of internal entropy production per unit volume times the absolute temperature) per unit volume of the system is always increasing. Hence, it is also called the *Dissipation inequality*.

Alternatively, (3.109) can rewritten as:

$$\rho\dot{\varphi} \leq \boldsymbol{\sigma} \cdot \dot{\boldsymbol{\varepsilon}} - \rho\dot{T}\eta - \boldsymbol{q} \cdot \frac{\nabla T}{T} \tag{3.110}$$

which highlights the fact that in an admissible process, the free energy of a system cannot increase - it is either always decreasing or stays constant. The isolated systems in equilibrium have the minimum free-energy.

Although $\varphi$ depends only on the six independent components of the symmetric strain tensor, it is more convenient to think of it as a function of all nine components of the strain tensor. This then leads to:

$$\frac{\partial\varphi}{\partial\varepsilon_{ij}} = \frac{\partial\varphi}{\partial\varepsilon_{ji}} \tag{3.111}$$

Revisiting the equation for the free energy (3.106) then the relation between free energy function and the stress-strain conjugate pair is as follows:

$$\dot{\varphi} = \frac{\partial\varphi}{\partial\boldsymbol{\varepsilon}} : \dot{\boldsymbol{\varepsilon}} + \frac{\partial\varphi}{\partial T}\dot{T} \tag{3.112}$$

which implies that the rate of stored energy comes from changes in strain and temperature. Substituting this value of $\dot{\varphi}$ in Eqn. 3.109:

$$\left(\boldsymbol{\sigma} - \rho\frac{\partial\varphi}{\partial\boldsymbol{\varepsilon}}\right) \cdot \dot{\boldsymbol{\varepsilon}} - \rho\left(\eta + \frac{\partial\varphi}{\partial T}\right)\dot{T} - \boldsymbol{q} \cdot \frac{\nabla T}{T} \geq 0; \qquad \forall\, \dot{\boldsymbol{\varepsilon}}, \dot{T} \tag{3.113}$$

This equations brings to attention that the $\dot{\varepsilon}$ and $\dot{T}$ are independent state variables, and can vary arbitrarily in a process. Therefore, the inequality can hold for all processes only if the coefficients of these rates vanish. This is the **Coleman–Noll argument.** By using (3.111), along with the symmetry of stress tensor $\boldsymbol{\sigma}$, we get:

$$\implies \quad \boldsymbol{\sigma} = \rho\frac{\partial\varphi}{\partial\boldsymbol{\varepsilon}} \quad \text{constitutive law for stresses, ie, stress must come from free energy} \tag{3.114}$$

and

$$\implies \quad \eta = -\frac{\partial\varphi}{\partial T} \quad \text{constitutive law for specific entropy} \tag{3.115}$$

Substituting these into (3.113), it is observed that the coefficients of $\dot{\boldsymbol{\varepsilon}}$ and $\dot{\boldsymbol{T}}$ become zero, leaving the following form of the equation

$$\implies -\boldsymbol{q} \cdot \frac{\nabla T}{T^2} \geq 0 \tag{3.116}$$

identifying that heat conduction is the only source of entropy production.

In the next step, starting with the first constitutive law for stresses (3.114) we differentiate it with respect to time:

$$\dot{\boldsymbol{\sigma}} = \underbrace{\rho\frac{\partial^2\varphi}{\partial\boldsymbol{\varepsilon}\,\partial\boldsymbol{\varepsilon}}}_{\mathbb{E}} \cdot [\dot{\boldsymbol{\varepsilon}}] + \underbrace{\rho\frac{\partial^2\varphi}{\partial T\,\partial\boldsymbol{\varepsilon}}}_{\boldsymbol{M}}\dot{T} \tag{3.117}$$

The terms $\mathbb{E}$ is a fourth order tensor, and is known as *Isothermal Elastic Tensor* which measures how stress changes with variations in strain at constant temperature, while $\boldsymbol{M}$ is a second order tensor known as *Stress temperature tensor* which provides information on the thermal sensitivity of stress. Thus the equation can be re-written to obtain **Rate of stress** as:

$$\dot{\boldsymbol{\sigma}} = \mathbb{E} : \dot{\boldsymbol{\varepsilon}} + \boldsymbol{M}\dot{T} \tag{3.118}$$

where the first term $\mathbb{E} : \dot{\boldsymbol{\varepsilon}}$ is the "elastic response" - stress change due to deformation, and the second part is responsible for the "thermal contribution" - stress change due to heating or cooling.

Naturally, as the next step, we now consider the second constitutive law for entropy (3.115). The time derivative of this equation provides:

$$\rho\dot{\eta} = \underbrace{\rho\frac{-\partial^2\varphi}{\partial\boldsymbol{\varepsilon}\,\partial T}}_{\boldsymbol{M}} : \dot{\boldsymbol{\varepsilon}} - \rho\underbrace{\frac{\partial^2\varphi}{\partial T^2}}_{c_E/T}\dot{T} \tag{3.119}$$

where $\boldsymbol{M}$ is the **stress-temperature tensor** and $c_E/T$ is the **specific heat at constant strain.**

Thus, the equation can be re-written to obtain the **Rate of entropy** as:

$$\rho\dot{\eta} = -\boldsymbol{M} : \dot{\boldsymbol{\varepsilon}} - \rho\frac{c_E}{T}\dot{T} \tag{3.120}$$

The first term in the equation above is *thermoelastic coupling term* that illustrates entropy change induced by elastic deformation in a thermoelastic material, due to coupling between mechanical strain and temperature in the free energy.

Both Rate of Stress (3.118) and Rate of Entropy (3.120) are linear equations (small deformations), and together form the *thermodynamic conjugate pair.*

### 3.3.4 Energy Equation for an Elastic Solid

We know that from (3.106), the free energy equation is given as:

$$\varphi = e - T\eta; \quad \varphi = \varphi(\boldsymbol{\varepsilon}, T) \tag{3.121}$$

And the differentiation of free energy with time gives:

$$\dot{\varphi} = \dot{e} - \dot{T}\eta - T\dot{\eta} \tag{3.122}$$

Also, from (3.112):

$$\dot{\varphi} = \frac{\partial\varphi}{\partial\boldsymbol{\varepsilon}} \cdot \dot{\boldsymbol{\varepsilon}} + \frac{\partial\varphi}{\partial T}\dot{T} \tag{3.123}$$

From the Constitutive law of stress (3.118) and entropy (3.120)

$$\frac{\partial\varphi}{\partial\boldsymbol{\varepsilon}} = \frac{1}{\rho}\boldsymbol{\sigma} \quad \text{and} \quad \frac{\partial\varphi}{\partial T} = -\eta \tag{3.124}$$

Substituting this value in (3.123) and equating with (3.122), we get:

$$\implies \quad \frac{1}{\rho}\boldsymbol{\sigma} \cdot \dot{\boldsymbol{\varepsilon}} - \eta\dot{T} = \dot{e} - T\dot{\eta} - \dot{T}\eta \tag{3.125}$$

Rearranging the equation in terms of internal energy:

$$\implies \quad \dot{e} = \frac{1}{\rho}\boldsymbol{\sigma} \cdot \dot{\boldsymbol{\varepsilon}} + T\dot{\eta} \tag{3.126}$$

Substituting this form of internal energy into the First law of Thermodynamics (3.97):

$$\rho \dot{e} = \boldsymbol{\sigma} \cdot \dot{\boldsymbol{\varepsilon}} - \operatorname{div} \boldsymbol{q} + Q = \boldsymbol{\sigma} \cdot \dot{\boldsymbol{\varepsilon}} + \rho T \dot{\eta}$$

$$\implies \quad \rho T \dot{\eta} = - \operatorname{div} \boldsymbol{q} + Q$$

This is the alternate form of the First Law of Thermodynamics in purely thermal form, indicating that entropy change arises only from heat flux and sources. But from (3.118) and (3.120)

$$\rho T \dot{\eta} = -T \boldsymbol{M} \cdot \dot{\boldsymbol{\varepsilon}} + \rho c_E \dot{T} \tag{3.127}$$

Substituting these values, and re-arranging the terms gives:

$$\rho c_E \dot{T} = - \operatorname{div} \boldsymbol{q} + Q + T \boldsymbol{M} \cdot \dot{\boldsymbol{\varepsilon}} \tag{3.128}$$

This is the equation for the **Energy of an Elastic Body.** From Fourier's law of heat conduction 3.7:

$$\boldsymbol{q} = -\boldsymbol{K}\left(\boldsymbol{x}, T\right) \nabla T \tag{3.129}$$

where $\boldsymbol{K}$ is the Conductivity tensor. Also, to have linear equations, we assume that the $\boldsymbol{K}$ is non-dependent on T. Then, substituting the value of $\boldsymbol{q}$ in (3.128):

$$\rho c_E \dot{T} = \operatorname{div}\left(\boldsymbol{K}\left(\boldsymbol{x}\right) \nabla T\right) + Q + T \boldsymbol{M} \cdot \dot{\boldsymbol{\varepsilon}} \tag{3.130}$$

Again applying the divergence theorem, and re-arranging the equations, we get:

$$\implies \qquad \rho c_E \dot{T} = \boldsymbol{K} \nabla^2 T + Q + T \boldsymbol{M} \cdot \dot{\varepsilon} \tag{3.131}$$

where

$$\nabla^2 = \frac{\partial^2}{\partial x^2} + \frac{\partial^2}{\partial y^2} + \frac{\partial^2}{\partial z^2} \tag{3.132}$$

is the Laplacian operator defined in 2.4. (3.131) is the **Heat Transport Equation** for an elastic body. It shows that for a purely elastic, reversible process, energy change is stored in the solid accounted for by the thermo-elastic coupling term $T \boldsymbol{M} \cdot \dot{\boldsymbol{\varepsilon}}$. For an isotropic material: $\boldsymbol{K} = K \boldsymbol{I}$, where $\boldsymbol{I}$ is Identity matrix.

### 3.3.5 Isotropic Linear Thermoelasticity

Isotropic linear thermoelasticity describes the coupled thermal and mechanical behavior of elastic solids under small deformations and small temperature changes, assuming isotropic behaviour of the material. The theory employs linear constitutive relations, isotropic thermal expansion, and Fourier heat conduction, while satisfying the first and second laws of thermodynamics. The linear thermoelasticity gives the tools to investigate the stresses produced by the temperature field and to calculate the distribution of the temperature due to the action of internal forces Ghiba, 2014.

It is assumed that the linearised strain tensor, defined in 3.41, can be split into its thermal and mechanical part, as

$$\boldsymbol{\varepsilon} = \boldsymbol{\varepsilon}_{mech} + \boldsymbol{\varepsilon}_{therm} \tag{3.133}$$

where $\boldsymbol{\varepsilon}_{mech}$ is the strain caused due to mechanical loads, and $\boldsymbol{\varepsilon}_{therm}$ is the strain produced in elastic solids due to thermal expansion, written as

$$\boldsymbol{\varepsilon}_{therm} = \Theta \boldsymbol{\alpha} \tag{3.134}$$

where $\boldsymbol{\alpha}$ is the symmetric tensor of second-order known as *thermal expansion tensor*. The reference temperature of the system is $T_0$ and its current temperature is given as $T$, and thus, $\Theta = T - T_0$. For a linearly isotropic material, $\boldsymbol{\alpha} = \alpha \boldsymbol{I}$.

For a simple case of linear isotropic elastic material, the free energy function is defined as:

$$\rho\varphi\left(\boldsymbol{\varepsilon}, T\right) = \underbrace{\frac{\lambda}{2}\left(\operatorname{tr}(\boldsymbol{\varepsilon})\right)^2 + \mu\boldsymbol{\varepsilon}\cdot\boldsymbol{\varepsilon}}_{\text{Strain-energy Function}} - 3\alpha\mathcal{K}\Theta\operatorname{tr}(\boldsymbol{\varepsilon}) - c_E T\log\frac{T}{T_0} + c_E\Theta - \Theta\eta_0 \tag{3.135}$$

where

$$\lambda, \mu = \text{Lame's elastic constants} \tag{3.136}$$
$$T_0 = \text{Reference Temperature} \tag{3.137}$$
$$\alpha = \text{coefficient of thermal expansion} \tag{3.138}$$
$$\mathcal{K} = (3\lambda + 2\mu)/3 \qquad \text{Bulk Modulus} \tag{3.139}$$
$$eta_0 = \text{entropy at } T = T_0 \text{ and } \boldsymbol{\varepsilon} = 0 \tag{3.140}$$

Substituting these values in the stress and entropy constitutive laws (3.118) and (3.120):

$$\boldsymbol{\sigma} = \rho\frac{\partial\varphi}{\partial\boldsymbol{\varepsilon}} = \lambda(\operatorname{tr}(\boldsymbol{\varepsilon})\underbrace{\frac{\partial\operatorname{tr}\boldsymbol{\varepsilon}}{\partial\boldsymbol{\varepsilon}}}_{\boldsymbol{I}} + 2\mu\boldsymbol{\varepsilon} - \underbrace{3\alpha\mathcal{K}}_{m}\Theta\underbrace{\frac{\partial\operatorname{tr}\boldsymbol{\varepsilon}}{\partial\boldsymbol{\varepsilon}}}_{\boldsymbol{I}} \tag{3.141}$$

$$\implies \qquad \boldsymbol{\sigma} = 2\,\mu\boldsymbol{\varepsilon} + \lambda\operatorname{tr}(\boldsymbol{\varepsilon})\boldsymbol{I} - m\Theta\boldsymbol{I} \tag{3.142}$$

and

$$\implies \qquad \eta = \eta_0 + c_E\left(\frac{T - T_0}{T_0}\right) - m\operatorname{tr}\varepsilon \tag{3.143}$$

(3.142) is the **stress-strain relation for an isotropic linear thermoelastic material** and (3.143) is the **entropy equation for an isotropic linear thermoelastic material** where $m$ is the **stress-temperature modulus**. The stress-temperature tensor, $\boldsymbol{M}$ is defined as:

$$\boldsymbol{M} = \rho\frac{\partial^2\varphi}{\partial T\partial\boldsymbol{\varepsilon}} = -3\alpha K\boldsymbol{I} = -m\boldsymbol{I} \tag{3.144}$$

### Coupled Linear Thermoelasticity

In coupled thermoelasticity, the thermal effects and the mechanical forces are the driving factors, as they both are interlinked. Temperature effects bring about deformation in elastic material, while these deformations in turn increases the temperature (and in turn, the entropy) of the system.

For such a case, the entropy and stress equations ((3.143) and (3.142)) remain the same.

The effect of the coupling term is predominant. As we saw in the derivation of Isotropic linear thermoelastic equations, the thermal subproblem is defined as:

$$\underbrace{\rho c_E\dot{T}}_{\text{thermal inertia}} = -\operatorname{div}\boldsymbol{q} + Q - \underbrace{mT_0\operatorname{tr}(\dot{\boldsymbol{\varepsilon}})}_{\text{coupling term}} \qquad in \quad B \tag{3.145}$$

where $\dot{\boldsymbol{\varepsilon}}$ is the *rate of volumetric strain*. The thermal coupling term $-mT_0\operatorname{tr}(\dot{\boldsymbol{\varepsilon}})$ can also be expressed in the following forms:

$$-mT_0\operatorname{tr}(\dot{\boldsymbol{\varepsilon}}) = T\boldsymbol{M}\cdot\dot{\boldsymbol{\varepsilon}} = -T(m\boldsymbol{I})\cdot\dot{\boldsymbol{\varepsilon}} = -mT\operatorname{tr}(\dot{\boldsymbol{\varepsilon}}) \tag{3.146}$$

The value of heat flux term $\boldsymbol{q}$ is computed from the Fourier law as: $\boldsymbol{q} = -K\nabla T$, which when substituted in the equation above, gives us the equation for the energy of an elastic solid:

$$\rho c_E \dot{T} = \boldsymbol{K}\nabla^2 T + Q + T\boldsymbol{M} \cdot \dot{\boldsymbol{\varepsilon}} \tag{3.147}$$

The thermal subproblem is further supplemented by providing the initial and the boundary conditions such as:

$$T(\boldsymbol{x}, 0) = T_0(\boldsymbol{x}) \qquad at \quad t = 0 \longrightarrow \text{Initial Conditions}$$

$$T(\boldsymbol{x}, t) = \boldsymbol{T}(\boldsymbol{x}, t) \qquad on \quad \partial B_T \longrightarrow \text{Dirichlet / Essential Boundary Conditions}$$

$$\boldsymbol{q}(\boldsymbol{x}, t) \cdot \boldsymbol{n} = \boldsymbol{q}_n(\boldsymbol{x}, t) \qquad on \quad \partial B_q \longrightarrow \text{Neumann / Natural Boundary Conditions}$$

The initial conditions (at $t = 0$) for the mechanical subproblem (3.142) is given as:

$$\boldsymbol{u}(\boldsymbol{x}, 0) = \boldsymbol{u}_0(\boldsymbol{x})$$

$$\dot{\boldsymbol{u}}(\boldsymbol{x}0) = \dot{\boldsymbol{u}}_0(\boldsymbol{x})$$

while the boundary conditions are specified as:

$$\boldsymbol{u}(\boldsymbol{x}, t) = \boldsymbol{u}(\boldsymbol{x}, t) \qquad on \quad \partial B_u \longrightarrow \text{Dirichlet / Essential Boundary Conditions}$$

$$\boldsymbol{\sigma}(\boldsymbol{x}, t) \cdot \boldsymbol{n} = \boldsymbol{t}_n(\boldsymbol{x}, t) \qquad on \quad \partial B_t \longrightarrow \text{Neumann / Natural Boundary Conditions}$$

Since there is a bi-directional coupling in this case (Temperature $\Leftrightarrow$ Mechanical), it is computationally exhaustive process and thus, a simply uncoupled form of linear thermoelasticity is commonly used.

**Comment on Effect of Coupling and Inertia** We first consider the mechanical coupling term $mT_0\,\mathrm{tr}(\dot{\boldsymbol{\varepsilon}})$ in the heat conduction equation. This equation shows that the variations in strain produced within a body, is generally accompanied by changes in temperature distributions within the body, and consequently the heat flow. This gives rise to an increase in entropy of the system, which is in turn linked with the increase in energy stored in a mechanically irrecoverable manner. This phenomenon is known as **thermoelastic dissipation**, and the mechanical coupling term in the heat transfer equation describes this dissipative process.

However, if the dissipation does not occur in the process, for instance, deformation due to external loads produce very little variation in temperature, and thus, these deformations can be calculated by without taking into account the thermal expansion. Similarly, is strains are produced in a body due to non-uniform distribution of temperature within the body, then there is no influence of the strains on the temperature itself.

### Uncoupled Linear Thermoelasticity

The equations and laws defined above are of the general form that can be employed in thermoelastic boundary value problems. If the coupling is only uni-directional, that is, only temperature variations affect mechanical deformations but not vice-versa, then it is known as *Uncoupled Thermoelasticity.* For such a case, the heat equation becomes independent of the thermoelastic coupling term $(-mT_0\,\mathrm{tr}(\dot{\boldsymbol{\varepsilon}}))$, as it is very very small. The thermal subproblem is then totally uncoupled from the $\dot{\boldsymbol{\varepsilon}}$ terms and consists of only thermal terms.

$$\rho c_E \dot{T} = -\operatorname{div} \boldsymbol{q} + Q \quad \longrightarrow \quad \text{fully uncoupled equation, solve it to find T}(\boldsymbol{x},\text{t}) \tag{3.148}$$

However, for the mechanical subproblem, the thermal change $\Theta = (T - T_0)$ exists and the effect is significant and the driving force of deformation. Thus, the equation for a mechanical subproblem is not fully uncoupled, and is solved by employing (3.142).

Such implementations are useful in situations where heat dominates the deformations in structures or cylic loadings, such as those in refractories. The uncoupled theory provides an accurate and computationally efficient approximation for many quasi-static engineering applications. In ABAQUS, it is known as **SEQUENTIALLY COUPLED**, with the temperature acting as the prescribed field.

#### Uncoupled Quasi-static Linear Thermoelasticity

This is a special case of uncoupled thermo-elastic problem, where the inertial term $\rho\ddot{\boldsymbol{u}}$ is considered to be very small and is neglected.

From the linear momentum balance equation:

$$\int_B (\operatorname{div} \boldsymbol{\sigma} + \boldsymbol{b} - \rho\ddot{\boldsymbol{u}}) \cdot \boldsymbol{v}\, dV \tag{3.149}$$

Thus, using localization theorem,

$$\operatorname{div} \boldsymbol{\sigma} + \boldsymbol{b} = 0 \tag{3.150}$$

The heat equation (3.131) remains independent of mechanical terms as given by (3.148), while effects of temperature variations still bring about a change in the stress tensor, computed according to (3.142).

### 3.3.6 Weak Form of Thermoelasticity

The weak form of thermoelasticity is the equation in which the order of derivative is lower than that of the strong form.

**Thermal Subproblem:**

$$G_T(T, \delta T) = \int_B \rho c_E \dot{T} \delta T\, dV + \int_B K \nabla T \cdot \nabla \delta T\, dV - \int_B (Q - \underbrace{m T_0 \operatorname{tr}(\dot{\boldsymbol{\varepsilon}})}_{\text{thermal coupling term}})\delta T\, dV \tag{3.151}$$

where $\delta T$ = Test Function

$\dot{T}$ = Temperature Field

$\delta T = 0$ on $\partial B_q$

$\int_{\partial B_q} \hat{q}_n \delta T\, dA = 0; \quad \forall \delta T$

**Mechanical Subproblem:**

$$G_u(\boldsymbol{u}, \delta \boldsymbol{u}) = \int_B \boldsymbol{\sigma} \cdot \delta \boldsymbol{\varepsilon}\, dV - \int_B \boldsymbol{b} \cdot \delta \boldsymbol{u}\, dV - \int_{\partial B_t} \boldsymbol{t}_n \cdot \delta \boldsymbol{u}\, dA \tag{3.152}$$

where

$\delta \boldsymbol{u} = 0$ on $\partial B_u \quad \forall \delta T$

$\boldsymbol{\sigma} = \mathbb{E} \cdot \boldsymbol{\varepsilon}$

$\boldsymbol{\varepsilon} = \frac{1}{2}\left(\nabla \boldsymbol{u} + \nabla \boldsymbol{u}^T\right)$

Also, we know that the total strain is given as: $\boldsymbol{\varepsilon} = \boldsymbol{\varepsilon}_e + \boldsymbol{\varepsilon}_T$, where the term $\boldsymbol{\varepsilon}_T$ is the thermal strain computed as, $\boldsymbol{\varepsilon}_T = \alpha \Delta T \boldsymbol{I}$. It is the thermal coupling term in the mechanical subproblem. Thus the elastic strain can be calculated as, $\boldsymbol{\varepsilon}_e = \boldsymbol{\varepsilon} - \boldsymbol{\varepsilon}_T$.

This value of elastic strain can then be substituted in the elastic constitutive law:

$\boldsymbol{\sigma} = \mathbb{E} \cdot (\boldsymbol{\varepsilon} - \boldsymbol{\varepsilon}_T)$

$\mathbb{E} \cdot \boldsymbol{\varepsilon}_e = \lambda(\mathrm{tr}(\boldsymbol{\varepsilon}_e)\boldsymbol{I} + 2\mu\boldsymbol{\varepsilon}_e$

# Chapter 4

# Transmission Conditions across a thin conductive interface

Thermally conductive interphases are formed as a result of a chemical reaction between two substances or by deposition of a material from one material to another, and the thermal conductivity mismatch between the materials accounts for the behaviour of this thin interphase as a thermal barrier or a conductive layer. Its numerous applications were highlighted in Chapter 1. In this chapter, the focus is placed on the development of two imperfect interface models derived from the thermal governing equations defined in (3.7) and (3.18). These transmission conditions aim to accurately capture the effect of a thin layer via jumps in temperature and heat flux. The novelty of the present method lies in the fact that both proposed models are based on the modified form of Bovik-Benveniste methodology to account for continuity of temperature and heat flux at any point inside the interface, while preserving accuracy at the boundaries. The two approaches presented in this paper are compared via implementation in different interphase geometries, with known classical models, to study the effect of geometric and material properties on the efficacy and validity of the proposed methods across a range of thermal conductivities.

The chapter is divided as follows: Sec.4.1 details the modification of Benveniste's equation accounting for continuity inside the interphase, while Sec.4.2 outlines the development of our proposed transmission conditions. Several classical benchmark models are outlined in Sec.4.3, and Sec. 4.4 presents the implementation of these methods to different geometries and subsequent analysis of the proposed schemes. The accuracy is also analyzed by comparison with the models from Sec.4.3, with the conclusions drawn in chapter 7.

## 4.1 Motivation

In his paper, Benveniste, 2006b used Taylor series expansion around point $A_1$ and $A_2$ to express the temperature and heat flux at point $A_3$, in the normal direction as:

$$\begin{aligned} T^{(i)}(\xi) &= T^{(i)}_{A_1} + \left.\frac{\partial T^{(i)}}{\partial n}\right|_{A_1} \xi + \frac{1}{2}\left.\frac{\partial^2 T^{(i)}}{\partial n^2}\right|_{A_1} \xi^2, \qquad 0 \le \xi \le t/2, \\ T^{(i)}(\xi) &= T^{(i)}_{A_2} + \left.\frac{\partial T^{(i)}}{\partial n}\right|_{A_2} (\xi - t) + \frac{1}{2}\left.\frac{\partial^2 T^{(i)}}{\partial n^2}\right|_{A_2} (\xi - t)^2, \qquad t/2 \le \xi \le t, \end{aligned} \tag{4.1}$$

It can be easily seen that the temperature values inside the interphase ($T^{(i)}(\xi)|_{A_3}$), obtained by Taylor series expansion, whether around point $A_1$ or point $A_2$, is discontinuous, as

illustrated with orange dashed lines in Fig.4.2. It provides us with a good approximation of the temperature and heat flux values at the interphase boundaries, but within the domain itself(i.e, away from the boundaries), the behavior of temperature and heat flux is seen to be discontinuous. This is in contrast to the intuitive assumption that material is continuous at all points within the interphase, and thus all the associated state variables such as temperature, displacement, etc. should be continuous as well inside the domain of the interphase.

To compute our model, we proceed the similar way by taking Taylor series expansion around point $A_1$ and $A_2$, to express temperature and heat flux at point $A_3$ in the normal direction:

$$\begin{aligned} T^{(i)}(\xi) &= T^{(i)}_{A_1} + \left.\frac{\partial T^{(i)}}{\partial n}\right|_{A_1} \xi + a_1\xi^2, \quad 0 \le \xi \le t_1, \\ T^{(i)}(\xi) &= T^{(i)}_{A_2} + \left.\frac{\partial T^{(i)}}{\partial n}\right|_{A_2} (\xi - t) + a_2(\xi - t)^2, \quad t_1 \le \xi \le t, \end{aligned} \tag{4.2}$$

From the Fourier's law, the heat flux at point $A_3$ is given as

$$q^{(i)}_n(\xi) = -k^{(i)} \left.\frac{\partial T^{(i)}}{\partial n}\right|_{\xi} \tag{4.3}$$

Substituting (4.2) here gives the following set of equations for the normal component of heat flux at a point inside the interphase,

$$\begin{aligned} q^{(i)}_n(\xi) &= -k^{(i)}(\xi) \left( \left.\frac{\partial T^{(i)}}{\partial n}\right|_{A_1} + 2a_1\xi \right), \quad 0 \le \xi \le t_1, \\ q^{(i)}_n(\xi) &= -k^{(i)}(\xi) \left( \left.\frac{\partial T^{(i)}}{\partial n}\right|_{A_2} + 2a_2(\xi - t) \right), \quad t_1 \le \xi \le t, \end{aligned} \tag{4.4}$$

where $T^{(i)}_{A_1}$ and $T^{(i)}_{A_2}$ are the temperature values at the point $A_1$ and $A_2$ taken *inside* the interphase, and $\xi$ is the arbitrary position of the point $A_3$ within the interphase, and $a_1$ and $a_2$ are the internal parameters that refine our model to provide a continuous temperature profile at all points within the domain. Moreover, computing the values of $T^{(i)}(\xi)$ and $q^{(i)}_n(\xi)$ at point $A_3$ by asymptotic expansion of Taylor series from point $A_1$ and $A_2$ ensures that the accuracy of the temperature and heat flux functions are retained at the boundary (much like Benveniste's model) while also preserving the continuity within the region. The constants $a_1$ and $a_2$ are computed from the continuity conditions at point $A_3$:

$$T^{(i)}_{A_3}(t_1^-) = T^{(i)}_{A_3}(t_1^+), \quad \left.\frac{\partial T^{(i)}}{\partial n}\right|_{A_3}(t_1^-) = \left.\frac{\partial T^{(i)}}{\partial n}\right|_{A_3}(t_1^+) \tag{4.5}$$

Assuming the continuity of $k^{(i)}(\xi)$ inside the interphase, the second condition above coincides with the continuity of heat flux.

Solving Eqs.(4.5) we get this:

$$\begin{aligned} a_1 &= \frac{2k^{(i)}_{A_1}k^{(i)}_{A_2}(T^{(i)}_{A_2} - T^{(i)}_{A_1}) + k^{(i)}_{A_1}q^{(i)}_n|_{A_2}t_2 + k^{(i)}_{A_2}q^{(i)}_n|_{A_1}(2t - t_2)}{2k^{(i)}_{A_1}k^{(i)}_{A_2}t_1 t}, \\ a_2 &= \frac{2k^{(i)}_{A_1}k^{(i)}_{A_2}(T^{(i)}_{A_1} - T^{(i)}_{A_2}) - k^{(i)}_{A_2}q^{(i)}_n|_{A_1}t_1 - k^{(i)}_{A_1}q^{(i)}_n|_{A_2}(2t - t_1)}{2k^{(i)}_{A_1}k^{(i)}_{A_2}t_2 t}, \end{aligned} \tag{4.6}$$

where there is a clear symmetry by changing $T_{A_1}^{(i)} \rightarrow T_{A_2}^{(i)}$ and $q_n^{(i)}|_{A_1} \rightarrow -q_n^{(i)}|_{A_2}$. Ideal interface conditions between the interphase and the adherents exists at point $A_1$ and $A_2$ for a perfect interphase condition:

$$\begin{aligned} T_{A_1}^{(i)} &= T_{A_1}^{(1)} \quad T_{A_2}^{(i)} = T_{A_2}^{(2)} \\ q_n^{(i)}|_{A_1} &= q_n^{(1)}|_{A_1} \quad q_n^{(i)}|_{A_2} = q_n^{(2)}|_{A_2} \end{aligned} \tag{4.7}$$

where for isotropic materials, the normal component of heat flux is computed from Fourier's law as:

$$q_n^{(i)} = -k^{(i)} \frac{\partial T^{(i)}}{\partial n}, \quad q_n^{(1)} = -k^{(1)} \frac{\partial T^{(1)}}{\partial n}, \quad q_n^{(2)} = -k^{(2)} \frac{\partial T^{(2)}}{\partial n} \tag{4.8}$$

We also can compute the temperature and the flux on the intermediate surface inside the interphase

$$T_{A_3}^{(i)}(t_1^-) = T_{A_3}^{(i)}(t_1^+) = \frac{1}{2k_{A_1}^{(i)} k_{A_2}^{(i)} t} \left[ k_{A_1}^{(i)} q_n^{(i)}|_{A_2} t_1 t_2 - k_{A_2}^{(i)} q_n^{(i)}|_{A_1} t_1 t_2 + 2k_{A_1}^{(i)} k_{A_2}^{(i)} (T_{A_1}^{(i)} t_2 + T_{A_2}^{(i)} t_1) \right] \tag{4.9}$$

$$q_n^{(i)}|_{A_3}(t_1^-) = q_n^{(i)}|_{A_3}(t_1^+) = \frac{-k_{A_3}^{(i)}}{k_{A_1}^{(i)} k_{A_2}^{(i)} t} \left[ k_{A_1}^{(i)} q_n^{(i)}|_{A_2} t_2 + k_{A_2}^{(i)} q_n^{(i)}|_{A_1} t_1 + 2k_{A_1}^{(i)} k_{A_2}^{(i)} (T_{A_2}^{(i)} - T_{A_1}^{(i)}) \right] \tag{4.10}$$

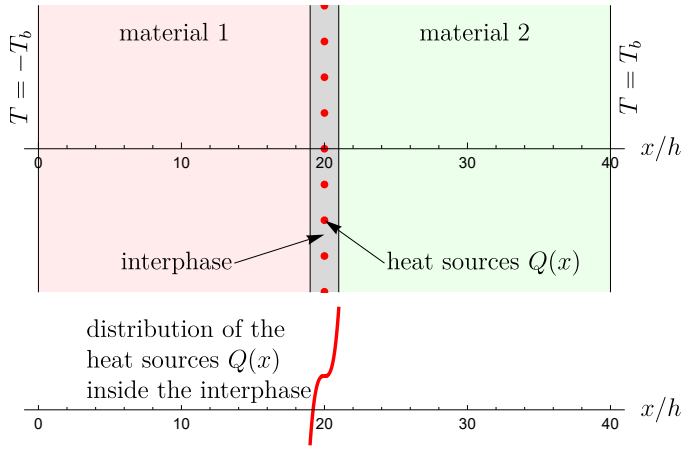


**Fig. 4.1.** Example of an interphase between two materials with non-uniform heat sources inside the interphase.

**The heat source function:** Consider a distributed heat source in the interphase given by:

$$Q(x) = Q_0 \left( \frac{x + \zeta - b_1 - h}{h} \right)^{\alpha} \tag{4.11}$$

where $\alpha$ is an integer number that represents the "type" of the heat source, i.e., constant ($\alpha = 0$), linear ($\alpha = 1$), quadratic ($\alpha = 2$) or cubic ($\alpha = 3$), while $|\zeta| < h$ is the position of the heat source within the interphase, indicating the distribution of the symmteric ($\zeta = 0$) or non-symmteric ($\zeta \neq 0$) heat source. In the numerical examples below, $\zeta$ will be taken as $h/2$, where $h = t/2$. Here, $t$ is the total thickness of the interphase. The volumetric heat source is presented by $Q_0$ ($W/m^3$), and $x$ is the position within the interphase.

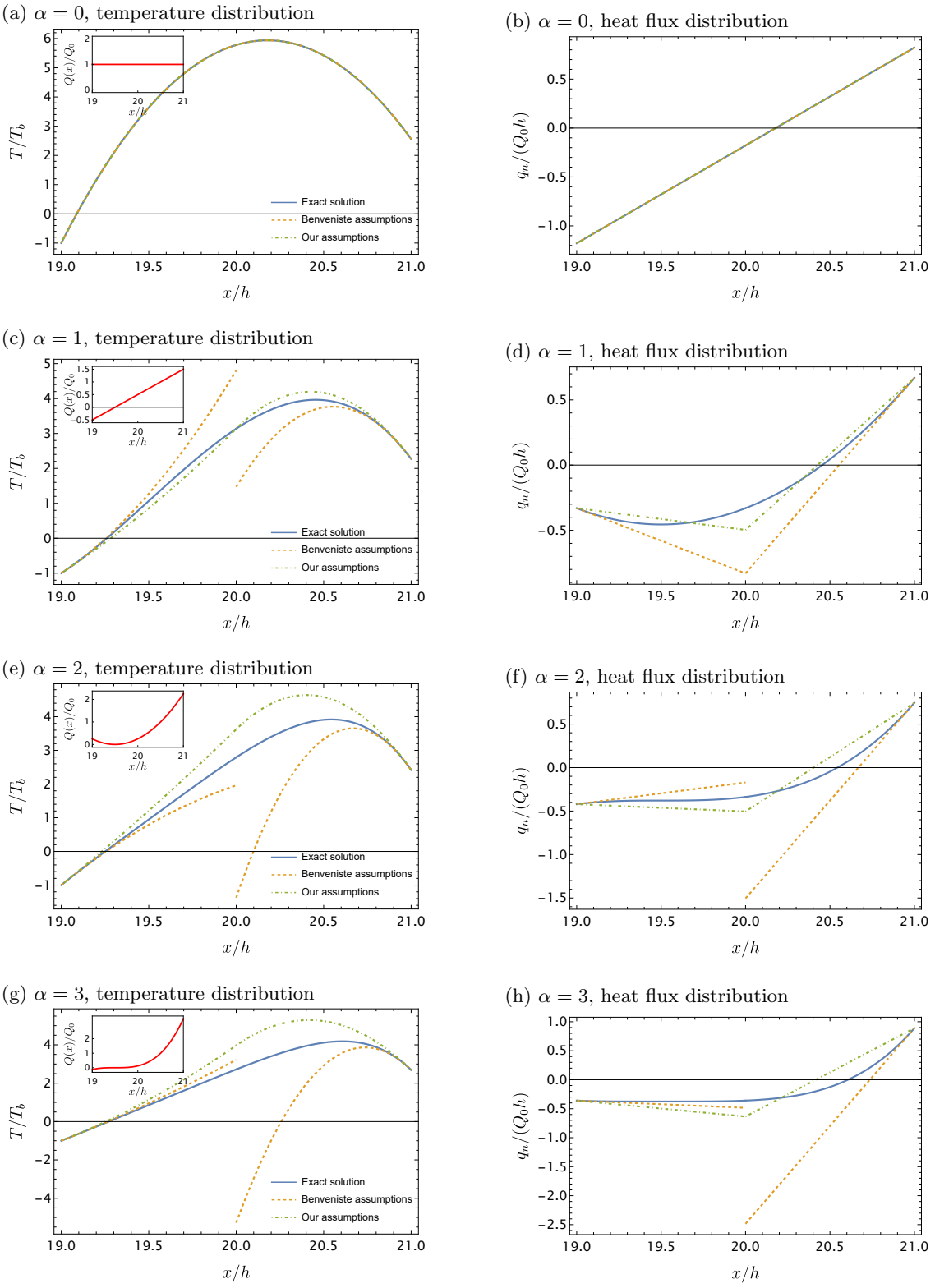


**Fig. 4.2.** Illustrative examples:0 Constant heat source, linear heat source, quadratic heat source and cubic heat source distribution. Also here we assume $t_1 = t_2 = t/2 = h$ and we take $\zeta = h/2$, while the heat source $Q_0 = 1.0 \times 10^{-}4(W/m^3)$

The following graphs represent the temperature and heat source profile across the planar domain, when 4 different cases of heat source distributions are used.

Fig.4.2 demonstrates the temperature and heat flux behaviour for the exact solution (shown in blue) and the temperature and heat flux in x-direction inside the interphase using Benveniste's assumptions (orange line) and using our assumptions (computed using $a_1$ and $a_2$ parameters, shown in green). It can be easily seen that the except for the constant heat source type, where all approximations are continuous, temperature approximations using Benveniste's assumptions are discontinuous inside the interphase, in the presence of a small heat source value, while our assumptions respects the continuity of the field variables inside the interphase at all points, for all types of body forces. Moreover, it can be seen that for quadratic and cubic heat sources, the fluxes inside the interphase are no longer continuous for Benveniste's approximations, while our assumptions show good approximation of the continuity inside the interphase. Hence, it can be said that the approximation of solution inside the interphase via asymptotic means is improved by taking the fields inside the interphase into account.

It is important to note here that the example presented here indicates that our approximation (that is continuous inside the interphase) is better than Taylor expansion from two different sides of the interface, when same order of approximation is used.

## 4.2 Development of Transmission Conditions

We now proceed to derive our proposed schemes, by making use of two points at the boundary of the interphase, namely points $A_1$ and $A_2$ (for the two points schemes) and a third point $A_3$ inside the interphase (for the three-points scheme). We begin by analyzing Fig.2.4a which gives the graphical representation of a perfect 3 phase system, with three distinct regions marked as material 1, material 2, and the thin interphase in between. For such a system, the normal component of heat flux and temperatures are continuous across the boundaries of the interphase such that,

$$T^{(1)}\Big|_{A_1} = T^{(i)}\Big|_{A_1} \quad ; \quad (q_j n_j)^{(1)}\Big|_{A_1} = (q_j n_j)^{(i)}\Big|_{A_1} \tag{4.12}$$

$$T^{(2)}\Big|_{A_2} = T^{(i)}\Big|_{A_2} \quad ; \quad (q_j n_j)^{(2)}\Big|_{A_2} = (q_j n_j)^{(i)}\Big|_{A_2} \tag{4.13}$$

Across the thin interface $\Gamma$ ($\lim t \to 0$) the thermal properties are no longer continuous and there is an accumulation of temperature or heat flux at the boundary, known as "jump" of the property, and is denoted as:

$$[\![\phi]\!] = \phi|_{A_2} - \phi|_{A_1} \tag{4.14}$$

where $\phi$ is the temperature or heat flux of the material.

Let us consider an isotropic, homogeneous, steady-state heat conduction within the interphase domain described above. The heat transfer through the arbitrary curvilinear composite system is obtained by the balance equation:

$$\operatorname{div} \boldsymbol{q} - Q(\xi, \alpha_2, \alpha_3, T) = 0. \tag{4.15}$$

where $\boldsymbol{q}$ is the heat flux vector, and $Q(\xi, \alpha_2, \alpha_3, T)$ is the heat source function, described in Eqn.(4.11) above. Since $\alpha_1$ is aligned in the normal direction, $q_1 = q_n$. In parallel

curvilinear coordinates, the equation can be expressed as

$$\frac{1}{h_2 h_3}\left\{\frac{\partial}{\partial n}(h_2 h_3 q_n^{(i)}) + \frac{\partial}{\partial \alpha_2}(h_3 q_2^{(i)}) + \frac{\partial}{\partial \alpha_3}(h_2 q_3^{(i)})\right\} - Q(\xi, \alpha_2, \alpha_3, T) = 0. \tag{4.16}$$

We solve this equation to obtain the derivative of the normal component of heat flux in the normal direction. This term represents the gradual change in the behaviour of normal component of heat flux when moving along the normal direction,ie, when one moves from point $A_1$ to $A_2$. This leads to the following two different forms of this equation.

$$\frac{\partial q_n^{(i)}}{\partial n} = Q(\xi, \alpha_2, \alpha_3, T) - \mathcal{D}_s \boldsymbol{q} - g\, q_n^{(i)}, \tag{4.17}$$

or

$$\frac{\partial}{\partial n}(h_2 h_3 q_n^{(i)}) = h_2 h_3 Q(\xi, \alpha_2, \alpha_3, T) - h_2 h_3 \mathcal{D}_s \boldsymbol{q}, \tag{4.18}$$

where

$$\mathcal{D}_s \boldsymbol{q} = \frac{1}{h_2 h_3}\frac{\partial}{\partial \alpha_2}(h_3 q_2^{(i)}) + \frac{1}{h_2 h_3}\frac{\partial}{\partial \alpha_3}(h_2 q_3^{(i)}) \tag{4.19}$$

is the *surface differential operator* known as *surface Laplacian* $\nabla_s \boldsymbol{q}$ (as denoted in Hashin, 2001), which denotes the gradient of the heat flux, or the diffusion of the heat flux, along the surface, that is, in the tangential directions, and

$$g(\xi, \alpha_2, \alpha_3) = \frac{1}{h_2 h_3}\frac{\partial h_2 h_3}{\partial n}. \tag{4.20}$$

represents the effect of *geometric curvature* on the transmission condition.

On the other hand, using Fourier's Law, (4.8) can be written in the form:

$$\frac{\partial T^{(i)}}{\partial n} = -\frac{1}{k^{(i)}} q_n^{(i)}. \tag{4.21}$$

This relates the normal derivative of the temperature, ie, the gradual change in the temperature profile from point $A_1$ to $A_2$ along the normal direction to the normal component of heat flux.

Comparison of the models from the literature, especially with Hashin, 2001 and Benveniste, 2006b model, we can see the following notable points: Firstly, the transmission conditions in these models do not account for heat sources inside the interphase. Thus, if the heat sources were considered, then these models would fail to provide accurate solution, as will be seen later in the results section. In Hashin's model, the surface differential term, $\mathcal{D}_s \boldsymbol{q}$, and the geometric curvature term, $g$, is taken at point $A_1$ (or from $A_2$) only, hence we only know the behaviour of the these terms around point $A_1$ in the vicinity of the interphase, but it does not accurately approximate the behaviour *inside* the interphase. In Benveniste's model, the thermal properties at points $A_1$ and $A_2$ are considered, but, as demonstrated in the previous section, we see the effect of these terms at points near the interphase, but it does not accurately capture the changes within the interphase, away from the boundary.

In the transmission conditions, which are derived in detail in the following sections, we have made use of Trapezoidal rule, between the appropriate intervals. Trapezoidal rule is numerical technique to compute the definite integral of a function between two given point (known as the "interval"). It is a simple technique whose accuracy improves with the increase in the number of intervals (or the sub-intervals) used to compute the solution, as we will see with the 2 points of integration and 3 points of integrations used in the schemes below.

### 4.2.1 Transmission conditions for the first integration scheme

For this scheme. we will implement Trapezoidal rule on Eqns (4.17) and (4.21), and obtain the first set of transmission conditions. The equations are integrated between 2 points (points $A_1$ and $A_2$) and between 3 points (between $A_1$ and $A_3$ and between $A_3$ and $A_2$).

#### Two integration points

Integrating (4.17) and (4.21) from 0 to $t$ (from $A_1$ to $A_2$) using the trapezoidal rule gives

$$q_n^{(i)}|_{A_2} - q_n^{(i)}|_{A_1} = \frac{t}{2}\Big(Q(0,\alpha_2,\alpha_3,T_{A_1}^{(i)}) + Q(t,\alpha_2,\alpha_3,T_{A_2}^{(i)}) - \mathcal{D}_s\boldsymbol{q}|_{A_1} - \mathcal{D}_s\boldsymbol{q}|_{A_2} - g\, q_n^{(i)}|_{A_1} - g\, q_n^{(i)}|_{A_2}\Big),$$

$$T_{A_2}^{(i)} - T_{A_1}^{(i)} = -\frac{t}{2}\left(\left.\frac{q_n^{(i)}}{k^{(i)}}\right|_{A_1} + \left.\frac{q_n^{(i)}}{k^{(i)}}\right|_{A_2}\right).$$

That can be written in a compact form, using the notation given in (2.116):

$$[\![q_n]\!] = t\Big(\langle Q\rangle - \langle \mathcal{D}_s\boldsymbol{q}\rangle - \langle g\, q_n^{(i)}\rangle\Big), \tag{4.22}$$

$$[\![T]\!] = -t\Big\langle \frac{q_n}{k^{(i)}}\Big\rangle, \tag{4.23}$$

The accuracy of the set of transmission conditions depends on the smoothness of the functions to be integrated.

#### Three integration points

The transmission conditions can be improved by a more accurate integration which exploits the division of the thin interphase into two sub-intervals. It is then natural to integrate with a two intervals trapezoidal rule

$$\begin{aligned}[\![q_n^{(i)}]\!] = {} & \frac{t_1}{2}\Big(Q(0,T_{A_1}^{(i)}) - \mathcal{D}_s\boldsymbol{q}|_{A_1} - g\, q_n^{(i)}|_{A_1}\Big) \\ & + \frac{t}{2}\Big(Q(t_1,T_{A_3}^{(i)}) - \mathcal{D}_s\boldsymbol{q}|_{A_3} - g\, q_n^{(i)}|_{A_3}\Big) + \frac{t_2}{2}\Big(Q(t,T_{A_2}^{(i)}) - \mathcal{D}_s\boldsymbol{q}|_{A_2} - g\, q_n^{(i)}|_{A_2}\Big),\end{aligned} \tag{4.24}$$

$$[\![T]\!] = -\left.\frac{t_1}{2}\,\frac{q_n^{(i)}}{k^{(i)}}\right|_{A_1} - \left.\frac{t}{2}\,\frac{q_n^{(i)}}{k^{(i)}}\right|_{A_3} - \left.\frac{t_2}{2}\,\frac{q_n^{(i)}}{k^{(i)}}\right|_{A_2}, \tag{4.25}$$

where the values of $T_{A_3}^{(i)}$ involved in (4.24) should be taken from the basic approximation (4.9) that is:

$$T_{A_3}^{(i)} = \frac{1}{2k_{A_1}^{(i)}k_{A_2}^{(i)}t}\left[k_{A_1}^{(i)}q_n^{(i)}|_{A_2}t_1t_2 - k_{A_2}^{(i)}q_n^{(i)}|_{A_1}t_1t_2 + 2k_{A_1}^{(i)}k_{A_2}^{(i)}(T_{A_1}^{(i)}t_2 + T_{A_2}^{(i)}t_1)\right], \tag{4.26}$$

while the eq. (4.10) is equivalent to eq. (4.25). The reason for this is very simple. Since our approximation lead to first order spline for the flux inside the interface, the respective integration is exact and coincides with the interpolation.

On the other hand, we can integrate each part of the interval separately to obtain:

$$q_n^{(i)}|_{A_3} - q_n^{(i)}|_{A_1} = \frac{t_1}{2}\Big(Q(0,T_{A_1}^{(i)}) - \mathcal{D}_s\boldsymbol{q}|_{A_1} - g\, q_n^{(i)}|_{A_1} + Q(t_1,T_{A_3}^{(i)}) - \mathcal{D}_s\boldsymbol{q}|_{A_3} - g\, q_n^{(i)}|_{A_3}\Big) \tag{4.27}$$

$$T^{(i)}_{A_3} - T^{(i)}_{A_1} = -\frac{t_1}{2}\left( \left.\frac{q_n^{(i)}}{k^{(i)}}\right|_{A_1} + \left.\frac{q_n^{(i)}}{k^{(i)}}\right|_{A_3}\right) \tag{4.28}$$

or

$$q_n^{(i)}|_{A_3} - q_n^{(i)}|_{A_2} = -\frac{t_2}{2}\Big(Q(0, T^{(i)}_{A_2}) - \mathcal{D}_s\boldsymbol{q}|_{A_2} - g\, q_n^{(i)}|_{A_2} + Q(t_1, T^{(i)}_{A_3}) - \mathcal{D}_s\boldsymbol{q}|_{A_3} - g\, q_n^{(i)}|_{A_3}\Big) \tag{4.29}$$

$$T^{(i)}_{A_3} - T^{(i)}_{A_2} = \frac{t_2}{2}\left( \left.\frac{q_n^{(i)}}{k^{(i)}}\right|_{A_2} + \left.\frac{q_n^{(i)}}{k^{(i)}}\right|_{A_3}\right) \tag{4.30}$$

Evidently, the sum of Eqns.(4.28) and (4.30) is identical to (4.25) and (4.26). Subtracting Eqn.(4.27) and (4.29) results in:

$$q_n^{(i)}|_{A_2} - q_n^{(i)}|_{A_1} = \frac{t_1}{2}\Big(Q - \mathcal{D}_s\boldsymbol{q} - g\, q_n^{(i)}\Big)|_{A_1} + \frac{t_2}{2}\Big(Q - \mathcal{D}_s\boldsymbol{q} - g\, q_n^{(i)}\Big)|_{A_2} + \frac{t_1 + t_2}{2}\Big(Q - \mathcal{D}_s\boldsymbol{q} - g\, q_n^{(i)}\Big)|_{A_3} \tag{4.31}$$

which is equivalent to (4.24).
Conversely, adding Eqn.(4.27) and (4.29) produces the following equation:

$$q_n^{(i)}|_{A_3} - \langle q_n\rangle = \frac{t_1}{4}\Big(Q - \mathcal{D}_s\boldsymbol{q} - g\, q_n^{(i)}\Big)|_{A_1} - \frac{t_2}{4}\Big(Q - \mathcal{D}_s\boldsymbol{q} - g\, q_n^{(i)}\Big)|_{A_2} + \frac{t_1 - t_2}{4}\Big(Q - \mathcal{D}_s\boldsymbol{q} - g\, q_n^{(i)}\Big)|_{A_3} \tag{4.32}$$

In case $t_1 = t_2$ equations (4.31) and (4.24) are identical, while (4.32) determines $q_n^{(i)}|_{A_3}$. Since $\mathcal{D}_s\boldsymbol{q}$ is the surface Laplacian term in the *tangential* direction, it can be assumed that it does not change dramatically along the normal direction. Thus,

$$\mathcal{D}_s\boldsymbol{q}|_{A_3} = \langle \mathcal{D}_s\boldsymbol{q}\rangle\,. \tag{4.33}$$

If we now assume the simplest possible choice for the middle point $t_1 = t_2 = t/2$ and we take into account the continuity of temperature and normal heat flux across the interfaces defined in (4.12), the transmission conditions take the form

$$[\![q_n^{(i)}]\!] = \frac{t}{2}\left(\langle Q\rangle + Q\left(\frac{t}{2}, T^{(i)}_{A_3}\right) - 2\langle \mathcal{D}_s\boldsymbol{q}\rangle\right) - \frac{t}{2}\left(\left\langle g\, q_n^{(i)}\right\rangle + (g\, q_n^{(i)})|_{A_3}\right), \tag{4.34}$$

$$[\![T^{(i)}]\!] = -\frac{t}{2}\left\langle \frac{q_n^{(i)}}{k^{(i)}}\right\rangle - \frac{t}{2}\frac{1}{k^{(i)}_{A_3}} q_n^{(i)}|_{A_3}, \tag{4.35}$$

where

$$k^{(i)}_{A_j} = k^{(i)}(A_j, T^{(i)}(A_j)), \quad j = 1, 2, 3, \tag{4.36}$$

and the values of $T^{(i)}_{A_3}$ and $q_n^{(i)}|_{A_3}$ used in the transmission conditions should be computed from the relationships:

$$q_n^{(i)}|_{A_3} = \langle q_n\rangle - \frac{t}{8}\Big([\![Q]\!] - [\![\mathcal{D}_s\boldsymbol{q}]\!] - [\![g\, q_n^{(i)}]\!]\Big) \tag{4.37}$$

$$T_{A_3}^{(i)} = \left\langle T^{(i)} \right\rangle + \frac{t}{8}\left[\!\left[ \frac{q_n^{(i)}}{k^{(i)}} \right]\!\right], \tag{4.38}$$

Invoking the identities defined in (2.117) (4.34) can be re-written equivalently as:

$$\left\{1 + \frac{t}{8}\left(\llbracket g \rrbracket + \frac{t}{2} g|_{A_3}\langle g\rangle\right)\right\}\llbracket q_n^{(i)}\rrbracket + \frac{t}{2}\left\{\langle g\rangle + g|_{A_3}\left(1 + \frac{t}{8}\llbracket g\rrbracket\right)\right\}\langle q_n^{(i)}\rangle = \frac{t}{2}\left\{\langle Q\rangle + Q\left(\frac{t}{2}, T_{A_3}^{(i)}\right) - 2\langle \mathcal{D}_s \boldsymbol{q}\rangle\right\} + \frac{t^2}{16} g|_{A_3}\Big(\llbracket Q\rrbracket - \llbracket \mathcal{D}_s \boldsymbol{q}\rrbracket\Big). \tag{4.39}$$

and

$$q_n^{(i)}|_{A_3} = \left\langle q_n^{(i)} \right\rangle - \frac{t}{8}\left(\llbracket Q\rrbracket - \llbracket \mathcal{D}_s \boldsymbol{q}\rrbracket - \langle g\rangle\llbracket q_n^{(i)}\rrbracket - \llbracket g\rrbracket\langle q_n^{(i)}\rangle\right). \tag{4.40}$$

This is equivalent to Eqns. (4.34) and (4.37).

For interphase situated between two plates we have $g = 0$, and the latter transforms to

$$\llbracket q_n^{(i)}\rrbracket = \frac{t}{2}\left(\langle Q\rangle + Q\left(\frac{t}{2}, T_{A_3}^{(i)}\right) - 2\langle \mathcal{D}_s \boldsymbol{q}\rangle\right), \quad q_n^{(i)}|_{A_3} = \left\langle q_n^{(i)} \right\rangle - \frac{t}{8}\left(\llbracket Q\rrbracket - \llbracket \mathcal{D}_s \boldsymbol{q}\rrbracket\right). \tag{4.41}$$

### 4.2.2 Transmission conditions for the second integration scheme

One can use Trapezoidal rule to integrate equation (4.18) instead of the equivalent equation (4.17). They are equivalent, but the final result will be slightly different as the same trapezoidal integration rule provides another approximation.

Here, as we can see from Eqn.(4.18), the geometric curvature term $g$ does not appear explicitly in the equation, so one may assume that the curvature does not play any role in the transmission conditions; however, as we will see the upcoming derivations, the curvature is involved, albeit indirectly, and thus, we arrive at a different form of transmission conditions than the ones seen in the preceding section.

#### Two integration points

Integrating (4.18) (instead of the equivalent equation (4.17)) and (4.21) from 0 to $t$ using the trapezoidal rule gives

$$\llbracket h_2 h_3 q_n^{(i)}\rrbracket = t\left\langle h_2 h_3\Big(Q - \mathcal{D}_s \boldsymbol{q}\Big)\right\rangle. \tag{4.42}$$

Again, implementing the identities defined in (2.117) here, the above equation be rewritten equivalently as:

$$\llbracket q_n\rrbracket + \beta\langle q_n\rangle = t\left\{\langle Q - \mathcal{D}_s \boldsymbol{q}\rangle + \frac{1}{4}\beta\,\llbracket Q - \mathcal{D}_s \boldsymbol{q}\rrbracket\right\} \tag{4.43}$$

where $\beta$ is the parameter defined in (2.118) as

$$\beta(t, \alpha_1, \alpha_2) = \frac{\llbracket h_2 h_3\rrbracket}{\langle h_2 h_3\rangle}, \quad -2 \le \beta \le 2. \tag{4.44}$$

Note that the second transmission condition, that is, $\llbracket T\rrbracket$, defined by Eqn.(4.23) remains the same.

**Three integration points**

Similar to the procedure

$$[\![h_2h_3q_n^{(i)}]\!] = \frac{t_1}{2}\, h_2h_3|_{A_1}\Big(Q(0,T_{A_1}^{(i)}) - \mathcal{D}_s\boldsymbol{q}|_{A_1}\Big) + \frac{t}{2}\, h_2h_3|_{A_3}\Big(Q(t_1,T_{A_3}^{(i)}) - \mathcal{D}_s\boldsymbol{q}|_{A_3}\Big) + \frac{t_2}{2}\, h_2h_3|_{A_2}\Big(Q(t,T_{A_2}^{(i)}) - \mathcal{D}_s\boldsymbol{q}|_{A_2}\Big) \quad (4.45)$$

while integrating separately within the two smaller interval we obtain:

$$h_2\, h_3|_{A_3} q_n^{(i)}|_{A_3} - h_2\, h_3|_{A_1} q_n^{(i)}|_{A_1} = \frac{t_1}{2}\Big\{h_2\, h_3|_{A_1}\Big(Q(0,T_{A_1}^{(i)}) - \mathcal{D}_s\boldsymbol{q}|_{A_1}\Big)\Big\} + \frac{t_1}{2}\Big\{h_2\, h_3|_{A_3}\Big(Q(t_1,T_{A_3}^{(i)}) - \mathcal{D}_s\boldsymbol{q}|_{A_3}\Big)\Big\} \quad (4.46)$$

and

$$h_2\, h_3|_{A_3} q_n^{(i)}|_{A_3} - h_2\, h_3|_{A_2} q_n^{(i)}|_{A_2} = -\frac{t_2}{2}\Big\{h_2h_3|_{A_2}\Big(Q(t,T_{A_2}^{(i)}) - \mathcal{D}_s\boldsymbol{q}|_{A_2}\Big)\Big\} - \frac{t_2}{2}\Big\{h_2h_3|_{A_3}\Big(Q(t_1,T_{A_3}^{(i)}) - \mathcal{D}_s\boldsymbol{q}|_{A_3}\Big)\Big\} \quad (4.47)$$

Subtracting Eqns.(4.47) from (4.46), we obtain Eqn.(4.45). On the other hand, summing Eqns.(4.47) and (4.46), we have:

$$h_2h_3|_{A_3}\, q_n^{(i)}|_{A_3} - \langle h_2h_3\, q_n^{(i)}\rangle = \frac{t_1}{4}\, h_2h_3|_{A_1}\Big(Q(0,T_{A_1}^{(i)}) - \mathcal{D}_s\boldsymbol{q}|_{A_1}\Big) - \frac{t_2}{4}\, h_2h_3|_{A_2}\Big(Q(t,T_{A_2}^{(i)}) - \mathcal{D}_s\boldsymbol{q}|_{A_2}\Big) + \frac{t_1-t_2}{4}\, h_2h_3|_{A_3}\Big(Q(t_1,T_{A_3}^{(i)}) - \mathcal{D}_s\boldsymbol{q}|_{A_3}\Big)\Big) \quad (4.48)$$

Assuming $t_1 = t_2 = t/2$ we can rewrite (4.48) and (4.45) as

$$h_2h_3|_{A_3}\, q_n^{(i)}|_{A_3} = \langle h_2h_3\, q_n^{(i)}\rangle + \frac{t}{8}\, h_2h_3|_{A_1}\Big(Q(0,T_{A_1}^{(i)}) - \mathcal{D}_s\boldsymbol{q}|_{A_1}\Big) - \frac{t}{8}\, h_2h_3|_{A_2}\Big(Q(t,T_{A_2}^{(i)}) - \mathcal{D}_s\boldsymbol{q}|_{A_2}\Big)$$

and

$$[\![h_2h_3\, q_n^{(i)}]\!] = \frac{t}{4}\, h_2h_3|_{A_1}\Big(Q(0,T_{A_1}^{(i)}) - \mathcal{D}_s\boldsymbol{q}|_{A_1}\Big) + \frac{t}{2}\, h_2h_3|_{A_3}\Big(Q(t/2,T_{A_3}^{(i)}) - \mathcal{D}_s\boldsymbol{q}|_{A_3}\Big) + \frac{t}{4}\, h_2h_3|_{A_2}\Big(Q(t,T_{A_2}^{(i)}) - \mathcal{D}_s\boldsymbol{q}|_{A_2}\Big)$$

Using (2.117) and (4.33), we arrive at:

$$[\![q_n^{(i)}]\!] = \frac{t}{2}\Big[\langle Q - \mathcal{D}_s\boldsymbol{q}\rangle + \frac{1}{4}\,\beta\,[\![Q - \mathcal{D}_s\boldsymbol{q}]\!] + \gamma\Big(Q(t/2,T_{A_3}^{(i)}) - \langle\mathcal{D}_s\boldsymbol{q}\rangle\Big)\Big] - \beta\,\langle q_n^{(i)}\rangle \quad (4.49)$$

and

$$q_n^{(i)}|_{A_3} = \frac{1}{\gamma}\left(\langle q_n^{(i)}\rangle + \frac{\beta}{4}[\![q_n^{(i)}]\!] - \frac{t}{8}\Big(\beta\langle Q - \mathcal{D}_s\boldsymbol{q}\rangle + [\![Q - \mathcal{D}_s\boldsymbol{q}]\!]\Big)\right) \quad (4.50)$$

where we have $\gamma$ defined in (2.119) introduced as:

$$\gamma(t,\alpha_1,\alpha_2) = \frac{h_2h_3|_{A_3}}{\langle h_2h_3\rangle} \tag{4.51}$$

Together with the set of Eqns.(4.35) and (4.38) for temperature, Eqns.(4.49) and (4.50) represent the entire set of transmission conditions when other form, that is, Eqn.(4.18) is integrated within the interphase.

### 4.2.3 Comparison of the transmission conditions

To compare those two slightly different representations of the transmission conditions, we need to have a link between the parameters $\beta$, $\gamma$, and the values of the function $g$ defined in (4.20), where

$$\beta = \frac{[\![h_2h_3]\!]}{\langle h_2h_3\rangle} = O(t), \quad \gamma = \frac{(h_2h_3)_{A_3}}{\langle h_2h_3\rangle} = 1 + O(t^2), \quad g(\xi) = \frac{1}{h_2h_3(\xi)}\left.\frac{\partial h_2h_3}{\partial n}\right|_{\xi}, \quad t \ll 1, \tag{4.52}$$

Using a forward and backward second-order approximation of the first derivative:

$$\left.\frac{\partial h_2h_3}{\partial n}\right|_{\xi=0} = \frac{1}{t}\Big\{4h_2h_3(t/2) - h_2h_3(t) - 3h_2h_3(0)\Big\} + O(t^2), \tag{4.53}$$

$$\left.\frac{\partial h_2h_3}{\partial n}\right|_{\xi=t} = \frac{1}{t}\Big\{3h_2h_3(t) - 4h_2h_3(t/2) + h_2h_3(0)\Big\} + O(t^2), \tag{4.54}$$

This gives

$$\begin{aligned}[\![g]\!] &= \frac{1}{t}\left\{6 + \frac{h_2h_3(0)}{h_2h_3(t)} + \frac{h_2h_3(t)}{h_2h_3(0)} - 4h_2h_3(t/2)\frac{h_2h_3(0)+h_2h_3(t)}{h_2h_3(0)h_2h_3(t)}\right\} + O(t^2) = \\ &= \frac{4}{t}\frac{8(1-\gamma)-\beta^2}{4-\beta^2} + O(t^2),\end{aligned} \tag{4.55}$$

$$\begin{aligned}\langle g\rangle &= \frac{1}{2t}\left\{\frac{h_2h_3(0)}{h_2h_3(t)} - \frac{h_2h_3(t)}{h_2h_3(0)} + 4h_2h_3(t/2)\frac{h_2h_3(t)-h_2h_3(0)}{h_2h_3(0)h_2h_3(t)}\right\} + O(t^2) = \\ &= \frac{4\beta}{t}\frac{2\gamma-1}{4-\beta^2} + O(t^2),\end{aligned} \tag{4.56}$$

Using the first order approximation for the derivative we obtain:

$$g_{A_1} = \frac{2}{t}\frac{\beta+2(\gamma-1)}{2-\beta}, \quad g_{A_2} = \frac{2}{t}\frac{\beta-2(\gamma-1)}{2+\beta}, \quad g_{A_3} = \frac{\beta}{\gamma t}, \tag{4.57}$$

Note that $g_{A_1} = g(t,\alpha_1,\alpha_2)|_{A_1}$. In turn, this allows us to compute the jump and the average:

$$[\![g]\!] = -\frac{4}{t}\frac{\beta^2+4(\gamma-1)}{4-\beta^2}, \quad \langle g\rangle = \frac{4\beta\gamma}{t(4-\beta^2)}. \tag{4.58}$$

It is also natural to assume that, for sufficiently smooth surfaces, the thickness is the dominating small parameter. Then, the following estimate can be posed:

$$\gamma(t) = 1 + \gamma_2 t^2 + O(t^4), \quad \beta(t) = \beta_1 t + O(t^3), \quad t \ll 1, \tag{4.59}$$

where

$$\gamma_2 = \gamma_2(\alpha_2,\alpha_3), \quad \beta_1 = \beta_1(\alpha_2,\alpha_3).$$

This brings us to the following estimate:

$$[\![g]\!] = -t\Big(4\gamma_2 + \beta_1^2 + O(t^2)\Big), \quad \langle g\rangle \text{ and } g|_{A_3} = \beta_1 + O(t^2), \quad t \ll 1. \tag{4.60}$$

Note that the average and the value in the middle point differ at the order of $O(t^2)$ for any reasonable surfaces. At the midpoint of the interphase, $\gamma_2$ is equal to zero for most of the cases. This allows us to suggest for comparison to use the following relationships between the parameters

$$\langle g\rangle = g_{A_3} = \mathcal{B}_0(t), \quad [\![g]\!] = -t\,\mathcal{B}_0^2(t), \quad \mathcal{B}_0(t) = \frac{\beta(t)}{t} = \beta_1 + O(t^2), \quad t \ll 1. \tag{4.61}$$

where the first estimate is valid with an accuracy of $O(t^2)$ as $t \ll 1$.

Substituting these estimations into the transmission condition obtained by the first integration approach, (equations (4.39) and (4.40)), we have

$$\left(1 - \frac{t^2}{16}\beta_1^2\right)[\![q_n^{(i)}]\!] + \beta_1 t\left(1 - \frac{t^2}{16}\beta_1\right)\langle q_n^{(i)}\rangle = \frac{t}{2}\left\{\langle Q\rangle + Q\left(\frac{t}{2}, T_{A_3}^{(i)}\right) - 2\langle \mathcal{D}_s \boldsymbol{q}\rangle\right\} + \frac{t^2}{16}\beta_1\Big([\![Q]\!] - [\![\mathcal{D}_s \boldsymbol{q}]\!]\Big) \tag{4.62}$$

and

$$q_n^{(i)}|_{A_3} = \left\langle q_n^{(i)}\right\rangle - \frac{t}{8}\left([\![Q]\!] - [\![\mathcal{D}_s \boldsymbol{q}]\!] - \beta_1[\![q_n^{(i)}]\!] - (-t\beta_1^2)\langle q_n^{(i)}\rangle\right). \tag{4.63}$$

Since $t \ll 1$, higher order terms can be neglected in the equation above, to arrive at the following form:

$$[\![q_n^{(i)}]\!] + \beta(t)\langle q_n^{(i)}\rangle = \frac{t}{2}\left\{\langle Q\rangle + Q\left(\frac{t}{2}, T_{A_3}^{(i)}\right) - 2\langle \mathcal{D}_s \boldsymbol{q}\rangle\right\} \tag{4.64}$$

and

$$q_n^{(i)}|_{A_3} = \left\langle q_n^{(i)}\right\rangle + \frac{\beta(t)}{8}\langle q_n^{(i)}\rangle - \frac{t}{8}\left\{[\![Q - \mathcal{D}_s \boldsymbol{q}]\!]\right\} \tag{4.65}$$

while the transmission conditions set for Second integration scheme (eqn.(4.49) and (4.50))is as follows:

$$[\![q_n^{(i)}]\!] + \beta(t)\langle q_n^{(i)}\rangle = \frac{t}{2}\left\{\langle Q\rangle + Q\left(\frac{t}{2}, T_{A_3}^{(i)}\right) - 2\langle \mathcal{D}_s \boldsymbol{q}\rangle + \frac{\beta(t)}{4}\Big([\![Q]\!] - [\![\mathcal{D}_s \boldsymbol{q}]\!]\Big)\right\} \tag{4.66}$$

and

$$q_n^{(i)}|_{A_3} = \frac{1}{\gamma(t)}\left\{\langle q_n^{(i)}\rangle + \frac{\beta(t)}{4}[\![q_n^{(i)}]\!] - \frac{t}{8}\Big(\beta(t)\langle Q - \mathcal{D}_s \boldsymbol{q}\rangle + [\![Q]\!] - [\![\mathcal{D}_s \boldsymbol{q}]\!]\Big)\right\} \tag{4.67}$$

which, after neglecting the $O(t^2)$ terms, can be re-written as

$$[\![q_n^{(i)}]\!] + \beta(t)\langle q_n^{(i)}\rangle = \frac{t}{2}\left\{\langle Q\rangle + Q\left(\frac{t}{2}, T_{A_3}^{(i)}\right) - 2\langle \mathcal{D}_s \boldsymbol{q}\rangle\right\} \tag{4.68}$$

and

$$q_n^{(i)}|_{A_3} = \langle q_n^{(i)}\rangle + \frac{\beta(t)}{4}[\![q_n^{(i)}]\!] - \frac{t}{8}\left\{[\![Q - \mathcal{D}_s \boldsymbol{q}]\!]\right\} \tag{4.69}$$

which is same as Eqns.(4.64) for jump of normal heat flux, while Eqn.(4.65) and (4.69) would differ slightly for the heat flux value at point $A_3$. Thus, for a thin interphase, the proposed two schemes (First and Second) using three points of integration are equivalent.

## 4.3 Overview of models in literature.

The existing models in literature for thin interphases are redefined below by including the volumetric heat source term $Q$. A comparison between these models and the approaches proposed in this paper will be presented in Sec.4.4 using illustrative examples.

- One-Point Schemes: These refer to the approaches based on Taylor series expansion around one point only, either $A_1$ or $A_2$ on the interface boundary.
  - Miloh and Y.Benveniste (1999b): In this work, the authors have implemented Taylor series expansion around point $A_1$ only to derive separate transmission conditions for a low and a high conductive interphase respectively.
    - Low-Conductive interface: For a thermally resistive interphase, the heat flux is continuous across the interface boundary, while the jump in temperature is computed as:

$$[\![T]\!] = t\left\{-\frac{q_n^{(1)}}{k^{(i)}}\right\}_{A_1} = t\left\{\frac{k^{(1)}}{k^{(i)}}\frac{\partial T^{(1)}}{\partial n}\right\}_{A_1} = t\left\{\frac{k^{(2)}}{k^{(i)}}\frac{\partial T^{(2)}}{\partial n}\right\}_{A_1} \tag{4.70}$$

$$[\![q_n]\!] = 0. \tag{4.71}$$

    - High-Conductive interface: For a highly conductive interphase, the temperature is continuous across the interface boundary, while the flux accumulation is given as:

$$[\![T]\!] = 0, \tag{4.72}$$

$$[\![q_n]\!] = t\left\{Q - \mathcal{D}_s\boldsymbol{q}\right\}_{A_1} = t\left\{Q - \mathcal{D}_s\boldsymbol{q}\right\}_{A_2} \tag{4.73}$$

    - General case: Since the original formulation did not account for the effect of heat sources present inside the interphase, a more generalized form using (4.70) and (4.73) has been implemented in this work.

$$[\![T]\!] = t\left\{-\frac{q_n^{(1)}}{k^{(i)}}\right\}_{A_1} \tag{4.74}$$

$$[\![q_n]\!] = t\left\{Q - \mathcal{D}_s\boldsymbol{q}\right\}_{A_1} \tag{4.75}$$

      The validity of this implementation is proved in Fig.4.3 for three different values of heat source magnitudes.
  - Hashin (2001): One of the main highlights of this paper was the simple yet effective model obtained from the asymptotic Taylor series expansion around point $A_1$ of the temperature field and the normal component of the heat flux for a wide range of thermal conductivity of interphase, but limited to a thin interphase. The accuracy of the model decreases with increasing the interphase thickness. The model is recapped here, with the inclusion of heat source term. The significance of this model was the modification of the transmission condition for the normal heat flux component of Miloh and Y.Benveniste, 1999b, to include the curvature term.

$$[\![T]\!] = t\left\{-\frac{q_n^{(1)}}{k^{(i)}}\right\}_{A_1} = t\left\{\frac{k^{(1)}}{k^{(i)}}\frac{\partial T^{(1)}}{\partial n}\right\}_{A_1}, \tag{4.76}$$

$$[\![q_n]\!] = t\left\{Q - \mathcal{D}_s\boldsymbol{q} - gq_n^{(i)}\right\}_{A_1} \tag{4.77}$$

- Two-Point Schemes: These refer to the approaches based on Taylor series expansion around both points $A_1$ and $A_2$ on the interface boundary, thus increasing the accuracy of the transmission conditions by estimating fields from both sides of the interphase.

  – Benveniste (2006b): Benveniste provided a simplified and a generalized form of BÖvik, 1994 method, of using Taylor series expansion around two points situated on either boundary of the interphase to arrive at the following transmission conditions for the jumps in temperature and heat flux. Thus, the resulting equation comprised of approximated field variables, and the surface differentials along the curve, in the vicinity of the interphase from two points, point $A_1$ situated on the boundary between the interphase and media "1" and from point $A_2$ which is located on the boundary between the interphase and media "2". Since the model was derived in anisotropic setting, it is assumed that the thermal conductivities are of the same order as that of the surrounding media, and for any bounded conductivities of material 1 ($k^{(1)}$) and material 2 ($k^{(2)}$), the thermal conductivity of the interphase $k^{(i)}$ is $k^{(i)} \ll (k^{(1)}, k^{(2)})$, or conversely, $k^{(i)} \gg (k^{(1)}, k^{(2)})$.

$$[\![T]\!] = \frac{t}{2}\left\{\left(\frac{1}{k^{(2)}} - \frac{1}{k^{(i)}}\right) q_n^{(2)}|_{A_2} + \left(\frac{1}{k^{(1)}} - \frac{1}{k^{(i)}}\right) q_n^{(1)}|_{A_1}\right\} \tag{4.78}$$

$$[\![q_n]\!] = t\left\{\langle Q\rangle - \left\langle \left(1 - \frac{k^{(j)}}{k^{(i)}}\right) \mathcal{D}_s \boldsymbol{q}\right\rangle\right\} \quad ; \quad j = \{1, 2\} \tag{4.79}$$

  – D. Andreeva et al:

    * Low-Conductive interface Andreeva, Miszuris, and Zagnetko, 2016 $\left(k^{(i)} \ll k_{A_1}^{(1)}, \; k^{(i)} \ll k_{A_2}^{(2)}\right)$: The study focuses on development of transmission conditions using non-linear material properties, and thus, the jumps in temperature and heat flux are defined as:

$$[\![q_n]\!] = t\int_{A_1}^{A_2} Q d\xi, \tag{4.80}$$

$$[\![T]\!] = -\left\langle q_n^{(i)}\right\rangle \int_{A_1}^{A_2} \frac{d\xi}{k^{(i)}} - \frac{1}{2}\int_{A_1}^{A_2}\left(\int_{A_1}^{\xi} Q dx + \int_{A_2}^{\xi} Q dx\right)\frac{d\xi}{k^{(i)}} \tag{4.81}$$

    where $k^{(i)} = k^{(i)}(z, T(z), \cdot)$, $Q = Q(z, T(z), \cdot)$, where $z$ is the direction perpendicular to the interface, and $\cdot$ indicates a dependence on the tangential variables.
    If, however, conductivity and the source both do not depend on the temperature ($k^{(i)} = k^{(i)}(z, \cdot)$, $Q = Q(z, \cdot)$), the conditions become linear.
    Next using 2 points integration scheme for equations (4.80) and (4.81) we have

$$[\![q_n]\!] = t\langle Q - \mathcal{D}_s \boldsymbol{q}\rangle, \tag{4.82}$$

$$[\![T]\!] = -t\left\langle q_n^{(i)}\right\rangle \left\langle \frac{1}{k^{(i)}}\right\rangle - \frac{t^2}{4}\left[\!\left[\frac{1}{k^{(i)}}\right]\!\right]\langle Q - \mathcal{D}_s \boldsymbol{q}\rangle \tag{4.83}$$

    Here we have taken into account that the derivation in Mishuris can easy include the remaining term (to write $Q - \mathcal{D}_s\boldsymbol{q}$ instead of $Q$, see for example (4.17)). Finally, note that the second condition can be rewritten in the form

$$[\![T]\!] = -t\left\langle q_n^{(i)}\right\rangle \left\langle \frac{1}{k^{(i)}}\right\rangle - \frac{t}{4}\left[\!\left[\frac{1}{k^{(i)}}\right]\!\right][\![q_n]\!] = -t\left\langle \frac{q_n^{(i)}}{k^{(i)}}\right\rangle \tag{4.84}$$

* High-Conductive interface Andreeva and Miszuris, 2018: For a highly conductive interphase, the derived conditions have similar form as in the Benveniste-Miloh Eqn.(4.72), (4.73) but in this case, the approximation is taken from both boundaries of the interphase. The simplified form of the equations can be written assuming that the material properties inside the interphase does not change:

$$[\![T]\!] = 0, \tag{4.85}$$

$$[\![q_n]\!] = t \int_{A_1}^{A_2} (Q - \mathcal{D}_s \boldsymbol{q}) d\xi, \tag{4.86}$$

In case of the two point integration coincides with (4.82).

* General case: For the boundary value problems considered in the next section, the following general case of jump conditions are used following the same approach as suggested above for the case of Miloh and Y.Benveniste, 1999a.

$$[\![T]\!] = -t \left\langle \frac{q_n^{(i)}}{k^{(i)}} \right\rangle \tag{4.87}$$

$$[\![q_n]\!] = t \int_{A_1}^{A_2} (Q - \mathcal{D}_s \boldsymbol{q}) d\xi, \tag{4.88}$$

The validity of this implementation is proved in Fig.4.3 for three different values of heat source magnitude.

– Han et al., 2021; Baranova et al., 2020: The work focuses on the Boundary Element Method (BEM) implementation of transmission conditions that are modified form of Benveniste, 2006b described by second-order differential operators and utilizing the *curvature correction factor* $\mathcal{F}_p$, where $p$ represents the materials $1, 2$ and the interphase $i$. The interphase is assumed to be isotropic, homogeneous with no heat source present inside the interphase.

$$[\![T]\!] = -\frac{t}{2}\left(\frac{1}{k^{(i)}}\mathcal{F}_2^{-1} - \frac{1}{k^{(2)}}\right) q_n^{(2)}|_{A_2} + \frac{t}{2}\left(\frac{1}{k^{(i)}}\mathcal{F}_1^{-1} - \frac{1}{k^{(1)}}\right) q_n^{(1)}|_{A_1} \tag{4.89}$$

$$[\![q_n]\!] = \frac{t}{2}\left\{\left(Q(0, T_{A_1}^{(i)}) + Q(t, T_{A_2}^{(i)})\right)\right\} - \frac{t}{2}\left\{\left(\frac{1}{\mathcal{F}_2} - \frac{k^{(2)}}{k^{(i)}})\right) \mathcal{D}_s \boldsymbol{q}\Big|_{A_2} - \left(\frac{1}{\mathcal{F}_1} - \frac{k^{(1)}}{k^{(i)}})\right) \mathcal{D}_s \boldsymbol{q}\Big|_{A_1}\right\} \tag{4.90}$$

where the term $\mathcal{F}_p$ represents the metric coefficient of the curvilinear coordinate system, responsible for illustrating how curvature in a thin layer affects the diffusion along the curve (in tangential direction), and is expressed as:

$$\mathcal{F}_p(s_0) = \begin{cases} 1, & p = i \\ 1 + (-1)^p \dfrac{t}{2}\kappa_0(s_0), & p = \{1, 2\} \end{cases} \tag{4.91}$$

where $\kappa_0(s_0) = 1/R_0(s_0)$ is the local curvature of the curve $\Gamma$ parametrized by its arc length $s_0$. If $\mathcal{F}_p = 1$ (as in the case of flat interphase, 4.4.1), then conditions 4.89 and (4.90) are the same as those of Benveniste's, (4.78) and (4.79).

Comparison of the two-point schemes with our proposed models highlights the presence of the geometric curvature term $g$, in transmission conditions obtained through First Integration Scheme.

As mentioned by Benveniste, 2006b in Appendix B, the Taylor series expansion was considered in the settings of Fig.2.4b as well to arrive at the final form of the transmission conditions in his paper, since the imperfect interface was assumed to be extension of material 1 and 2. This assumption is not valid in the present paper, thus, if the Taylor series expansion is neglected in the imperfect interface settings, the transmission conditions then obtained (for both Benveniste, 2006b and Han et al., 2021) are equivalent to (4.23) and (4.22) of the First Integration Scheme. If the approximations are considered from one side of the interphase boundaries only (either $A_1$ or $A_2$), then the conditions outlined in Hashin, 2001 are recovered.

In the cases of Benveniste, 2006b,Benveniste, 2006c, and Han et al., 2021,Baranova et al., 2020, the transmission conditions are derived based on the underlying assumption that the perfect interphase is replaced by extending the materials 1 and 2, up to the interface $\Gamma$, and thus the resulting conditions contain only the material properties of the replaced interphase, as well as the surrounding media. Because of this assumption, the term

$$\mathcal{P}_s(q_n)_\Gamma = -g = \frac{1}{R}$$

becomes zero. For our proposed methods, we have replaced the interphase with an appropriate surface of zero-thickness. Thus, our proposed schemes contain not only the material properties ($\mathcal{D}_s\boldsymbol{q}$ terms), but the geometric data ($g$) of the interphase (taken at midpoint $A_3$), as well as the material properties of the three domains.

## 4.4 Results and Discussion

The boundary value problem of perturbative effect of a coated interphase embedded in an otherwise homogeneous medium is studied in settings of three different geometries of the interphase:

1. Flat interphase demonstrating the behaviour of transmission conditions in the presence of heat source only.

2. Coated circular inclusion, emphasizing the impact of the presence of surface differentials on the transmission conditions and

3. A wavy interphase of varying oscillations in radial direction, highlighting the impact of rapidly varying curvature on the transmission conditions .

It must be noted that for each case:

- The interphase has properties different from that of the surrounding material, its thermal conductivity is denoted as $k_i \neq (k_1, k_2)$, where $k_1$ and $k_2$ are the thermal conductivities of the inclusion and surrounding matrix, respectively, and may or may not be similar. For all the three cases considered below, we take $k_1 = 10.0\ W/m.K$ an $k_2 = 1.0\ W/m.K$, thus taking the inclusion to be more conductive than the matrix.

- The heat source $Q(x)$, as defined in Eqn.(4.11), is taken to be linear ($\alpha = 1$) and is positioned asymmetrically toward the inner boundary of the interphase. However, it is located sufficiently far from the edge to avoid introducing edge effects into the analysis.

Each case is discussed with an emphasis on how the geometric variations influence the outcomes. The findings are compared with the existing literature to highlight the accuracy of the proposed models. The following subsections present the results for each geometry case, highlighting the accuracy of the methods with increasing curvature and presence of the heat source.

The results are presented in terms of dimensionless parameter $\epsilon \ll 1$, which is defined as $\epsilon = t/L$ (or R in case of circular and non-circular interphase). For the case of flat interphase and circular coated inclusion, the analytical solutions exists while the non-circular interphase case is solved by means of numerical methods.

It must also be noted that unless stated otherwise, all the results presented below for $[\![T]\!]$ and $[\![q_n]\!]$ in the case of circular and non-circular interphases are presented for $\theta = 0\,\text{deg}$.

For each case, the absolute errors $\Delta$ are presented alongside the jumps in temperature and heat fluxes, which are computed as:

$$\Delta_T = \left| \frac{[\![T]\!]_{exact} - [\![T]\!]_{imperf}}{T^*} \right| \quad ; \quad \Delta_{q_n} = \left| \frac{[\![q_n]\!]_{exact} - [\![q_n]\!]_{imperf}}{q_n^*} \right| \tag{4.92}$$

where $T^*$ and $q_n^* = -k^{(2)}\,\beta$ represent the temperature value and heat flux at the remote boundary. The ratio $k^{(i)}/k^{(2)}$ is shown on a logarithmic scale along the x-axis in all the graphs presented below.

**Quick comparison of the general conditions of Miloh & Benevniste, and Andreeva, including the heat source term.**

Before proceeding with the analysis of the individual geometric cases, a quick validation of general cases of Miloh and Y.Benveniste, 1999a represented by (4.74), (4.75) as well as the general case of Andreeva, Miszuris, and Zagnetko, 2016, given by Eqns.(4.87) and (4.88) is made by including the effects of heat source inside the thin interphase. The three-phase solution, corresponding to jumps in temperature and heat flux across a perfect coated circular interphase are represented by the light green solid line. The generalized conditions (4.74), (4.75) are represented by orange dashed lines with star shaped markers, while the low ((4.70) and (4.71)) and high ((4.72),(4.73)) conductive interface jump conditions of Miloh and Y.Benveniste, 1999a are illustrated with dark green dashed line and solid light blue colored line respectively. For the conditions proposed by Andreeva et al, the plots of the original form of the equations are represented by solid magenta colored curve for low conductive((4.84),(4.82)) and with dashed red curve for high conductive ((4.84),(4.86)), while Dashed blue line with filled circle markers indicates the values plotted using the general case given by Eqns.(4.87) and (4.88). The results are presented for a case of circular inclusion having a coating whose thickness is characterized by $\epsilon$. The interphase conductivity varies from $\{10^{-8}$ to $10^{8}\}$, and the radius of inclusion is $a = 1$. The conductivities of the two materials is $k^{(1)}/k^{(2)} = 10$. The circular geometry is chosen as it takes into account the curvature and surface differentials along the surface.

The following three different cases of heat sources are considered:

- $Q_0 = 0\ \ W/m^3$: This represents the limiting case originally considered by Benveniste and Miloh. In the absence of volumetric heat sources within a circular coating of thickness $\epsilon = 0.05$, as illustrated in 4.3a and 4.3b, the generalized transmission conditions ((4.74) and (4.75)) Miloh and Y.Benveniste, 1999a coincide exactly with the low-conductivity ((4.70), (4.71)) and high-conductivity ((4.72), (4.73)) interface jump conditions. Likewise, the conditions proposed by Andreeva et al. for low-((4.83) and (4.82)) and high-conductivity ((4.85) and (4.86)) interphases are fully consistent

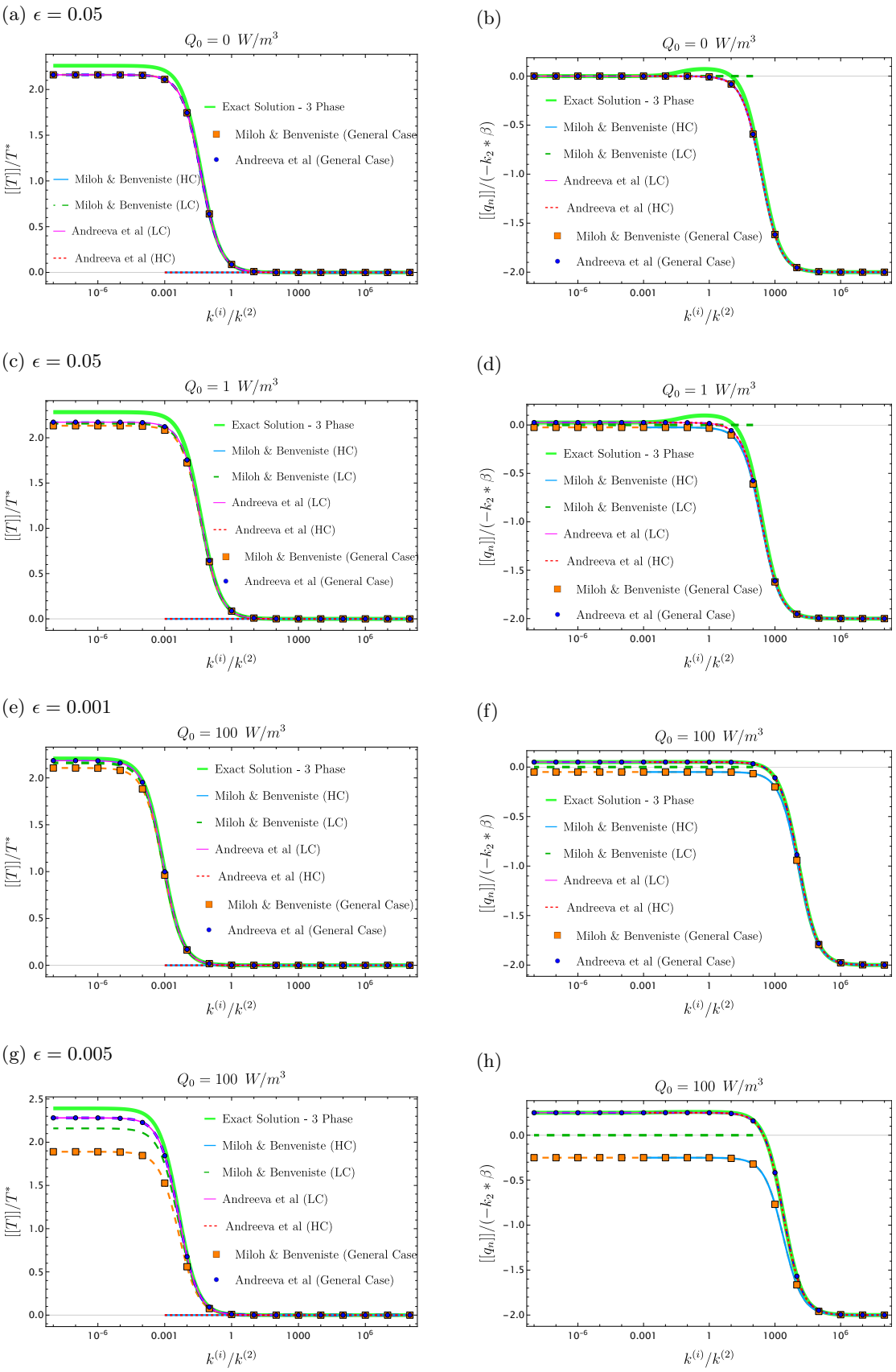


**Fig. 4.3.** Comparison of jumps conditions given by Benveniste-Miloh and Andreeva et al, for three increasing heat source magnitude $Q_0$: (4.3a, 4.3b) shows $[\![T]\!]$ and $[\![q_n]\!]$ for limiting case of $Q_0 = 0$, ie, no heat source inside the interphase (original formulation), (4.3c, 4.3d) shows $[\![T]\!]$ and $[\![q_n]\!]$ for the case of low heat source magnitude $Q_0 = 1$, and (4.3e, 4.3f and 4.3g, 4.3h) shows $[\![T]\!]$ and $[\![q_n]\!]$ for higher heat source consideration inside the interphase $Q_0 = 100$. *HC* stands for High conductive and *LC* stands for Low Conductive interphase and the thickness of the interphase is depicted by $\epsilon$.

with the general formulation ((4.87) and (4.88)) in this limiting regime. It should be emphasized that these transmission conditions do not coincide with the solution corresponding to a perfect interphase when the thickness of the interphase exceeds 0.001.

- $Q_0 = 1\ W/m^3$: When a volumetric heat source of a small magnitude, 1.0 $W/m^3$ is present inside the interphase of thickness $\epsilon = 0.05$, as illustrated in 4.3c, 4.3d, the error for the jumps in temperature between Eqn.(4.70) and general case (4.74) is of $\mathcal{O}(\epsilon)$, while in case of of jumps in normal heat flux component the error is less than $\mathcal{O}(\epsilon^2)$ for Miloh and Benveniste. For the case of Andreeva et al, it is observed that the jumps in temperature values changes with the introduction of heat source term, and at higher conductivity, (4.83) and (4.84) are almost similar, with maximum error between the two being $\mathcal{O}(\epsilon)$ at $k^{(i)}/k^{(2)} = k^{(1)}$ and decreases to $\mathcal{O}(\epsilon^2)$ with increasing conductivity beyond this point.

- $Q_0 = 100\ W/m^3$: When a higher volumetric heat source is considered to be present inside the interphase, the temperature curves begin to show a slight divergence. For a thin interphase of thickness $\epsilon = 0.001$, the temperature graph (4.3e) shows divergence between the generalized case and the actual formulation for temperature jumps in low conductive interphase. The absolute error between these equations is upto $10^{-2}$ for $k^{(i)}/k^{(2)} \leq 0.001$, and beyond these conductivity values, the error diminishes to $\ll \mathcal{O}(\epsilon^2)$. Moreover, once can easily see that the jumps in temperature obtained from the eqns.(4.70),(4.71) are constant for all values of interphase thickness and increasing heat source magnitudes, which contradicts the physics involved. This discrepancy arises from the fact that Miloh and Benveniste did not account for a volumetric heat source in their original formulation. Nevertheless, as is clearly observed, the presence of a heat source influences the temperature jump conditions and is manifested explicitly in their modified behavior. For jumps in normal component of heat flux, (4.3f) the absolute error between our assumed combined case, and (4.73), (4.72) is less than $\mathcal{O}(\epsilon^2)$ for increasing interphase conductivity values. For jumps in temperature, the error between (4.83) and (4.84) is always less than $\mathcal{O}(\epsilon)$.

Thus, it can safely assumed that taking the generalized case of opting (4.74) for temperature jumps and (4.75) for heat flux jumps for Miloh and Y.Benveniste, 1999a, and considering (4.87) and (4.88) for a generalized case of Andreeva, is valid for the above mentioned interphase thicknesses and heat source magnitudes.

A point of interest is the localized heat flux occurring in Figs.4.3b and 4.3d for $10^{-2} \leq k^{(i)}/k^{(2)} \leq 10^{1}$. For $k^{(i)}/k^{(2)} \leq 10^{-3}$, the interphase is highly resistive(also known as Kapitza resistance) and temperature along the normal direction accumulates at the boundaries of the interphase. This creates a jumps in temperature across the boundaries of the interphase, while heat flux is continuous ($[\![q_n]\!] = 0$).

As the thermal conductivity of the interphase increases and approaches that of the adherents, heat transfer into the interphase becomes progressively more efficient, and the interphase transitions from a strong thermal barrier to a partially conducting medium. In this regime, $[\![q_n]\!]$ increases slightly, although residual resistance still induces temperature accumulation within the interphase.

The heat flux distribution is further affected by the curvature term $g(\xi, \alpha_1, \alpha_3)$ resulting in unequal fluxes at the interphase boundaries, with higher values at the outer boundary (r=a+t). Depending on interphase thickness and internal heat generation (type of heat source: linear, quadratic, etc), the flux profile may be linear or nonlinear. For very thin

coatings ($\epsilon \leq 0.001$), curvature effects are negligible yielding a smooth distribution. In contrast, strong heat sources (e.g., $Q_0 = 100$) induce nonlinear flux profiles without boundary localization (Fig. 4.3f).

For $k^{(i)}/k^{(2)} = 1$, the interphase is thermally matched with the matrix, eliminating its barrier effect at the outer boundary (or point $A_2$), while a mild resistance persists at the inner boundary (at point $A_1$). Under these conditions, the jump in normal heat flux reaches its maximum, corresponding to peak values of localized heat accumulation within the interphase. As $k^{(i)}$ increases further to match the inclusion conductivity, heat transfer across the inner boundary becomes unhindered and temperature jumps vanish ($[\![T]\!] = 0$), reducing localization effects.

In the high-conductivity limit ($k^{(i)}/k^{(2)} \geq 10^3$), the interphase behaves as a highly conductive medium, allowing nearly unrestricted heat flow across both boundaries, and $[\![q_n]\!]$ approaches an asymptotic value.

### 4.4.1 Parallel Interphase

We will first consider a very simple example of a thin interphase, situated between two parallel plates, with a uni-directional heat flow. The geometry is defined in Cartesian coordinates, which implies that the geometric curvature $g$ the surface differential terms $\mathcal{D}_s \boldsymbol{q}$ become zero.

The main objective of presenting this example is to provide the estimation and comparison of accuracy of transmission conditions when only the heat source term inside the interphase comes into play, while the effect in the tangential direction and the curvature remain absent.

#### Problem Setup

Consider a steady state, one-dimensional geometry, as shown in Fig.4.4a. By steady state, we mean that the temperature, and thus the heat flux, are constant with time.

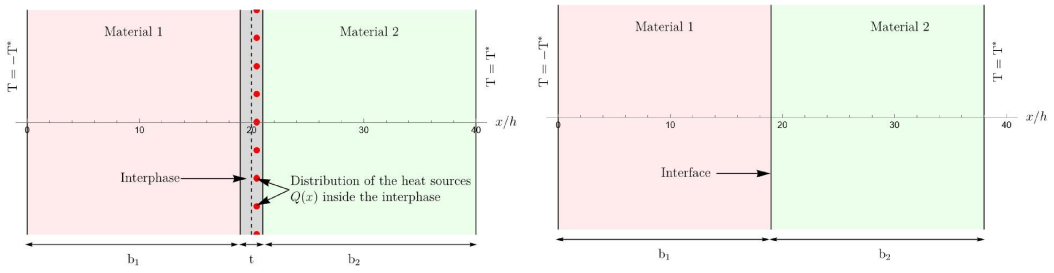


(a) 3 Phase representation. (b) 2 Phase representation.

**Fig. 4.4.** Perfect and Imperfect flat interphase between two materials with different thermal conductivity.

The scale factors for a Cartesian geometry as given as $h_1 = h_2 = h_3 = 1$. The heat sources are present only inside the interphase, while the material 1 and material 2 have steady state heat transfer through them, without any heat source. This is the problem of heat flow through plane walls, and the analytical solution for heat transfer through material 1 and 2 is obtained as follows. Consider the Balance equation (4.15) as given in Sec 4.2:

$$\operatorname{div} \boldsymbol{q} = 0 \tag{4.93}$$

$$\nabla^2 T = \frac{\partial^2 T}{\partial x^2} = 0 \tag{4.94}$$

where, the heat flux is related to the temperature gradient, through Fourier's law:

$$q = -k\frac{\partial T}{\partial x} \tag{4.95}$$

Equation (4.94) above can be integrated twice to obtain the temperature function.

$$T(x) = C_1 + C_2 x \tag{4.96}$$

Thus, the temperature profiles in material 1 and 2 are obtained by the following equations:

$$T^{(1)}(x) = A_1 + B_1 x \tag{4.97}$$

$$T^{(2)}(x) = A_2 + B_2 x \tag{4.98}$$

Now, for the temperature flow inside the interphase, we must take into account the heat source. Thus, the balance equation becomes the following.

$$\operatorname{div} \boldsymbol{q}^{(i)} = Q(x) \tag{4.99}$$

$$\nabla^2 T^{(i)} = \frac{\partial^2 T^{(i)}}{\partial x^2} = \frac{Q(x)}{k^{(i)}} \tag{4.100}$$

This is a non-homogeneous equation, which can be solved by implementing *Method of Variations* to find the Particular Integral of the equation. Then, the solution, which the equation of temperature inside the interphase can be given as:

$$T^{(i)}(x) = A_i + B_i x - \frac{h^2 Q_0}{k_i}\frac{1}{(\alpha+1)(\alpha+2)}\left(\frac{x+\zeta-b1-h}{h}\right)^{\alpha+2} \tag{4.101}$$

where, $A_1, B_1, A_2, B_2, A_i, B_i$ are constants. Within each domain - inclusion, interphase and the matrix - the equilibrium equation is respected. At the extreme ends of the geometry, remote temperature values are applied as:

$$T(x)\Big|_{x=0} = -T^* \quad ; \quad T(x)\Big|_{x=L} = T^* \tag{4.102}$$

Thus, the values of these constants can be solved for by enforcing the continuity conditions (4.12) across a perfect interphase. This provides the following temperature distributions within the domain of each material, in terms of thermal conductivity $k^{(i)}$, heat source magnitude $Q_0$ and thickness parameter $\epsilon$.

$$T^{(1)}(x) = \frac{\epsilon\,(1.82 - 0.015\,Q_0\,\epsilon\,x) + k^{(i)}\left[40 - 0.36\,x + 0.045\,Q_0\,\epsilon^2\,x + \epsilon\,(-1 - 1.82\,Q_0\,x)\right]}{-40\,k^{(i)} - 1.82\,\epsilon + k^{(i)}\epsilon} \tag{4.103}$$

$$T^{(2)}(x) = \frac{k^{(i)}\left[105.46 + Q_0\,\epsilon^2\,(1.82 - 0.046\,x) - 3.64\,x + \epsilon\,(1 - 72.7\,Q_0 + 1.82\,Q_0\,x)\right]}{-40\,k^{(i)} - 1.82\,\epsilon + k^{(i)}\epsilon} + \frac{\epsilon\,[Q_0\,\epsilon\,(0.76\,x - 30.3) - 1.82]}{-40\,k^{(i)} - 1.82\,\epsilon + k^{(i)}\epsilon} \tag{4.104}$$

$$T^{(i)}(x) = \frac{72.7 - 3.64\,x + Q_0\,\epsilon\left[413.64 + 0.26\,\epsilon^2 + 0.52\,\epsilon\,x - 2 - 20.68\,x\right]}{-40\,k^{(i)} - 1.82\,\epsilon + k^{(i)}\,\epsilon} +$$

$$\frac{Q_0\,\epsilon^2\,(5.3 - 0.12\,\epsilon - 0.27\,x)}{k^{(i)}\left(-40\,k^{(i)} - 1.82\,\epsilon + k^{(i)}\,\epsilon\right)} + \frac{k^{(i)}\left(32.7 - 0.02\,Q_0\epsilon^3 + 1.82\,Q_0\,\epsilon^2 - 36.4\,Q_0\epsilon + 0.82\,\epsilon\right)}{-40\,k^{(i)} - 1.82\,\epsilon + k^{(i)}\,\epsilon}$$

$$+ \frac{Q_0\epsilon^2\left[0.009\,\epsilon + k^{(i)}\,(0.21 - 0.005\,\epsilon)\right]}{k^{(i)}\left(-40\,k^{(i)} - 1.82\,\epsilon + k^{(i)}\,\epsilon\right)}\left(\frac{\epsilon + 4\,x - 80}{\epsilon}\right)^3 \tag{4.105}$$

The jumps in temperature and normal component of heat flux for a three-phase solution is the difference in the properties across the interphase thickness, that is, at points $A_2$ and $A_1$.

$$[\![T]\!] = T^{(i)}(b_1 + t)\Big|_{A_2} - T^{(i)}(b_1)\Big|_{A_1} \tag{4.106}$$

$$= \frac{k^{(i)}\,\epsilon\left(-3.64 + 0.37\,Q_0\,\epsilon^2 - 14.85\,Q_0\,\epsilon - 3.64\right) + 3.7\times 10^{-17}\,Q_0\,\epsilon^3}{k^{(i)}\left(-40\,k^{(i)} - 1.82\,\epsilon + k^{(i)}\,\epsilon\right)} \tag{4.107}$$

and

$$[\![q_n]\!] = q_n^{(i)}(b_1 + t)\Big|_{A_2} - q_n^{(i)}(b_1)\Big|_{A_1} = 0.05\,Q_0\,\epsilon \tag{4.108}$$

These jumps in temperature and normal component of heat flux across an imperfect interface is approximated by the transmission conditions proposed by the two-point schemes, and the three-point schemes. The temperature distributions in material 1 and 2 retain their form, and thus, the jump conditions are given as

1. One Point Schemes

   - Miloh and Y.Benveniste, 1999a

$$[\![T]\!] = -\frac{\epsilon\left(0.56\,Q_0\,\epsilon^2 + 22.2\,Q_0\,\epsilon - 4.44\right)}{48.89\,k^{(i)} + 2.2\,\epsilon + k^{(i)}\,\epsilon} \tag{4.109}$$

$$[\![q_x]\!] = -0.5\,Q_0\,\epsilon \tag{4.110}$$

   - Hashin, 2001

$$[\![T]\!] = -\frac{\epsilon\left(0.56\,Q_0\,\epsilon^2 + 22.2\,Q_0\,\epsilon - 4.44\right)}{48.89\,k^{(i)} + 2.2\,\epsilon + k^{(i)}\,\epsilon} \tag{4.111}$$

$$[\![q_x]\!] = -0.5\,Q_0\,\epsilon \tag{4.112}$$

2. Two Point Schemes

   - Benveniste, 2006a

$$[\![T]\!] = \frac{\epsilon\left[20 + 1.38\,Q_0\,\epsilon^2 + 45\,Q_0\,\epsilon - 4.44 - k^{(i)}\left(11 + 0.25\,Q_0\,\epsilon^2\right)\right]}{220\,k^{(i)} + 10\,\epsilon - k^{(i)}\,\epsilon} \tag{4.113}$$

$$[\![q_x]\!] = 0.5\,Q_0\,\epsilon \tag{4.114}$$

   - Andreeva and Miszuris, 2017

$$[\![T]\!] = \frac{\epsilon\left(4.4 + 0.31\,Q_0\,\epsilon^2 + 10\,Q_0\,\epsilon\right)}{48.89\,k^{(i)} + 2.2\,\epsilon + k^{(i)}\,\epsilon} \tag{4.115}$$

$$[\![q_x]\!] = 0.5\,Q_0\,\epsilon \tag{4.116}$$

- Han et al., 2021

$$[\![T]\!] = \frac{\epsilon\left[20 + 1.38\,Q_0\,\epsilon^2 + 45\,Q_0\,\epsilon - 4.44 - k^{(i)}\left(11 + 0.25\,Q_0\,\epsilon^2\right)\right]}{220\,k^{(i)} + 10\,\epsilon - k^{(i)}\,\epsilon} \tag{4.117}$$

$$[\![q_x]\!] = 0.5\,Q_0\,\epsilon \tag{4.118}$$

- For the parallel interphase, the two proposed schemes of First ((4.23),(4.22)) and Second Integration ((4.23),(4.43)) using two-points of integration become equivalent, and take the following form:

$$[\![T]\!] = \frac{\epsilon\left(4.4 + 0.31\,Q_0\,\epsilon^2 + 10\,Q_0\,\epsilon\right)}{48.89\,k^{(i)} + 2.2\,\epsilon + k^{(i)}\,\epsilon} \tag{4.119}$$

$$[\![q_x]\!] = 0.5\,Q_0\,\epsilon \tag{4.120}$$

3. Three Point Schemes

- Similarly, the First ((4.35),(4.34)) and Second ((4.35),(4.49)) Integration Schemes using three-points of integration are equivalent, and are given as:

$$[\![T]\!] = \frac{\epsilon\left(4.44 + 0.43\,Q_0\,\epsilon^2 + 16.1\,Q_0\,\epsilon\right)}{48.89\,k^{(i)} + 2.2\,\epsilon + k^{(i)}\,\epsilon} \tag{4.121}$$

$$[\![q_x]\!] = 0.5\,Q_0\,\epsilon \tag{4.122}$$

For simplicity, $T^* = 1K$ and $\epsilon = t/L, \epsilon \ll 1$. The comparison is shown between the proposed two points scheme (4.119) and the three points scheme (4.121) along with the classical methods from the literature discussed above. For a flat interphase, the models proposed by Benveniste, 2006b and Han et al., 2021 are equivalent, and only Eqns.(4.113) is presented in the plots illustrated below.

**Verification**

- Low magnitude of heat source: Fig.4.5a and 4.5b depict the temperature jumps across a perfect interphase of thickness $\epsilon = 0.05$ with a small volumetric heat source $Q_0 = 1\ W/m^3$, along with the approximations computed from all the different methods. For extremely small conductivities ($k^{(i)}/k^{(2)} \leq 10^{-4}$), the one point schemes of Hashin and Miloh & Benveniste, given by Eqns.(4.111) and (4.109) respectively, the absolute error is about $\Delta_{[\![T]\!]} = \mathcal{O}(10^{-1})$ for low conductive interphase ($k^{(i)}/k^{(2)} < 10^{-2}$). In the region where the interphase conductivity approaches that of its neighbouring materials ($k^{(1)} \leq k^{(i)}/k^{(2)}$), the absolute error is less than or equal to $\mathcal{O}(\epsilon)$, and goes on to decrease to about $\mathcal{O}(\epsilon^3)$ for increasing conductivity values. The relative errors for jumps in temperature across the interphase remains $\approx 37.8\%$ of the exact solution. The absolute error of $[\![q_x]\!]$ remains constant for all values of conductivities, as it is independent of the thermal conductivities of the interphase, and is $\mathcal{O}(\epsilon)$ or about 200% relative to the exact solution, which is extremely high.

  The two-points schemes representing formulations proposed by Benveniste, 2006a (Eqn(4.113)), Andreeva and Miszuris, 2017 (Eqn.(4.115)) and including the method proposed by us (Eqn. (4.119)) show similar behaviours for lower thermal conductivities up to ($k^{(i)}/k^{(2)} \leq 10^{-3}$) and report absolute errors of $\mathcal{O}(10^{-1})$ or relative errors of approximately 7.6%. However, the two-points model proposed by Benveniste, 2006b

(and Han et al., 2021) show divergence in the region $k^{(i)}/k^{(2)} \geq 10^{-2}$ and approaches the finite asymptotic values with increasing conductivity. This behaviour can be explained by observing the values of ratios of thermal conductivities of the interphase with that of the adherents. As the thermal conductivity of the interphase approaches the values of its neighbouring material 2, the ratio $(k^{(i)}/k^{(2)} \to k_2)$, the temperature jump drops, as the thermal properties around point $A_1$ become dominant, while those around point $A_2$ become negligible. Also, with increasing values of $k_i$, the ratio $k^{(i)}/k^{(1)}$ and $k^{(i)}/k^{(2)}$ tend to reduce, becoming negligible. The temperature gradient in the normal direction becomes less significant as the thermal conductivity of the interphase $k^{(i)}/k^{(2)} \geq 1$. These causes a very slow temperature variation within the interphase, and thus, the $[\![T]\!]$ term reaches an asymptotic value of $2.0 \times 10^{-3}$. The deviation of the jumps in temperatures obtained by (4.115) and (4.119) for thermal conductivities $k^{(i)}/k^{(2)} \geq 1$ is about $\mathcal{O}(\epsilon^2)$ and decreases with increasing conductivity. For a superconductive interphase, the absolute error $\Delta_{[\![T]\!]} \approx \mathcal{O}(\epsilon^4)$. The relative error is approximately 7.8% of the exact solution, for all values of the thermal conductivity. The heat flux values are completely coincident with the exact solution, and therefore the absolute and relative errors become zero.

As illustrated, our proposed schemes using three-points of integration (4.121) represented by blue curve with filled circles, shows good approximation of the original solution for both cases of jumps in temperature and heat flux. The method provides the lowest absolute error of about $\mathcal{O}(\epsilon)$ or in terms of relative error which is about 1.86% of the original solution for the highly resistive interphase $(k^{(i)}/k^{(2)} \leq 10^{-4})$. For the highly conductive interphase $(k^{(i)}/k^{(2)} \geq 10^{1})$, the absolute error of the method is $\Delta_{[\![T]\!]} \leq \mathcal{O}(\epsilon^3)$, or $\delta_{[\![T]\!]} = 2.08\%$ of the exact solution. The jumps in heat flux values also has good agreement with the exact solution, and the absoute error is $\Delta_{[\![q_x]\!]} \leq \mathcal{O}(\epsilon^9)$, or $\delta_{[\![q_x]\!]} = 2.78 \times 10^{-14}\%$, which are extremely small, and thus, effectively, the deviation of the approximation of our proposed three-points scheme from the exact solution is zero. Therefore, it can be concluded that the proposed formulation of using three-points of Integration shows good approximation with the exact solution.

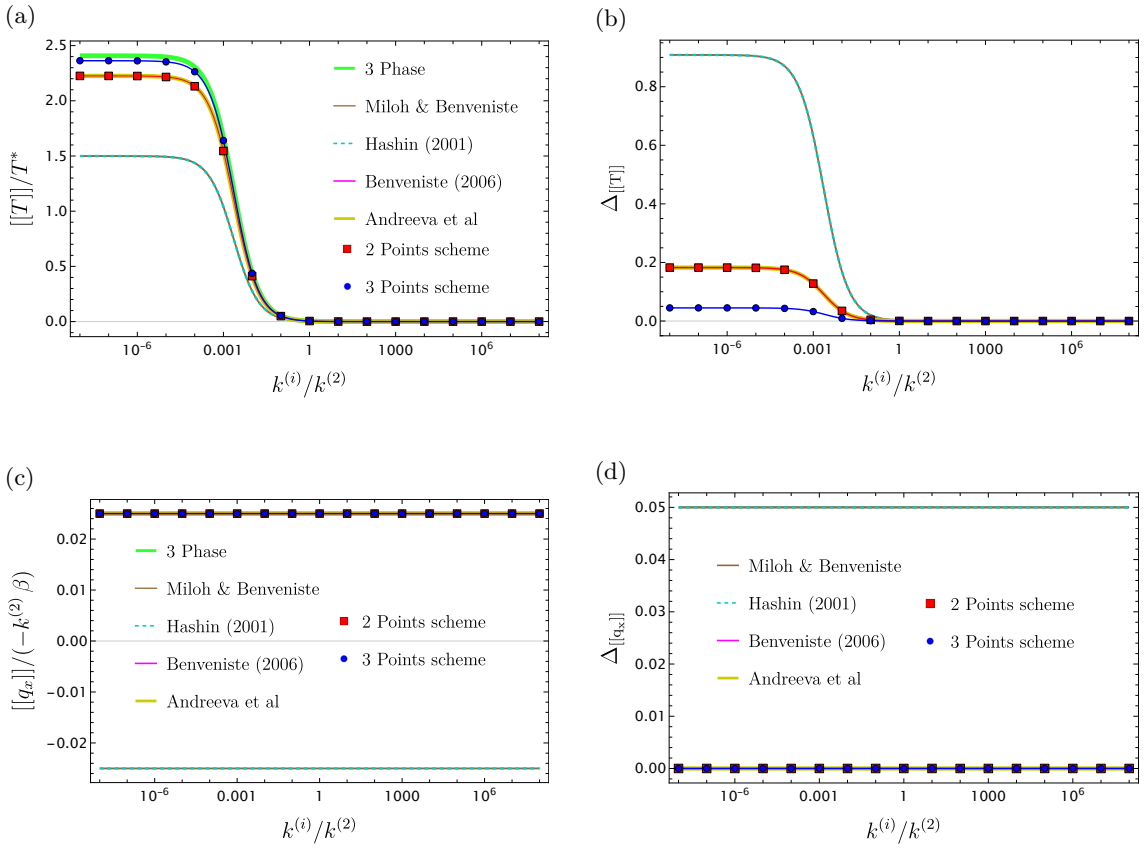


**Fig. 4.5.** Normalized $[\![T]\!]$ and $[\![q_x]\!]$ for a flat interphase of thickness, $\epsilon = 0.05$ and heat source $Q_0 = 1.0$. The red curve with square markers represent the proposed two points scheme (Eqns,(4.23),(4.22)), and blue curve with filled circles represents the proposed three-points scheme (Eqns,(4.35),(4.34)).

- High magnitude of heat source: The plots of $[\![T]\!]$ and $[\![q_n]\!]$ are illustrated in Fig.4.6 for an interphase of thickness $\epsilon = 0.001$, having a higher volumetric heat source $Q_0 = 100.0\, W/m^3$. It is obviously clear that even for the thin interphase, the evaluated jumps in temperature from all methods are not consistent with the results of the exact solution for low conductive interphase ($k^{(i)}/k^{(2)} \leq 10^{-3}$). The relative error between the exact solution and the models follow the same behaviour as seen previously in the case of low heat source magnitude. The presence of the higher heat source increases the absolute error computed for each model.

  The jumps in temperature predicted by the one-point schemes (4.111) and (4.109) show a huge deviation from the exact solution with absolute errors reported to be approximately $\mathcal{O}(10^{-1})$ or less for resistive interphase. With the increasing conductivity of the interphase, the absolute error becomes $\mathcal{O}(\epsilon)$ and decreases to $\mathcal{O}(\epsilon^2)$ with increasing conductivity. For a highly superconductive interphase, the error is $\mathcal{O}(\epsilon^3)$. The heat flux values reported from these schemes shows huge variation, with absolute error $\mathcal{O}(10^{-1})$ or the relative error of 200% of the exact solution.

  The two point schemes given by (4.113) and (4.115) including our proposed model (4.119) show the absolute error of order $\mathcal{O}(10^{-1})$ for a highly resistive interphase ($k^{(i)}/k^{(2)} \leq 10^{-3}$), and increases to $\mathcal{O}(\epsilon)$ with increasing thermal conductivity of the interphase. For higher thermal conductivities, ($k^{(i)}/k^{(2)} \geq k^{(1)}$), the absolute error

becomes $\mathcal{O}(\epsilon^2)$ and continues to decrease with increasing conductivity. The relative error for these methods is approximately 13.02% of the exact solution. However, for the schemes of Benveniste, 2006b and Han et al., 2021, which for the reason similar to the previous case of low magnitude of heat source increase asymptotically for $k^{(i)}/k^{(2)} > k^{(2)}$ and reach a value of $5 \times 10^{-4}$. As in the previous case, the heat flux jumps reports values that are in good agreement with the exact solution, and therefore the errors, both relative and absolute are zero.

The jumps in temperatures obtained from the three-points scheme (4.121) shows better approximation of the temperature variations across a perfect interphase, although it begins to diverge from the solution for a resistive interphase ($k^{(i)}/k^{(2)} \leq 10^{-3}$). Beyond this, with increasing conductivity, the absolute error becomes $\mathcal{O}(\epsilon)$. At higher conductivities, the error is approximately less than $\mathcal{O}(\epsilon^3)$. The jumps in heat flux also shows excellent agreement with the exact solution and the reported absolute error is $\Delta_{[\![q_x]\!]} = 0$.

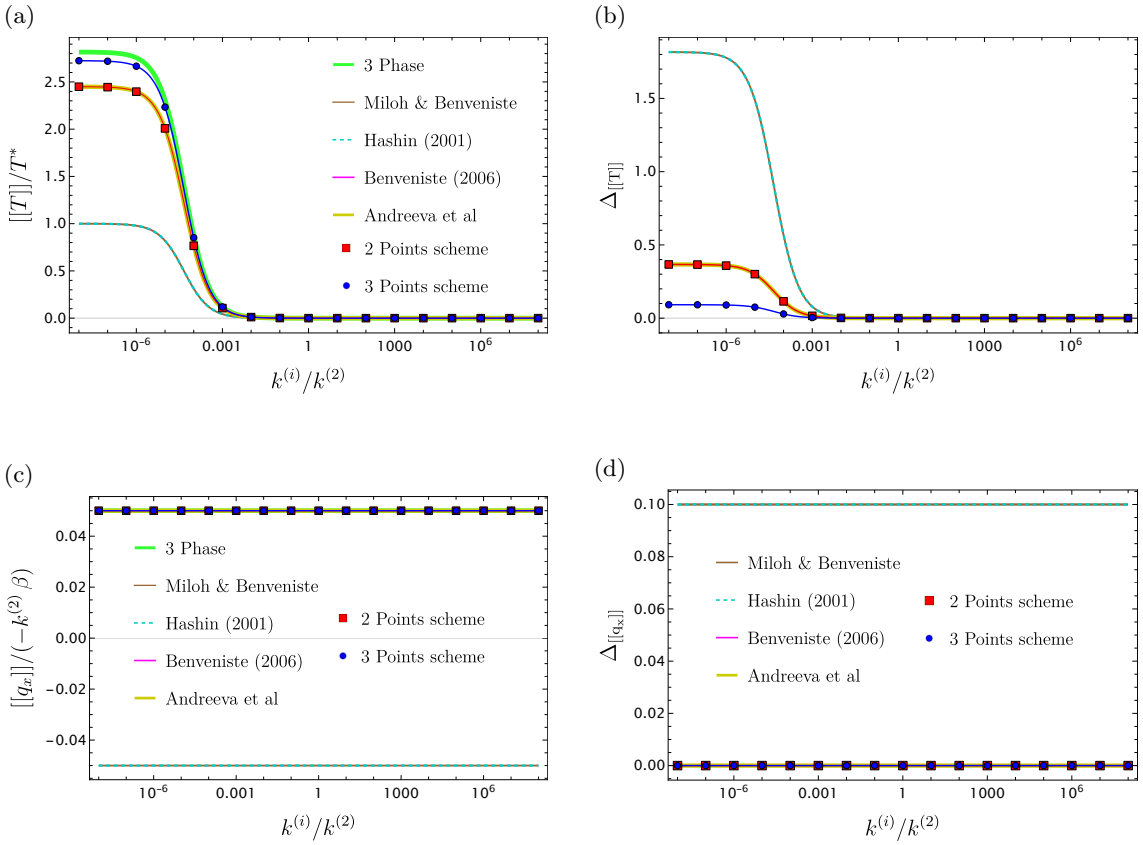


**Fig. 4.6.** Normalized $[\![T]\!]$ and $[\![q_x]\!]$ for a flat interphase of thickness, $t = 0.001$ and heat source $Q_0 = 100.0$. The red curve with square markers represent the proposed two points scheme (Eqns.(4.23),(4.22)), and blue curve with filled circles represents the proposed three-points scheme (Eqns,(4.35),(4.34)).

### 4.4.2 Circular And Non-circular Interphase

From the examples, we have seen the conduct of the transmission conditions in the case of flat geometry and a constant curvature. We will now consider a geometry that has a rapidly changing curvature, or oscillations in the radial direction. Such a geometry is

characterized by variations in the parameter $N$, which induce corresponding changes in the curvature of the configuration, as illustrated in Fig.4.10. The geometry of these parametric curves of the interphase is defined by the equations given in Sec.2.5

### Circular Interphase: Problem Setup

The first case we will discuss will be that of $N = 0$ which represents a perfect circle. For this class of geometry, analytical solutions are available, thereby facilitating direct verification of the numerical results against the exact solutions.

Let us consider a two-dimensional case of a circular inclusion of radius $R(\theta) = r_i = a$, with a coating of thickness $\xi = t$. The tangent (2.106) and normal (2.107) unit vectors simply take the form

$$\hat{\boldsymbol{t}} = \frac{\partial \boldsymbol{r}(\theta)}{\partial \theta} = \{-\sin(\theta), \cos(\theta)\} \tag{4.123}$$

$$\hat{\boldsymbol{n}} = \frac{\partial \boldsymbol{r}(\theta)}{\partial \theta} = \{\cos(\theta), \sin(\theta)\} \tag{4.124}$$

For a simple circular case, Eqn.(2.105) becomes $h_1 = h_r = 1, h_\theta = h_2 = r$ and curvature from (2.108) simplifies to $1/r$. The surface Laplacian given by Eqn.(2.111) is simplified to:

$$\mathcal{D}_s \boldsymbol{q} = -\frac{k^{(i)}}{r^2}\left\{\frac{\partial^2 T(r,\theta)}{\partial \theta^2}\right\} \tag{4.125}$$

For such a geometry, the normal direction is aligned in the radial direction, while the tangential direction is in the $\theta$-direction.

The inclusion of thermal conductivity $k^{(1)} = 10\ W/m.K$ is embedded in an uniaxial flow field having thermal conductivity $k^{(2)} = 1\ W/m.K$, as shown in Fig.4.7a and 4.7b. The thermal conductivity of the coating is $k^{(i)}$ which ranges from super resistive $10^{-8}\ W/m.K$ to super conductive $10^{8}\ W/m.K$.

The coated circular interphase, embedded in a homogeneous flow-field is shown in Fig.4.7.

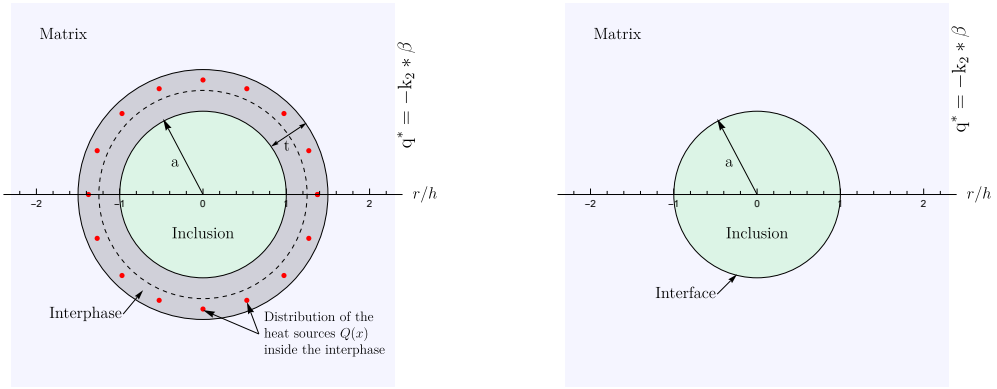


(a) 3 Phase representation.

(b) 2 Phase representation.

**Fig. 4.7.** Geometric representation of the problem.

In polar coordinates, the heat equation takes the following form:

$$\nabla^2 T^{(i)}(r,\theta) = \frac{\partial^2}{\partial r^2}T^{(i)}(r,\theta) + \frac{1}{r}\frac{\partial}{\partial r}T^{(i)}(r,\theta) + \frac{1}{r^2}\frac{\partial^2}{\partial \theta^2}T^{(i)}(r,\theta) \tag{4.126}$$

whereas, the heat flux is related to the temperature gradient, through Fourier's law:

$$q_j = -k\frac{\partial}{\partial \alpha_j}T(r,\theta) \quad ; \quad (\alpha_j = \{r,\theta\}) \tag{4.127}$$

Eqn.4.126 is a homogeneous Laplacian equation. It is assumed that the temperature distribution within material 1 (inclusion of radius 'a') and material 2, which is the surrounding matrix, exhibits angular dependence, ie, it has asymmetric behaviour.

$$T^{(1)}(r_1,\theta) = A_1 \cdot r_1 \cdot \cos\theta \quad ; \quad 0 \le r_1 \le a \tag{4.128}$$

$$T^{(2)}(r_2,\theta) = \left(A_2 r_2 + \frac{B_2}{r_2}\right) \cdot \cos\theta \quad ; \quad a+t \le r_2 \le \infty \tag{4.129}$$

The temperature inside the interphase is influenced by the presence of symmetrically distributed heat source, $Q(r)$ which is defined in 4.1. Thus, the balance equation becomes,

$$\operatorname{div} \boldsymbol{q}^{(i)} = Q(r) \tag{4.130}$$

$$\nabla^2 T^{(i)}(r,\theta) = \frac{Q(r,\theta)}{k^{(i)}} \tag{4.131}$$

$$T^{(i)}(r_i,\theta) = \left(A_i r_i + \frac{B_i}{r_i}\right)\cos(\theta) - \frac{Q(r,\theta)}{k^{(i)}} \tag{4.132}$$

where $Q_0$ is the magnitude of the volumetric heat source in $W/m^3$, with the parameters: $h = t/2$, $\zeta = h/2$. The results are presented for a linear heat source, $\alpha = 1$. The Eqn.(4.132) is a non-homogeneous equation, which can be solved by implementing *Method of Variations*. This will result in two sets of three equations each for temperature and the heat flux distribution derived from these temperature distributions inside the three materials. It is seen that these temperature fields satisfy the equilibrium conditions inside each domain. Therefore the set of six arbitrary constants $(A_1, B_1, A_i, B_i, A_2, B_2)$ can be solved by enforcing the continuity of temperature and heat flux across the boundaries of a perfect interphase, as well as by employing remote boundary conditions:

$$q^{(2)}(r_2,\theta) = q^*(r_2,\theta)|_{r_2\to\infty} = -k^{(2)} * \beta = 1 \ \ W/m^3 \tag{4.133}$$

where $\beta = -1K/m$ is a constant temperature gradient at the remote boundary. Therefore, the temperature field within the respective domains is described in terms of thickness $\epsilon$, volumetric heat source magnitude $Q_0$ and thermal conductivity of the interphase $k^{(i)}$.

$$T^{(1)}(r,\theta) = \left[\frac{k^{(i)}\left[0.83\,\epsilon^3 + \epsilon^2\,(1.83\,Q_0+4) + \epsilon\,(1.17\,Q_0+8)+4\right]}{(\epsilon^2\,\left\{k^{(i)}\left(11+k^{(i)}\right)+10\right\} + \epsilon\left\{2\,k^{(i)}\left(k^{(i)}+11\right)+2\,\left(11\,k^{(i)}+10\right)\right\}}\right] r\,\cos\theta$$

$$+\left[\frac{1.67\,Q_0\,\epsilon^2\,(1+\epsilon)}{(\epsilon^2\,\left\{k^{(i)}\left(11+k^{(i)}\right)+10\right\} + \epsilon\left\{2\,k^{(i)}\left(k^{(i)}+11\right)+2\,\left(11\,k^{(i)}+10\right)\right\}}\right] r\,\cos\theta \tag{4.134}$$

$$T^{(2)}(r,\theta) = \left[\frac{1}{22\,k^{(i)} + 2\,\epsilon\,\left(1+k^{(i)}\right)\left(10+k^{(i)}\right) + \epsilon^2\,\left(1+k^{(i)}\right)\left(10+k^{(i)}\right)}\right]\cos\theta +$$

$$\left[\frac{0.04\,(1.08+\epsilon)^2\left\{-48\,\epsilon\left(10+k^{(i)}\right)\,\left(k^{(i)}-1-0.42\,Q_0\,\epsilon\right)\right\}}{22\,k^{(i)} + 2\,\epsilon\,\left(1+k^{(i)}\right)\left(10+k^{(i)}\right) + \epsilon^2\,\left(1+k^{(i)}\right)\left(10+k^{(i)}\right)}\right]\frac{\cos\theta}{r} +$$

$$\left[\frac{0.04\,(1.08+\epsilon)^2\left\{\epsilon^2\left(10+k^{(i)}\right)\,\left(24-24\,k^{(i)}+8\,Q_0\,\epsilon\right)+k^{(i)}\,(24\,Q_0\,\epsilon-432)\right\}}{22\,k^{(i)} + 2\,\epsilon\,\left(1+k^{(i)}\right)\left(10+k^{(i)}\right) + \epsilon^2\,\left(1+k^{(i)}\right)\left(10+k^{(i)}\right)}\right]\frac{\cos\theta}{r} \tag{4.135}$$

$$T^{(i)}(r,\theta) = \left[\frac{-0.25\,Q_0\,\left(0.33+r+0.83\,\epsilon\right)\,\left(r-1-0.25\,\epsilon^2\right)}{\epsilon}\right]\,\frac{\cos\theta}{k^{(i)}\,r}$$

$$r^2\,\left[\frac{Q_0\,\epsilon^3\,\left\{1.15+k^{(i)}\,\left(4.59+0.45\,k^{(i)}\right)\right\}+2\,k^{(i)}\,\left(k^{(i)}+10\right)}{\epsilon^2\left\{10+k^{(i)}\,(ki+11)\right\}+2\,\epsilon\,k^{(i)}\,\left(k^{(i)}+11\right)+2\,\left(11\,k^{(i)}+10\,\epsilon\right)}\right]\,\frac{\cos\theta}{k^{(i)}\,r}+$$

$$r^2\,\left[\frac{\epsilon^2\,\left\{k^{(i)}\,\left(k^{(i)}+10\right)+Q_0\left\{1.46+k^{(i)}\,\left(0.98+9.94\,Q_0\right)\right\}\right\}}{\epsilon^2\left\{10+k^{(i)}\,(ki+11)\right\}+2\,\epsilon\,k^{(i)}\,\left(k^{(i)}+11\right)+2\,\left(11\,k^{(i)}+10\,\epsilon\right)}\right]\,\frac{\cos\theta}{k^{(i)}\,r}+$$

$$r^2\,\left[\frac{k^{(i)}\,\epsilon\,\left\{k^{(i)}\,\left(4+0.5\,Q_0\right)+5.69\,Q_0+40\right\}}{\epsilon^2\left\{10+k^{(i)}\,(ki+11)\right\}+2\,\epsilon\,k^{(i)}\,\left(k^{(i)}+11\right)+2\,\left(11\,k^{(i)}+10\,\epsilon\right)}\right]\,\frac{\cos\theta}{k^{(i)}\,r}+\mathcal{A} \quad (4.136)$$

where

$$\mathcal{A} = -\left[\frac{Q_0\,\epsilon^5\,\left\{0.003+0.004\,k^{(i)}\,\left(1+0.09\,k^{(i)}\right)\right\}}{\epsilon^2\left\{10+k^{(i)}\,(ki+11)\right\}+2\,\epsilon\,k^{(i)}\,\left(k^{(i)}+11\right)+2\,\left(11\,k^{(i)}+10\,\epsilon\right)}\right]\,\frac{\cos\theta}{k^{(i)}\,r}-$$

$$\left[\frac{Q_0\,\epsilon^4\,\left\{0.06+0.064\,k^{(i)}\,\left(1+0.09\,k^{(i)}\right)\right\}}{\epsilon^2\left\{10+k^{(i)}\,(ki+11)\right\}+2\,\epsilon\,k^{(i)}\,\left(k^{(i)}+11\right)+2\,\left(11\,k^{(i)}+10\,\epsilon\right)}\right]\,\frac{\cos\theta}{k^{(i)}\,r}+$$

$$\left[\frac{Q_0\,\epsilon^3\,\left\{-1.25-4.55\,k^{(i)}\,\left(1-0.08\,k^{(i)}\right)\right\}}{\epsilon^2\left\{10+k^{(i)}\,(ki+11)\right\}+2\,\epsilon\,k^{(i)}\,\left(k^{(i)}+11\right)+2\,\left(11\,k^{(i)}+10\,\epsilon\right)}\right]\,\frac{\cos\theta}{k^{(i)}\,r}+$$

$$\left[\frac{\epsilon^2\,\left\{2\,k^{(i)}\,\left(k^{(i)}-10\right)+Q_0\,\left(1.45-9.88\,k^{(i)}\,\left(1-0.086\,k^{(i)}\right)\right)\right\}}{\epsilon^2\left\{10+k^{(i)}\,(ki+11)\right\}+2\,\epsilon\,k^{(i)}\,\left(k^{(i)}+11\right)+2\,\left(11\,k^{(i)}+10\,\epsilon\right)}\right]\,\frac{\cos\theta}{k^{(i)}\,r}+$$

$$\left[\frac{k^{(i)}\,\epsilon\,\left\{k^{(i)}\,\left(4+05\,Q_0\right)-5.69\,Q_0-40\right\}+2\,k^{(i)}\,\left(k^{(i)}-10\right)}{\left\{10+k^{(i)}\,(ki+11)\right\}+2\,\epsilon\,k^{(i)}\,\left(k^{(i)}+11\right)+2\,\left(11\,k^{(i)}+10\,\epsilon\right)}\right]\,\frac{\cos\theta}{k^{(i)}\,r}$$

The jumps in temperature and normal component of heat flux for a three-phase solution is the difference in the properties across the interphase thickness, that is, at points $A_2$ and $A_1$.

$$[\![T]\!] = T^{(i)}(a+t,\theta)\Big|_{A_2} - T^{(i)}(a,\theta)\Big|_{A_1}$$

$$= \left[\frac{\epsilon^2\left(20+k^{(i)}\,(2+0.36\,Q_0)+12.42\,Q_0\right)+Q_0\,\epsilon^3\left(3.33+0.33\,k^{(i)}\right)}{\epsilon^2\left[k^{(i)}\left(11+k^{(i)}\right)+10\right]+\epsilon\left[21.6+k^{(i)}\left(2.16\,k^{(i)}+23.76\right)\right]+25.66\,k^{(i)}}\right]\,\epsilon\,\cos\theta$$

$$+\left[\frac{46.66+\epsilon\left(64.8+2.16\,k^{(i)}+9.53\,Q_0\right)}{\epsilon^2\left[k^{(i)}\left(11+k^{(i)}\right)+10\right]+\epsilon\left[21.6+k^{(i)}\left(2.16\,k^{(i)}+23.76\right)\right]+25.66\,k^{(i)}}\right]\,\epsilon\,\cos\theta \quad (4.137)$$

and

$$[\![q_n]\!] = q_n^{(i)}(a+t,\theta)\Big|_{A_2} - q_n^{(i)}(a,\theta)\Big|_{A_1}$$

$$= \left[\frac{\epsilon^2\left(5\,Q_0 + 8.67\,k^{(i)}\,Q_0\right) + \epsilon\left[10.8\,Q_0 + k^{(i)}\left(20 - 2.2\,k^{(i)} + 20.7\,Q_0\right)\right]}{\epsilon^2\left[k^{(i)}\left(11 + k^{(i)}\right) + 10\right] + \epsilon\left[21.6 + k^{(i)}\left(2.16\,k^{(i)} + 23.76\right)\right] + 25.66\,k^{(i)}}\right]\epsilon\,\cos\theta$$

$$+ \left[\frac{k^{(i)}\left(43.2 + 12.83\,Q_0 - 4.32\,k^{(i)}\right)}{\epsilon^2\left[k^{(i)}\left(11 + k^{(i)}\right) + 10\right] + \epsilon\left[21.6 + k^{(i)}\left(2.16\,k^{(i)} + 23.76\right)\right] + 25.66\,k^{(i)}}\right]\epsilon\,\cos\theta \tag{4.138}$$

These jumps in temperature and normal component of heat flux across an imperfect interface is approximated by the transmission conditions proposed by the two-point schemes, and the three-point schemes. The temperature distributions in material 1 and 2 retain their form, and thus, the jump conditions are given as

1. One Point Schemes

   - Miloh and Y.Benveniste, 1999a

$$[\![T]\!] = \left[\frac{20 - 5\,Q_0\,\epsilon}{10\,\epsilon + k^{(i)}\left(\epsilon\,k^{(i)} + 11\right)}\right]\epsilon\,\cos\theta \tag{4.139}$$

$$[\![q_r]\!] = \left[\frac{-k^{(i)}\left(2\,k^{(i)} + 5.5\,Q_0\right) - 5\,Q_0\,\epsilon}{10\,\epsilon + k^{(i)}\left(\epsilon\,k^{(i)} + 11\right)}\right]\epsilon\,\cos\theta \tag{4.140}$$

   - Hashin, 2001

$$[\![T]\!] = \left[\frac{20 - 5\,Q_0\,\epsilon}{10\,\epsilon\left(1 - k^{(i)}\right) + k^{(i)}\left(11 + k^{(i)}\,\epsilon\right)}\right]\epsilon\,\cos\theta \tag{4.141}$$

$$[\![q_r]\!] = \left[\frac{2\,k^{(i)}\left(10 - k^{(i)}\right) - Q_0\left(5.5\,k^{(i)} + 5\,\epsilon\right)}{10\,\epsilon\left(1 - k^{(i)}\right) + k^{(i)}\left(11 + k^{(i)}\,\epsilon\right)}\right]\epsilon\,\cos\theta \tag{4.142}$$

2. Two Point Schemes

   - Benveniste, 2006a

$$[\![T]\!] = \left[\frac{\epsilon\left\{k^{(i)}\left(2\,k^{(i)} - 13\right) + 11 - 4.5\,Q_0\right\} + 22\,k^{(i)} - 40}{\mathcal{P}(\epsilon, k^{(i)})}\right]\epsilon\,\cos\theta \tag{4.143}$$

$$[\![q_r]\!] = \left[\frac{\epsilon\left[k^{(i)}\left(31 - 11\,k^{(i)} + 5.5\,Q_0\right) - 20 - 10\,Q_0\right]}{\mathcal{P}(\epsilon, k^{(i)})}\right]\epsilon\,\cos\theta + \left[\frac{k^{(i)}\left(4\,k^{(i)} - 11\,Q_0 - 22\right)}{\mathcal{P}(\epsilon, k^{(i)})}\right]\epsilon\,\cos\theta \tag{4.144}$$

   where

$$\mathcal{P}(\epsilon, k^{(i)}) = \epsilon^2\left[k^{(i)}\left(k^{(i)} - 11\right) + 10\right] + \epsilon\left[k^{(i)}\left(22 - 2\,k^{(i)}\right) - 20\right] - 22\,k^{(i)}$$

   - Andreeva and Miszuris, 2017

$$[\![T]\!] = \left[\frac{\epsilon\left(0.36\,k^{(i)} + 0.82\,Q_0\right) + 7.27}{\epsilon^2\,k^{(i)} + \epsilon\,k^{(i)}\left(0.36\,k^{(i)} + 3.64\right) + 4\,k^{(i)}}\right]\epsilon\,\cos\theta \tag{4.145}$$

$$[\![q_r]\!] = \left[\frac{\epsilon\left(1.82\,Q_0 - 3.64\,k^{(i)}\right) + k^{(i)}\left(2\,Q_0 - 0.73\,k^{(i)}\right)}{\epsilon^2\,k^{(i)} + \epsilon\,k^{(i)}\left(0.36\,k^{(i)} + 3.64\right) + 4\,k^{(i)}}\right]\epsilon\,\cos\theta \tag{4.146}$$

- Han et al., 2021

$$[\![T]\!] = \left[\frac{\epsilon^3\left(2\,\epsilon\,k^{(i)} - 2\,Q_0 - 4\right) + \epsilon^2\left(1.45 - 7.27\,Q_0 - 16\,k^{(i)}\right)}{\mathcal{Q}(\epsilon, k^{(i)})}\right]\epsilon\,\cos\theta$$
$$\left[\frac{\epsilon\left\{2.91\,k^{(i)}\left(k^{(i)} - 1\right) - 6.55\,Q_0 - 13.09\right\} - 32\,k^{(i)} - 58.18}{\mathcal{Q}(\epsilon, k^{(i)})}\right]\epsilon\,\cos\theta \quad (4.147)$$

$$[\![q_r]\!] = \left[\frac{\epsilon\left\{k^{(i)}\left(29.09 - 13.09\,k^{(i)}\right) - 14.55\,Q_0 - 29.09\right\}}{\mathcal{Q}(\epsilon, k^{(i)})}\right]\epsilon\,\cos\theta$$
$$\left[\frac{k^{(i)}\,\epsilon^3\left\{\epsilon\left(Q_0 - 2\right) + 4\,k^{(i)}\right\} + \epsilon^2\left\{8\,k^{(i)}\left(Q_0 + 2\right) - 7.27\,Q_0 - 14.55\right\}}{\mathcal{Q}(\epsilon, k^{(i)})}\right]\epsilon\,\cos\theta$$
$$\left[\frac{k^{(i)}\left(5.82\,k^{(i)} - 16\,Q_0 - 32\right)}{\mathcal{Q}(\epsilon, k^{(i)})}\right]\epsilon\,\cos\theta \quad (4.148)$$

where

$$\mathcal{Q}(\epsilon, k^{(i)}) = \epsilon^3\left[k^{(i)}\left(\epsilon^2 - 2\,\epsilon + 0.73\,k^{(i)} - 12\right) + 7.27\right] + 8\epsilon^2\,k^{(i)}$$
$$+\epsilon\left[k^{(i)}\left(16 - 2.91\,k^{(i)}\right) - 29.09\right] - 32\,k^{(i)}$$

- First Integration Schemes (4.23) and (4.22)

$$[\![T]\!] = \left[\frac{\epsilon\left(0.82\,Q_0 + 0.36\,k^{(i)}\right) + 7.27}{\epsilon^2\,k^{(i)} + \epsilon\left[k^{(i)}\left(0.36\,k^{(i)} - 1.64\right) + 3.64\right] + 4\,k^{(i)}}\right]\epsilon\,\cos\theta \quad (4.149)$$

$$[\![q_r]\!] = \left[\frac{\epsilon\left(1.82\,Q_0 - 3.64\,k^{(i)}\right) + k^{(i)}\left(2\,Q_0 + 7.3 - 0.73\,k^{(i)}\right)}{\epsilon^2\,k^{(i)} + \epsilon\left[k^{(i)}\left(0.36\,k^{(i)} - 1.64\right) + 3.64\right] + 4\,k^{(i)}}\right]\epsilon\,\cos\theta \quad (4.150)$$

- Second Integration Schemes (4.23) and (4.43)

$$[\![T]\!] = \left[\frac{\epsilon^2\left(0.2\,k^{(i)} + 1.35\,Q_0\right) + \epsilon\left(0.4\,k^{(i)} + 0.9\,Q_0 + 4\right)}{(2+\epsilon)\,\left[\epsilon^2\,k^{(i)} + \epsilon\left(k^{(i)}\left(0.2\,k^{(i)} - 0.9\right) + 2\right) + 2.2\,k^{(i)}\right]}\right]\epsilon\,\cos\theta$$

(4.151)

$$[\![q_r]\!] = \left[\frac{\epsilon^2\left(3\,Q_0 - 4\,k^{(i)}\right) + \epsilon\left[Q_0\left(2 + 3.3\,k^{(i)}\right) - k^{(i)}\left(4 + 0.4\,k^{(i)}\right)\right]}{(2+\epsilon)\,\left[\epsilon^2\,k^{(i)} + \epsilon\left(k^{(i)}\left(0.2\,k^{(i)} - 0.9\right) + 2\right) + 2.2\,k^{(i)}\right]}\right]\epsilon\,\cos\theta$$
$$\left[\frac{k^{(i)}\left(8 - 0.8\,k^{(i)} + 2.2\,Q_0\right)}{(2+\epsilon)\,\left[\epsilon^2\,k^{(i)} + \epsilon\left(k^{(i)}\left(0.2\,k^{(i)} - 0.9\right) + 2\right) + 2.2\,k^{(i)}\right]}\right]\epsilon\,\cos\theta$$

(4.152)

3. Three Point Schemes

- First Integration Schemes (4.35) and (4.34)

$$[\![T]\!] = \left[\frac{2\,\epsilon^3\left\{k^{(i)}\,(1+Q_0) - 5\,(1+Q_0)\right\} + \epsilon^2\left\{4\,k^{(i)}\,(5+Q_0) + 47\,Q_0\right\}}{\mathcal{R}(\epsilon, k^{(i)})}\right]\,\epsilon\,\cos\theta$$
$$\left[\frac{4\,\epsilon\left(29\,Q_0 + 8\,k^{(i)} + 80\right) + 640}{\mathcal{R}(\epsilon, k^{(i)})}\right]\,\epsilon\,\cos\theta \quad (4.153)$$

$$[\![q_r]\!] = \left[\frac{\epsilon^3\left\{10\left(k^{(i)} - Q_0\right) - k^{(i)}\left(2\,k^{(i)} + 3.5\,Q_0\right)\right\}}{\mathcal{R}(\epsilon, k^{(i)})}\right]\,\epsilon\,\cos\theta$$
$$\left[\frac{\epsilon^2\left\{Q_0\left(80 - 7\,k^{(i)}\right) - 4\,k^{(i)}\left(k^{(i)} + 160\right)\right\}}{\mathcal{R}(\epsilon, k^{(i)})}\right]\,\epsilon\,\cos\theta$$
$$\left[\frac{4\,\epsilon\left\{40\,Q_0 + k^{(i)}\left(33\,Q_0 - 8\,k^{(i)}\right)\right\} + 16\,k^{(i)}\left(11\,Q_0 - 4\,k^{(i)} + 40\right)}{\mathcal{R}(\epsilon, k^{(i)})}\right]\,\epsilon\,\cos\theta \quad (4.154)$$

where

$$\mathcal{R}(\epsilon, k^{(i)}) = \epsilon^4\left[k^{(i)}\left(k^{(i)} - 6.75\right) - 5\right] + 2\,\epsilon^3 k^{(i)}\left(k^{(i)} + 23\right)$$
$$+16\epsilon^2\left[10 + k^{(i)}\left(k^{(i)} + 6\right)\right] + 32\,\epsilon\left[k^{(i)}\left(k^{(i)} + 1\right) + 10\right] - 352\,k^{(i)}$$

- Second Integration Schemes (4.35) and (4.49)

$$[\![T]\!] = \left[\frac{2\,\epsilon^3\left\{Q_0\left(34 + \epsilon\,k^{(i)}\right) + 8\,k^{(i)}\,(2+Q_0)\right\}}{\mathcal{T}(\epsilon, k^{(i)})}\right]\,\epsilon\,\cos\theta$$
$$\left[\frac{4\,\epsilon^2\left\{Q_0\left(123 + k^{(i)}\right) + 2\,k^{(i)}\,(18+Q_0) + 80\right\}}{\mathcal{T}(\epsilon, k^{(i)})}\right]\,\epsilon\,\cos\theta$$
$$+\left[\frac{\epsilon\left(160 + 29\,Q_0 + 8\,k^{(i)} + 2560\right)}{\mathcal{T}(\epsilon, k^{(i)})}\right]\,\epsilon\,\cos\theta \quad (4.155)$$

$$[\![q_r]\!] = \left[\frac{-k^{(i)}\,\epsilon^4\left(3.5\,Q_0 + 2\,k^{(i)}\right) + 2560\,k^{(i)}}{\mathcal{T}(\epsilon, k^{(i)})}\right]\,\epsilon\,\cos\theta$$
$$+\left[\frac{4\,\epsilon^3\left\{Q_0\left(50 - 7\,k^{(i)}\right) - 4\,k^{(i)}\left(20 + k^{(i)}\right)\right\}}{\mathcal{T}(\epsilon, k^{(i)})}\right]\,\epsilon\,\cos\theta$$
$$+\left[\frac{4\,\epsilon^2\left\{Q_0\left(200 + 81\,k^{(i)}\right) - 20\,k^{(i)}\left(18 + k^{(i)}\right)\right\}}{\mathcal{T}(\epsilon, k^{(i)})}\right]\,\epsilon\,\cos\theta$$
$$+\left[\frac{16\,\epsilon\left\{Q_0\left(40 + 33\,k^{(i)}\right) + k^{(i)}\left(33\,Q_0 - 16\,k^{(i)}\right)\right\}}{\mathcal{T}(\epsilon, k^{(i)})}\right]\,\epsilon\,\cos\theta \quad (4.156)$$

where

$$\mathcal{T}(\epsilon, k^{(i)}) = \epsilon^4\, k^{(i)} \left(\epsilon\, k^{(i)} + 8\, k^{(i)} + 66\right) + 40\,\epsilon^3 \left[4 + k^{(i)} \left(k^{(i)} + 11\right)\right] + 8\,\epsilon^2 \left[160 + k^{(i)} \left(16\, k^{(i)} + 63\right)\right] + 1408\, k^{(i)} + 64\,\epsilon \left[20 + k^{(i)} \left(2\, k^{(i)} + 13\right)\right]$$

**Numerical Verification**

The results obtained from the exact solution (which is the three-phase solution) are compared with the approximated values computed from each method as given above. The behavior of transmission conditions with their absolute errors which is evaluated as per (4.92) and is illustrated in the following graphs to pinpoint the accuracy of each method.

- Low magnitude of heat source:

  Fig.4.8a and 4.8b present the temperature discontinuities across a perfect interphase of thickness $\epsilon = 0.05$, subjected to a small volumetric heat source $Q_0 = 1\,\mathrm{W/m^3}$. These figures also include the corresponding approximations of both the temperature and heat flux jumps obtained using the various methods under consideration.

  For the jumps in normal component of heat flux illustrated in Fig.4.8c, localization is perceived in the region where $10^{-2} \leq k^{(i)}/k^{(2)} \leq 10$, that is, in the regions where the thermal conductivity of the interphase begins to approach that of its surrounding materials. Such behavior is consistent with the trends previously identified in 4.3d. The effect is more pronounced in terms of errors Fig.4.8d.

  The effect of thermal conductivity mismatch ($k^{(i)}/k^{(2)}$ within the interphase $< k^{(1)}$) causes the interphase boundary to behaves as a "barrier", creating local pocket of intense heat flux accumulation, illustrated in Fig.4.8d as absolute error in $[\![q_r]\!]$. The curves of Benveniste, 2006b and Han et al., 2021, provided by Eqns.(4.143) and (4.147) respectively, show dipping at two points, which mark the conductivities at which the $[\![q_r]\!]$ computed from these methods, coincide with the perfect interphase solution, at points $k^{(i)}/k^{(2)} \approx 10^{-2}$ and $k^{(i)}/k^{(2)} \approx 10^{1}$. The effect of the absence of the term $g\, q_n^{(i)}$ on the transmission conditions can be understood by the higher relative errors of the schemes of Benveniste, 2006b, Han et al., 2021 with the generalized scheme of Andreeva et al (Eqn.(4.145)) as well as Miloh & Benveniste (Eqn.(4.139)), as illustrated in Figs.4.8c, where, in the region of localization, these methods show higher divergence from the three-phase solution, resulting in higher relative errors pertaining to this range of thermal conductivities. Although the Hashin's model given by (4.141) contains the geometric curvature term for the jump in normal heat flux component, it still produces higher error because the method focuses on expansion on one side of the interphase only. This is also the reason why we see the deviation of Hashin, 2001 and Miloh and Y.Benveniste, 1999a model within this region.

- High magnitude of heat source: For a thin interphase thickness ($\epsilon = t/a = 0.001$), a volumetric heat source $Q(r, \theta)$ of large magnitude $Q_0 = 100.0\, W/m^3$ is considered. The interphase thickness is chosen such that the assumption of generalized conditions of Miloh & Beneveniste is valid, as discussed in 4.4.

  The comparative graph of jumps of $[\![T]\!]$ and $[\![q_r]\!]$ of the three-phase solution with the solution computed from each models, along with their respective relative errors,

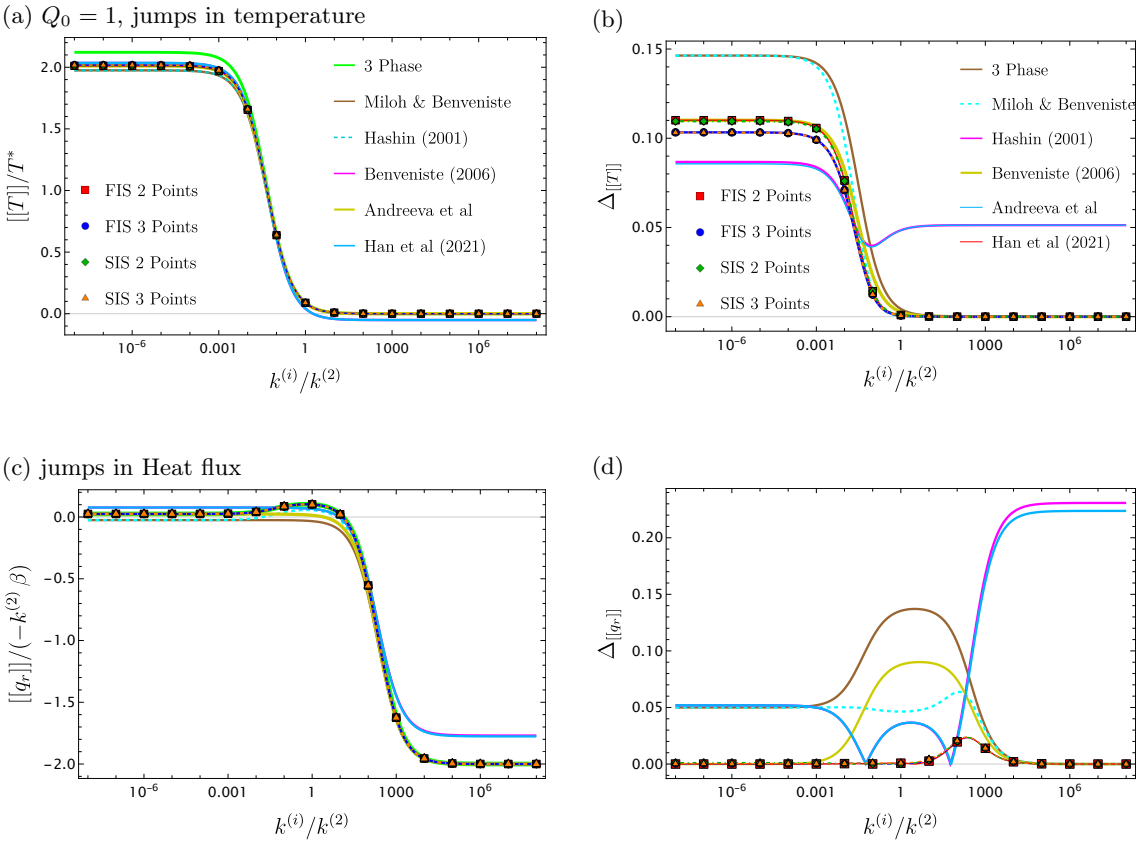


**Fig. 4.8.** Plots of normalized temperature jumps and normal component of heat flux jumps, with their corresponding relative errors for circular interphase of thickness $\epsilon = 0.05$ having heat source of magnitude $Q_0 = 1.0\ W/m^3$.

is shown in Fig.4.9. For a thin interphase with high volumetric heat source, it seen that the temperature jumps for the one-point schemes show complete deviance from the exact (three-phase) solution, while the jumps in normal component of heat flux deviates for conductivities $k^{(i)}/k^{(2)} \approx 10^4$. The temperature jumps computed from the generalized case of Miloh & Benveniste, and Hashin, 2001 show constant relative error of 4.5% for the thermal conductivities $k^{(i)}/k^{(2)} \leq 10^2$, beyond this value, the error increases steadily to 99.98%. The high relative error is because $[\![T]\!]$ for Hashin, 2001 and Miloh & Benveniste becomes equal in magnitude to the solution obtained from exact solution. It can also be observed that our proposed three-points schemes (4.35) and (4.49), the absolute error is for low conductive interphase is approximately $\mathcal{O}(\epsilon)$ while the high conductive interphase has absolute error of $\mathcal{O}(\epsilon^2)$, and thus show least relative error values for the entire range of thermal conductivities $(0.3 - 0.4\%)$, while the proposed two point schemes show an absolute error of order $10^{-2}$ or less for low conductive interphase, while the absolute error for high conductive interphase is $\mathcal{O}(\epsilon^2)$. Similar to the case of $Q_0 = 1$, the localized heat flux zone is observed in the case of higher heat source, even though the thickness is small. For our proposed three-points scheme, the absolute error is of the order $\mathcal{O}(\epsilon^2)$

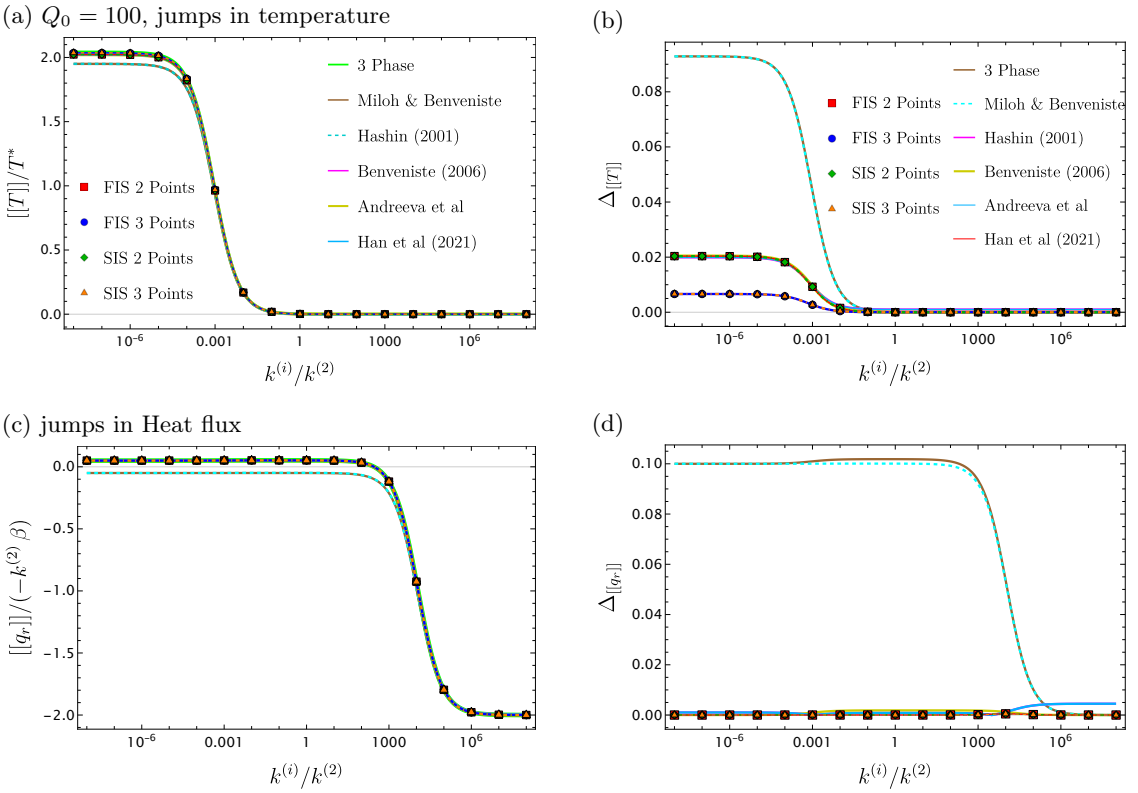


**Fig. 4.9.** Plots of normalized $[\![T]\!]$ and $[\![q_n]\!]$, with their corresponding relative errors for circular interphase of thickness $\epsilon = 0.001$ having heat source of magnitude $Q_0 = 100.0\ W/m^3$.

### 4.4.3 Wavy Interphase

The next case is that of a rapidly varying curvature in the tangential direction and its impact on the efficiency and accuracy of the proposed schemes. The geometry of such an inclusion is given by the parametric form of the radius as defined in (2.103).

In the parametric form of the equations above, $r_i$ is the radius of the inclusion (the inner boundary of the interphase) and $r_o$ is the outer boundary of the interphase, as shown in the Fig.4.11a. $N$ is the number of oscillations or wavelengths in the tangential directions. The amplitude of these oscillations is represented by $A = 0.05$, which remains constant for all values of $N$. Higher values of N represent complex geometries that have higher variations in boundary normals and are thus the limiting case for our wavy interphase geometry.

To understand this, we have considered the following six different but increasing values of $N = \{0, 5, 10, 20, 30, 40\}$. At $N = 50$, there is overlap of the outer boundaries of the interphase, which is characteristic of the parallel surfaces.

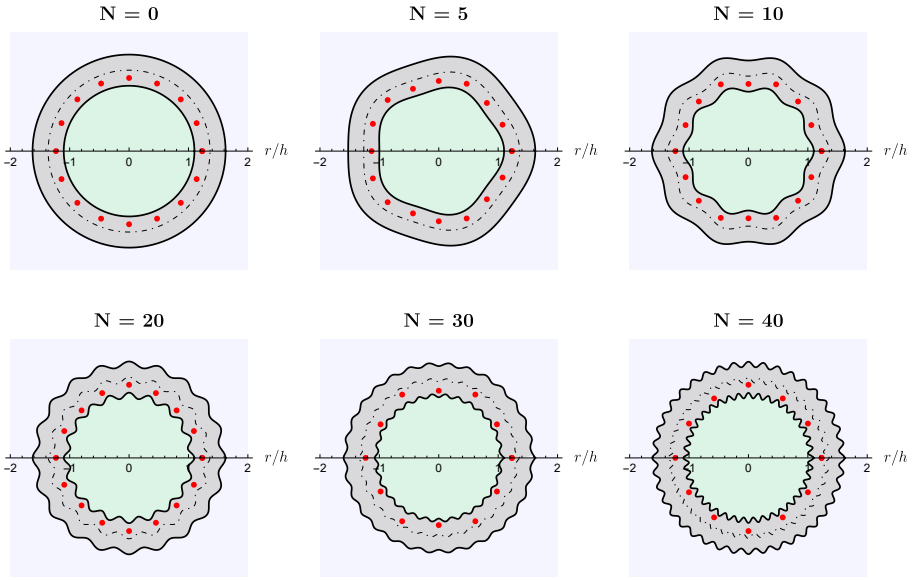


**Fig. 4.10.** Circular and non-circular geometries with varying curvature.

For simplicity, $T^* = 1K$ and $\beta = \frac{\partial T^*}{\partial L} = -1K/m$, while the surrounding matrix is modeled as a square of length $L = 30\,m$. The matrix dimensions $L >> \epsilon$, so that the remote boundary conditions are far-off from the inclusion, where $\epsilon \ll 1$ is the dimensionless parameter, $\epsilon = t/a$. The top and bottom of the domain are assumed to be thermally insulated, so that the flow is uni-directional. The temperature and heat flux values are affected by local variations in the tangential directions and changing curvature. All the values are computed at $\theta = 0\,\text{deg}$.

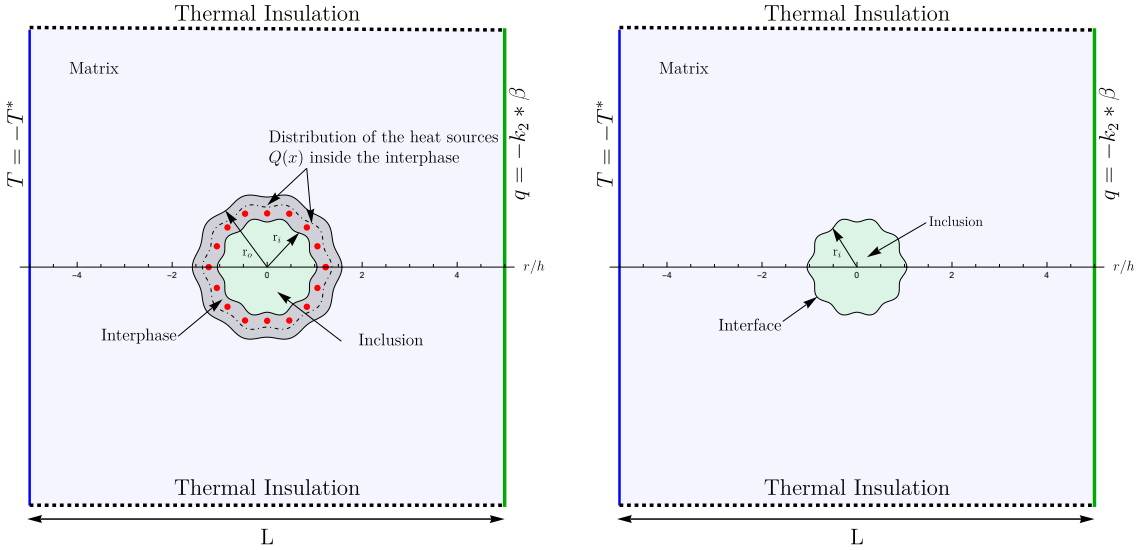


(a) 3 Phase representation.

(b) 2 Phase representation.

**Fig. 4.11.** Geometric representation of the wavy interphase.

The commercial finite element software Comsol Multiphysics is used to perform the simulations for a thermally conductive wavy interphase. The 2D domain as illustrated in Fig.4.11a, is meshed using unstructured triangular mesh elements having Quadratic

Lagrange shape functions, and as well as Quadratic Lagrange discretization to maintain the accuracy of the solution, without increasing the computational load. The triangular elements are chosen instead of quadrilaterals elements because of their ability to provide accurate solutions in highly complex geometries. To achieve the accuracy of the solution within the interphase, very fine mesh having 1422929 elements is used within the interphase while the matrix and inclusion have coarse mesh away from the interphase boundaries. The effect of mesh density within the interphase on the solution is negligible when varied from coarse to fine to very fine mesh within the interphase region.

**Numerical Verification**

For the first case, that is, $N = 0$ which represents a perfect circular inclusion, we have the analytical solution, as seen in the previous example. To verify the accuracy of the numerical solution presented below, we have compared the jumps in temperature and heat flux obtained from the analytical solution and the numerical solution and is presented in Fig.4.12. The corresponding errors are computed as:

$$\Delta_{[\![T]\!]} = \frac{1}{T^*}|[\![T]\!]_{ana} - [\![T]\!]_{num}| \quad ; \quad \Delta_{[\![q_n]\!]} = \frac{1}{q_n^*}|[\![q_n]\!]_{ana} - [\![q_n]\!]_{num}| \tag{4.157}$$

where $T^*$ represent the values of temperature at the remote boundary, and $q_n^* = -k^{(2)}\,\beta$ is the heat flux at the remote boundary. It can be seen that for the $[\![T]\!]$, the maximum error is of the order $\mathcal{O}(10^{-3})$, for the highly resistive interphase, and similarly, the maximum error of order $\mathcal{O}(10^{-1})$ for the extremely conductive interphase. Since the errors for both jumps in temperature and jumps in normal component of heat flux is close to zero for $k^{(i)}/k^{(2)} = \{10^{-2}, 10^{2}\}$, for all the numerical results presented below, we will consider the low conductive interphase to have thermal conductivity of $k^{(i)} = 10^{-2}\,W/m.K$ and for the high conductive interphase, the value is taken to be $k^{(i)} = 100\,W/m.K$

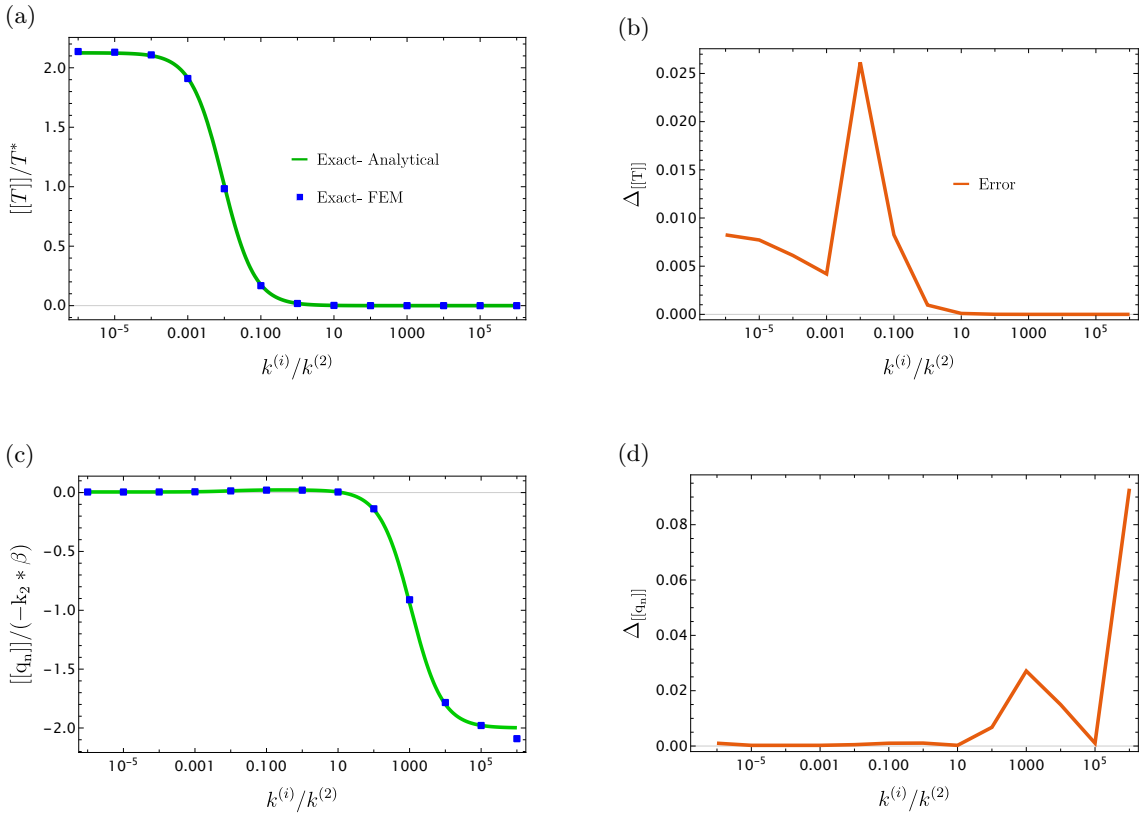


**Fig. 4.12.** Verification of the numerical solutions by comparison with known analytical solution, for a perfect circular inclusion, having low heat source value, $Q_0 = 1W/m^3$ of volumetric heat source. The results illustrated in this graph are the $[\![T]\!]$ and $[\![q_n]\!]$ computed across the boundaries of the perfect interphase setting.

Next, we will begin our analysis by inspecting the behaviour of parameters $g, \beta$ and $\gamma$ with the increasing oscillations, as highlighted in Fig.4.13. These parameters are computed from Eqns.(4.20), (2.118), (2.119) respectively. The values of $\gamma$ remains constant at 1.0 for all values of $N$, as it simply represents the ratio of $(h_1\, h_2)$ at point $A_3$ to the average values of same taken at points $A_1$ and $A_2$. Since, we consider point $A_3$ to lie exactly at the midpoint of the interphase thickness this ratio naturally becomes 1. From Fig.4.13a it is also observed that the curvature at the inner boundary of the interphase increases rapidly as compared to the curvature computed at the outer edge. This is becuase the curvature is inversely proportional to the tangent vector of the curve $(R'(\theta))$, and thus the curvature increases with increasing values of $R(\theta)$. From the graph, it is clearly observed that for the small curvatures $N = \{0, 5, 10\}$, the variation of $g, \beta$ is very small, and thus the resulting solutions from the First and Second Integration scheme will be similar, and will diverge for the higher curvature terms $N = \{20, 30, 40\}$.

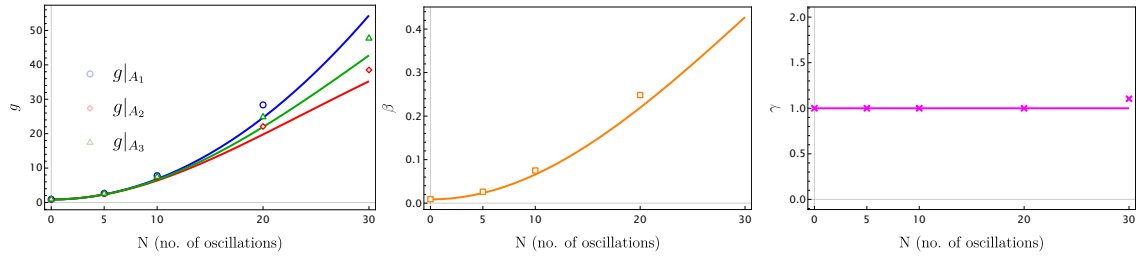


(a) (b) (c)

**Fig. 4.13.** Variation of parameters $g, \beta, \gamma$ computed from the Eqns.(4.20) (for the First Integration Scheme) and (2.118), (2.119) for the Second Integration Scheme respectively.

We also take into account the validation of the approximation of surface Laplacian term $\mathcal{D}_s\boldsymbol{q}$ at point $A_3$ made in (4.33), with $LHS$ denoting the value at point $A_3$ obtained directly from the numerical solution, and $RHS$ representing the average of the surface Laplacian values evaluated via FEM at points $A_1$ and $A_2$ of the interphase boundaries. The corresponding relative $\delta$ error is reported alongside each graph.

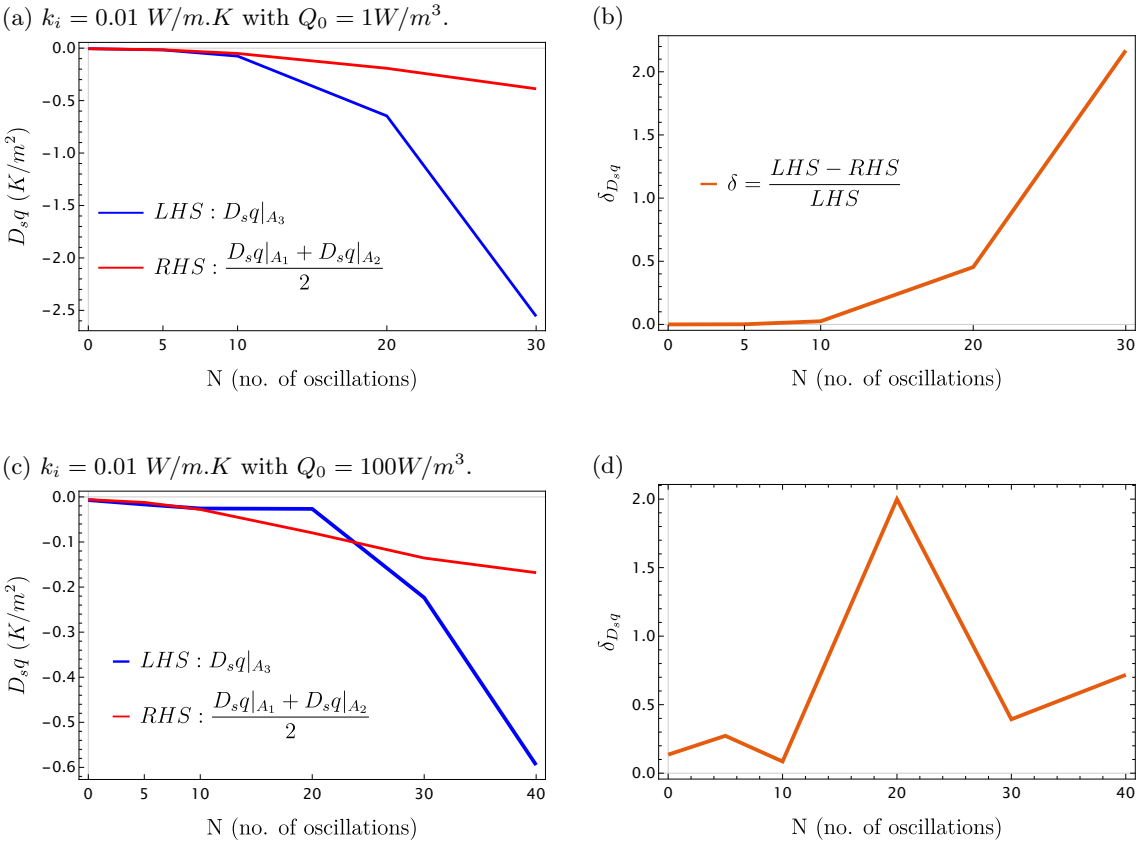


**Fig. 4.14.** Values of LHS and RHS of Eqn.(4.33), along with corresponding relative error, $\delta$ for a low conductive (LC) interphase, $k^{(i)} = 0.01\,W/m.K$ and $\epsilon = 0.01$.

Fig.4.14 shows the $\mathcal{D}_s\boldsymbol{q}$ for a low conductive interphase ($k^{(i)} = 0.01\,W/m.K$) having a low heat source value $Q_0 = 1.0\,W/m^3$ (Figs.4.14a,4.14b) and a high heat source $Q_0 = 100.0\,W/m^3$ (Figs.4.14c,4.14d), whereas Fig.4.15 shows the $\mathcal{D}_s\boldsymbol{q}$ for a high conductive interphase ($k^{(i)} = 100\,W/m.K$) having a low heat source value $Q_0 = 1.0\,W/m^3$

(Figs.4.15a,4.15b) and a high heat source $Q_0 = 100.0\,W/m^3$ (Figs.4.15c,4.15d) present inside the interphase. From both graphs, it can be clearly understood that the approximation is valid only for small curvature, up to $N = 10$, and beyond this, the temperature variation along the tangential direction is more rapid, leading to increasing deviations between the LHS and the RHS of (4.33), thus rendering the solutions obtained from our proposed schemes inaccurate.

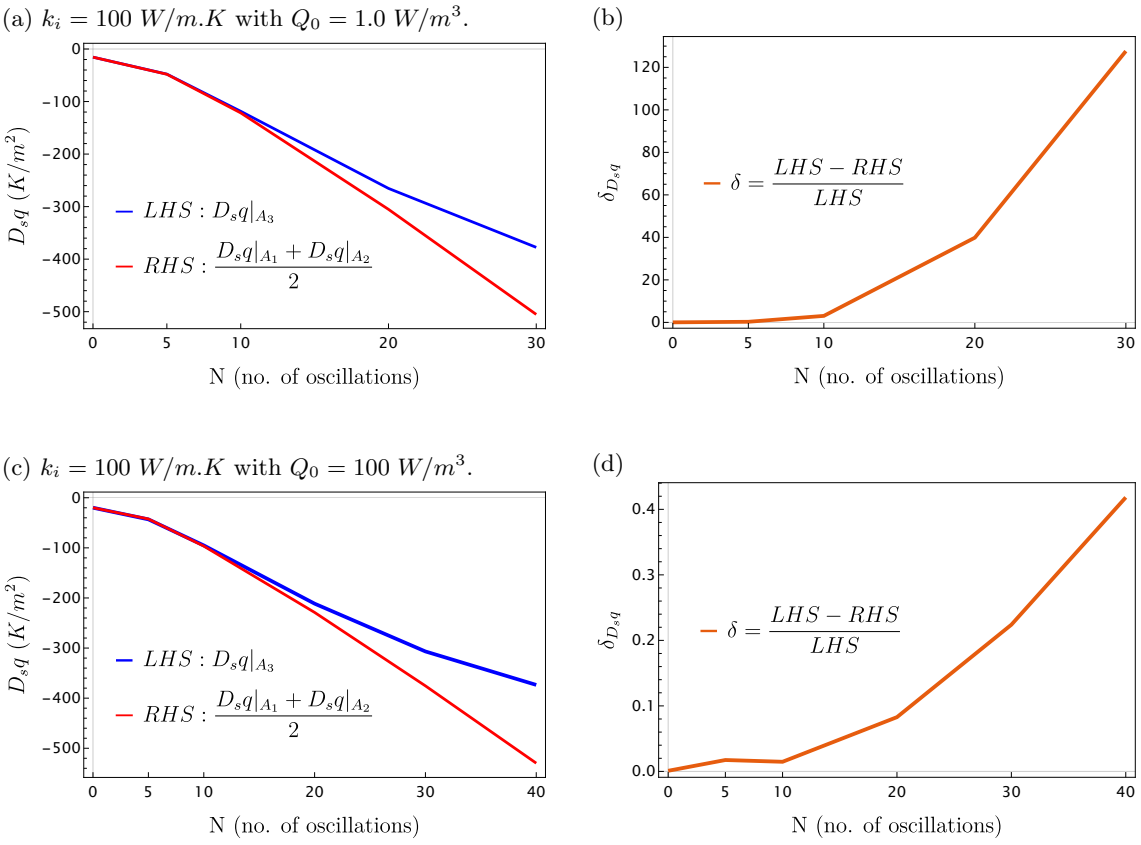


**Fig. 4.15.** Values of LHS and RHS of Eqn.(4.33), along with corresponding relative error, $\delta$ for a high conductive (HC) interphase, $k^{(i)} = 100\,W/m.K$ and $\epsilon = 0.01$.

Another key aspect to consider is the behaviour of the heat flux $q_n$ at point $A_3$, which is approximated for the First and Second Integration schemes via Eqns.(4.37) and (4.50) respectively. The value is also obtained numerically at the point $A_3$ via numerical solution, and the comparative analysis of these three values is made in Figs.4.16 for a low conductive interphase and 4.17 for a high conductive interphase. It can be gleaned from the presented figures that the three values coincide for small curvature and deviate considerably for the increasing oscillations. The deviation is more observable for the high conductive interphase. These graphs also highlight the comparison made in section 4.2.3 between the First and Second Integration Schemes. It can be seen that with increasing curvatures the values of $q_n|_{A_3}$ from the approximations Eqns.(4.37) and (4.50) diverge from each other. For the low conductive interphase, this deviation is very small ($\mathcal{O}(10^{-3})$) for the extreme values of oscillations, while for the high conductive interphase, the deviation between the two approximations is of the order $\mathcal{O}(10^{-1})$. Thus, based on these results, immediate observations can be made on the behaviour of proposed schemes with increasing curvatures, and it can be said with confidence, that the proposed schemes would work well for the small

curvature of $N \leq 10$. Beyond this, other accurate approximations are needed to increase the efficiency of the proposed schemes.

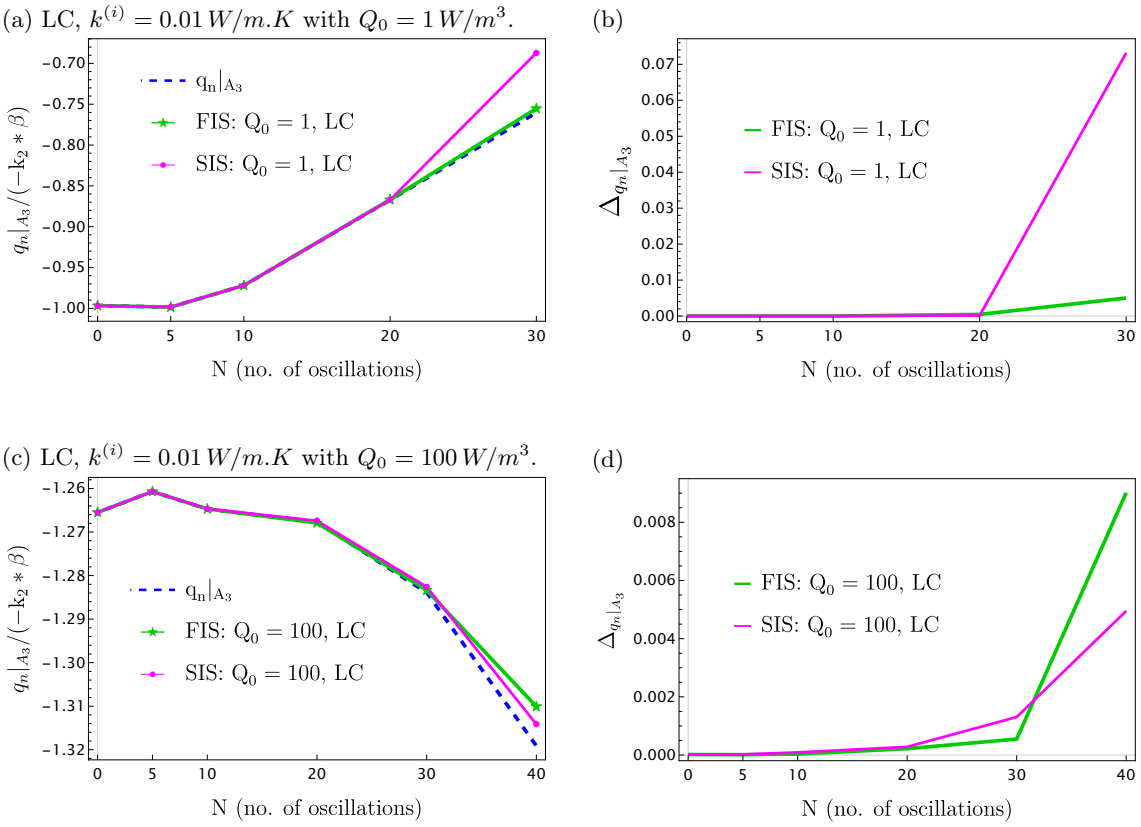


**Fig. 4.16.** Normalized heat flux values at point $A_3$ taken as: exact value from numerical simulation, represented by blue dashed line, green curve with star markers represents values computed from the Eqns.(4.37) for FIS (First Integration Scheme) and magenta curve with filled circle markers represents values computed from (4.50) for SIS (Second Integration Scheme), for a low conductive (LC) type interphase having thickness $\epsilon = 0.01$.

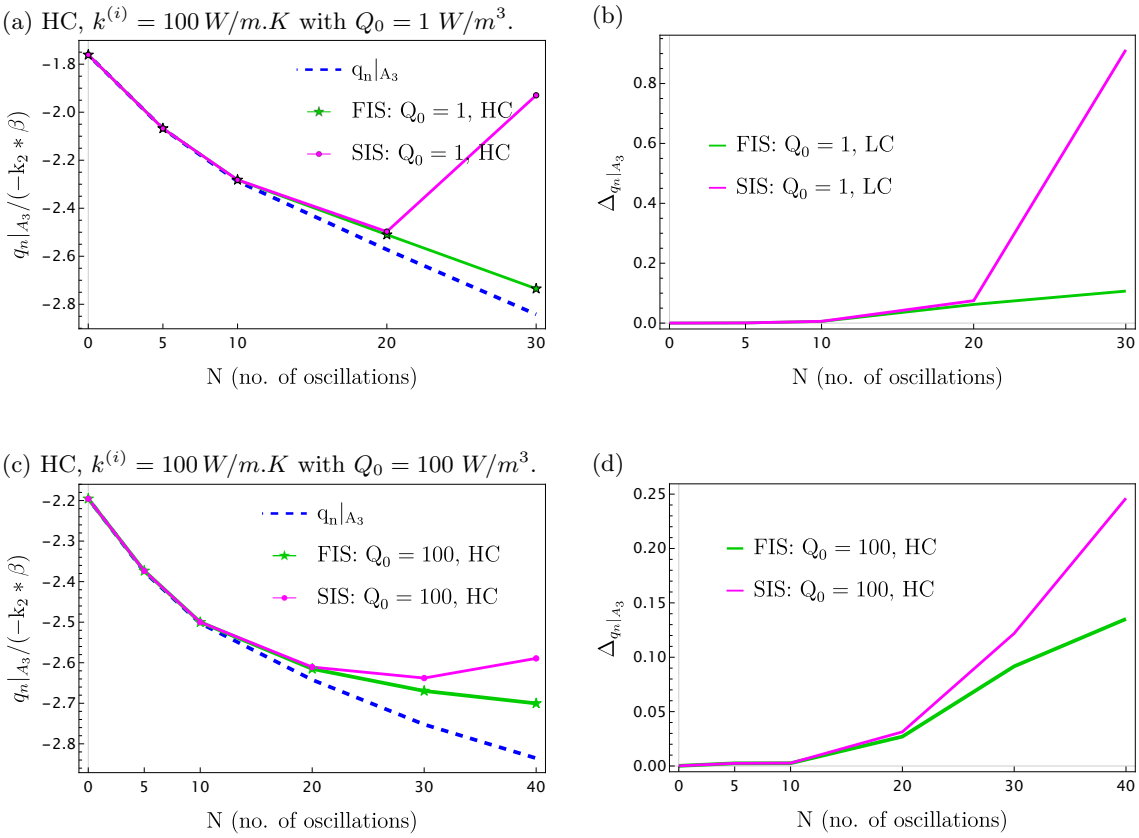


**Fig. 4.17.** Normalized heat flux values at point $A_3$ taken as: exact value from numerical simulation, represented by blue dashed line, green curve with star markers represents values computed from the Eqns.(4.37) for FIS (First Integration Scheme) and magenta curve with filled circle markers represents values computed from (4.50) for SIS (Second Integration Scheme), for a high conductive (HC) type interphase having thickness $\epsilon = 0.01$.

Fig.4.18 represents the normalized values of $[\![T]\!]$ and $[\![q_n]\!]$ in a perfect interphase (original solution) having two heat sources: small ($Q_0 = 1$) and high ($Q_0 = 100$) $W/m^3$, with respect to increasing curvature of the interphase boundaries. Figs.4.18a and 4.18b illustrate the behaviour of $[\![T]\!]$ and $[\![q_n]\!]$ of a low conductive interphase $k^{(i)} = 0.01\ W/m.K$ along-with increasing curvature in the tangential direction. It can be seen that for small curvatures $N = \{0, 5, 10\}$, the $[\![T]\!]$ and $[\![q_n]\!]$ are constant, and for higher curvatures, the jumps in temperatures and in the normal component of the heat flux decrease. This is because with increasing curvature, the surface area increases, which enables the interphase to transfer heat across its boundaries more efficiently. The temperature at point $A_2$ is higher as the interphase is resistant to the incoming heat flow from the matrix, and thus the heat flux passing through that point is also small. On the other side of the interphase, the heat transfer between interphase and the inclusion at point $A_1$ is rapid, as the inclusion is more conductive than the interphase, and hence the heat flux at that point is also along the natural thermal flow. For the case of a perfect circle ($N = 0$), the curvature is constant and thus the fluctuation of the heat flux along the normal direction at the boundaries is only due to the mismatch of the thermal conductivities at the boundaries of the interphase. With the increasing curvature, the heat flux becomes more localized near the boundaries of the interphase, in the regions where the normal aligns with the incoming

heat flow. The effect of rapidly varying boundary normals also causes the flux to be more concentrated in the region near the inner boundaries of the interphase - between inclusion and the interphase, because of the thermal conductivity mismatch. This causes a drop in the jumps of temperatures and in the heat flux across the boundaries. A representation of this is illustrated in Fig.4.28, where the localization of temperatures and heat fluxes can be clearly observed, as well as the accumulation of temperatures within the interphase, with increasing curvature. The presence of a higher heat source, represented by red curve with filled circles in Figs.4.18a,4.18b, in the interphase dominates the temperature and heat flux profiles, and the phenomenon explained above becomes more significant, as depicted in Fig.4.29, where higher temperatures and heat fluxes are seen near the boundary between the interphase and the matrix.

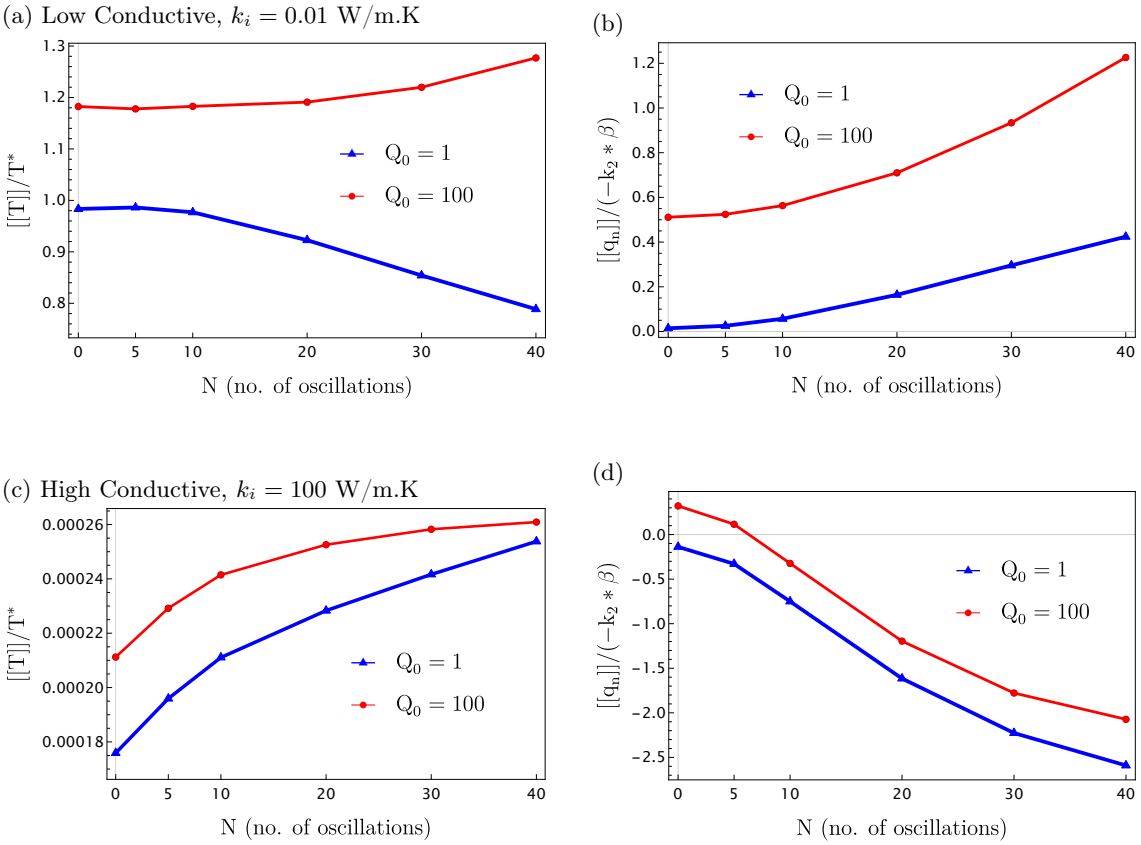


**Fig. 4.18.** Normalized jumps of temperature and heat flux across a perfect interphase (three-phase solution) setting, with respect to increasing curvature for a wavy interphase of thickness $\epsilon = 0.01$, having a low conductive ($k_i = 0.01W/m.K$ Figs.4.18a,4.18b) and high conductive ($k_i = 100W/m.K$ Figs.4.18c,4.18d) interphase.

In the case of a highly conductive interphase (Figs.4.18c,4.18d), the interphase is now more conductive ($k^{(i)} = 100W/m.K$) then the surroundings. Thus, the jumps in temperature and heat flux increases rapidly as the curvature increases, in both cases of heat sources term, $Q$. Although the increase in $[\![T]\!]$ is not much, the heat flux graph shows a significant increase. This can be clearly understood from the temperature and heat flux graphs shown in Figs.4.30 and 4.31 for both cases of heat sources. The conductivity mismatch at the boundary between the interphase and the matrix (at point $A_2$) causes the heat flux to flow rapidly along the natural flow of the heat, as the interphase is more conductive than

the matrix. Conversely, at the boundary between the interphase and the inclusion, the conductivity mismatch hinders the flux flowing across the boundaries, as the inclusion is now less conductive than the interphase. If the curvature is increased, the flux is more concentrated in the regions, where the normal of the curvature is aligned with the normal flow of heat, and the increasing boundary normals at the concave side of the boundary "trap" the heat flux, and thus, we see higher contours of flux at point $A_2$ than at $A_1$. With the presence of the high heat source inside the interphase, the heat source dominates the temperature and flux inside the interphase, and this hinders the temperature and heat flux at the boundaries of the interphase. Although the heat flux across the boundaries follows the same principle as explained above, only the magnitude of the flux at the boundaries is small.

- Low magnitude of heat source: Fig.4.19 represents jumps in temperature and heat flux computed numerically using FEM, for a low conductive interphase for each imperfect interface model discussed earlier. The comparison with temperature jump across a perfect interphase (solid green line) is shown (Figs.4.19a,4.19c) along with their corresponding absolute errors (Figs.4.19b,4.19d). The values of $[\![T]\!]$ and $[\![q_n]\!]$ for each model is computed by plugging in the values at point $A_1$ of the material 1, and at point $A_2$ of material 2, obtained from FEM simulations, into the respective equations. The absolute error, as defined in 4.157, plotted alongside each graphs. Here $[\![T]\!]_{ana}$ replaced by the temperature jump across the perfect interphase (between points $A_1$ and $A_2$ inside the interphase) and $[\![T]\!]_{num}$ is the temperature jump approximation computed from each model, and similarly for the heat flux.

  From the illustrated graphs, it is clear that our proposed schemes show good approximation of the exact solution, up to $N = 20$ oscillations, and beyond this the divergence between the schemes and the exact solution increases. In case of $[\![T]\!]$ the proposed schemes of three-points for both First and Second Integration (Eqns.(4.35) and (4.49) respectively) show very good approximation of the exact solution as compared to other schemes, and the relative error from these methods is $\mathcal{O}(\epsilon^2)$, and at the extreme value of $N = 40$ the methods diverge by $\mathcal{O}(10^{-3})$, which is quite small. The $[\![T]\!]$ approximated by general method of (4.84) is exactly same as those of our proposed schemes using two-points of integrations. In case of $[\![q_n]\!]$, depicted in Fig.4.19c and the corresponding relative errors graphs 4.19d, the error for small curvatures (upto $N \leq 10$) is approximately $\mathcal{O}(\epsilon^2)$ for all the methods in literature as well as the proposed First and Second Integration schemes using two points of integration. However, for the First and second integrations schemes employing three-points, the error is $\mathcal{O}(\epsilon^3)$, which is lowest than that of the competing methods. With increasing oscillations, the errors increase to $\mathcal{O}(\epsilon)$, with Second Integration schemes showing lower values than the First Integration scheme. The error between the two schemes is approximately $\mathcal{O}(10^{-3})$ for small curvatures and increases to $\mathcal{O}(\epsilon)$ for highly oscillating curves.

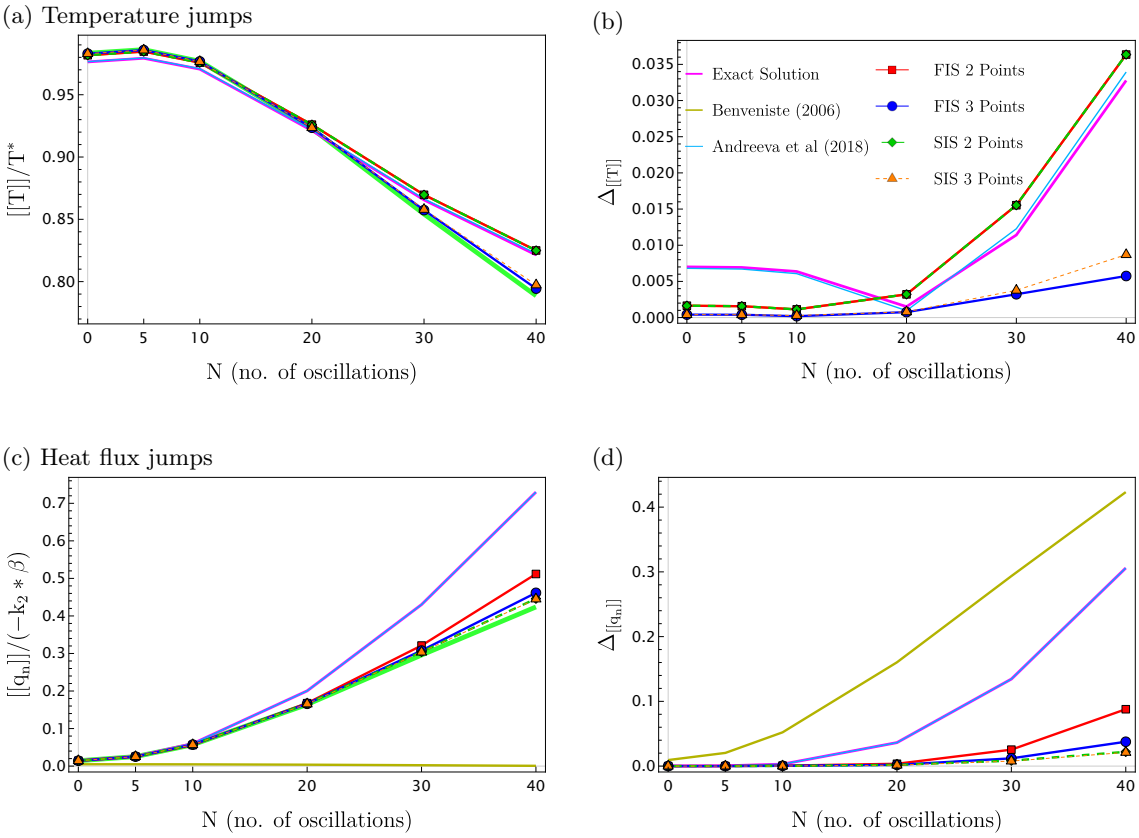


**Fig. 4.19.** $[\![T]\!]$ and $[\![q_n]\!]$ for a wavy interphase of thickness $\epsilon = 0.01$, with heat source of $Q_0 = 1.0$. Fig.4.19a and 4.19b show the temperature jumps and relative errors, respectively, and Figs.4.19c,4.19d represent jumps in normal component of heat flux for low conductive interphase ($k^{(i)}/k^{(2)} = 0.01$), against increasing curvature values, $N$.

Fig.4.20 represents jumps in normal component of heat flux obtained from each imperfect interface model discussed earlier. The comparison with flux jump across a perfect interphase (solid green line) is shown (Figs.4.20a,4.20c) along with their corresponding relative errors (Figs.4.20b,4.20d). For a high conductive type interphase, the jumps in temperature is negligible. Thus, from Fig.4.20b that the error values in very small, except for those obtained from Benveniste, 2006b and Han et al., 2021, which is consistent with the results for the analytical solution of the circular interphase, in sec.4.4.2. These methods show high deviation from the exact solution, ($\mathcal{O}(\epsilon)$). The errors, reported by all other schemes, including our proposed schemes is less than $\mathcal{O}(\epsilon^2)$, where it is clear that the First and Second Integration schemes using three-points of integration are more accurate than those using two points of integration.

For the case of $[\![q_n]\!]$, the proposed schemes of three-points integration show the least deviation from the exact solution, that is, they have least absolute error for $N \leq 20$, beyond which the errors start to grow. It must also be brought to attention that the methods show similar solutions; the error between the two methods is approximately $\mathcal{O}(\epsilon^2)$ for small curvatures, while it increases from $\mathcal{O}(10^{-1})$ to $\mathcal{O}(10^0)$. It can also be seen that the First and Second Integration schemes show almost similar approximations of the exact solution, upto smaller curvatures.

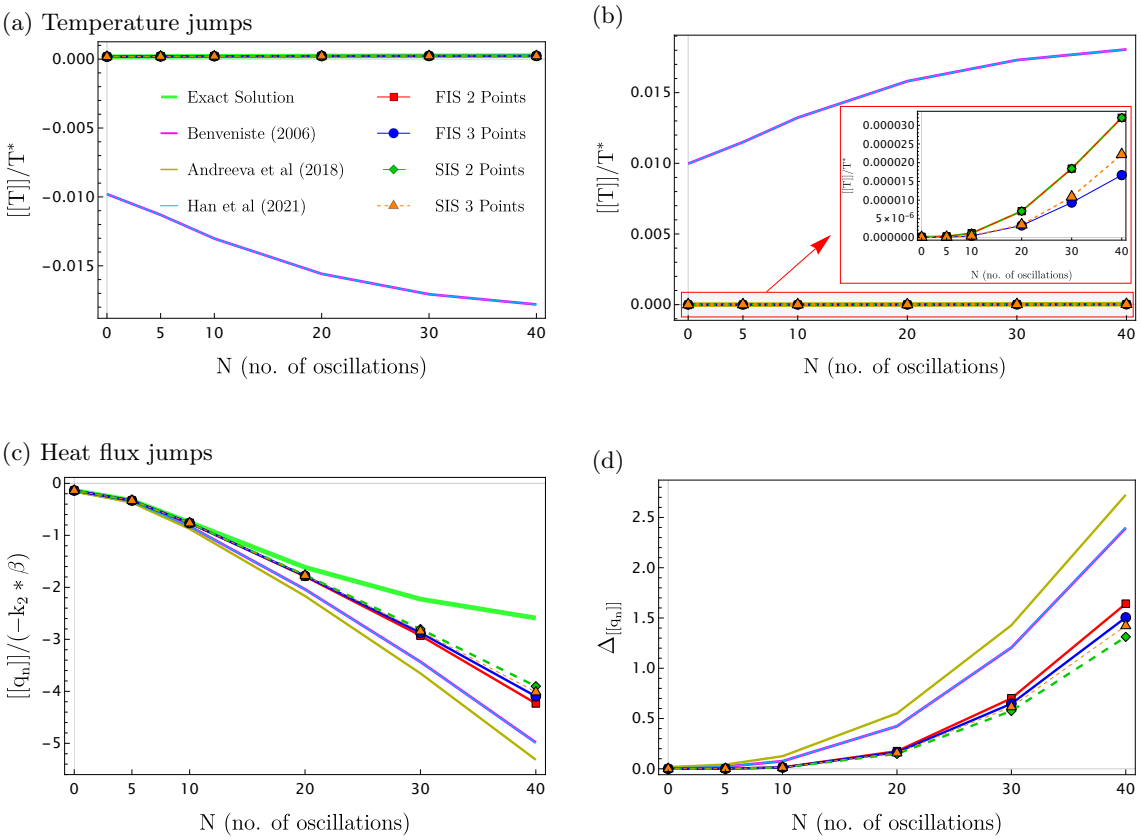


**Fig. 4.20.** $[\![T]\!]$ and $[\![q_n]\!]$ for a wavy interphase of thickness $\epsilon = 0.01$, with heat source of $Q_0 = 1.0$. Fig.4.20a and 4.20b show the temperature jumps and relative errors, respectively, and Figs.4.20c,4.20d represent jumps in normal component of heat flux for high conductive interphase ($k^{(i)}/k^{(2)} = 100$), against increasing curvature values, $N$.

Fig.4.21 represents the temperatures and heat fluxes at the inner and outer boundaries of the interphase, that is, moving along the interphase boundaries, from $0 \leq \theta \leq 2\pi$, as obtained from the COMSOL solution of three-phase problem. The values are presented for each case of increasing curvatures, $N$ for a low conductive interphase $k^{(i)}/k^{(2)} = 0.01$ having a thickness of $\epsilon = 0.01$ and volumetric heat source of magnitude $Q_0 = 1\, W/m^3$. Figs.4.21a and 4.21b represent temperatures at the inner and outer boundaries of the interphase, while Figs.4.21c and 4.21d depict heat flux values at the inner and outer boundaries of the interphase. The maximum value of temperatures is obtained at $\theta = 0$ rad. As is clear from the graph, the temperatures at the inner boundary (between the interphase and material 1) is lower than that at the outer boundary. This can be explained by the thermal conductivity mismatch at the boundary. At the inner boundary, the inclusion behaves as a conductive material, in comparison to the interphase, and thus the heat transfer from the interphase to the inclusion is rapid, lowering the temperature at this boundary. When curvature is increased, naturally the localization of corresponding boundary normals also increases. Due to this, the temperature at the concave surface of the interphase increases. Thus, we see slightly higher temperatures for $N = 40$ than the perfect circle $N = 0$ at $\theta = 0$.

At the outer boundary of the interphase, the temperature is higher than that at

the inner boundary. The thermal conductivity mismatch at this boundary causes localization of temperature at the boundary, for all values of $N$. This is primarily because the interphase, which has lower conductivity than that of the surrounding matrix, thus, creating the barrier or a resistance for the incoming thermal flow. With increasing curvatures, and consequently increasing surface areas, the rate of heat transfer becomes slightly more efficient, and thus the temperature at this point ($\theta = 0$) is lower for the highly oscillating curves, as compared to that of the small curvatures or the constant curvature, that is, a circle at the same point.

The heat fluxes are illustrated in Figs.4.21c for the inner boundary and in 4.21d for the outer boundary. It is observed that the heat fluxes at the outer boundary is lower than than at the inner boundary of a low conductive interphase, and it decreases further for the high "waviness" of the curve.

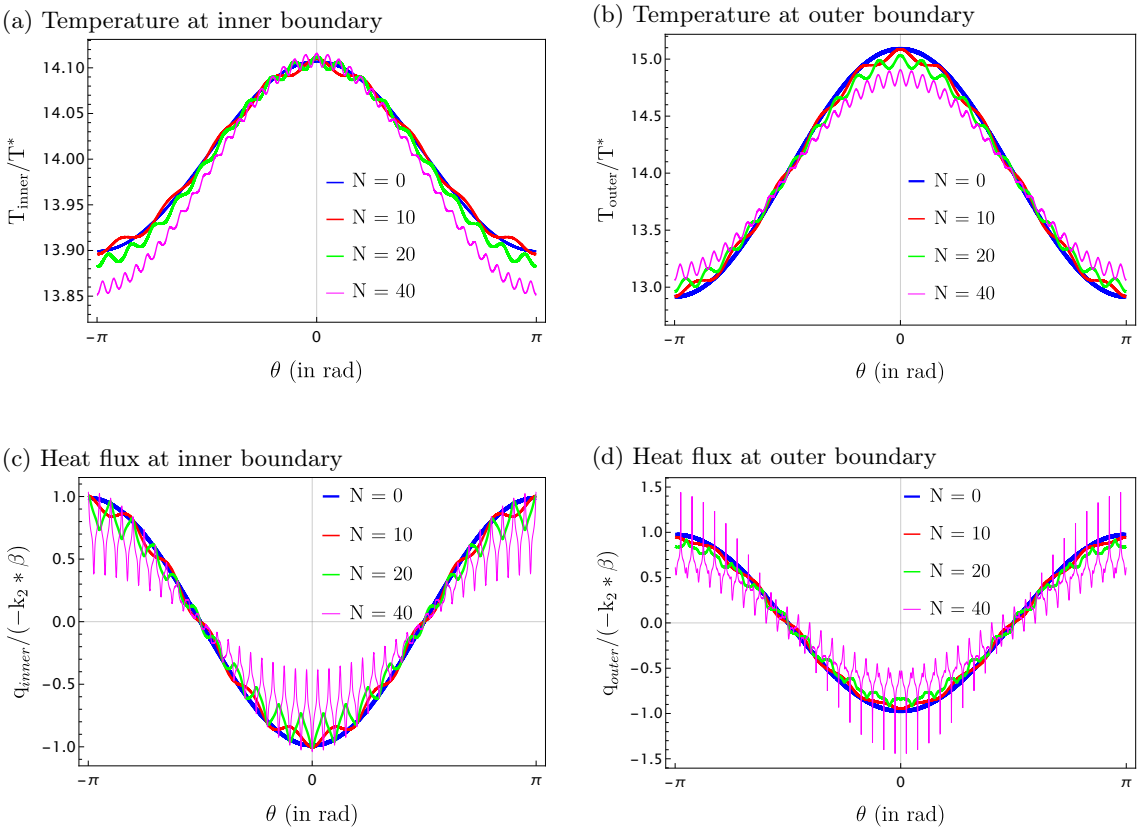


**Fig. 4.21.** Variation of temperature and heat flux at the inner and outer boundaries of the interphase, for different values of oscillations, $N$, for an interphase of thickness $\epsilon = 0.01$, and thermal conductivity $k^{(i)}/k^{(2)} = 0.01$, having an internal heat source of magnitude $Q_0 = 1\,W/m^3$.

Fig.4.22 represents the temperatures and heat fluxes at the inner and outer boundaries of the interphase, that is, moving along the interphase boundaries, from $0 \leq \theta \leq 2\pi$, for a high conductive interphase $k^{(i)}/k^{(2)} = 100$ having a thickness of $\epsilon = 0.01$ and volumetric heat source of magnitude $Q_0 = 1\,W/m^3$. Figs.4.22a and 4.22b represent temperatures at the inner and outer boundaries of the interphase, while Figs.4.22c and 4.22d depict heat flux values at the inner and outer boundaries of the interphase. Since the interphase has higher conductivity than the bonding media on either side, the flow of temperature and the heat flux occurs along the natural flow direction at

the boundaries. However, the flow is more rapid between boundary of material 2 and the interphase, as $k^{(i)}/k^{(2)} = 100$. With increasing curvatures, the heat transfer is more rapid, and thus lower values of heat flux is obtained for highly curved boundary.

On the boundary between the inclusion and the interphase, the heat transfer has some impediment, as material 1 behaves like an insulator, due to lower thermal conductivity than the interphase $k^{(i)}/k^{(2)} = 0.1$. As the curvature is increased, the flux is more concentrated in the regions, where the normal of the curvature is aligned with the normal flow of heat, and the increasing boundary normals at the concave side of the boundary "trap" the heat flux. This "slows" the heat flux flow, and at the boundary between inclusion and the interphase, the heat flux values are lower, as seen from the graph.

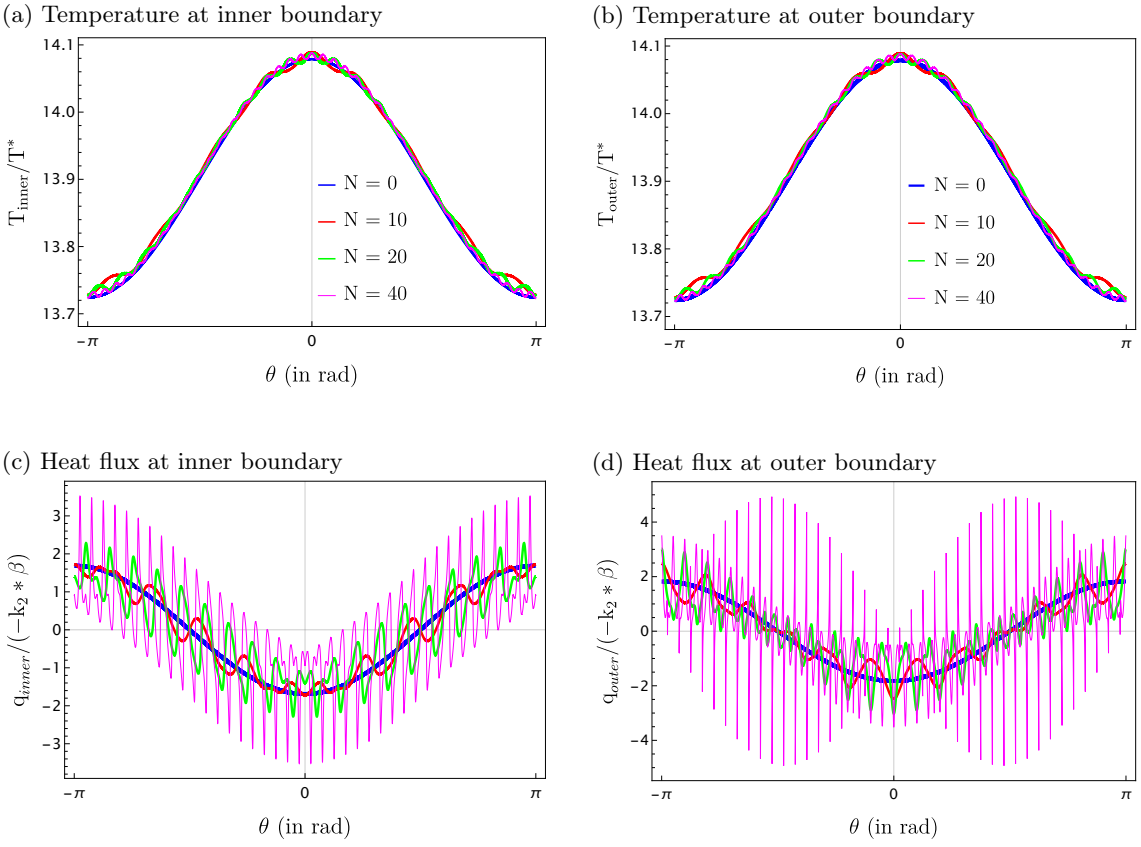


**Fig. 4.22.** Variation of temperature and heat flux at the inner and outer boundaries of the interphase, for different values of oscillations, $N$, for an interphase of thickness $\epsilon = 0.01$, and thermal conductivity $k^{(i)}/k^{(2)} = 100$, having an internal heat source of magnitude $Q_0 = 1\,W/m^3$.

- Higher Heat Source: Fig.4.23 represents jumps in temperature and heat flux computed numerically using FEM, for a low conductive interphase havinf a higher magnitude of volumetric heat source term $Q_0 = 100\,W/m^3$. The figure illustrates $[\![T]\!]$ and $[\![q_n]\!]$ for each imperfect interface model discussed earlier. The comparison with temperature jump across a perfect interphase (solid green line) is shown (Figs.4.23a,4.23c) along with their corresponding absolute errors (Figs.4.23b,4.23d).

  The presence of a higher heat source inside the interphase dominates the temperature distribution inside the interphase, as seen in Figs.4.18a,4.18b. This in turn

influences the heat flux profile inside the interphase. With increasing curvatures, the localization of temperature and heat flux increases at the interphase boundaries. From the illustrated graphs, it is clear that that while our proposed schemes does not coincide with the exact solution for $[\![T]\!]$, Fig.4.23a, the three-points scheme show least deviation as compared to the two -points scheme or the classical methods. The $[\![T]\!]$ approximated by general method of (4.84) is exactly same as those of our proposed schemes using two-points of integrations. In case of $[\![q_n]\!]$, depicted in Fig.4.23c and the corresponding relative errors graph 4.23d, it can be seen that the proposed scheme of First integration method using three-points shows good approximation of the exact solution, and has the least error of all proposed schemes, approx $\mathcal{O}(\epsilon^2)$ to $\mathcal{O}(10^{-3})$ for small curvatures (upto $N \leq 20$). For all the methods in literature as well as the proposed First and Second Integration schemes using two points of integration, the error is approximately $\mathcal{O}(10^{-3})$, while for the $[\![q_n]\!]$ approximations from (4.86) has a relative error of $\mathcal{O}(\epsilon)$ for the First Integration schemes, and the three-point schemes of Second Integration method.

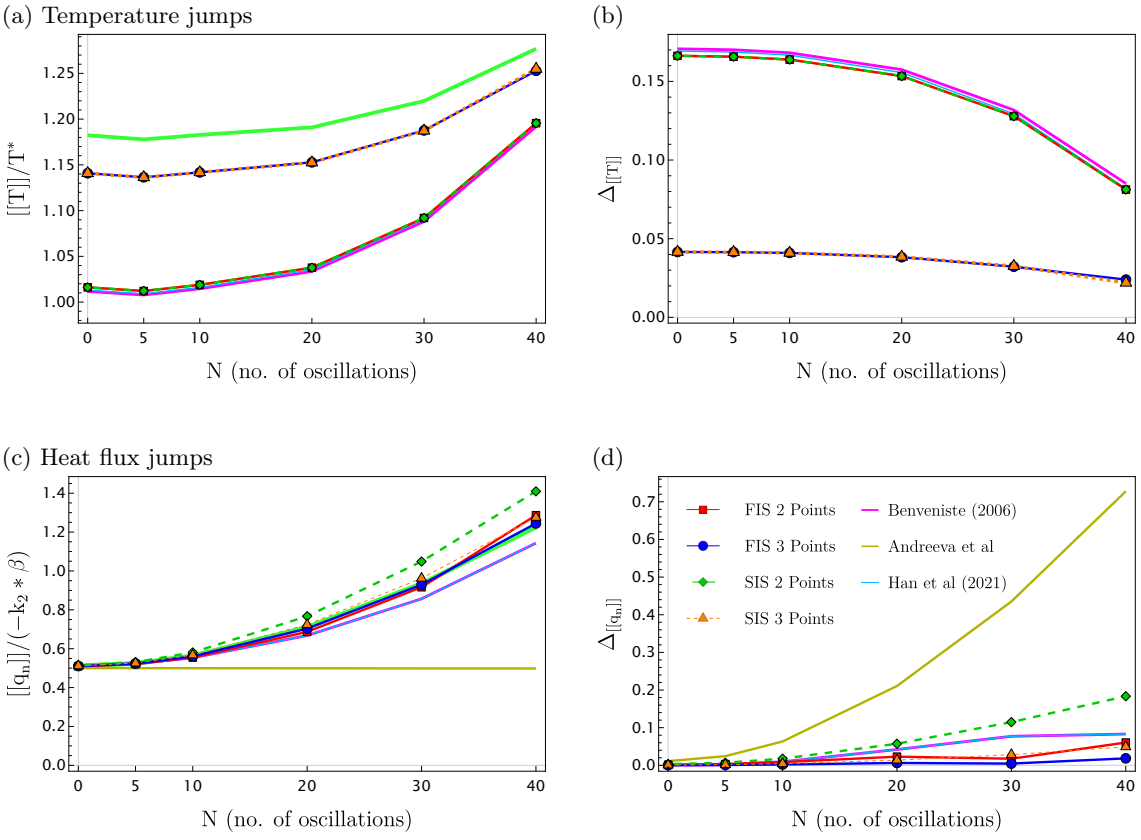


**Fig. 4.23.** $[\![T]\!]$ and $[\![q_n]\!]$ for a wavy interphase of thickness $\epsilon = 0.01$, with heat source of $Q_0 = 100.0$. Fig.4.23a and 4.23b show the temperature jumps and relative errors, respectively, and Figs.4.23c,4.23d represent jumps in normal component of heat flux for low conductive interphase ($k^{(i)}/k^{(2)} = 0.01$), against increasing curvature values, $N$.

Fig.4.24 represents jumps in temperature and normal component of heat flux for a conductive type interphase ($k^{(i)}/k^{(2)} = 100$) having a high heat source term ($Q_0 = 100\,W/m^3$) present inside the interphase. The comparison with flux jump across a perfect interphase (solid green line) is shown (Figs.4.24a,4.24c) along with their

corresponding relative errors (Figs.4.24b,4.24d) for jumps in temperature and heat flux respectively.

For a high conductive type interphase, the jumps in temperature is negligible, as discussed in Fig.4.20b. Although none of the methods coincide with the exact solution, but the deviation reported by the proposed methods is very small. Thus, from Fig.4.24b jumps in temperature and the corresponding absolute errors values is very small, except for those obtained from Benveniste, 2006b and Han et al., 2021, which is consistent with the results for the analytical solution of the circular interphase, in sec.4.4.2. These methods show high deviation from the exact solution, ($\mathcal{O}(\epsilon)$). The errors, reported by all other schemes, including our proposed schemes is less than $\mathcal{O}(\epsilon^2)$, while those reported by the proposed three-point schemes of the First and Second Integration schemes are more accurate, with error of $\mathcal{O}(\epsilon^3)$ upto $N \leq 20$, and increasing to $\mathcal{O}(\epsilon^2)$ for the higher oscillations.

The jumps in normal components of heat flux $[\![q_n]\!]$, the proposed schemes of three-points integration for the First and Second Method show the least deviation from the exact solution, that is, they have least absolute error for $N \leq 5$, beyond which the errors start to grow. It must also be brought to attention that the methods show similar solutions; the error between the two methods is approximately $\mathcal{O}(10^{-3})$ for small curvatures, while it increases to $\mathcal{O}(10^{-1})$ at the extreme value of curvature. It can also be seen that the First and Second Integration schemes show almost similar approximations of the exact solution, upto smaller curvatures. With increasing curvatures, the Second Integration scheme using two points shows better approximations than all other methods.

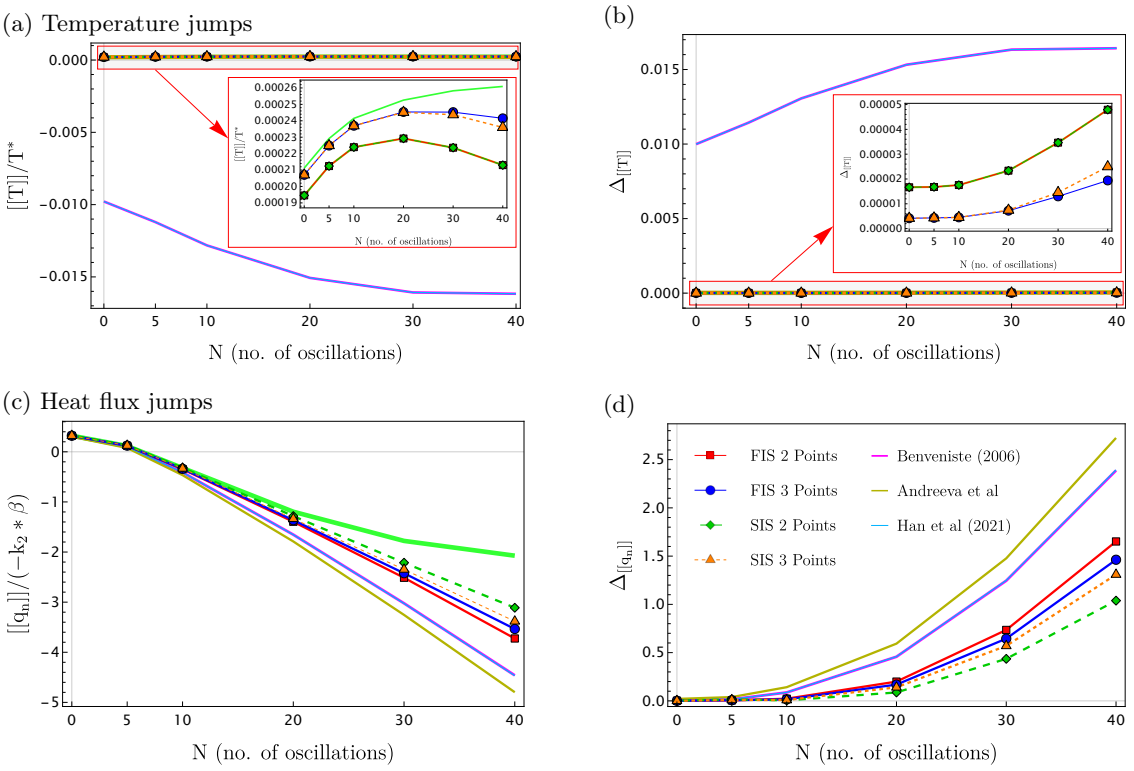


**Fig. 4.24.** $[\![T]\!]$ and $[\![q_n]\!]$ for a wavy interphase of thickness $\epsilon = 0.01$, with heat source of $Q_0 = 100.0\, W/m^3$. Fig.4.24a and 4.24b show $[\![T]\!]$ and relative errors, respectively, and Figs.4.24c,4.24d represent $[\![q_n]\!]$ for high conductive interphase ($k^{(i)}/k^{(2)} = 100$), against increasing curvature values, $N$.

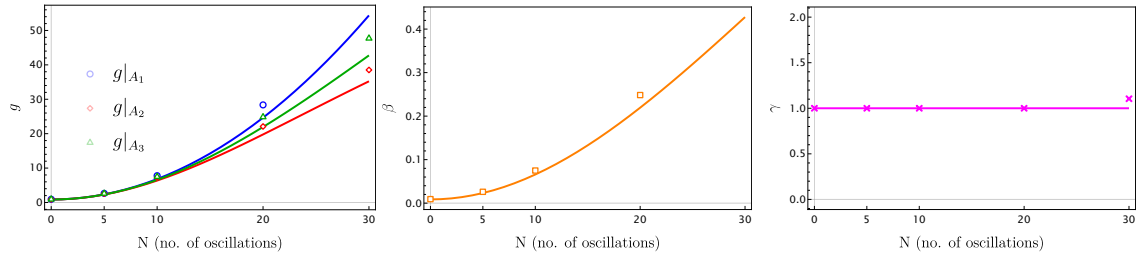


(a) (b) (c)

**Fig. 4.25.** Variation of parameters $g, \beta, \gamma$ for a wavy interphase of amplitude $A = 0.08m$ computed from the Eqns.(4.20) (for the First Integration Scheme) and (2.118), (2.119) for the Second Integration Scheme respectively.

**Effect of amplitude of the oscillatory curve:** Increasing the amplitude of the oscillatory curve increases the height of the peaks (and the troughs) of the wavy curve. This causes the outer edge of the curve to create overlapping or self-intersecting geometry, and thus making it difficult to produce reasonable solutions. For example, increasing the amplitude to 0.08 in appropriate units creates overlapping geometry for $N = 40$, and increasing further to 0.1 produces self-intersecting elements for a geometry having $N = 30$ oscillations in a period of $0 \leq \theta \leq 2\pi$, and so on. The Fig.4.25 plotted below illustrate the variations of parameters $g, \beta, \gamma$ with increasing curvature values.

Fig.4.26 portrays approximation of surface Laplacian term $\mathcal{D}_s\boldsymbol{q}$ at point $A_3$ made in (4.33), with $LHS$ denoting the value at point $A_3$ obtained from the numerical solution, and $RHS$ representing the average of the surface Laplacian values at points $A_1$ and $A_2$. The corresponding relative $\delta$ error is reported alongside each graph.

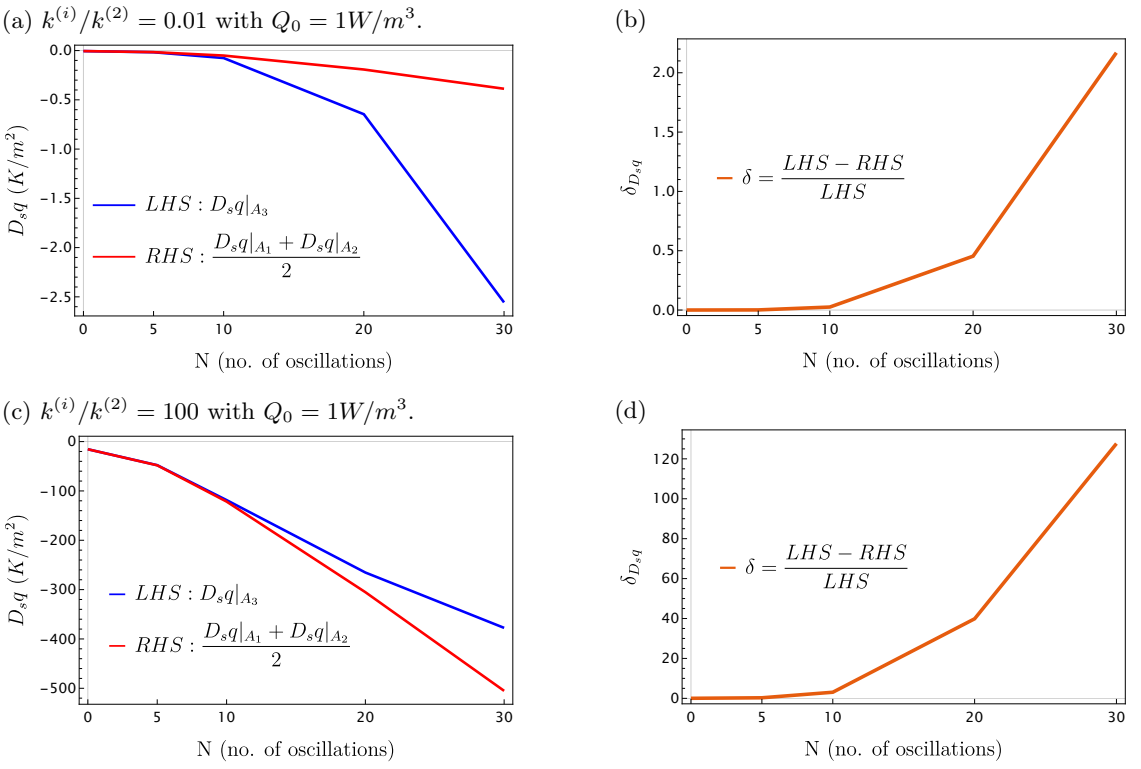


**Fig. 4.26.** Values of LHS and RHS of Eqn.(4.33), along with corresponding relative error, $\delta$ for an interphase of thickness $\epsilon = 0.01$, and amplitude $A = 0.08$.

The plots of 4.27 gives an idea of the behaviour of the heat flux $q_n$ at point $A_3$, which is approximated for the First and Second Integration schemes via Eqns.(4.37) and (4.50) respectively. The value is also obtained numerically at the point $A_3$ via numerical solution, and the comparative analysis of these three values is made in Figs.4.27. It is observed from the presented figures that the three values coincide for small curvature and deviate considerably for the increasing oscillations. For a low conductive interphase, the approximations hold true until $N = 20$, while for the high conductive interphase, the deviation can be observed beyonf $N = 10$.

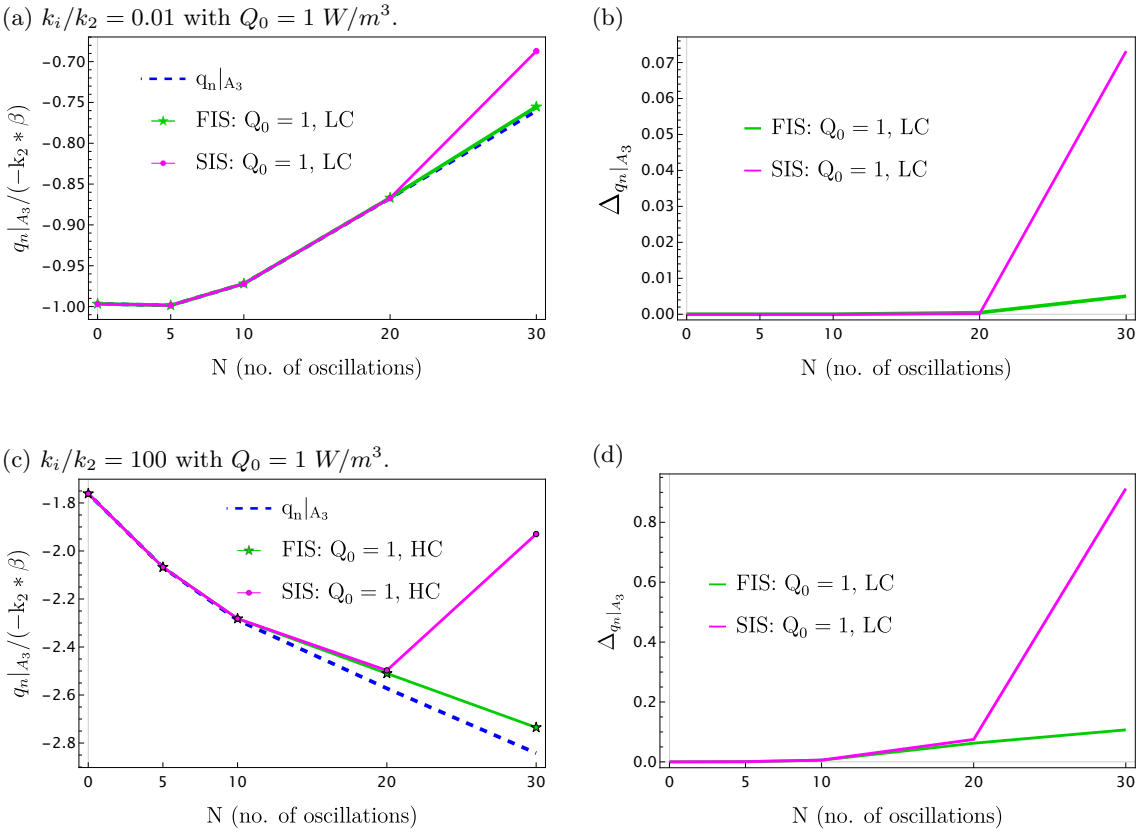


**Fig. 4.27.** Normalized heat flux values at point $A_3$ taken as: exact value from numerical simulation, represented by blue dashed line, green curve with star markers represents values computed from the Eqns.(4.37) for FIS (First Integration Scheme) and magenta curve with filled circle markers represents values computed from (4.50) for SIS (Second Integration Scheme), for an interphase having thickness $\epsilon = 0.01$ and amplitude of $A = 0.08m$.

It can be concluded from this section that the proposed transmission conditions would provide a good approximation of the jumps in temperature and heat fluxes for small curvatures, (up to $N \leq 10$) for high amplitudes of the curves, while the high curvatures demonstrate the invalidity of the parallel surfaces approach.

## 4.5 Appendix

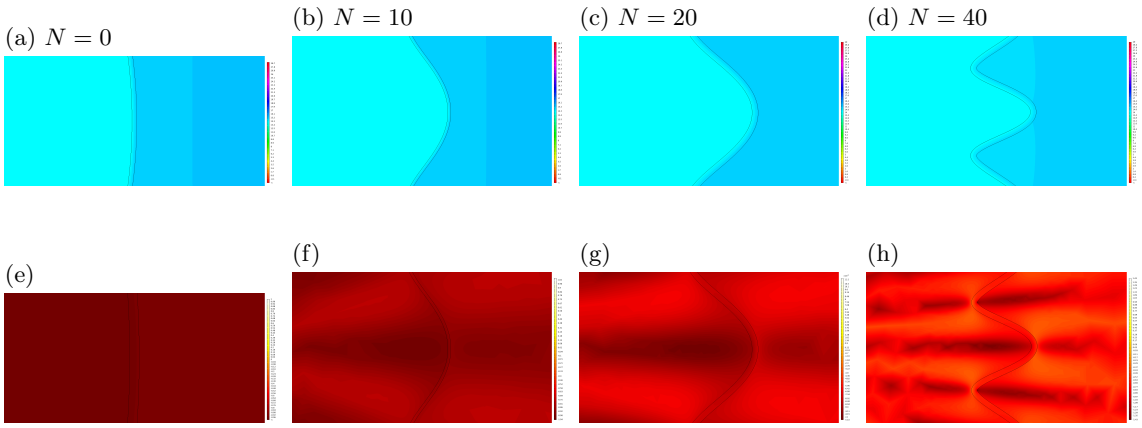


**Fig. 4.28.** Zoomed in view of temperatures (4.28a-4.28d) and heat fluxes (4.28e-4.28h) at $\theta = 0\,\text{deg}$, for increasing values of N. The volumetric heat source is small $Q_0 = 1$. The plot shows the effect of curvature geometry on the temperature contours for a low conductive interphase ($k_i/k_2 = 0.01, \epsilon = 0.01$).

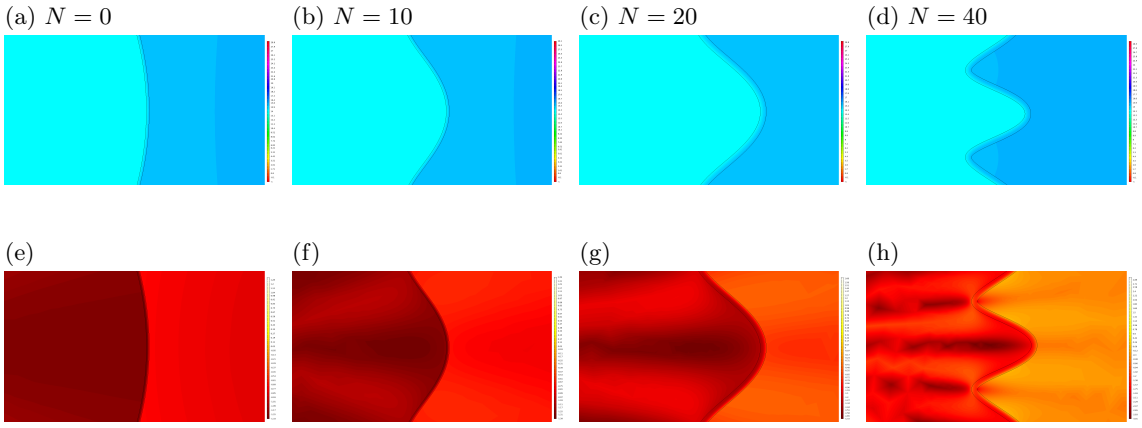


**Fig. 4.29.** Zoomed in view of temperatures (4.29a-4.29d) and heat fluxes (4.29e-4.29h) at $\theta = 0\,\text{deg}$, for increasing values of N. The volumetric heat source is high $Q_0 = 100$. The plot shows the effect of curvature geometry on the temperature contours for a low conductive interphase ($k_i/k_2 = 0.01, \epsilon = 0.01$).

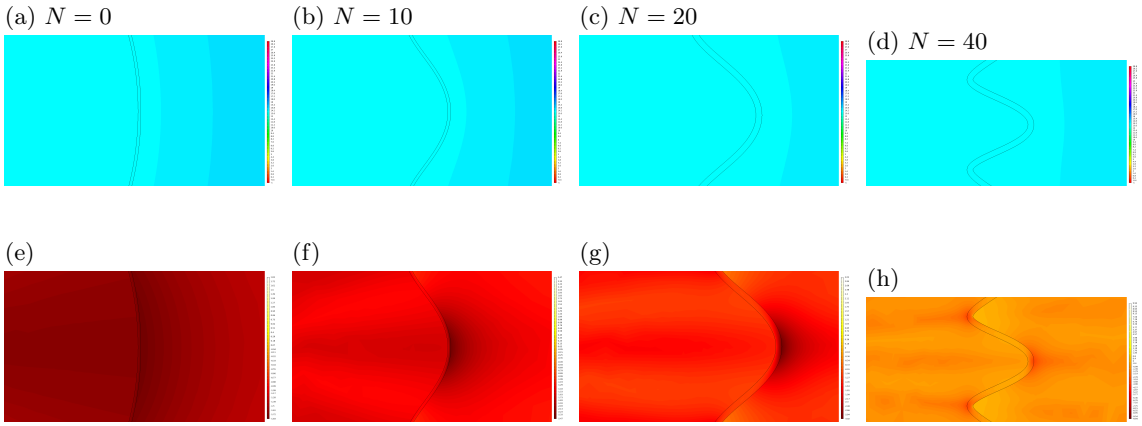


**Fig. 4.30.** Zoomed in view of temperatures (4.30a-4.30d) and heat fluxes (4.30e-4.30h) at $\theta = 0$ rad, for increasing values of N. The volumetric heat source is small $Q_0 = 1$. The plot shows the effect of curvature geometry on the temperature contours for a high conductive interphase ($k_i/k_2 = 100, \epsilon = 0.01$).

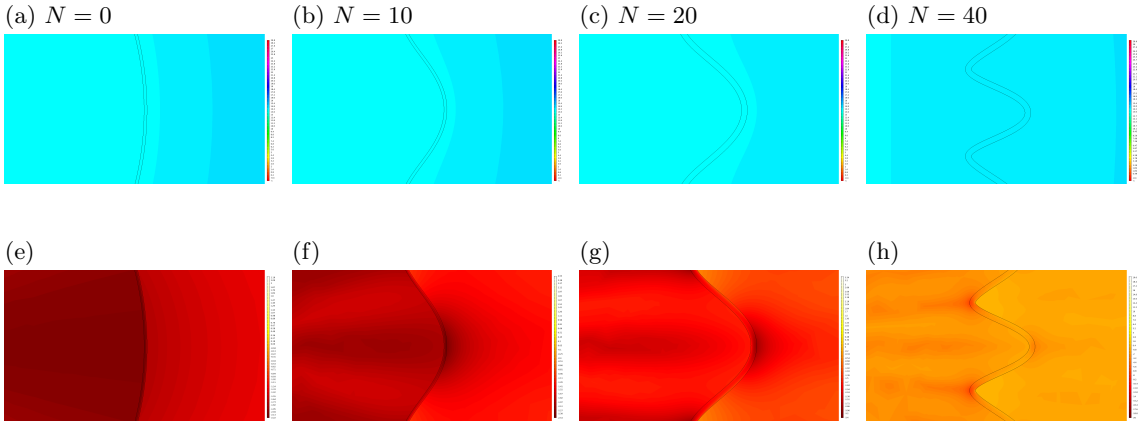


**Fig. 4.31.** Zoomed in view of temperatures (4.31a-4.31d) and heat fluxes (4.31e-4.31h) at $\theta = 0\,\text{deg}$, for increasing values of N. The volumetric heat source is high $Q_0 = 100$. The plot shows the effect of curvature geometry on the temperature contours for a high conductive interphase ($k_i/k_2 = 100, \epsilon = 0.01$).

# Chapter 5

# Transmission conditions across a thin, spring-type elastic interface

## 5.1 Introduction

The present study focuses on the development of transmission conditions for higher order, using three point formulation. The transmission conditions are obtained by implementing Trapezoidal rule at two intervals, between points $A_1$ situated at the boundary $S_1$ between interphase and the media "1" and point $A_3$ which is an arbitrary point inside the interphase, while the second interval is between the points $A_2$, lying on the boundary between interphase boundary $S_2$ and surrounding media "2", and point $A_3$ inside the interphase.

The chapter is organized as follows. Sec.5.2 presents the governing equations in curvilinear coordinates and introduces the geometric relations required for the asymptotic analysis. Sec.5.3 to 5.5 details the derivation of the higher-order transmission conditions based on the three-point trapezoidal formulation. Sec.5.7 assesses the accuracy and applicability of the proposed methodology through the boundary value problem of a coated fiber embedded in a unidirectional flow field. The chapter concludes with a discussion of the numerical results and an evaluation of the accuracy and limitations of the developed model.

## 5.2 Governing Equations in Curvilinear Coordinates

Consider $(\alpha_1, \alpha_2, \alpha_3)$ to be the curvilinear coordinates, with the axis of $\alpha_1$ aligned with the normal to the system. The scale factors are $h_1, h_2, h_3$ with $h_1 = 1$. The governing equations for any linear, isotropic elastic material in curvilinear coordinates are:

1. Strain Displacement Equations:

$$\varepsilon_{ij} = \frac{1}{2}\Big\{ (\operatorname{grad} \boldsymbol{u})_{ij} + (\operatorname{grad} \boldsymbol{u})_{ji} \Big\} \tag{5.1}$$

2. Balance Equations:

$$\operatorname{div} \sigma + \rho \boldsymbol{F} = 0 \tag{5.2}$$

3. Hooke's Law:

$$\sigma_{ij} = \lambda \varepsilon_{kk} \delta_{ij} + 2\mu \varepsilon_{ij} \tag{5.3}$$

In terms of strain tensor, this equation can also be rewritten as:

$$\varepsilon_{ij} = \frac{1}{E}\Big[\sigma_{ij} - \nu\left(\sigma_{kk}\delta_{ij} - \sigma_{ij}\right)\Big] \tag{5.4}$$

where $E$ is the Young's modulus, and $\nu$ is the Poisson's ratio.

## 5.3 Motivation

In his paper, Benveniste, 2006b used Taylor series expansion around point $A_1$ and $A_2$ to express the displacement and stress vector $\boldsymbol{t}^{(i)}$ at point $A_3$ as:

$$\begin{aligned}
\boldsymbol{u}^{(i)}(\xi) &= \boldsymbol{u}^{(i)}_{A_1} + \left.\frac{\partial \boldsymbol{u}^{(i)}}{\partial n}\right|_{A_1} \xi + \frac{1}{2}\left.\frac{\partial^2 \boldsymbol{u}^{(i)}}{\partial n^2}\right|_{A_1} \xi^2, \quad 0 \le \xi \le t/2, \\
\boldsymbol{u}^{(i)}(\xi) &= \boldsymbol{u}^{(i)}_{A_2} + \left.\frac{\partial \boldsymbol{u}^{(i)}}{\partial n}\right|_{A_2} (\xi - t) + \frac{1}{2}\left.\frac{\partial^2 \boldsymbol{u}^{(i)}}{\partial n^2}\right|_{A_2} (\xi - t)^2, \quad t/2 \le \xi \le t, \\
\boldsymbol{t}^{(i)}(\xi) &= \boldsymbol{t}^{(i)}_{A_1} + \left.\frac{\partial \boldsymbol{t}^{(i)}}{\partial n}\right|_{A_1} \xi + \frac{1}{2}\left.\frac{\partial^2 \boldsymbol{t}^{(i)}}{\partial n^2}\right|_{A_1} \xi^2, \quad 0 \le \xi \le t/2, \\
\boldsymbol{t}^{(i)}(\xi) &= \boldsymbol{t}^{(i)}_{A_2} + \left.\frac{\partial \boldsymbol{t}^{(i)}}{\partial n}\right|_{A_2} (\xi - t) + \frac{1}{2}\left.\frac{\partial^2 \boldsymbol{t}^{(i)}}{\partial n^2}\right|_{A_2} (\xi - t)^2, \quad t/2 \le \xi \le t,
\end{aligned} \tag{5.5}$$

It can be easily seen that the displacement values inside the interphase ($\boldsymbol{u}^{(i)}(\xi)|_{A_3}$), obtained by Taylor series expansion whether around the point $A_1$ or the point $A_2$, are discontinuous, as illustrated in Fig.5.2. The expansion above provides us with a good approximation of the displacement and stress values at the interphase boundaries, but within the domain itself (i.e, away from the boundaries), the behavior of displacement and surface flux is seen to be discontinuous. This is in contrast to the intuitive assumption that material is continuous at all points within the interphase, and thus all the associated state variables such as displacement, stresses, etc. should be continuous as well inside the domain of the interphase.

To compute our model, we proceed in a similar way as in the thermal case in Sec.4.1 by taking the Taylor series expansion around point $A_1$ and $A_2$, to express displacement at point $A_3$:

$$\begin{aligned}
\boldsymbol{u}^{(i)}(\xi) &= \boldsymbol{u}^{(i)}_{A_1} + \left.\frac{\partial \boldsymbol{u}^{(i)}}{\partial \alpha_1}\right|_{A_1} \xi + \boldsymbol{a}\xi^2, \quad 0 \le \xi \le t_1, \\
\boldsymbol{u}^{(i)}(\xi) &= \boldsymbol{u}^{(i)}_{A_2} + \left.\frac{\partial \boldsymbol{u}^{(i)}}{\partial \alpha_1}\right|_{A_2} (\xi - t) + \boldsymbol{b}(\xi - t)^2, \quad t_1 \le \xi \le t,
\end{aligned} \tag{5.6}$$

where

$$\frac{\partial \boldsymbol{u}^{(i)}}{\partial \alpha_1} = \frac{\partial \boldsymbol{u}^{(i)}}{\partial n} = (\nabla \boldsymbol{u}^{(i)}) \cdot \hat{\boldsymbol{n}} \tag{5.7}$$

since the coordinate $\alpha_1$ is aligned with the normal direction. From the constitutive relation for an isotropic linearly elastic material, the stress is given as:

$$\boldsymbol{\sigma}^{(i)}_n = \mathbb{C} \cdot \boldsymbol{\epsilon} = \mathbb{C} \cdot (\nabla \boldsymbol{u}^{(i)}), \tag{5.8}$$

$$\mathbb{C}^{-1} \cdot \boldsymbol{\sigma}^{(i)}_n = \nabla \boldsymbol{u}^{(i)} \tag{5.9}$$

The gradient of displacement vector $\boldsymbol{u}^{(i)}$ can be decomposed into its normal and tangential components as:

$$\nabla \cdot \boldsymbol{u}^{(i)} = \operatorname{grad} \boldsymbol{u}^{(i)} = \operatorname{grad}_s \boldsymbol{u}^{(i)} + \operatorname{grad} \boldsymbol{u}^{(i)} \cdot \hat{\boldsymbol{n}} \tag{5.10}$$

where $\text{grad}_s\, \boldsymbol{u}^{(i)}$ is the second order tensor that comprises all the tangential components of the displacement vector, that is, along the $\alpha_2$ and $\alpha_3$ directions, and $\text{grad}\, \boldsymbol{u}^{(i)} \cdot \hat{\boldsymbol{n}}$ is the normal derivative of the gradient of the displacement vector. It consists of the normal component and the tangential components of the displacement vector, taken along the normal direction. Thus,

$$\text{grad}\, \boldsymbol{u}^{(i)} \cdot \hat{\boldsymbol{n}} = \frac{\partial \boldsymbol{u}^{(i)}}{\partial n} \tag{5.11}$$

Substituting this value into the constitutive equation, we get:

$$\mathbb{C}^{-1} \cdot \boldsymbol{\sigma}_n^{(i)} = \text{grad}\, \boldsymbol{u}^{(i)} \tag{5.12}$$

$$= \text{grad}_s\, \boldsymbol{u}^{(i)} + \text{grad}\, \boldsymbol{u}^{(i)} \cdot \hat{\boldsymbol{n}} \tag{5.13}$$

$$= \text{grad}_s\, \boldsymbol{u}^{(i)} + \boldsymbol{B}\, \frac{\partial \boldsymbol{u}^{(i)}}{\partial n} \tag{5.14}$$

where $\boldsymbol{B} = B_{klp} = \delta_{k1}\delta_{lp}$ is a kinematic selector tensor which only allows the $B_{1kk}$ terms, and also converts the vector $(\text{grad}\, \boldsymbol{u}^{(i)} \cdot \hat{\boldsymbol{n}})$ to the second-order tensor form maintaining the mathematical equality, near the interface in a local Cartesian coordinate. It simply identifies the elements of the displacement vector that are aligned or projected along the unit normal vector. $\mathbb{C}^{-1}$ is a second order tensor. Here, in place of $\boldsymbol{u}^{(i)}$ for the normal derivative, we substitute the asymptotic expansion of (5.6), which gives us the following set of equations. We do not substitute (5.6) into $\text{grad}_s$ because there is no expansion of the vector along the tangential direction.

$$\mathbb{C}^{-1}\boldsymbol{\sigma}_n^{(i)}(\xi) = \text{grad}_s\, \boldsymbol{u}^{(i)}\Big|_{A_3} + \boldsymbol{B}\left(\frac{\partial \boldsymbol{u}^{(i)}}{\partial \alpha_1}\Big|_{A_1} + 2\,\boldsymbol{a}\,\xi\right) \tag{5.15}$$

and

$$\mathbb{C}^{-1}\boldsymbol{\sigma}_n^{(i)}(\xi) = \text{grad}_s\, \boldsymbol{u}^{(i)}\Big|_{A_3} + \boldsymbol{B}\left(\frac{\partial \boldsymbol{u}^{(i)}}{\partial \alpha_1}\Big|_{A_2} + 2\,\boldsymbol{b}\,(\xi - t)\right) \tag{5.16}$$

Across a perfect interphase,

$$\boldsymbol{u}^{(i)}(\xi)(t_1^+) = \boldsymbol{u}^{(i)}(\xi)(t_1^-) \quad ; \quad \boldsymbol{\sigma}_n^{(i)}(\xi)(t_1^+) = \boldsymbol{\sigma}_n^{(i)}(\xi)(t_1^-) \tag{5.17}$$

Thus, we get the following two equations:

$$\text{grad}_s\, \boldsymbol{u}^{(i)}\Big|_{A_3} + \boldsymbol{B}\left(\frac{\partial \boldsymbol{u}^{(i)}}{\partial \alpha_1}\Big|_{A_1} + 2\,\boldsymbol{a}\,\xi\right) = \text{grad}_s\, \boldsymbol{u}^{(i)}\Big|_{A_3} + \boldsymbol{B}\left(\frac{\partial \boldsymbol{u}^{(i)}}{\partial \alpha_1}\Big|_{A_2} + 2\,\boldsymbol{b}\,(\xi - t)\right) \tag{5.18}$$

and from (5.6)

$$\boldsymbol{u}_{A_1}^{(i)} + \frac{\partial \boldsymbol{u}^{(i)}}{\partial \alpha_1}\Big|_{A_1} \xi + \boldsymbol{a}\xi^2 = \boldsymbol{u}_{A_2}^{(i)} + \frac{\partial \boldsymbol{u}^{(i)}}{\partial \alpha_1}\Big|_{A_2} (\xi - t) + \boldsymbol{b}(\xi - t)^2 \tag{5.19}$$

Solving these two sets of equations (5.18) and (5.19), we get a general form of the internal parameter vectors $\boldsymbol{a}$ and $\boldsymbol{b}$:

$$\boldsymbol{a} = \frac{2\,(\boldsymbol{u}^{(i)}|_{A_2} - \boldsymbol{u}^{(i)}|_{A_1}) - t_2\left(\frac{\partial \boldsymbol{u}^{(i)}}{\partial \alpha_1}\Big|_{A_2} - \frac{\partial \boldsymbol{u}^{(i)}}{\partial \alpha_1}\Big|_{A_1}\right) - 2\,t\,\frac{\partial \boldsymbol{u}^{(i)}}{\partial \alpha_1}\Big|_{A_1}}{2\,t\,t_1} \tag{5.20}$$

$$\boldsymbol{b} = \frac{2\,(\boldsymbol{u}^{(i)}|_{A_1} - \boldsymbol{u}^{(i)}|_{A_2}) + t_1\left(\frac{\partial \boldsymbol{u}^{(i)}}{\partial \alpha_1}\Big|_{A_1} - \frac{\partial \boldsymbol{u}^{(i)}}{\partial \alpha_1}\Big|_{A_2}\right) + 2\,t\,\frac{\partial \boldsymbol{u}^{(i)}}{\partial \alpha_1}\Big|_{A_2}}{2\,t\,t_2} \tag{5.21}$$

where $\nabla_s \boldsymbol{u}^{(i)}$ is the surface gradient of the displacement vector, and $\xi = t_1$, and $(\xi - t) = -t_2$. The normal components of the displacement vector can be replaced by substituting the stress-strain relationship defined in terms of curvilinear coordinates as given in (3.46)

$$\boldsymbol{\varepsilon}^{(i)} = \frac{1}{2}\left(\nabla \boldsymbol{u}^{(i)} + (\nabla \boldsymbol{u}^{(i)})^T\right) \tag{5.22}$$

$$\varepsilon_{km} = \frac{1}{2}\sum_{k,m}\left(\frac{1}{h_m}\frac{\partial}{\partial \alpha_m}(u_k^{(i)}\,\hat{e}_k)\otimes \hat{e}_m + \frac{1}{h_k}\frac{\partial}{\partial \alpha_k}(u_m\,\hat{e}_m)\otimes \hat{e}_k\right) \tag{5.23}$$

The complete equation is as given in (3.47):

$$\varepsilon_{km}^{(i)} = \frac{1}{2}\left[\frac{1}{h_k}\frac{\partial u_m^{(i)}}{\partial \alpha_k} + \frac{1}{h_m}\frac{\partial u_k^{(i)}}{\partial \alpha_m} - \left(\frac{u_k^{(i)}}{h_m\,h_k}\frac{\partial h_k}{\partial \alpha_m} + \frac{u_m^{(i)}}{h_m\,h_k}\frac{\partial h_m}{\partial \alpha_k}\right)\right] \tag{5.24}$$

To obtain components along the normal direction, we fix $k = 1$, while $m = \{1, 2, 3\}$. This means the normal and tangential components of the displacement vector with respect to the normal direction are: $\partial u_1/\partial \alpha_1, \partial u_2/\partial \alpha_1, \partial u_3/\partial \alpha_1$, represented by the first term on the RHS and since $\alpha_1$ is aligned with the normal, $h_1 = 1$. Therefore, the equation presented above can be re-written in the following form:

$$\frac{\partial u_m^{(i)}}{\partial \alpha_1} = 2\,\varepsilon_{1m}^{(i)} - \left(\frac{1}{h_m}\frac{\partial u_1^{(i)}}{\partial \alpha_m} - \frac{u_m^{(i)}}{h_m}\frac{\partial h_m}{\partial \alpha_1}\right) \tag{5.25}$$

isolating the derivative of the displacement vector along the normal direction. From the constitutive Hooke's Law, the strain term can also be replaced with the corresponding term of stress tensor. However, since only terms along the normal direction are considered, this gives the traction vector $\boldsymbol{t}^{(i)}$ written as

$$t_m^{(i)} = \sigma_{im}^{(i)} \cdot \hat{n}_i = \sigma_{n_m}^{(i)} \tag{5.26}$$

where $\sigma_{n_m}^{(i)}$ is the traction vector. Thus, from Hooke's Law

$$\varepsilon_{1m}^{(i)} = \mathbb{C}_{1j1m}^{-1}\,\sigma_{n_j}^{(i)} \tag{5.27}$$

The normal derivative of the displacement in (5.25) can then be given as

$$\frac{\partial u_m^{(i)}}{\partial \alpha_1} = 2\,\mathbb{C}_{1j1m}^{-1}\,\sigma_{n_j}^{(i)} - \left(\frac{1}{h_m}\frac{\partial u_1^{(i)}}{\partial \alpha_m} - \frac{u_m^{(i)}}{h_m}\frac{\partial h_m}{\partial \alpha_1}\right) = 2\,\mathbb{C}_{1j1m}^{-1}\,\sigma_{n_j}^{(i)} - \mathcal{P}_m^{(i)} \tag{5.28}$$

where $\mathcal{P}_m$ is the vector operator that represents:

$$\mathcal{P}_m = \frac{1}{h_m}\frac{\partial u_1}{\partial \alpha_m} - \frac{u_m}{h_m}\frac{\partial h_m}{\partial \alpha_1} \tag{5.29}$$

We can now substitute (5.28) into (5.20) to get a different form of the internal parameters $\boldsymbol{a}$ and $\boldsymbol{b}$ in terms of the surface gradients components of the displacement vector and the traction vector. Upon rearranging the terms, we get the following form for $\boldsymbol{a}$

$$\begin{aligned}\implies \quad a_m = &\frac{2\,(u_m^{(i)}|_{A_2} - u_m^{(i)}|_{A_1}) - 2\,t_2\,C_{1j1m}^{-1}\left(\sigma_{n_j}^{(i)}|_{A_2} - \sigma_{n_j}^{(i)}|_{A_1}\right)}{2\,t\,t_1} \\ &\frac{+t_2\left(\mathcal{P}_m|_{A_2} - \mathcal{P}_m|_{A_1}\right) - 2\,t\left(2\,C_{1j1m}^{-1}\sigma_{n_j}^{(i)} - \mathcal{P}_m^{(i)}\right)|_{A_1}}{2\,t\,t_1}\end{aligned} \tag{5.30}$$

And similarly, for the second parameter $\boldsymbol{b}$, we get the following form

$$\begin{aligned}\implies \quad b_m = \frac{2\,(u_m^{(i)}|_{A_1} - u_m^{(i)}|_{A_2}) + 2\,t_1\,C^{-1}_{1j1m}\left(\sigma_{n_j}^{(i)}|_{A_1} - \sigma_{n_j}^{(i)}|_{A_2}\right)}{2\,t\,t_2} \\ \frac{-t_1\left(\mathcal{P}_m|_{A_1} - \mathcal{P}_m|_{A_2}\right) + 2\,t\left(2\,C^{-1}_{1j1m}\sigma_{n_j}^{(i)} - \mathcal{P}_m^{(i)}\right)|_{A_2}}{2\,t\,t_2}\end{aligned} \tag{5.31}$$

Eqns.(5.30) and (5.31) are symmetric in nature $(A_1, t_1) \leftrightarrow (A_2, t_2)$. Thus, the internal parameters $\boldsymbol{a}, \boldsymbol{b}$ depend on the normal component of the displacement and stress vector. Ideal interphase conditions exists between the interphase and the surrounding materials at points $A_1$ and $A_2$, and displacement and stress vector (traction) for each material is continuous across the interphase boundaries.

$$\begin{aligned}\boldsymbol{u}^{(i)}|_{A_1} &= \boldsymbol{u}^{(1)}|_{A_1} \quad ; \quad \boldsymbol{u}^{(i)}|_{A_2} = \boldsymbol{u}^{(2)}|_{A_2} \\ \boldsymbol{\sigma}_n^{(i)}|_{A_1} &= \boldsymbol{\sigma}_n^{(1)}|_{A_1} \quad ; \quad \boldsymbol{\sigma}_n^{(i)}|_{A_2} = \boldsymbol{\sigma}_n^{(2)}|_{A_2}\end{aligned} \tag{5.32}$$

This allows us to compute the displacements and stress vectors at the intermediate surface (at point $A_3$) inside the interphase, expressed as

$$\begin{aligned}\boldsymbol{u}^{(i)}|_{A_3}(t_1^+) = \boldsymbol{u}^{(i)}|_{A_3}(t_1^-) = \frac{t_1\,t_2\left(\mathcal{P}_m^{(i)}|_{A_2} - \mathcal{P}_m^{(i)}|_{A_1}\right) + 2\,t_1\,t_2\left(\mathbb{C}^{-1}\boldsymbol{\sigma}_{A_1}^{(i)} - \mathbb{C}^{-1}\,\boldsymbol{\sigma}^{(i)}|_{A_2}\right)}{2\,t} \\ + \frac{2\left(t_1\,\boldsymbol{u}^{(i)}|_{A_2} + t_2\,\boldsymbol{u}^{(i)}|_{A_1}\right)}{2\,t}\end{aligned} \tag{5.33}$$

To compute the stress vector at the intermediate surface, we make use of Hooke's law again,

$$\boldsymbol{\sigma}_n^{(i)} = \mathbb{C}\cdot\boldsymbol{\varepsilon}_n^{(i)} = \mathbb{C}\cdot\left(\operatorname{grad}\boldsymbol{u}^{(i)} + \left(\operatorname{grad}\boldsymbol{u}^{(i)}\right)^{\mathsf{T}}\right) = \mathbb{C}\cdot\left\{\frac{1}{2}\left(\frac{\partial\boldsymbol{u}^{(i)}}{\partial\alpha_1} + \mathcal{P}^{(i)}\right)\right\} \tag{5.34}$$

At point $A_3$ which forms the intermediate surface, the normal derivative of the displacement term becomes

$$\frac{\partial\boldsymbol{u}^{(i)}}{\partial\alpha_1}_{A_3} = \frac{\partial\boldsymbol{u}^{(i)}}{\partial n}_{A_3} = 2\left(\frac{\partial\boldsymbol{u}^{(i)}|_{A_3}}{\partial t_1} - \frac{\partial\boldsymbol{u}^{(i)}|_{A_3}}{\partial t_2}\right) \tag{5.35}$$

Substituting these values into the stress vector equations provides us with the following equation

$$\begin{aligned}\boldsymbol{\sigma}_n^{(i)}|_{A_3}(t_1^-) = \boldsymbol{\sigma}_n^{(i)}|_{A_3}(t_1^+) = \frac{\mathbb{C}\cdot\mathcal{P}^{(i)}|_{A_1}\,t_1 + \mathbb{C}\cdot\mathcal{P}^{(i)}|_{A_2}\,t_2 - 2\left(\boldsymbol{\sigma}_n^{(i)}|_{A_1}\,t_1 + \boldsymbol{\sigma}_n^{(i)}|_{A_2}\,t_2\right)}{2\,t} \\ \frac{-4\,\mathbb{C}\left(\boldsymbol{u}^{(i)}|_{A_2} - \boldsymbol{u}^{(i)}|_{A_1}\right) + \mathcal{P}^{(i)}|_{A_3}}{2\,t}\end{aligned} \tag{5.36}$$

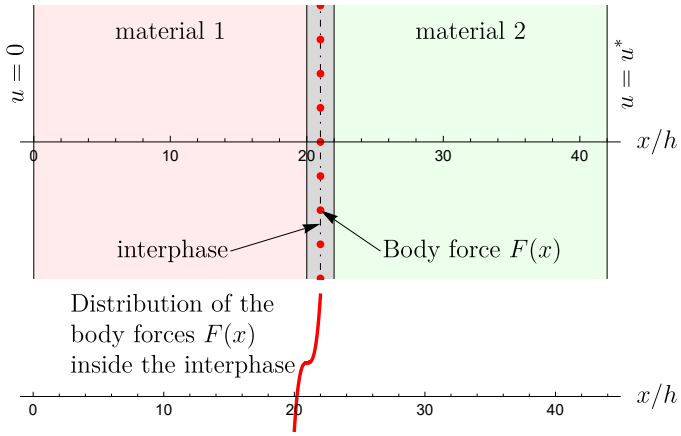


**Fig. 5.1.** Example of an interphase between two materials with uniformly distributed body forces inside the interphase.

**Body Force Function:** Consider a uniformly distributed body force function in the interphase given as:

$$F(x) = F_0 \left( \frac{x + \zeta - b_1 - h}{h} \right)^{\alpha} \tag{5.37}$$

where $\alpha$ is an integer number, representing the "type" of heat source, ie, constant ($\alpha = 0$), linear ($\alpha = 1$), quadratic ($\alpha = 2$) or cubic ($\alpha = 3$), while $|\zeta| < h$ is the position of the heat source within the interphase, denoting the symmteric ($\zeta = 0$) or the unsymmteric ($\zeta \neq 0$) heat source distribution within the interphase. In the numerical examples below, $\zeta$ will be taken as $h/2$, where $h = t/2$. Here, $t$ is the total thickness of the interphase. The volumetric heat source is presented by $Q_0$ ($W/m^3$), and $x$ is the position or the point within the interphase where the heat source will be computed.

Fig.5.2 demonstrates the displacement and the stress behaviour for the exact solution (shown in blue) and the displacement and stress in x-direction inside the interphase using Benveniste's assumptions (orange line) and using our assumptions (computed using $a_1$ and $a_2$ parameters, shown in green). It can be easily seen that the except for the constant body force type (Fig.5.2a,5.2b), where all approximations are continuous, displacement approximations using Benveniste's assumptions are discontinuous inside the interphase, in the presence of a small body force value, while our assumptions respects the continuity of the field variables inside the interphase at all points, for all types of body forces. Moreover, it can be seen that for quadratic (Fig.5.2e,5.2f) and cubic body forces (Fig.5.2g,5.2h), the stresses inside the interphase are no longer continuous for Benveniste's approximations, while our assumptions shows good approximation of the continuity.

It is important to note here that the example presented here indicates that our approximation (that is, continuous inside the interphase) is better than Taylor expansion from two different sides of the interface when the same order of approximation is used.

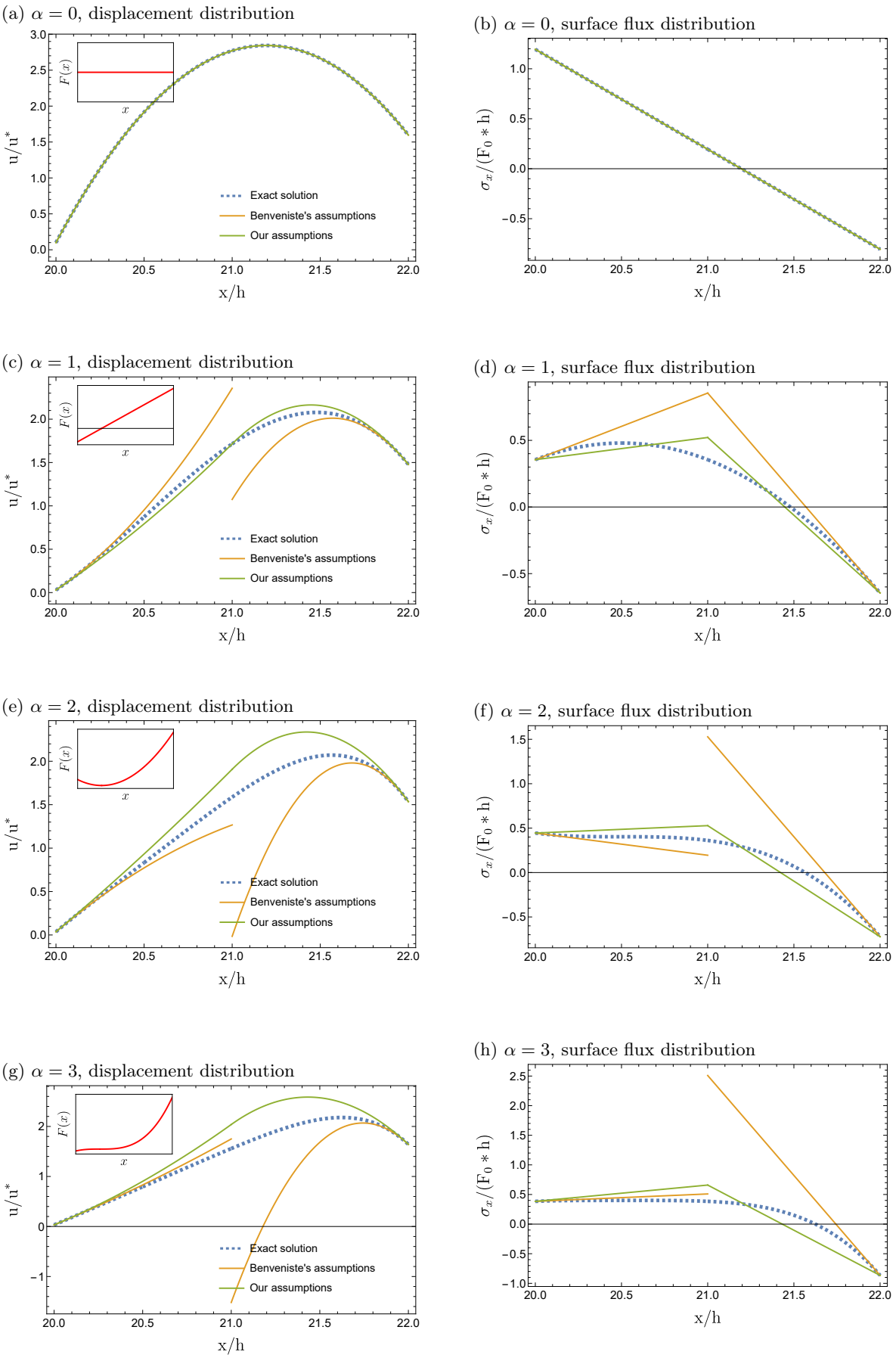


**Fig. 5.2.** Illustrative example for a constant, linear, quadratic and cubic body force distributed uniformly inside the interphase. Here we have assumed $t_1 = t_2 = t/2 = h$ and $\zeta = h/2$, while the body force $Q_0 = 1.0 \times 10^-4(N/m^2)$

## 5.4 Modified Transmission Conditions

Fig.2.4a gives the graphical representation of a perfect 3 phase system, with three distinct regions marked as material 1, material 2, and the thin interphase in between. For such a system, the surface fluxes and displacements are continuous across the boundaries of the interphase such that,

$$\boldsymbol{u}^{(1)}\Big|_{A_1} = \boldsymbol{u}^{(i)}\Big|_{A_1} \quad ; \quad (\sigma_{ij}\, n_j)^{(1)}\Big|_{A_1} = (\sigma_{ij}\, n_j)^{(i)}\Big|_{A_1} \quad \text{across } S_1 \tag{5.38}$$

$$\boldsymbol{u}^{(2)}\Big|_{A_2} = \boldsymbol{u}^{(i)}\Big|_{A_2} \quad ; \quad (\sigma_{ij}\, n_j)^{(2)}\Big|_{A_2} = (\sigma_{ij}\, n_j)^{(i)}\Big|_{A_2} \quad \text{across } S_2 \tag{5.39}$$

Across the thin interface $\Gamma$ the elastic properties are no longer continuous and there is an accumulation of displacement or tractions at the boundary, known as "jump" of the property, and is denoted as:

$$[\![\phi]\!] = \phi\Big|_{A_2} - \phi\Big|_{A_1}$$

where $\phi$ is the elastic function (displacement or surface flux) of the material.

Let us consider a homogeneous, isotropic elastic material as the interphase domain described above. The arbitrary curvilinear composite system is governed by the following equations:

$$\operatorname{div} \boldsymbol{\sigma} + \boldsymbol{F}(\xi) = 0 \tag{5.40}$$

where $\boldsymbol{\sigma}$ is the surface flux tensor, and where $\boldsymbol{F}(\xi) = \{F_1, F_2, F_3\}$ is the internal body force, distributed within the interphase.

For each equation, the derivative of the surface flux in the normal direction represents the gradual change in the surface fluxes when moving along the normal direction, that is, when one moves from point $A_1$ to $A_2$. This leads to the following two different forms of this equation.

$$\frac{\partial \boldsymbol{\sigma}^{(i)}}{\partial n} = \left(\boldsymbol{A} - \boldsymbol{F}(\xi) - \mathcal{D}_s\boldsymbol{\sigma} - g\,\sigma_{1k}^{(i)}\right) \tag{5.41}$$

or

$$\frac{\partial}{\partial n}(h_2h_3\boldsymbol{\sigma}^{(i)}) = \left(h_2h_3\boldsymbol{A} - h_2h_3\boldsymbol{F}(\xi,\alpha_2,\alpha_3,u) + h_2h_3\mathcal{D}_s\boldsymbol{\sigma}\right) \tag{5.42}$$

where

$$\mathcal{D}_s\boldsymbol{\sigma} = \frac{1}{h_2h_3}\frac{\partial(h_3\sigma_{k2}^{(i)})}{\partial\alpha_2} + \frac{1}{h_2h_3}\frac{\partial(h_2\sigma_{k3}^{(i)})}{\partial\alpha_3} \quad ; \quad k = (1,2,3) \tag{5.43}$$

is the *surface differential operator*, which denotes the stress gradient or the diffusion of the surface flux, along the surface, in the tangential directions, and

$$g(\xi,\alpha_2,\alpha_3) = \frac{1}{h_2h_3}\frac{\partial h_2h_3}{\partial n}. \tag{5.44}$$

represents the effect of *geometric curvature* on the transmission condition.

The term $\boldsymbol{A}$ contains all the directional derivatives of the scale factors in curvilinear coordinates, expressed explicitly as:

$$A_{11} = \left(\frac{\sigma_{22}}{h_2}\frac{\partial h_2}{\partial\alpha_1} + \frac{\sigma_{33}}{h_3}\frac{\partial h_3}{\partial\alpha_1}\right) \tag{5.45}$$

$$A_{12} = \frac{\sigma_{21}}{h_2}\frac{\partial h_2}{\partial\alpha_1} + \frac{\sigma_{23}}{h_2h_3}\frac{\partial h_2}{\partial\alpha_3} - \frac{\sigma_{33}}{h_3}\frac{\partial h_3}{\partial\alpha_2} \tag{5.46}$$

$$A_{13} = \frac{\sigma_{31}}{h_3}\frac{\partial h_3}{\partial\alpha_1} + \frac{1}{h_2h_3}\left(\sigma_{32}\frac{\partial h_3}{\partial\alpha_2} - \sigma_{22}\frac{\partial h_2}{\partial\alpha_3}\right) \tag{5.47}$$

These terms can be further simplified and written as:

$$A_{11} = \frac{\nu_i}{1-\nu_i} g\,\sigma_{11} + \frac{2\,G^{(i)}}{1-\nu^{(i)}}\,\mathcal{B}(\alpha_2,\alpha_3,\boldsymbol{u}) \tag{5.48}$$

$$A_{12} = \frac{\sigma_{21}}{h_2}\frac{\partial h_2}{\partial \alpha_1} + \frac{\sigma_{23}}{h_2 h_3}\frac{\partial h_2}{\partial \alpha_3} - \frac{\sigma_{33}}{h_3}\frac{\partial h_3}{\partial \alpha_2} \tag{5.49}$$

$$A_{13} = \frac{\sigma_{31}}{h_3}\frac{\partial h_3}{\partial \alpha_1} + \frac{1}{h_2 h_3}\left(\sigma_{32}\frac{\partial h_3}{\partial \alpha_2} - \sigma_{22}\frac{\partial h_2}{\partial \alpha_3}\right) \tag{5.50}$$

where $\mathcal{B}(\alpha_2,\alpha_3,\boldsymbol{u})$ is defined as:

$$\mathcal{B}(\alpha_2,\alpha_3,\boldsymbol{u}) = \frac{1}{h_2 h_3}\left(h_3\frac{\partial h_2}{\partial \alpha_1}\left(\epsilon_{22}+\nu_i\epsilon_{33}\right) + h_2\frac{\partial h_3}{\partial \alpha_1}\left(\epsilon_{33}+\nu_i\epsilon_{22}\right)\right) \tag{5.51}$$

while for the normal derivatives of the displacement term is obtained from the (5.28).

$$\frac{\partial u_m^{(i)}}{\partial \alpha_1} = 2\,\mathbb{C}^{-1}_{1j1m}\,\sigma^{(i)}_{n_j} - \mathcal{P}^{(i)}_m \tag{5.52}$$

The derivatives of the normal component $u_1^{(i)}$ of the displacement vector along the normal direction can be written as

$$\frac{\partial u_1^{(i)}}{\partial n} = \frac{1-2\,\nu_i}{2\,\mu_i(1-\nu_i)}\,\sigma_{11}^{(i)} - \frac{\nu_i}{1-\nu_i}\left(\varepsilon_{22}+\varepsilon_{33}\right) \tag{5.53}$$

in the normal direction.

The derivative of the tangential component of the displacement vector along the normal direction is expressed as:

$$\frac{\partial u_k^{(i)}}{\partial n} = \frac{\sigma_{1p}^{(i)}}{\mu_i} - \frac{1}{h_p}\left(\frac{\partial u_1^{(i)}}{\partial \alpha_p} - u_p^{(i)}\frac{\partial h_p}{\partial \alpha_1}\right) \quad ; \quad p=(2,3) \tag{5.54}$$

where $\mu_i$ is the shear modulus, and $\nu_i$ is the Poisson's ratio for the interphase.

It is interesting to note here that in comparison of the models from the literature, especially with Hashin's and Benveniste's models, we can see the following notable points: Firstly, the transmission conditions in these models do not account for body forces inside the interphase, thus, if the body forces were considered, then these models would fail to provide accurate solution, as will be seen later in the results section. In Hashin's model, the surface differential term, $\mathcal{D}_s\boldsymbol{\sigma}$, and the geometric curvature term, $g$, is taken at point $A_1$ (or from $A_2$) only, thus we only know the behaviour of the surface differential terms around point $A_1$ in the vicinity of the interphase, but it does not accurately approximate the behaviour *inside* the interphase. In Benveniste's model, the thermal properties at points $A_1$ and $A_2$ are considered, but again, and as has been illustrated in the previous section, we see the effect of surface differential terms again at points near the interphase,but it does not accurately capture the changes within the interphase, away from the boundary.

As in the previous case of thermally conductive interphase, the transmission conditions are derived in detail in the following sections by employing the Trapezoidal rule between the appropriate intervals.

## 5.5 Development of Transmission conditions for a thin interphase.

Now, that we have obtained our necessary forms of derivatives of stresses (Eqn.(5.41) and (5.42)), we will make use of either form in the forthcoming sections, by integrating them along the thickness of the interphase, to arrive at two different schemes of transmission conditions across an imperfect interface. It must be noted that the accuracy of the transmission conditions depends on the smoothness of the displacement functions to be integrated.

### 5.5.1 First Integration Scheme

For the first scheme, we integrate Eqn.(5.41) along the thickness of the interphase, approximating it by implementing the trapezoidal rule at the points on the boundaries of the interphase.

#### Two Integration Points

The jump of the elastic field variables are defined as the difference in the values at the points $A_1$ and $A_2$ lying on the the boundary of the interphase:

$$[\![\boldsymbol{u}^{(i)}]\!] = \int_0^t \frac{\partial \boldsymbol{u}^{(i)}}{\partial n} = \frac{t}{2}\left\{ \frac{\partial \boldsymbol{u}^{(i)}}{\partial n}\bigg|_{A_1} + \frac{\partial \boldsymbol{u}^{(i)}}{\partial n}\bigg|_{A_2} \right\} = t\left\langle \frac{\partial \boldsymbol{u}^{(i)}}{\partial n} \right\rangle$$

and similarly, for the jumps in surface fluxes, we can integrate between the two points,

$$[\![\boldsymbol{\sigma}^{(i)}]\!] = \int_0^t \frac{\partial \boldsymbol{\sigma}^{(i)}}{\partial n} = \frac{t}{2}\left\{ \frac{\partial \boldsymbol{\sigma}^{(i)}}{\partial n}\bigg|_{A_1} + \frac{\partial \boldsymbol{\sigma}^{(i)}}{\partial n}\bigg|_{A_2} \right\} = t\left\langle \frac{\partial \boldsymbol{\sigma}^{(i)}}{\partial n} \right\rangle$$

Thus, the jump of the displacement vector along the normal direction is:

$$[\![\boldsymbol{u}^{(i)}]\!] = t\left\{ 2\,\mathbb{C}^{-1}\left\langle \boldsymbol{\sigma}_n^{(i)} \right\rangle - \left\langle \mathcal{P}^{(i)} \right\rangle \right\} \tag{5.55}$$

Explicitly, the jumps in each component of displacement and stress are obtained by substituting the values of normal derivatives of each component from Eqn.(5.53)

$$[\![u_1]\!] = t\left\{ \frac{1-2\,\nu_i}{2\,\mu_i(1-\nu_i)}\left\langle \sigma_{11}^{(i)} \right\rangle - \frac{\nu_i}{1-\nu_i}\left\langle \varepsilon_{22}+\varepsilon_{33} \right\rangle \right\} \tag{5.56}$$

and the from Eqn.(5.54) for jumps in tangential components of displacement in the normal direction:

$$[\![u_m^{(i)}]\!] = t\left\langle \frac{\partial u_m^{(i)}}{\partial n} \right\rangle = \frac{t}{2}\left\{ \left\langle \frac{\sigma_{1m}^{(i)}}{\mu_i} \right\rangle - \left\langle \mathcal{P}_m^{(i)} \right\rangle \right\} \quad ; \quad m = \{2,3\} \tag{5.57}$$

The jumps in stress vector along the normal direction can also be expressed by substituting the normal derivative values from (5.41), giving

$$[\![\boldsymbol{\sigma}_n^{(i)}]\!] = t\left\{ \langle \boldsymbol{F} \rangle + \langle \mathcal{A} \rangle - \left\langle \mathcal{D}_s \boldsymbol{\sigma}_n^{(i)} \right\rangle - \left\langle g\boldsymbol{\sigma}_n^{(i)} \right\rangle \right\} \tag{5.58}$$

The explicit form of these equations can be obtained by substituting the corresponding values of the differential operators $\boldsymbol{A}, \mathcal{D}_s\boldsymbol{\sigma}$ and $g$ in the equations. For jumps in the

$\sigma_{11}$, substituting the value of $\mathcal{A}_{11}$ from Eqn.(5.45) gives the following form of the jump condition:

$$[\![\sigma_{11}]\!] = t\left\{\langle F_1\rangle + \frac{2\,G_i}{1-\nu_i}\langle\mathcal{B}(\alpha_2,\alpha_3,\boldsymbol{u})\rangle - \langle\mathcal{D}_s\boldsymbol{\sigma}\rangle - \frac{1-2\nu_i}{1-\nu_i}\langle g\sigma_{11}^{(i)}\rangle\right\} \tag{5.59}$$

and of the tangential component is:

$$[\![\sigma_{12}]\!] = t\left\{\langle F_2\rangle + \langle\mathcal{A}_{12}\rangle - \langle\mathcal{D}_s\boldsymbol{\sigma}\rangle - \langle g\sigma_{12}^{(i)}\rangle\right\} \tag{5.60}$$

and

$$[\![\sigma_{13}]\!] = t\left\{\langle F_3\rangle + \langle\mathcal{A}_{13}\rangle - \langle\mathcal{D}_s\boldsymbol{\sigma}\rangle - \langle g\sigma_{13}^{(i)}\rangle\right\} \tag{5.61}$$

Together the jumps in displacements (5.56),(5.57) and the jumps in tractions (5.59), (5.60), (5.61) represent the entire set of transmission conditions for the First Integration scheme using two points.

### Three Integration Points

To improve the accuracy of the transmission conditions, trapezoidal rule can be implemented using three points lying within the interphase. The domain can be split into two sub-domains, and the variation of displacements and the tractions can be approximated by integration between these three points of integration, ie, between points $A_1$ and $A_3$ (0 to $t_1$), and between $A_3$ and $A_2$ ($t_1$ to $t$). The generalized form is given as:

$$[\![\boldsymbol{u}^{(i)}]\!] = \int_0^t \frac{\partial\boldsymbol{u}^{(i)}}{\partial n} = \int_0^{t_1}\frac{\partial\boldsymbol{u}^{(i)}}{\partial n} + \int_{t_1}^{t}\frac{\partial\boldsymbol{u}^{(i)}}{\partial n} \tag{5.62}$$

$$[\![\boldsymbol{u}]\!] = \frac{t_1}{2}\left(\frac{\partial\boldsymbol{u}}{\partial\alpha_1}\right)\Big|_{A_1} + \frac{t_2}{2}\left(\frac{\partial\boldsymbol{u}}{\partial\alpha_1}\right)\Big|_{A_2} + \frac{t}{2}\left(\frac{\partial\boldsymbol{u}}{\partial\alpha_1}\right)\Big|_{A_3} \quad ; \quad t = t_1 + t_2 \tag{5.63}$$

and for the stresses:

$$[\![\boldsymbol{\sigma}^{(i)}]\!] = \int_0^t \frac{\partial\boldsymbol{\sigma}^{(i)}}{\partial n} = \int_0^{t_1}\frac{\partial\boldsymbol{\sigma}^{(i)}}{\partial n} + \int_{t_1}^{t}\frac{\partial\boldsymbol{\sigma}^{(i)}}{\partial n} \tag{5.64}$$

$$[\![\boldsymbol{\sigma}]\!] = \frac{t_1}{2}\left(\frac{\partial\boldsymbol{\sigma}}{\partial\alpha_1}\right)\Big|_{A_1} + \frac{t_2}{2}\left(\frac{\partial\boldsymbol{\sigma}}{\partial\alpha_1}\right)\Big|_{A_2} + \frac{t}{2}\left(\frac{\partial\boldsymbol{\sigma}}{\partial\alpha_1}\right)\Big|_{A_3} \quad ; \quad t = t_1 + t_2 \tag{5.65}$$

Integrating each part of the interval in (5.62),(5.64) separately, we get:

$$\boldsymbol{u}^{(i)}|_{A_3} - u_k^{(i)}|_{A_2} = -\frac{t_2}{2}\left\{\frac{\partial\boldsymbol{u}^{(i)}}{\partial n}\Big|_{A_3} + \frac{\partial\boldsymbol{u}^{(i)}}{\partial n}\Big|_{A_2}\right\} \tag{5.66}$$

and

$$\boldsymbol{u}^{(i)}|_{A_3} - \boldsymbol{u}^{(i)}|_{A_1} = \frac{t_1}{2}\left\{\frac{\partial\boldsymbol{u}^{(i)}}{\partial n}\Big|_{A_3} + \frac{\partial\boldsymbol{u}^{(i)}}{\partial n}\Big|_{A_1}\right\} \tag{5.67}$$

for the displacements. In terms of the stresses, we get the following set of equations:

$$\boldsymbol{\sigma}^{(i)}|_{A_3} - \boldsymbol{\sigma}^{(i)}|_{A_2} = -\frac{t_2}{2}\left\{\frac{\partial\boldsymbol{\sigma}^{(i)}}{\partial n}\Big|_{A_3} + \frac{\partial\boldsymbol{\sigma}^{(i)}}{\partial n}\Big|_{A_2}\right\} \tag{5.68}$$

and

$$\boldsymbol{\sigma}^{(i)}|_{A_3} - \boldsymbol{\sigma}^{(i)}|_{A_1} = \frac{t_1}{2}\left\{\left.\frac{\partial \boldsymbol{\sigma}^{(i)}}{\partial n}\right|_{A_3} + \left.\frac{\partial \boldsymbol{\sigma}^{(i)}}{\partial n}\right|_{A_1}\right\} \tag{5.69}$$

Subtracting the Eqns.(5.67) from (5.66) (and (5.69) from (5.68)), results in the form of equation which is equivalent to (5.63) for the displacement vector (and to (5.63) for the traction vector)

$$\boldsymbol{u}|_{A_2} - \boldsymbol{u}|_{A_1} = \frac{t_2}{2}\left(\left.\frac{\partial \boldsymbol{u}^{(i)}}{\partial n}\right|_{A_2}\right) + \frac{t_1+t_2}{2}\left(\frac{\partial \boldsymbol{u}^{(i)}}{\partial n}\right)\Big|_{A_3} + \frac{t_1}{2}\left(\left.\frac{\partial \boldsymbol{u}^{(i)}}{\partial n}\right|_{A_2}\right) \tag{5.70}$$

$$\boldsymbol{\sigma}|_{A_2} - \boldsymbol{\sigma}|_{A_1} = \frac{t_2}{2}\left(\left.\frac{\partial \boldsymbol{\sigma}^{(i)}}{\partial n}\right|_{A_2}\right) + \frac{t_1+t_2}{2}\left(\frac{\partial \boldsymbol{\sigma}^{(i)}}{\partial n}\right)\Big|_{A_3} + \frac{t_1}{2}\left(\left.\frac{\partial \boldsymbol{\sigma}^{(i)}}{\partial n}\right|_{A_2}\right) \tag{5.71}$$

On the other hand, adding Eqns.(5.66),(5.67) and (5.68),(5.69), gives the displacement and stress components at point $A_3$:

$$\boldsymbol{u}^{(i)}|_{A_3} - \left\langle \boldsymbol{u}^{(i)} \right\rangle = -\frac{t_2}{4}\left(\left.\frac{\partial \boldsymbol{u}^{(i)}}{\partial n}\right|_{A_2}\right) + \frac{t_1-t_2}{4}\left(\frac{\partial \boldsymbol{u}^{(i)}}{\partial n}\right)\Big|_{A_3} + \frac{t_1}{4}\left(\left.\frac{\partial \boldsymbol{u}^{(i)}}{\partial n}\right|_{A_2}\right) \tag{5.72}$$

$$\boldsymbol{\sigma}^{(i)}|_{A_3} - \left\langle \boldsymbol{\sigma}^{(i)} \right\rangle = -\frac{t_2}{4}\left(\left.\frac{\partial \boldsymbol{\sigma}^{(i)}}{\partial n}\right|_{A_2}\right) + \frac{t_1-t_2}{4}\left(\frac{\partial \boldsymbol{\sigma}^{(i)}}{\partial n}\right)\Big|_{A_3} + \frac{t_1}{4}\left(\left.\frac{\partial \boldsymbol{\sigma}^{(i)}}{\partial n}\right|_{A_2}\right) \tag{5.73}$$

If we take the simple case of $t_1 = t_2 = t/2$, then jumps in displacements and tractions simplify to:

$$[\![\boldsymbol{u}^{(i)}]\!] = \frac{t}{2}\left\{\left\langle 2\,\mathbb{C}^{-1}\,\boldsymbol{\sigma}_n^{(i)}\right\rangle - 2\left\langle \mathcal{P}^{(i)}\right\rangle + \left.2\,\mathbb{C}^{-1}\,\boldsymbol{\sigma}_n^{(i)}\right|_{A_3}\right\} \tag{5.74}$$

where it is assumed that at point $A_3$ the derivatives of the displacement vector along the tangential direction does not vary much along the normal direction, then

$$\mathcal{P}_k^{(i)}|_{A_3} = \left\langle \mathcal{P}_k^{(i)} \right\rangle \tag{5.75}$$

$$[\![\boldsymbol{\sigma}_n^{(i)}]\!] = \frac{t}{2}\left\{\langle \boldsymbol{F} + \mathcal{A} - g\,\boldsymbol{\sigma}_n\rangle - 2\,\langle \mathcal{D}_s\boldsymbol{\sigma}\rangle + \left.(\mathcal{F} + \mathcal{A} - g\,\boldsymbol{\sigma}_n)\right|_{A_3}\right\} \tag{5.76}$$

where the same assumption has been made for the tangential derivatives. The values at point $A_3$ are computed from the following:

$$\boldsymbol{u}^{(i)}|_{A_3} = \langle \boldsymbol{u}\rangle - \frac{t}{8}\left\{[\![2\,\mathbb{C}^{-1}\,\boldsymbol{\sigma}_n^{(i)} - \mathcal{P}^{(i)}]\!]\right\} \tag{5.77}$$

$$\boldsymbol{\sigma}_n^{(i)}|_{A_3} = \langle \boldsymbol{\sigma}_n\rangle - \frac{t}{8}\left\{[\![\boldsymbol{F} + \mathcal{A} - \mathcal{D}_s\boldsymbol{\sigma} - g\,\boldsymbol{\sigma}_n]\!]\right\} \tag{5.78}$$

where the continuity of displacement and stress across the boundaries of the interphase (from (5.38)) is invoked.

The Eqns.(5.74),(5.76) along with (5.77).(5.78) give a general form of the jumps of displacements and stresses across the interphase boundaries. Substitution of the normal derivatives of the displacement from Eqn.(5.53) gives the explicit form of jumps in displacement components across an imperfect interphase.

$$[\![u_1]\!] = \frac{t}{2}\left\{\frac{1-2\,\nu_i}{2\,G_i(1-\nu_i)}\left(\langle \sigma_{11}^{(i)}\rangle + \sigma_{11}^{(i)}|_{A_3}\right) - \frac{\nu_i}{1-\nu_i}\left(\langle \varepsilon_{22}+\varepsilon_{33}\rangle + (\varepsilon_{22}+\varepsilon_{33})|_{A_3}\right)\right\} \tag{5.79}$$

where $\sigma_{11}^{(i)}|_{A_3}$ is the normal component of the stress at point $A_3$ defined in (5.88), and $u_1^{(i)}|_{A_3}$ is the displacement component $u_1$ at point $A_3$ given as:

$$u_1^{(i)}|_{A_3} = \langle u_1 \rangle - \frac{t}{8}\left\{\frac{1-2\,\nu_i}{2\,\mu_i(1-\nu_i)}\left[\!\left[\sigma_{11}^{(i)}\right]\!\right] - \frac{\nu_i}{1-\nu_i}[\![\varepsilon_{22}+\varepsilon_{33}]\!]\right\} \tag{5.80}$$

For a thin interphase, it can assumed that the gradients of the displacement vector and the stresses, for a sufficiently smooth displacement field, do not vary much along the surface of the interphase (in tangential direction), and thus, for a linearly varying gradient in the normal direction, the following assumption can be made:

$$\text{Assumption 1:}\quad (\varepsilon_{22}+\varepsilon_{33})\,|_{A_3} = \langle \varepsilon_{22}+\varepsilon_{33}\rangle \tag{5.81}$$

So, the jump of the normal component of the displacement vector can be re-written as:

$$[\![u_1]\!] = \frac{t}{2}\left\{\frac{1-2\,\nu_i}{2\,G_i(1-\nu_i)}\left(\langle\sigma_{11}^{(i)}\rangle + \sigma_{11}^{(i)}|_{A_3}\right) - \frac{\nu_i}{1-\nu_i}\left(2\,\langle\varepsilon_{22}+\varepsilon_{33}\rangle\right)\right\} \tag{5.82}$$

Similarly, $[\![u_k]\!]$ is obtained as:

$$[\![u_k]\!] = \frac{t}{2}\left\{\left\langle\frac{\sigma_{1k}}{\mu_i} + \frac{\sigma_{1k}^{(i)}}{\mu_i}\bigg|_{A_3}\right\rangle - \left(\left\langle\mathcal{P}_k^{(i)}\right\rangle + \mathcal{P}_m^{(i)}\bigg|_{A_3}\right)\right\} \tag{5.83}$$

where $u_k^{(i)}|_{A_3}$ is the displacement component $u_1$ at point $A_3$ given as:

$$u_k^{(i)}|_{A_3} = \langle u_k\rangle - \frac{t}{8}\left\{\left[\!\left[\frac{\sigma_{1k}}{\mu_i}\right]\!\right] + \left[\!\left[\mathcal{P}_k^{(i)}\right]\!\right]\right\} \quad ; \quad k=(2,3) \tag{5.84}$$

The tangential derivative of the $u_1$ that appears in the expression for $G_m^{(i)}$ given in (5.29) can be expressed at the point $A_3$ as the average of the tangential derivative at points $A_1$ and $A_2$:

$$\text{Assumption 2:}\quad \left(\frac{1}{h_k}\frac{\partial u_1}{\partial\alpha_k}\right)\bigg|_{A_3} = \left\langle\frac{1}{h_k}\frac{\partial u_1}{\partial\alpha_k}\right\rangle \tag{5.85}$$

where $k=(2,3)$ represents the tangential directions.

Thus, the expression for $[\![u_k]\!]$ can be re-written as:

$$[\![u_k]\!] = \frac{t}{2}\left\{\left\langle\frac{\sigma_{1k}}{\mu_i}\right\rangle + \frac{\sigma_{1k}^{(i)}|_{A_3}}{\mu_i} - \left\langle 2\,\frac{1}{h_k}\frac{\partial u_1}{\partial\alpha_k}\right\rangle + \left\langle\left(u_k\frac{\partial h_k}{\partial\alpha_1}\right)\right\rangle + \frac{1}{h_k|_{A_3}}\left(u_k|_{A_3}\frac{\partial h_k}{\partial\alpha_1}\bigg|_{A_3}\right)\right\} \tag{5.86}$$

where $\sigma_{1k}^{(i)}|_{A_3}$ is taken from the expression (5.88) and $u_k|_{A_3}$ is taken from (5.84).

To obtain expressions of jumps in normal and shearing components of stresses across an imperfect interface, we will begin by substituting the normal derivatives of the stresses from Eqn.(5.41) which gives the explicit form of jumps in stress components across an imperfect interface.

$$[\![\sigma_{1k}]\!] = \frac{t}{2}\left\{F_k + \left\langle A_{1k} - \mathcal{D}_s\boldsymbol{\sigma} - g\sigma_{1k}^{(i)}\right\rangle\right) + \left(F_k + A_{1k} - \mathcal{D}_s\boldsymbol{\sigma} - g\sigma_{1k}^{(i)}\right)\bigg|_{A_3}\right\} \tag{5.87}$$

where $\sigma_{1k}^{(i)}|_{A_3}$ is the stress at point $A_3$ given as:

$$\sigma_{1k}^{(i)}|_{A_3} = \langle\sigma_{1k}\rangle - \frac{t}{8}\left\{F_k + \left[\!\left[A_{1k} - \mathcal{D}_s\boldsymbol{\sigma} - g\sigma_{1k}^{(i)}\right]\!\right]\right\} \tag{5.88}$$

The term $\mathcal{D}_s\boldsymbol{\sigma}$ represents the surface gradient of the stress tensor, that is, the sum of the gradients of the stresses in the tangential direction, while $A_{11}$ depicts the derivatives of scale factor of curvilinear coordinate system in the tangential direction. For a thin interphase, it can assumed that these terms do not exhibit huge variations along the surface of the interphase (in tangential direction), and thus,

$$\text{Assumption 3: } \mathcal{D}_s\boldsymbol{\sigma}|_{A_3} = \langle \mathcal{D}_s\boldsymbol{\sigma} \rangle \quad ; \quad \text{Assumption 4: } A^{(i)}_{1k}|_{A_3} = \left\langle A^{(i)}_{1k} \right\rangle \tag{5.89}$$

So, the jump of the normal component of the stress can be re-written as:

$$[\![\sigma_{1k}]\!] = \frac{t}{2}\left\{ \langle F_k \rangle + F_k|_{A_3} + 2\langle A_{1k}\rangle - 2\langle \mathcal{D}_s\boldsymbol{\sigma}\rangle - \langle g\,\sigma^{(i)}_{1k}\rangle - g\,\sigma^{(i)}_{1k} \Big)\Big|_{A_3} \right\} \tag{5.90}$$

The explicit form of each term for normal and shear stress is defined in the preceding sections in Eqns.(5.44),(5.48) and (5.43), and can be substituted here to get the explicit form of each jump equation.

$$[\![\sigma_{11}]\!] = \frac{t}{2}\left\{ \langle F_1 \rangle + F_1|_{A_3} + \frac{4\,G_i}{1-\nu_i}\langle \mathcal{B}(\alpha_2,\alpha_3,\boldsymbol{u})\rangle - 2\langle \mathcal{D}_s\boldsymbol{\sigma}\rangle - \frac{1-2\nu_i}{1-\nu_i}\left( \langle g\,\sigma^{(i)}_{11}\rangle + g\,\sigma^{(i)}_{11}|_{A_3} \right) \right\} \tag{5.91}$$

where the $\mathcal{B}(\alpha_2,\alpha_3,\boldsymbol{u})$ is defined in(5.51).

Eqn.(5.88) and subsequently (5.90) can be written in an alternate form using the identities defined in (2.117). The equation for stress vector at point $A_3$ can then be written as

$$\boldsymbol{\sigma}^{(i)}_n|_{A_3} = \langle \boldsymbol{\sigma}_n \rangle - \frac{t}{8}\left\{ \boldsymbol{F} + [\![\boldsymbol{A} - \mathcal{D}_s\boldsymbol{\sigma}]\!] - \langle g\rangle [\![\boldsymbol{\sigma}^{(i)}_n]\!] - [\![g]\!]\langle \boldsymbol{\sigma}^{(i)}_n\rangle \right\} \tag{5.92}$$

while the jump in stress vector $[\![\boldsymbol{\sigma}_n]\!]$ from (5.90) can be expressed equivalently as

$$[\![\boldsymbol{\sigma}_n]\!]\left\{ 1 + \frac{t}{8}\left( [\![g]\!] + \frac{t}{2}\,g|_{A_3}\,\langle g\rangle \right) \right\} + \frac{t}{2}\langle \boldsymbol{\sigma}_n\rangle \left\{ \langle g\rangle + g|_{A_3} + \frac{t}{8}\,g|_{A_3}\,[\![g]\!] \right\} =$$
$$\frac{t}{2}\left\{ \langle \boldsymbol{F}\rangle + \boldsymbol{F}|_{A_3} - 2\langle \boldsymbol{A} - \mathcal{D}_s\boldsymbol{\sigma}\rangle \right\} + \frac{t^2}{16}\,g|_{A_3}\,[\![\boldsymbol{F} - \boldsymbol{A} - \mathcal{D}_s\boldsymbol{\sigma}]\!] \tag{5.93}$$

### 5.5.2 Second Integration Scheme

To develop transmission conditions for this scheme, we make use of Eqn 5.42. Although Eqns.(5.41) and (5.42) are equivalent, but the final result will be slightly different, as the same trapezoidal integration rule provides another approximation.

Here, as we can see from Eqn (5.42), the geometric curvature term $g$ does not come into the picture, and thus one can mistakenly assume that the derived conditions do not involve the geometric curvature. However, as we will see, the curvature enters the equations in a form different from the one seen so far.

It must also be noted that the transmission conditions for the jumps in the normal and tangential components of the displacement vector remain the same, given by Eqns.(5.56),(5.57) for the two-point scheme and Eqns.(5.82),(5.83) for the three-points scheme.

#### Two integration points

Here, as in the case of First Integration Scheme (Sec. 5.5.1), we will simply integrate (5.42) (instead of the equivalent equation (5.41)) and (5.53), (5.54) from 0 to $t$ using the

trapezoidal rule gives

$$[\![h_2 h_3 \boldsymbol{\sigma}^{(i)}]\!] = t \left\langle h_2 h_3 \left( \boldsymbol{F} + \mathcal{A} - \mathcal{D}_s \boldsymbol{\sigma} \right) \right\rangle \tag{5.94}$$

Applying the following identities:

$$[\![ab]\!] = \langle a \rangle [\![b]\!] + [\![a]\!] \langle b \rangle, \quad \langle ab \rangle = \langle a \rangle \langle b \rangle + \frac{1}{4} [\![a]\!] [\![b]\!], \tag{5.95}$$

Then the above equation be rewritten as

$$[\![\boldsymbol{\sigma}]\!] + \beta \langle \boldsymbol{\sigma} \rangle = t \left\{ \langle \boldsymbol{F} + \mathcal{A} - \mathcal{D}_s \boldsymbol{\sigma} \rangle + \frac{1}{4} \beta [\![ \boldsymbol{F} + \mathcal{A} - \mathcal{D}_s \boldsymbol{\sigma} ]\!] \right\} \tag{5.96}$$

where the parameter, $\beta$ is introduced and defined in (2.118).

It must be noted that the second transmission condition for $[\![\boldsymbol{u}]\!]$ remains the same, as defined in (5.56) and (5.57). Together with (5.96), they form a complete set of transmission conditions for Second Integration Scheme using two points of integration.

### Three Points

The transmission conditions derived above can be improved further by a more accurate integration with a two intervals trapezoidal rule:

$$\begin{aligned} [\![h_2\, h_3 \boldsymbol{\sigma}^{(i)}]\!] = \frac{t_1}{2}\, h_2 h_3|_{A_1} \left( \boldsymbol{F}|_{A_1} + \mathcal{A}|_{A_1} - \mathcal{D}_s \boldsymbol{\sigma}|_{A_1} \right) \\ + \frac{t}{2}\, h_2 h_3|_{A_3} \left( \boldsymbol{F}|_{A_3} + \mathcal{A}|_{A_3} - \mathcal{D}_s \boldsymbol{\sigma}|_{A_3} \right) + \frac{t_2}{2}\, h_2 h_3|_{A_2} \left( \boldsymbol{F}|_{A_2} + \mathcal{A}|_{A_2} - \mathcal{D}_s \boldsymbol{\sigma}|_{A_2} \right) \end{aligned} \tag{5.97}$$

As in the previous section, we can integrate the equation above with two separate intervals:

$$\begin{aligned} h_2\, h_3|_{A_3}\, \boldsymbol{\sigma}^{(i)}|_{A_3} - h_2\, h_3|_{A_1}\, \boldsymbol{\sigma}^{(i)}|_{A_1} = \frac{t_1}{2} \left\{ h_2\, h_3|_{A_1} \left( \boldsymbol{F}|_{A_1} + \mathcal{A}|_{A_1} - \mathcal{D}_s \boldsymbol{\sigma}|_{A_1} \right) \right\} + \\ \frac{t_1}{2} \left\{ h_2\, h_3|_{A_3} \left( \boldsymbol{F}|_{A_3} + \mathcal{A}|_{A_3} - \mathcal{D}_s \boldsymbol{\sigma}|_{A_3} \right) \right\} \end{aligned} \tag{5.98}$$

and

$$\begin{aligned} h_2\, h_3|_{A_3}\, \boldsymbol{\sigma}^{(i)}|_{A_3} - h_2\, h_3|_{A_2}\, \boldsymbol{\sigma}^{(i)}|_{A_2} = -\frac{t_2}{2} \left\{ h_2\, h_3|_{A_1} \left( \boldsymbol{F}|_{A_2} + \mathcal{A}|_{A_2} - \mathcal{D}_s \boldsymbol{\sigma}|_{A_2} \right\} \right. \\ \left. - \frac{t_2}{2} \left\{ h_2\, h_3|_{A_3} \left( \boldsymbol{F}|_{A_3} + \mathcal{A}|_{A_3} - \mathcal{D}_s \boldsymbol{\sigma}|_{A_3} \right) \right) \right. \end{aligned} \tag{5.99}$$

Again, adding Eqns.(5.98) and (5.99), provides us with an expression of stress terms at point $A_3$ within the interphase.

$$\begin{aligned} h_2\, h_3|_{A_3}\, \boldsymbol{\sigma}^{(i)}|_{A_3} - \langle h_2 h_3\, \boldsymbol{\sigma}^{(i)} \rangle = \frac{t_1}{4} h_2 h_3|_{A_1} \left( \boldsymbol{F}|_{A_1} + \mathcal{A}|_{A_1} - \mathcal{D}_s \boldsymbol{\sigma}|_{A_1} \right) \\ - \frac{t_2}{4} h_2 h_3|_{A_2} \left( \boldsymbol{F}|_{A_2} + \mathcal{A}|_{A_2} - \mathcal{D}_s \boldsymbol{\sigma}|_{A_2} \right) + \frac{t_1 - t_2}{4} h_2 h_3|_{A_3} \left( \boldsymbol{F}|_{A_3} + \mathcal{A}|_{A_3} - \mathcal{D}_s \boldsymbol{\sigma}|_{A_3} \right) \right) \end{aligned} \tag{5.100}$$

Assuming $t_1 = t_2 = t/2$, we can rewrite the equation above as:

$$h_2h_3|_{A_3}\,\boldsymbol{\sigma}^{(i)}|_{A_3} = \langle h_2h_3\,\boldsymbol{\sigma}^{(i)}\rangle - \frac{t}{8}\left\{\left[\!\left[h_2h_3\Big(\boldsymbol{F}+\mathcal{A}-\mathcal{D}_s\boldsymbol{\sigma}\Big)\right]\!\right]\right\} \tag{5.101}$$

while subtracting Eqns.(5.98) and (5.99) gives us the jump across the interface, which is equivalent to Eqn.(5.97)

$$[\![h_2h_3\boldsymbol{\sigma}^{(i)}]\!] = \frac{t}{2}\left\{\Big\langle h_2h_3\Big(\boldsymbol{F}+\mathcal{A}-\mathcal{D}_s\boldsymbol{\sigma}\Big)\Big\rangle + h_2h_3|_{A_3}\Big(\boldsymbol{F}|_{A_3}-\boldsymbol{A}|_{A_3}-\mathcal{D}_s\boldsymbol{\sigma}|_{A_3}\Big)\right\} \tag{5.102}$$

Invoking the identities defined in Eqn.(5.95), we get

$$[\![\boldsymbol{\sigma}^{(i)}]\!] = \frac{t}{2}\left\{\langle\boldsymbol{F}+\mathcal{A}-\mathcal{D}_s\boldsymbol{\sigma}\rangle + \frac{\beta}{4}[\![\boldsymbol{F}+\mathcal{A}-\mathcal{D}_s\boldsymbol{\sigma}]\!] + \gamma\left(\boldsymbol{F}+\mathcal{A}-\mathcal{D}_s\boldsymbol{\sigma}\right)\Big|_{A_3}\right\} - \beta\langle\boldsymbol{\sigma}^{(i)}\rangle \tag{5.103}$$

Aa defined in the previous section, at point $A_3$, employing (5.89) gives the following form of jump condition:

$$[\![\boldsymbol{\sigma}_n^{(i)q}]\!] = \frac{t}{2}\left\{\langle\boldsymbol{F}+\mathcal{A}-\mathcal{D}_s\boldsymbol{\sigma}\rangle + \frac{1}{4}\beta[\![\boldsymbol{F}+\mathcal{A}-\mathcal{D}_s\boldsymbol{\sigma}]\!] + \gamma\left(\boldsymbol{F}|_{A_3}+\langle\mathcal{A}-\mathcal{D}_s\boldsymbol{\sigma}\rangle\right)\right\} - \beta\langle\boldsymbol{\sigma}^{(i)}\rangle \tag{5.104}$$

while the stress at point $A_3$ is expressed as:

$$\boldsymbol{\sigma}_n^{(i)}|_{A_3} = \frac{1}{\gamma}\left\{\langle\boldsymbol{\sigma}\rangle + \frac{\beta}{4}[\![\boldsymbol{\sigma}]\!] - \frac{t}{8}\left([\![\boldsymbol{F}+\mathcal{A}-\mathcal{D}_s\boldsymbol{\sigma}]\!] + \beta\langle\boldsymbol{F}+\mathcal{A}-\mathcal{D}_s\boldsymbol{\sigma}\rangle\right)\right\} \tag{5.105}$$

where $\gamma$ is a new parameter introduced as:

$$\gamma(t,\alpha_1,\alpha_2) = \frac{h_2h_3|_{A_3}}{\langle h_2h_3\rangle} \tag{5.106}$$

The second transmission condition for jumps in displacement vector is obtained from (5.82) and (5.86). Together with (5.104), it forms a complete set of transmission conditions for the Second Integration Scheme employing three-points of integration.

### 5.5.3 Comparison of the transmission conditions

Similar to the comparison made in Sec.4.2.3 for a thermally conductive interphase, the equivalence of the two schemes using three-points of integration is presented as follows. Substituting the estimations from (4.61) into the transmission condition obtained by the first integration approach, (equations (5.93) and (5.92)), we have

$$\left(1-\frac{t^2}{16}\beta_1^2\right)[\![\boldsymbol{\sigma}_n^{(i)}]\!] + \beta_1 t\left(1-\frac{t^2}{16}\beta_1\right)\langle\boldsymbol{\sigma}_n^{(i)}\rangle =$$
$$\frac{t}{2}\left\{\langle\boldsymbol{F}\rangle + \boldsymbol{F}\left(\frac{t}{2},\boldsymbol{u}_{A_3}^{(i)}\right) - 2\langle\boldsymbol{A}-\mathcal{D}_s\boldsymbol{\sigma}\rangle\right\} + \frac{t^2}{16}\beta_1\Big([\![\boldsymbol{F}-\boldsymbol{A}-\mathcal{D}_s\boldsymbol{\sigma}]\!]\Big) \tag{5.107}$$

and

$$\boldsymbol{\sigma}_n^{(i)}|_{A_3} = \Big\langle\boldsymbol{\sigma}_n^{(i)}\Big\rangle - \frac{t}{8}\left([\![\boldsymbol{F}-\boldsymbol{A}-\mathcal{D}_s\boldsymbol{\sigma}]\!] - \beta_1[\![\boldsymbol{\sigma}_n^{(i)}]\!] - (-t\beta_1^2)\langle\boldsymbol{\sigma}_n^{(i)}\rangle\right). \tag{5.108}$$

Since $t \ll 1$, higher order terms can be neglected in the equation above, to arrive at the following form:

$$[\![\boldsymbol{\sigma}_n^{(i)}]\!] + \beta(t)\langle\boldsymbol{\sigma}_n^{(i)}\rangle = \frac{t}{2}\left\{\langle\boldsymbol{F}\rangle + \boldsymbol{F}\left(\frac{t}{2},\boldsymbol{u}_{A_3}^{(i)}\right) - 2\langle\boldsymbol{A}-\mathcal{D}_s\boldsymbol{\sigma}\rangle\right\} \tag{5.109}$$

and

$$\boldsymbol{\sigma}_n^{(i)}|_{A_3} = \left\langle \boldsymbol{\sigma}_n^{(i)} \right\rangle + \frac{\beta(t)}{8} \langle \boldsymbol{\sigma}_n^{(i)} \rangle - \frac{t}{8} \left\{ [\![ \boldsymbol{F} + \boldsymbol{A} - \mathcal{D}_s \boldsymbol{q} ]\!] \right\} \tag{5.110}$$

while the transmission conditions set for Second integration scheme (eqn.(5.104) and (5.105))is as follows:

$$[\![ \boldsymbol{\sigma}_n^{(i)} ]\!] + \beta(t) \langle \boldsymbol{\sigma}_n^{(i)} \rangle = \frac{t}{2} \left\{ \langle \boldsymbol{F} \rangle + \boldsymbol{F} \left( \frac{t}{2}, \boldsymbol{u}_{A_3}^{(i)} \right) + 2 \langle \boldsymbol{A} - \mathcal{D}_s \boldsymbol{q} \rangle + \frac{\beta(t)}{4} \Big( [\![ \boldsymbol{F} + \boldsymbol{A} - \mathcal{D}_s \boldsymbol{\sigma} ]\!] \Big) \right\} \tag{5.111}$$

and

$$\boldsymbol{\sigma}_n^{(i)}|_{A_3} = \frac{1}{\gamma(t)} \left\{ \langle \boldsymbol{\sigma}_n^{(i)} \rangle + \frac{\beta(t)}{4} [\![ \boldsymbol{\sigma}_n^{(i)} ]\!] - \frac{t}{8} \Big( \beta(t) \langle \boldsymbol{F} + \boldsymbol{A} - \mathcal{D}_s \boldsymbol{\sigma} \rangle + [\![ \boldsymbol{F} + \boldsymbol{A} - \mathcal{D}_s \boldsymbol{\sigma} ]\!] \Big) \right\} \tag{5.112}$$

which, after neglecting the $O(t^2)$ terms, can be re-written as

$$[\![ \boldsymbol{\sigma}_n^{(i)} ]\!] + \beta(t) \langle \boldsymbol{\sigma}_n^{(i)} \rangle = \frac{t}{2} \left\{ \langle \boldsymbol{F} \rangle + \boldsymbol{F} \left( \frac{t}{2}, \boldsymbol{u}_{A_3}^{(i)} \right) + 2 \left\langle \boldsymbol{A} - \mathcal{D}_s \boldsymbol{\sigma} \right\rangle \right\} \tag{5.113}$$

and

$$\boldsymbol{\sigma}_n^{(i)}|_{A_3} = \langle \boldsymbol{\sigma}_n^{(i)} \rangle + \frac{\beta(t)}{4} [\![ \boldsymbol{\sigma}_n^{(i)} ]\!] - \frac{t}{8} \left\{ [\![ \boldsymbol{F} + \boldsymbol{A} - \mathcal{D}_s \boldsymbol{\sigma} ]\!] \right\} \tag{5.114}$$

which is same as Eqns.(5.109) for jump of normal heat flux, and Eqn.(5.112) for the heat flux value at point $A_3$. Thus, for a thin interphase, the proposed two schemes (First and Second) using three points of integration are equivalent.

## 5.6 Overview of models in literature.

A comparison between these models and the approaches proposed in this paper will be presented in Sec.5.7 using illustrative examples.

- **One-Point Schemes:** These refer to the approaches based on Taylor series expansion around one point only, either $A_1$ or $A_2$ on the interface boundary.
  - Hashin (2002): One of the main highlights of this paper was the simple yet effective model obtained from the asymptotic Taylor series expansion around point $A_1$ of the elastic fields of interphase, but limited to a thin interphase. The accuracy of the model decreased with the increase in interphase thickness.

$$[\![ u_1 ]\!] = t \left[ \frac{1 - 2\,\nu^{(i)}}{2\,G^{(i)} \left(1 - \nu^{(i)}\right)} \sigma_{11}^{(i)} - \frac{\nu^{(i)}}{1 - \nu^{(i)}} \left( \varepsilon_{22} + \varepsilon_{33} \right) \right]_{A_1}, \tag{5.115}$$

$$[\![ u_k ]\!] = t \left[ \frac{\sigma_{1k}^{(i)}}{G^{(i)}} - \mathcal{P}_k^{(i)} \right]_{A_1}, \qquad k = \{2, 3\} \tag{5.116}$$

$$[\![ \sigma_{11} ]\!] = t \left[ \mathcal{B} - \mathcal{D}_s \boldsymbol{q} - \frac{1 - 2\,\nu^{(i)}}{1 - \nu^{(i)}} g\, \sigma_{11}^{(i)} \right]_{A_1} \tag{5.117}$$

$$[\![ \sigma_{1k} ]\!] = t \left[ \mathcal{A}_{1k} - \mathcal{D}_s \boldsymbol{q} - g\, \sigma_{1k}^{(i)} \right]_{A_1} \tag{5.118}$$

## 5.7 Results and Discussion

The transmission conditions developed up to this point will now be tested against the analytical solution of a perfect circular interphase in plane strain setting subjected to remote shear strain. The inclusion has a radius $a$, and a coating of thickness $\epsilon = t/a, \epsilon \ll 1$. No body forces are assumed to be present inside the interphase. Let us consider a two-dimensional case of a circular inclusion of radius $R(\theta) = r_i = a$, with a coating of thickness $\xi = t$. The tangent (2.106) and normal (2.107) unit vectors simply take the form

$$\hat{\boldsymbol{t}} = \frac{\partial}{\partial\theta} R(\theta) = \{-\sin(\theta), \cos(\theta)\} \tag{5.119}$$

$$\hat{\boldsymbol{n}} = \frac{\partial}{\partial\theta} R(\theta) = \{\cos(\theta), \sin(\theta)\} \tag{5.120}$$

For a simple circular case, Eqn.(2.105) becomes $h_1 = h_r = 1, h_\theta = h_2 = r$ and (2.108) simplifies to $1/r$. For such a geometry, the normal direction is aligned in the radial direction, while the tangential direction is in the $\theta$-direction.

The main objective of presenting this example is to provide the estimation and comparison of accuracy of transmission conditions obtained from the different methods proposed, in the effect of surface Laplacian and geometric curvature.

The properties of the materials is provided in Table 5.1.

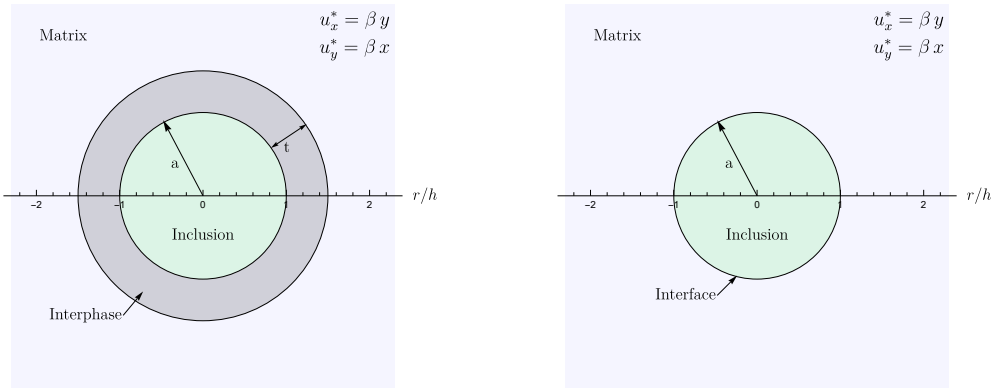


(a) 3 Phase representation.

(b) 2 Phase representation.

**Fig. 5.3.** Geometric representation of the problem.

The absolute error ($\Delta$) of each method given in the following sections is non-dimensionalized as

$$\Delta_{u_r} = \frac{[\![u_r]\!]|_{exact} - [\![u_r]\!]|_{\text{2 Phase solution}}}{u_r^*} \tag{5.121}$$

$$\Delta_{u_r} = \frac{[\![u_\theta]\!]|_{exact} - [\![u_\theta]\!]|_{\text{2 Phase solution}}}{u_r^*} \tag{5.122}$$

$$\Delta_{u_r} = \frac{[\![\sigma_{rr}]\!]|_{exact} - [\![\sigma_{rr}]\!]|_{\text{2 Phase solution}}}{\sigma_{rr}^*} \tag{5.123}$$

$$\Delta_{u_r} = \frac{[\![\sigma_{r\theta}]\!]|_{exact} - [\![\sigma_{r\theta}]\!]|_{\text{2 Phase solution}}}{\sigma_{r\theta}^*} \tag{5.124}$$

### Circular Interphase: Problem Setup

Consider a circular interphase of radius $a$ and a coating of thickness $t$ embedded in an infinite elastic matrix subjected to shear strain $\varepsilon_{xy}^0 = \beta$ at the remote ends. This is the

classical problem of a circular hole in an shear strain medium, and the analytical solution for such classical problem exists. Let us consider that the displacement vector in polar coordinates is give nas $\boldsymbol{u} = \{u_r(r,\theta), u_\theta(r,\theta)\}$.

$$G\,\nabla^2\,\boldsymbol{u} + (\lambda + G)\;\nabla\;(\nabla\cdot\boldsymbol{u}) = 0 \tag{5.125}$$

Substituting the values of $\boldsymbol{u}$ in the equation above leads to the following two forms of PDEs: Using separation of variables method

$$u_r(r,\theta) = R(r)\;\sin(n\,\theta) \qquad ; \qquad u_r(r,\theta) = \Theta(r)\;\cos(n\,\theta) \tag{5.126}$$

The problem is subjected to a uniform remote shear strain, which possesses quadrupolar symmetry. Consequently, the displacement field is sought in separable form using the second angular harmonic ($n = 2$). Thus,

$$u_r(r,\theta) = R(r)\;\sin(2\,\theta) \qquad ; \qquad u_\theta(r,\theta) = \Theta(r)\;\cos(2\,\theta) \tag{5.127}$$

which can be solved to obtain the following

$$R(r) = A\,r^3 + B\,r + \frac{C}{r} + \frac{D}{r^3} \tag{5.128}$$

$$\Theta(r) = \frac{3-2\nu}{2\nu}A\,r^3 + B\,r + \frac{1-2\nu}{2\nu}\frac{C}{r} - \frac{D}{r^3} \tag{5.129}$$

Thus, the displacement field are given as

$$u_r(r,\theta) = R(r)\;\sin(2\,\theta) = \left(A\,r^3 + B\,r + \frac{C}{r} + \frac{D}{r^3}\right)\sin(2\,\theta) \tag{5.130}$$

$$u_\theta(r,\theta) = \Theta(r)\;\cos(2\,\theta) = \left(\frac{3-2\nu}{2\nu}A\,r^3 + B\,r + \frac{1-2\nu}{2\nu}\frac{C}{r} - \frac{D}{r^3}\right)\cos(2\,\theta) \tag{5.131}$$

Plugging these values into strain-strain relation fives the following expressions for strain

$$\varepsilon_{rr} = \left(B - \frac{3D}{r^4} - \frac{C}{r^2} + 3Ar^2\right)\sin(2\,\theta) \tag{5.132}$$

$$\varepsilon_{\theta\theta} = \left(\frac{B}{\nu} + \frac{C}{r^2\,(1-\nu)} - \frac{3\,(1-\nu)}{\nu}Ar^2 - \frac{3D}{r^4}\right)\sin(2\,\theta) \tag{5.133}$$

$$\varepsilon_{r\theta} = \frac{1}{2}\left(2B + \frac{C}{r^2\,(1-\nu)} + \frac{3Ar^2}{\nu} + \frac{6D}{r^4}\right)\cos(2\,\theta) \tag{5.134}$$

and from the Hooke's law for isotropic elastic solids, we can obtain the expression for the stress fields

$$\sigma_{rr} = 2\,G\left(B - \frac{3D}{r^4} - \frac{1}{1-\nu}\frac{C}{r^2}\right)\sin(2\,\theta) \tag{5.135}$$

$$\sigma_{\theta\theta} = 2\,G\left(\frac{3D}{r^4} - B - \frac{3}{\nu}Ar^2 - \frac{3D}{r^4}\right)\sin(2\,\theta) \tag{5.136}$$

$$\sigma_{r\theta} = G\left(2B + \frac{C}{r^2\,(1-\nu)} + \frac{3Ar^2}{\nu} + \frac{6D}{r^4}\right)\cos(2\,\theta) \tag{5.137}$$

For a exact solution, that is the perfect interphase problem, the displacement fields (5.130) exists for all the three materials as $\boldsymbol{u}^{(1)}, \boldsymbol{u}^{(i)}, \boldsymbol{u}^{(2)}$, where $\boldsymbol{u}$ is the displacement vector and $1, 2$ refers to inclusion and matrix respectively, while the superscript $i$ indicates the field inside the interphase. Consequently, we have 3 strain fields and 3 stress fields for the three different materials. For the inclusion, as $r \to 0$, in order to avoid singularity the terms $C$ and $D$ in (5.130) become zero.

$$C_1 = D_1 = 0 \tag{5.138}$$

At the remote boundary, as $r \to \infty$, in order to avoid singularity the terms $A$ becomes zero and $B$ in (5.130) takes the remote shear strain value.

$$A_2 = 0 \quad , \quad B_2 = \beta \tag{5.139}$$

This simplifies our set of unknown values, and the system of equations can be solved to obtain the value of the constants - $\{A_1, B_1, A_i, B_i, C_i, D_i, C_2, D_2\}$. The elastic material properties of the three domains are given in the Table 5.1.

Therefore, the jumps in the elastic fields is given as:

$$[\![u_r]\!] = [R(a+t) - R(a)] \sin 2\,\theta \tag{5.140}$$

$$= \left[ A_i\, t^3 + 3\, a\, A_i\, t^2 + \left(3\, a^2\, A_i + B_i\right) t + C_i \left( \frac{1}{a+t} - \frac{1}{a} \right) + D_i \left( \frac{1}{(a+t)^3} - \frac{1}{a} \right) \right] \sin 2\theta \tag{5.141}$$

$$[\![u_\theta]\!] = [\Theta(a+t) - \Theta(a)] \cos 2\,\theta \tag{5.142}$$

$$= \left[ \frac{3 - 2\,\nu_i}{2\,\nu_i}\, A_i \left((a+t)^3 - a^3\right) + B_i((a+t) - a) + \right.$$
$$\left. \frac{1 - 2\,\nu_i}{2\,(1-\nu_i)}\, C_i \left( \frac{1}{a+t} - \frac{1}{a} \right) + D_i \left( \frac{1}{(a+t)^3} - \frac{1}{a^3} \right) \right] \cos 2\theta \tag{5.143}$$

$$[\![\sigma_{rr}]\!] = [\sigma_{rr}(a+t) - \sigma_{rr}(a)] \sin 2\,\theta$$

$$= 2\, G^{(i)} \left(2\, a + t\right) \left[ \frac{1}{1-\nu_i}\, C_i \left( \frac{1}{(a+t)^2} - \frac{1}{a^2} \right) + 6\, D_i \left( \frac{1}{(a+t)^3} - \frac{1}{a^3} \right) \right] \sin 2\theta \tag{5.144}$$

$$[\![\sigma_{r\theta}]\!] = [\sigma_{r\theta}(a+t) - \sigma_{r\theta}(a)] \cos 2\,\theta$$

$$= G^{(i)} \left[ \frac{3\,t}{t\nu_i}\, A_i \left((a+t) + a\right) + \frac{1}{1-\nu_i}\, C_i \left( \frac{1}{(a+t)^2} - \frac{1}{a^2} \right) + \right.$$
$$\left. 6\, D_i \left( \frac{1}{(a+t)^4} - \frac{1}{a^4} \right) \right] \cos 2\theta \tag{5.145}$$

| | $E$ | $\nu$ | $G$ |
|---|---|---|---|
| Material 1 (inclusion) | 24 | 0.20 | $10\,G^{(2)}$ |
| Material 2 (matrix) | 2.7 | 0.35 | 1 |
| Material 3 (interphase) | $2.5\,G^{(i)}$ | 0.25 | $\{10^{-8}$ to $10^{8}\}$ |

**Table 5.1.** Elastic properties of the material in perfect interphase setting.

### Numerical Verification

The results presented here refer to a circular inclusion with an imperfect interface compared to results from the exact solution (the perfect interphase setting). The results are presented at $\theta = 22.5\,\text{deg}$ and radius of inclusion $a = 1$.

Fig.5.4 illustrates the jumps in radial and angular component of the displacement vector along the normal direction for interphase thickness of $\epsilon = 0.01$. For jumps in radial direction Fig.5.4a presents the comparison of the results with respect to the three-phase solution, while Fig.5.4b demonstrates the absolute error computed for each method. From the graphs it is observed that the jump in radial component of displacement is ...

For the jumps of the angular component, Fig.5.4c highlights the plots of each method compared against the three-phase solution, while Fig.5.4d illustrates the absolute errors. It can be clearly seen that while Hashin, 2002 method shows good approximation of the jumps for soft interphases, it begins to deviate slightly with increasing rigidity. The method proposed by Hashin, 2002 and the two-point schemes proposed by us begin to deviate at around $G^{(i)}/G^{(2)} = 10^5$, while the three-point scheme proposed by us shows good results for $G^{(i)}/G^{(2)} = 10^8$. This highlights the efficiency of the proposed schemes for computing jumps of the radial and tangential displacement components.

The values of the jumps of the radial component $[\![u_r]\!]$ and the angular component $[\![u_\theta]\!]$ of the displacement vector of the circular interphase which is computed via classical models from literature as well as our proposed schemes, the comparison of their absolute values is tabulated in Table.5.2 for a soft $G^{(i)}/G^{(2)} = 0.001$ and a rigid interphase $G^{(i)}/G^{(2)} = 1000$. From the values below, it can be concurred that our proposed schemes provide good approximation of the exact solution, with absolute error being less than $\mathcal{O}(\epsilon)$.

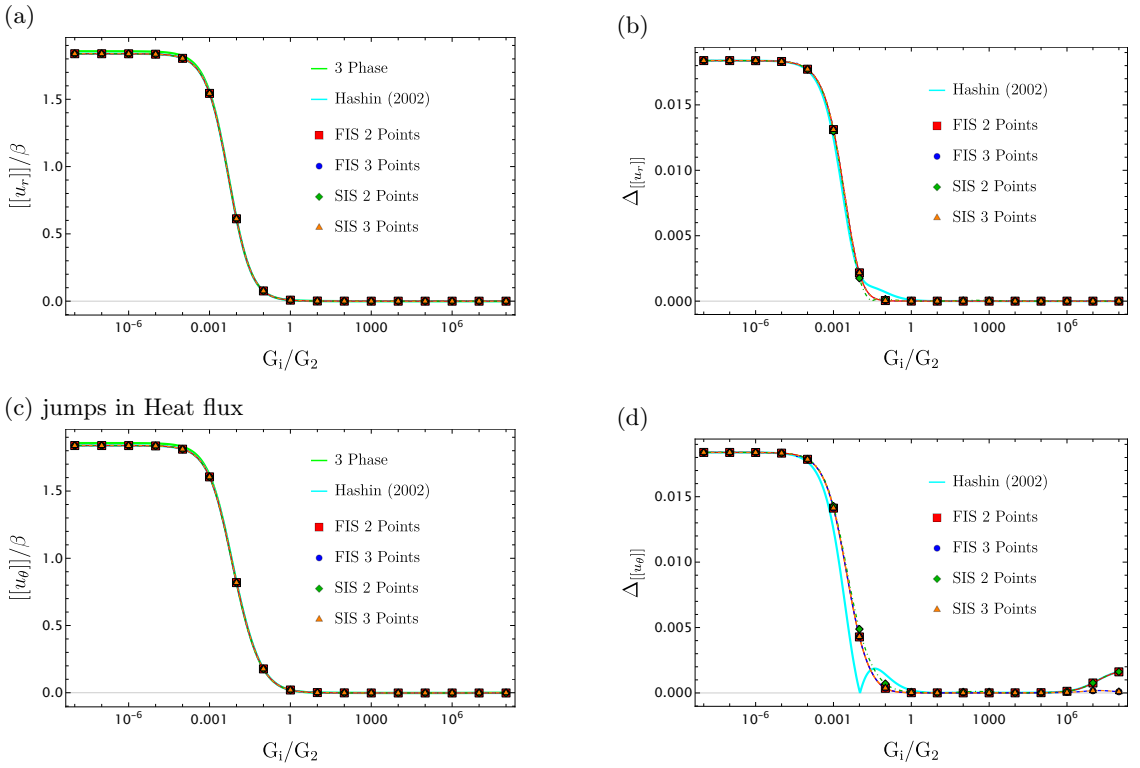


**Fig. 5.4.** Plots of normalized displacement jumps with their corresponding absolute errors for circular interphase of thickness $\epsilon = 0.01$.

Fig.5.5 highlights the plots of the jumps in normal components of the stress vector $\sigma_{rr}$ and the shear component $\sigma_{r\theta}$ across a wide range of elastic shear modulus of the interphase. Fig.5.5a compares the jumps in the normal component of the stress vector, and Fig.5.5b illustrates the absolute errors computed as defined in (5.121) for each method. It is clearly seen that our proposed schemes show good approximation of the exact solution. The one-point scheme of Hashin, along with our proposed two point scheme show good approximation upto $G^{(i)}/G^{(2)} \approx 10^5$, and beyond this value, the error increases. However, the proposed three-point scheme show good approximation, and error of $\mathcal{O}(\epsilon)$ at $G^{(i)}/G^{(2)} = 10^6$. Also, for higher thickness of $\epsilon = 0.05$, while Hashin's results are no longer accurate (as mentioned by himself in Hashin, 2002) we see that the three point schemes show error of $\mathcal{O}(\epsilon)$ for shear values of $G^{(i)}/G^{(2)} \approx 10^4$ which is quite a good approximation. For the jumps of the tangential components of the stress vector $\sigma_{r\theta}$ Fig.5.5c plots the values obtained from the perfect solution, and from the imperfect interface solution via the scheme of Hashin and our proposed methods. It is observed that the methods deviate from the exact solution somewhere around $10^5 \leq G^{(i)}/G^{(2)} < 10^6$ except for our proposed three-points methods show good approximation of the solution with error being approximately $\leq \mathcal{O}(\epsilon)$. Again for $\epsilon = 0.05$, while the other methods deviate largely, it is seen that our proposed scheme shows least error, about $\mathcal{O}(\epsilon)$ for $G^{(i)}/G^{(2)} \approx 10^8$ which demonstrates the robustness of the proposed transmission conditions.

| Absolute Error $\Delta$ with $\boldsymbol{F} = 0$ | | | | | | |
|---|---|---|---|---|---|---|
| $[\![u_r]\!]$ | $G^{(i)}/G^{(2)} = 10^{-3}$ | | | $G^{(i)}/G^{(2)} = 10^{3}$ | | |
| | $t = 0.01$ | $t = 0.05$ | $t = 0.1$ | $t = 0.01$ | $t = 0.05$ | $t = 0.1$ |
| Hashin, 2002 | 0.013 | 0.085 | 0.176 | $1.33 \times 10^{-6}$ | $9.96 \times 10^{-6}$ | $3.4 \times 10^{-5}$ |
| FIS - 2 points (Eqn.(5.56)) | 0.013 | 0.086 | 0.177 | $1.4 \times 10^{-7}$ | $6.5 \times 10^{-7}$ | $1.2 \times 10^{-5}$ |
| FIS - 3 points (Eqn.(5.82)) | 0.013 | 0.086 | 0.177 | $1.55 \times 10^{-7}$ | $1.39 \times 10^{-7}$ | $6.31 \times 10^{-6}$ |
| SIS - 2 points (Eqn.(5.56)) | 0.013 | 0.085 | 0.177 | $4.62 \times 10^{-5}$ | $7.6 \times 10^{-5}$ | $1.2 \times 10^{-4}$ |
| SIS - 3 points (Eqn.(5.82)) | 0.013 | 0.086 | 0.177 | $1.51 \times 10^{-7}$ | $6.79 \times 10^{-7}$ | $1.3 \times 10^{-5}$ |
| $[\![u_\theta]\!]$ | | | | | | |
| Hashin, 2002 | 0.013 | 0.085 | 0.176 | $2.03 \times 10^{-5}$ | 0.0005 | 0.003 |
| FIS - 2 points (Eqn.(5.57)) | 0.014 | 0.087 | 0.179 | $8.48 \times 10^{-6}$ | 0.0003 | 0.002 |
| FIS - 3 points (Eqn.(5.86)) | 0.014 | 0.087 | 0.179 | $9.99 \times 10^{-6}$ | 0.0003 | 0.001 |
| SIS - 2 points (Eqn.(5.57)) | 0.014 | 0.087 | 0.179 | $8.27 \times 10^{-5}$ | 0.0003 | 0.002 |
| SIS - 3 points (Eqn.(5.86)) | 0.014 | 0.087 | 0.179 | $9.93 \times 10^{-6}$ | 0.0002 | 0.001 |

**Table 5.2.** Relative errors ($\delta$) values computed for displacement vectors from all models for a soft ($G^{(i)}/G^{(2)} = 10^{-3}$) and rigid interphase ($G^{(i)}/G^{(2)} = 10^{3}$). Here, FIS refers to the proposed methods in First Integration Scheme and SIS stands for Second Integration scheme.

The values of the jumps of the radial component $[\![\sigma_{rr}]\!]$ and the angular component $[\![\sigma_{r\theta}]\!]$ of the displacement vector of the circular interphase which is computed via classical models from literature as well as our proposed schemes, the comparison of their absolute values is tabulated in Table.5.3 for a soft $G^{(i)}/G^{(2)} = 0.001$ and a rigid interphase $G^{(i)}/G^{(2)} = 1000$. From the values below, it can be concurred that our proposed schemes provide good approximation of the exact solution, with absolute error being less than $\mathcal{O}(\epsilon)$.

The absolute error for the interphase of thickness $\epsilon = 0.01$ is of the order of $\mathcal{O}(\epsilon)$ and confirms that employing three points of integration inside the interphase would provide very good approximation of the jumps of displacements and surface fluxes across an imperfect interface, and would be in good agreement with those obtained from the exact solution.

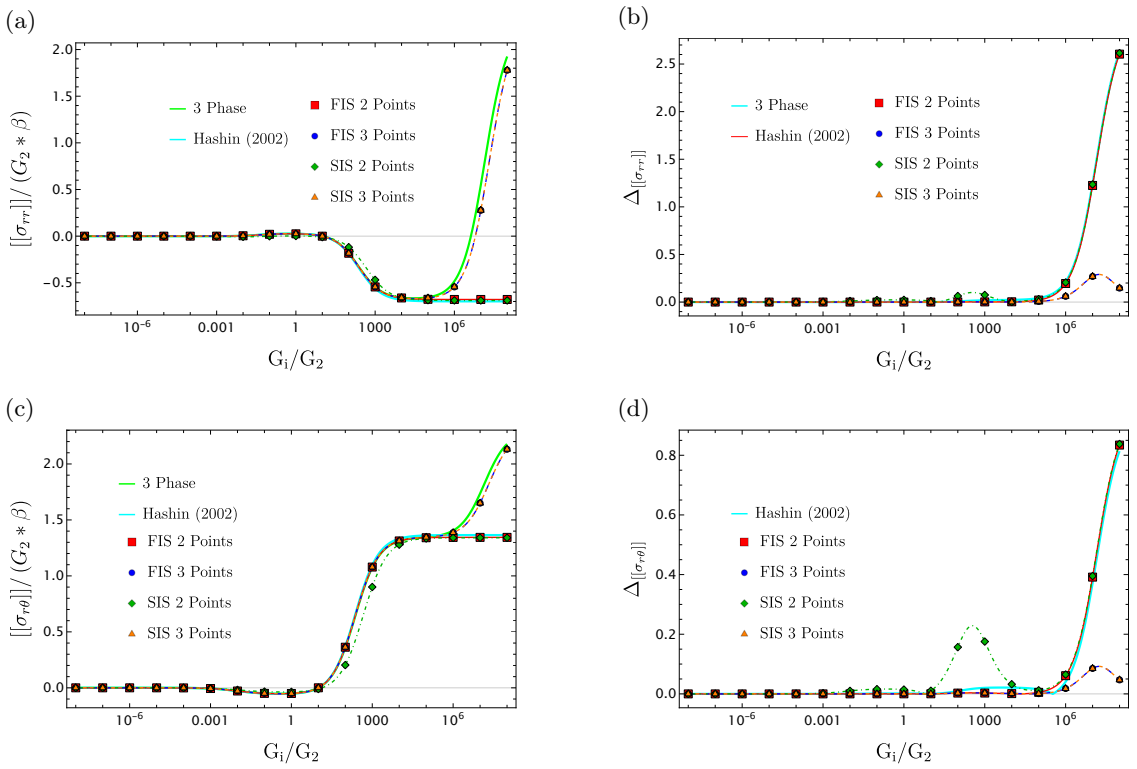


**Fig. 5.5.** Plots of normalized displacement jumps with their corresponding absolute errors for circular interphase of thickness $\epsilon = 0.01$.

| Absolute Error $\Delta$ with $\boldsymbol{F} = 0$ | | | | | | |
|---|---|---|---|---|---|---|
| $[\![\sigma_{rr}]\!]$ | Soft $G^{(i)}/G^{(2)} = 0.001$ | | | Rigid $G^{(i)}/G^{(2)} = 1000$ | | |
| | $t = 0.01$ | $t = 0.05$ | $t = 0.1$ | $t = 0.01$ | $t = 0.05$ | $t = 0.1$ |
| | $t = 0.01$ | $t = 0.05$ | $t = 0.1$ | $t = 0.01$ | $t = 0.05$ | $t = 0.1$ |
| Hashin, 2002 | $2.7 \times 10^{-6}$ | $1.02 \times 10^{-5}$ | $3.17 \times 10^{-5}$ | 0.0188 | 0.1313 | 0.3887 |
| FIS - 2 points (Eqn.(5.59)) | $1.13 \times 10^{-6}$ | $5.74 \times 10^{-6}$ | $2.71 \times 10^{-5}$ | 0.0017 | 0.0286 | 0.1688 |
| FIS - 3 points (Eqn.(5.91)) | $1.55 \times 10^{-6}$ | $2.48 \times 10^{-6}$ | $1.6 \times 10^{-5}$ | 0.0015 | 0.0107 | 0.0404 |
| SIS - 2 points (Eqn.(5.96)) | 0.002 | 0.0025 | 0.0024 | 0.0745 | 0.0537 | 0.2524 |
| SIS - 3 points (Eqn.(5.96)) | $9.82 \times 10^{-6}$ | $6.32 \times 10^{-5}$ | 0.00013 | 0.0014 | 0.0085 | 0.0325 |
| $[\![\sigma_{r\theta}]\!]$ | | | | | | |
| Hashin, 2002 | $1.75 \times 10^{-5}$ | $4.4 \times 10^{-5}$ | 0.0001 | 0.02 | 0.0972 | 0.145 |
| FIS - 2 points (Eqn.(5.57)) | $2.2 \times 10^{-5}$ | 0.0001 | 0.0003 | 0.0028 | $7.78 \times 10^{-5}$ | 0.05 |
| FIS - 3 points (Eqn.(5.86)) | $3.04 \times 10^{-5}$ | 0.0002 | 0.0004 | 0.0028 | 0.0042 | 0.008 |
| SIS - 2 points (Eqn.(5.57)) | 0.0024 | 0.0028 | 0.0029 | 0.1754 | 0.0743 | 0.126 |
| SIS - 3 points (Eqn.(5.86)) | $3.4 \times 10^{-5}$ | 0.0002 | 0.0004 | 0.0028 | 0.0042 | 0.008 |

**Table 5.3.** Relative errors ($\delta$) values computed for displacement vectors from all models for a soft ($G^{(i)}/G^{(2)} = 10^{-5}$) and rigid interphase ($G^{(i)}/G^{(2)} = 10^{5}$). Here, FIS refers to the proposed methods in First Integration Scheme and SIS stands for Second Integration scheme.

# Chapter 6

# Transmission conditions across a thin thermoelastic interface

## 6.1 Introduction

Composite materials are a common part in the industries, due to their high performance and better endurance to structural and thermal loading. The ceramics are subjected to cyclic thermal shock loading, leading to development of thermal stresses within the material, which progresses to the ultimate failure of the material. The presence of inclusions although contributes to the increased performance of the material, at the boundary of the matrix and inclusion, however, there exists an *imperfect interface*, across which there is a finite jump in the properties of the material due to mismatch of the thermal or mechanical material properties (thermal conductivities, shear modulus, Poisson ration, CTEs, etc). These accumulations, or "jumps" across the interphase boundaries creates hotspots which initiate microcracks which propagate on cyclic loading.

The work presented in this chapter is devoted to the development of transmission conditions for a thin thermoelastic interphase, making use of models developed in the previous chapters dealing with thermal and spring type interphase. The constitutive model is derived from the governing equations, and numerically validated via an appropriate example, and concluded with discussion on the results obtained.

## 6.2 Motivation

As in the previous cases of thermal (sec.4.1) and elastic interface (sec.5.3), temperature $\Theta^{(i)}$, and displacement vector $\boldsymbol{u}^{(i)}$ are expanded asymptotically inside the interphase around point $A_1$ and $A_2$, to express temperature and heat flux at point $A_3$ in the normal

direction using Taylor series.

$$\begin{aligned}
\Theta^{(i)}(\xi) &= \Theta^{(i)}_{A_1} + \left.\frac{\partial \Theta^{(i)}}{\partial n}\right|_{A_1} \xi + a_1\xi^2, \quad 0 \le \xi \le t_1, \\
\Theta^{(i)}(\xi) &= T^{(i)}_{A_2} + \left.\frac{\partial \Theta^{(i)}}{\partial n}\right|_{A_2} (\xi - t) + a_2(\xi - t)^2, \quad t_1 \le \xi \le t, \\
\boldsymbol{u}^{(i)}(\xi) &= \boldsymbol{u}^{(i)}_{A_1} + \left.\frac{\partial \boldsymbol{u}^{(i)}}{\partial \alpha_1} \cdot \hat{\boldsymbol{n}}\right|_{A_1} \xi + \boldsymbol{c}\xi^2, \quad 0 \le \xi \le t_1, \\
\boldsymbol{u}^{(i)}(\xi) &= \boldsymbol{u}^{(i)}_{A_2} + \left.\frac{\partial \boldsymbol{u}^{(i)}}{\partial \alpha_1} \cdot \hat{\boldsymbol{n}}\right|_{A_2} (\xi - t) + \boldsymbol{d}(\xi - t)^2, \quad t_1 \le \xi \le t,
\end{aligned} \tag{6.1}$$

Here $a_1, a_2$ are the scalar internal parameters in the expansion of the temperature field inside the interphase $\Theta^{(i)}$, as given in (4.2), and $\boldsymbol{c}, \boldsymbol{d}$ are the vector quantities of the internal parameters, when the displacement vector $\boldsymbol{u}^{(i)}$ inside the interphase, is expanded. From the thermoelastic constitutive laws, given in 3.3.5, and re-written here for the sake of brevity,

$$\text{Fourier's Law: } q^{(i)}_n = -k^{(i)} \frac{\partial \Theta^{(i)}}{\partial n} \tag{6.2}$$

$$\text{Hooke's Law: } \sigma^{(i)}_{mn} = C^{(i)}_{mnkl}(\varepsilon^{(i)}_{kl} - m^{(i)}\delta_{mn}\Theta^{(i)}) \quad ; \quad \mathbb{C} \in \mathsf{Sym} \tag{6.3}$$

where $m = (3\lambda + 2\mu)\alpha$ is the coupling factor and $\Theta = T - T_0$ is the variation of the temperature. Thus, from Hooke's law, no thermoelastic effect exists for the the temperature field. Substituting the temperature expansion around points $A_1$ and $A_2$ (6.1) into the Hooke's law, we get the heat flux approximation as

$$\begin{aligned}
q^{(i)}_n(\xi) &= -k^{(i)}(\xi)\left(\left.\frac{\partial \Theta^{(i)}}{\partial n}\right|_{A_1} + 2a_1\xi\right), \quad 0 \le \xi \le t_1, \\
q^{(i)}_n(\xi) &= -k^{(i)}(\xi)\left(\left.\frac{\partial \Theta^{(i)}}{\partial n}\right|_{A_2} + 2a_2(\xi - t)\right), \quad t_1 \le \xi \le t,
\end{aligned} \tag{6.4}$$

The first two equations of (6.1) along with (6.4) can be solved to obtain internal parameters $a_1, a_2$ for the temperature field, which have the same form as obtained in (4.6), as the temperature and heat flux are not affected by the thermoelastic coupling term. Thus,

$$\begin{aligned}
a_1 &= \frac{2k^{(i)}_{A_1}k^{(i)}_{A_2}(\Theta^{(i)}_{A_2} - \Theta^{(i)}_{A_1}) + k^{(i)}_{A_1}q^{(i)}_n|_{A_2}t_2 + k^{(i)}_{A_2}q^{(i)}_n|_{A_1}(2t - t_2)}{2k^{(i)}_{A_1}k^{(i)}_{A_2}t_1 t}, \\
a_2 &= \frac{2k^{(i)}_{A_1}k^{(i)}_{A_2}(\Theta^{(i)}_{A_1} - \Theta^{(i)}_{A_2}) - k^{(i)}_{A_2}q^{(i)}_n|_{A_1}t_1 - k^{(i)}_{A_1}q^{(i)}_n|_{A_2}(2t - t_1)}{2k^{(i)}_{A_1}k^{(i)}_{A_2}t_2 t},
\end{aligned} \tag{6.5}$$

where there is a clear symmetry by changing $T^{(i)}_{A_1} \to T^{(i)}_{A_2}$ and $q^{(i)}_n|_{A_1} \to -q^{(i)}_n|_{A_2}$, as seen previously in the thermal case. Next, the Hooke's law can be re-written as

$$C^{-1}_{mnkl}\sigma^{(i)}_{mn} = \varepsilon^{(i)}_{kl} - m^{(i)}\delta_{mn}\Theta^{(i)} \tag{6.6}$$

and the symmetric tensor $\varepsilon_{kl}$ can be further decomposed into the tangential and normal components, as seen as earlier in the elastic interphase case (5.14). Thus, the modified form of Hooke's law is then written as:

$$\mathbb{C}^{-1}\boldsymbol{\sigma}^{(i)} = \operatorname{grad}_s \boldsymbol{u}^{(i)} - \boldsymbol{B} : (\operatorname{grad} \boldsymbol{u}^{(i)} \cdot \hat{\boldsymbol{n}}) - m^{(i)}\Theta^{(i)}\boldsymbol{I} \tag{6.7}$$

The coordinate $\alpha_1$ is aligned with the outward normal $\hat{\boldsymbol{n}}$, this means that the normal component of the displacement vector becomes:

$$\operatorname{grad} \boldsymbol{u}^{(i)} \cdot \hat{\boldsymbol{n}} = \frac{\partial \boldsymbol{u}^{(i)}}{\partial n} = \frac{\partial \boldsymbol{u}^{(i)}}{\partial \alpha_1} \tag{6.8}$$

The equations for the expansion of the displacement vector field $\boldsymbol{u}^{(i)}$ from (6.1) is substituted in the modified Hooke's law above:

$$\mathbb{C}^{-1}\boldsymbol{\sigma}^{(i)}(\xi) = \nabla_s \boldsymbol{u}^{(i)}|_{A_3} + \boldsymbol{B}\left(\left.\frac{\partial \boldsymbol{u}^{(i)}}{\partial \alpha_1}\right|_{A_1} + 2\,\boldsymbol{c}\,\xi\right) - m\boldsymbol{I}\left(\Theta^{(i)}|_{A_1} - \left.\frac{q_n^{(i)}}{k^{(i)}}\right|_{A_1}\xi + a_1\,\xi^2\right), \quad 0 \le \xi \le t_1, \tag{6.9}$$

$$\begin{aligned}\mathbb{C}^{-1}\boldsymbol{\sigma}^{(i)}(\xi) = \nabla_s \boldsymbol{u}^{(i)}|_{A_3} + \boldsymbol{B}&\left(\left.\frac{\partial \boldsymbol{u}^{(i)}}{\partial \alpha_1}\right|_{A_2} + 2\,\boldsymbol{d}\,(\xi - t)\right) \\ &- m\boldsymbol{I}\left(\Theta^{(i)}|_{A_2} - \left.\frac{q_n^{(i)}}{k^{(i)}}\right|_{A_2}(\xi - t) + a_2\,(\xi - t)^2\right), \quad t_1 \le \xi \le t,\end{aligned} \tag{6.10}$$

The last two equations of (6.1) (6.9) and (6.10), the system of equations obtained can be solved for, and the internal parameters $\boldsymbol{c}, \boldsymbol{d}$ can be solved for. The parameters $a_1, a_2$ are the internal parameters in the expansion of $\Theta^{(i)}$ and their values are obtained above. Alternatively, the value of $\Theta^{(i)}|_{A_3}$ can be plugged in here. But since the parameters $a_1$ and $a_2$ are symmetric in nature then the coupling factor $(m\Theta^{(i)}\boldsymbol{I})|_{A_3}$ will cancel each other, and (6.9) and (6.10) will reduce to the same form as that of elastic case Sec5.3. Thus, with internal parameters $a_1, a_2, \boldsymbol{c}$ and $\boldsymbol{d}$ known the temperature $\Theta^{(i)}$ and the heat flux $q_n^{(i)}$ values at the intermediate surface along with the displacement fields $\boldsymbol{u}^{(i)}$ and stress vector $\boldsymbol{\sigma}_n^{(i)}$ can also be determined. It must be notes that this values of stress vector is not the same as that obtained in the purely elastic case (5.36) previously as the coupling factor now exists. Therefore

$$\Theta^{(i)}_{A_3}(t_1^-) = \Theta^{(i)}_{A_3}(t_1^+) = \frac{1}{2k^{(i)}_{A_1}k^{(i)}_{A_2}t}\left[k^{(i)}_{A_1}q^{(i)}_n|_{A_2}t_1t_2 - k^{(i)}_{A_2}q^{(i)}_n|_{A_1}t_1t_2 + 2k^{(i)}_{A_1}k^{(i)}_{A_2}(\Theta^{(i)}_{A_1}t_2 + \Theta^{(i)}_{A_2}t_1)\right] \tag{6.11}$$

$$\begin{aligned}\boldsymbol{u}^{(i)}|_{A_3}(t_1^+) = \boldsymbol{u}^{(i)}|_{A_3}(t_1^-) = &\frac{t_1\,t_2\left(\mathcal{P}^{(i)}_m|_{A_2} - \mathcal{P}^{(i)}_m|_{A_1}\right) + 2\,t_1\,t_2\left(\mathbb{C}^{-1}\boldsymbol{\sigma}^{(i)}_{A_1} - \mathbb{C}^{-1}\,\boldsymbol{\sigma}^{(i)}|_{A_2}\right)}{2\,t} \\ &+ \frac{2\left(t_1\,\boldsymbol{u}^{(i)}|_{A_2} + t_2\,\boldsymbol{u}^{(i)}|_{A_1}\right)}{2\,t}\end{aligned} \tag{6.12}$$

while the fluxes are computed as

$$q^{(i)}_n|_{A_3}(t_1^-) = q^{(i)}_n|_{A_3}(t_1^+) = \frac{-k^{(i)}_{A_3}}{k^{(i)}_{A_1}k^{(i)}_{A_2}t}\left[k^{(i)}_{A_1}q^{(i)}_n|_{A_2}t_2 + k^{(i)}_{A_2}q^{(i)}_n|_{A_1}t_1 + 2k^{(i)}_{A_1}k^{(i)}_{A_2}(\Theta^{(i)}_{A_2} - \Theta^{(i)}_{A_1})\right] \tag{6.13}$$

$$\boldsymbol{\sigma}_n^{(i)}|_{A_3}(t_1^-) = \boldsymbol{\sigma}_n^{(i)}|_{A_3}(t_1^+) = \frac{\mathbb{C}\cdot\mathcal{P}^{(i)}|_{A_1}\,t_1 + \mathbb{C}\cdot\mathcal{P}^{(i)}|_{A_2}\,t_2 - 2\left(\boldsymbol{\sigma}_n^{(i)}|_{A_1}\,t_1 + \boldsymbol{\sigma}_n^{(i)}|_{A_2}\,t_2\right)}{2\,t}$$

$$\frac{-4\,\mathbb{C}\left(\boldsymbol{u}^{(i)}|_{A_2} - \boldsymbol{u}^{(i)}|_{A_1}\right)}{2\,t} + \mathbb{C}\mathcal{P}^{(i)}|_{A_3} - m\Theta^{(i)}|_{A_3}\boldsymbol{I} \quad (6.14)$$

where the value of $\Theta^{(i)}|_{A_3}$ is the same as in (6.11). Thus,

$$\boldsymbol{\sigma}_n^{(i)}|_{A_3}(t_1^-) = \boldsymbol{\sigma}_n^{(i)}|_{A_3}(t_1^+) = \frac{\mathbb{C}\cdot\mathcal{P}^{(i)}|_{A_1}\,t_1 + \mathbb{C}\cdot\mathcal{P}^{(i)}|_{A_2}\,t_2 - 2\left(\boldsymbol{\sigma}_n^{(i)}|_{A_1}\,t_1 + \boldsymbol{\sigma}_n^{(i)}|_{A_2}\,t_2\right)}{2\,t}$$

$$\frac{-4\,\mathbb{C}\left(\boldsymbol{u}^{(i)}|_{A_2} - \boldsymbol{u}^{(i)}|_{A_1}\right)}{2\,t} + \mathbb{C}\mathcal{P}^{(i)}|_{A_3}$$

$$- m\frac{1}{2\,k_{A_1}^{(i)}k_{A_2}^{(i)}t}\left[k_{A_1}^{(i)}q_n^{(i)}|_{A_2}t_1t_2 - k_{A_2}^{(i)}q_n^{(i)}|_{A_1}t_1t_2 + 2k_{A_1}^{(i)}k_{A_2}^{(i)}(\Theta_{A_1}^{(i)}t_2 + \Theta_{A_2}^{(i)}t_1)\right]\boldsymbol{I} \quad (6.15)$$

$$\boldsymbol{\sigma}_n^{(i)}|_{A_3}(t_1^-) = \boldsymbol{\sigma}_n^{(i)}|_{A_3}(t_1^+) = \frac{\mathcal{M}^{(i)}|_{A_1}\,t_1 + \mathcal{M}^{(i)}|_{A_2}\,t_2 - 4\,\mathcal{A}\left(\boldsymbol{u}^{(i)}|_{A_2} - \boldsymbol{u}^{(i)}|_{A_1}\right)}{2\,k_{A_1}^{(i)}\,k_{A_2}^{(i)}t}$$

$$\frac{-1}{t}\left(\boldsymbol{\sigma}_n^{(i)}|_{A_1}\,t_1 + \boldsymbol{\sigma}_n^{(i)}|_{A_2}\,t_2\right) + \mathcal{M}^{(i)}|_{A_3} - m\Theta_{A_3}^{(i)}\boldsymbol{I} \quad (6.16)$$

where

$$\mathcal{A} = \mathbb{C}\,k_{A_1}^{(i)}\,k_{A_2}^{(i)} \quad ; \quad \mathcal{M} = \mathcal{A}\mathcal{P}^{(i)} \quad (6.17)$$

## 6.3 Problem Statement

Let us consider a homogeneous, isotropic thermoelastic material as the interphase domain. The arbitrary curvilinear composite system is governed by the following equations:

For the material 1, 2, and i, the corresponding components of displacements are $u^{(1)}, u^{(2)}$ and $u^{(i)}$, and the temperature is $T^{(1)}, T^{(2)}$ and $T^{(i)}$. The governing equations for a coupled thermoelastic body is given as:

$$\sigma_{ij} = \lambda\,\delta_{ij}\,\epsilon_{kk} + 2\,\mu\,\epsilon_{ij} - m\,\delta_{ij}\,\Theta \quad (6.18)$$

$$kT_{,ii} = \rho\,c_E\,\dot{T} + m\,T_0\,\dot{\epsilon}_{kk} \quad (6.19)$$

where $m = (3\lambda + 2\mu)\alpha$ is the coupling factor and $\Theta = T - T_0$ is the variation of the temperature with $T_0$ being the volumetric reference temperature.

The mechanical strain terms are computed from the linear isotropic strain-displacement relations:

$$\boldsymbol{\epsilon}^{mech} = \frac{1}{2}\left\{\nabla\boldsymbol{u} + (\nabla\boldsymbol{u})^T\right\} \quad (6.20)$$

and the thermal strain is presented by the term $\boldsymbol{\epsilon}^{therm} = m\,\Theta\,\boldsymbol{I}$, where $\boldsymbol{I}$ is the identity matrix.

## 6.4 Development of Transmission Conditions

The proposed transmission conditions to model the jumps in thermoelastic fields across the thin interphase are now developed, starting from the governing equations described in the previous section.

As in the previous cases of thermal and elastic interphase, the thermoelastic fields are defined at two points $A_1$ and $A_2$ which are situated on the boundaries of the interphase in Fig.2.4a, and a third point $A_3$ lying inside the interphase domain. The temperature and displacement, along with the fluxes, are continuous across the boundaries of interphase. These usual classical (perfect/ideal) interface conditions are:

$$[\![\boldsymbol{u}]\!] = 0, \quad [\![\Theta]\!] = 0$$

$$[\![\boldsymbol{\sigma} \cdot \boldsymbol{n}]\!] = 0, \quad [\![\boldsymbol{q} \cdot \boldsymbol{n}]\!] = 0$$

Across the thin interface $\Gamma$ ($\lim t \to 0$) that separates the two materials, as depicted in Fig. 2.4b the elastic and thermal properties are no longer continuous across this surface, and there is an accumulation of state variables or surface fluxes at the boundary, known as "jump" of the property.

The jumps in relative temperature $\Theta$ is expressed using Fourier's Law and is independent of the mechanical effects, as it is an independent state variable:

$$\frac{\partial \Theta^{(i)}}{\partial \alpha_1} = \frac{\partial \Theta^{(i)}}{\partial n} = -\frac{q_n^{(i)}}{k^{(i)}} \tag{6.21}$$

From the elastic case, we know that the components of the displacement vector $\boldsymbol{u}^{(i)}$ along the normal direction $\alpha_1$ is given by (5.28) as

$$\frac{\partial \boldsymbol{u}^{(i)}}{\partial \alpha_1} = \left\{ 2\,\mathbb{C}^{-1}\boldsymbol{\sigma}_n^{(i)} - \mathcal{P}^{(i)} \right\} \tag{6.22}$$

where $\mathcal{G}^{(i)} = \mathcal{P}_m^{(i)}$ is the term that contains all surface gradients of $\boldsymbol{u}^{(i)}$ as defined in (5.29). The governing balance equations are:

1. Thermal Equilibrium:

$$\operatorname{div} \boldsymbol{q}^{(i)} - Q(\xi, \alpha_2, \alpha_3, T) = \rho c_E \dot{T^{(i)}} + m\dot{\varepsilon}_{kk}^{(i)} \tag{6.23}$$

2. Mechanical Equilibrium:

$$\rho \ddot{\boldsymbol{u}}^{(i)} = \operatorname{div} \boldsymbol{\sigma}^{(i)} = \operatorname{div} \left( \lambda^{(i)}\, \operatorname{tr} \boldsymbol{\varepsilon}^{(i)} \boldsymbol{I} + 2\,\mu^{(i)} \boldsymbol{\varepsilon}^{(i)} - m\Theta^{(i)} \boldsymbol{I} \right) \tag{6.24}$$

where $m = \boldsymbol{M} = -3\alpha K$ is the stress-temperature modulus, defined in (3.144).

From the development of transmission conditions for a thermally conductive interphase, we know that the term $\operatorname{div} \boldsymbol{q}$ in (6.23) can be re-written in terms of curvilinear coordinates as:

$$\operatorname{div} \boldsymbol{q}^{(i)} = \frac{1}{h_2\, h_3} \left\{ \frac{\partial}{\partial n}(h_2\, h_3\, q_n^{(i)}) + \frac{\partial}{\partial \alpha_2}(h_3\, q_2^{(i)}) + \frac{\partial}{\partial \alpha_3}(h_2\, q_3^{(i)}) \right\} \tag{6.25}$$

$$= \frac{1}{h_2 h_3} \left\{ \frac{\partial}{\partial n}(h_2\, h_3\, q_n^{(i)}) \right\} + \frac{1}{h_2\, h_3} \left\{ \frac{\partial}{\partial \alpha_2}(h_3\, q_2^{(i)}) + \frac{\partial}{\partial \alpha_3}(h_2\, q_3^{(i)}) \right\} \tag{6.26}$$

$$= \frac{1}{h_2\, h_3} \left\{ \frac{\partial}{\partial n}(h_2\, h_3\, q_n^{(i)}) \right\} + \mathcal{D}_s \boldsymbol{q}^{(i)} \tag{6.27}$$

where $\mathcal{D}_s \boldsymbol{q}^{(i)}$ is the surface differential term defined in (4.19). Following the same process as in the thermal interphase case outlined in Sec 4.2, we have the following two forms of equations obtained from the first term on the LHS

$$\frac{1}{h_2 h_3}\left\{\frac{\partial}{\partial n}(h_2 h_3 q_n^{(i)})\right\} \quad \text{or} \quad \frac{\partial q_n^{(i)}}{\partial n} + g\, q_n^{(i)} \tag{6.28}$$

where $g$ is the curvature term defined in (4.20). This leads to the following two forms of the normal derivative of the normal component of the heat flux term:

$$\frac{\partial q_n^{(i)}}{\partial n} = Q(\xi, \alpha_2, \alpha_3, T) - \mathcal{D}_s \boldsymbol{q}^{(i)} - g\, q_n^{(i)} + \rho\, c_E\, \dot{T}^{(i)} + m\, \mathrm{tr}\, \dot{\boldsymbol{\varepsilon}}^{(i)} \tag{6.29}$$

and

$$\frac{\partial}{\partial n}(h_2 h_3 q_n^{(i)}) = h_2\, h_3 \left(Q(\xi, \alpha_2, \alpha_3, T) - \mathcal{D}_s \boldsymbol{q}^{(i)} + \rho\, c_E\, \dot{T}^{(i)} + m\, \Theta^{(i)}\, \mathrm{tr}\, \dot{\boldsymbol{\varepsilon}}^{(i)}\right) \tag{6.30}$$

where the mechanical presence can be seen via presence of coupling term $m\, \mathrm{tr}\, \dot{\boldsymbol{\varepsilon}}^{(i)}$ and $Q(\xi, \alpha_2, \alpha_3, T)$ is the heat source term distributed within the interphase. If the heat transfer is assumed to be steady state, and free of mechanical coupling effects, then the transmission conditions for heat flux (4.17) and (4.18) can be retrieved from the above equations.

The next step is to define the derivative of the normal component of the stress vector $\boldsymbol{\sigma}_n^{(i)}$ along normal direction. In parallel curvilinear coordinates, the balance equations (6.24) can be expanded as:

$$\mathrm{div}\, \boldsymbol{\sigma}^{(i)} = \frac{1}{h_2 h_3}\left\{\frac{\partial}{\partial n}(h_2 h_3 \boldsymbol{\sigma}_n^{(i)}) + \frac{\partial}{\partial \alpha_2}(h_3 \boldsymbol{\sigma}_2^{(i)}) + \frac{\partial}{\partial \alpha_3}(h_2 \boldsymbol{\sigma}_3^{(i)})\right\} + \boldsymbol{A}^{(i)} \tag{6.31}$$

$$= \frac{1}{h_2 h_3}\left\{\frac{\partial}{\partial n}(h_2 h_3 \boldsymbol{\sigma}_n^{(i)})\right\} + \frac{1}{h_2 h_3}\left\{\frac{\partial}{\partial \alpha_2}(h_3 \boldsymbol{\sigma}_2^{(i)}) + \frac{\partial}{\partial \alpha_3}(h_2 \boldsymbol{\sigma}_3^{(i)})\right\} + \boldsymbol{A}^{(i)} \tag{6.32}$$

$$= \frac{1}{h_2 h_3}\left\{\frac{\partial}{\partial n}(h_2 h_3 \boldsymbol{\sigma}_n^{(i)})\right\} + \mathcal{D}_s \boldsymbol{\sigma}_n^{(i)} + \boldsymbol{A}^{(i)} \tag{6.33}$$

where $\mathcal{D}_s \boldsymbol{\sigma}_n^{(i)}$ are the surface gradients of the normal stress vector $\boldsymbol{\sigma}_n^{(i)}$ defined in (5.43) and $\boldsymbol{A}$ is the tensor comprising of all the terms involving derivatives of scale factors given in (5.48). Thus, the evolution of the surface fluxes along the normal direction are obtained from Eqn.(6.24), and are expressed below explicitly as:

$$\frac{\partial \boldsymbol{\sigma}_n^{(i)}}{\partial \alpha_1} = \rho\, \ddot{\boldsymbol{u}}^{(i)} - \mathcal{D}_s \boldsymbol{\sigma}_n^{(i)} - g\, \boldsymbol{\sigma}_n^{(i)} - \boldsymbol{A}^{(i)} \tag{6.34}$$

or

$$\frac{\partial}{\partial \alpha_1}(h_2 h_3 \boldsymbol{\sigma}_n^{(i)}) = h_2\, h_3 \left(\rho\, \ddot{\boldsymbol{u}}^{(i)} - \boldsymbol{A} - \mathcal{D}_s \boldsymbol{\sigma}_n^{(i)}\right) \tag{6.35}$$

Following the definition of tensor $\boldsymbol{A}$ from (5.48),

$$A_{11} = \left(\frac{\sigma_{22}}{h_2}\frac{\partial h_2}{\partial \alpha_1} + \frac{\sigma_{33}}{h_3}\frac{\partial h_3}{\partial \alpha_1}\right) \tag{6.36}$$

$$A_{12} = \frac{\sigma_{21}}{h_2}\frac{\partial h_2}{\partial \alpha_1} + \frac{\sigma_{23}}{h_2 h_3}\frac{\partial h_2}{\partial \alpha_3} - \frac{\sigma_{33}}{h_3}\frac{\partial h_3}{\partial \alpha_2} \tag{6.37}$$

$$A_{13} = \frac{\sigma_{31}}{h_3}\frac{\partial h_3}{\partial \alpha_1} + \frac{1}{h_2 h_3}\left(\sigma_{32}\frac{\partial h_3}{\partial \alpha_2} - \sigma_{22}\frac{\partial h_2}{\partial \alpha_3}\right) \tag{6.38}$$

The term $A_{11}$ corresponding to $\sigma_{11}^{(i)}$ is redefined as follows for the linear isotropic thermoelastic case,

$$A_{11} = \mathcal{B} + g\left\{\frac{1-2\,\nu_i}{1-\nu_i}\sigma_{11} - m\,\Theta^{(i)}\right\} \tag{6.39}$$

where

$$\mathcal{B} = \frac{1}{h_2 h_3}\left\{\frac{2G_i}{1-\nu_i}\left(h_3\frac{\partial h_2}{\partial \alpha_1}\left(\epsilon_{22}+\nu_i\epsilon_{33}\right) + h_2\frac{\partial h_3}{\partial \alpha_1}\left(\epsilon_{33}+\nu_i\epsilon_{22}\right)\right)\right\} \tag{6.40}$$

while the terms $A_{12}$ and $A_{13}$ remain the same, as the thermo-elastic coupling effect does not come into play in the tangential stress components.

In the schemes proposed in the following sections, we will make use of either Eqns. ((6.29),(6.34)) or Eqns.((6.30),(6.35)) to arrive at more explicit expressions of the transmission conditions across the interface boundaries.

The effect of the thermal coupling term is represented by the thermal strain term in the normal component of the displacement (6.22), via the term $m\Theta$, while the jumps in tangential components show the same behaviour as that of linear elasticity as we shall see in the transmission conditions in the next section.

## 6.5 First Integration Scheme

For this scheme, we make use of the first set of eqns, (6.29) and (6.34), by integrating them between two or three points within the interphase. The solution for the integrated solution is obtained by employing Trapezoidal rule between these points (intervals), and thus, arriving at the required transmission conditions.

### 6.5.1 Two points Integration scheme

The eqns are integrated between two points, from 0 to $t$ that is between points $A_1$ and $A_2$ using the trapezoidal rule. This gives:

$$[\![f^{(i)}]\!] = \int_0^t \frac{\partial f^{(i)}}{\partial \alpha_1} = \frac{t}{2}\left(\frac{\partial f^{(i)}}{\partial \alpha_1}\bigg|_{A_1} + \frac{\partial f^{(i)}}{\partial \alpha_1}\bigg|_{A_2}\right) \tag{6.41}$$

This gives the following transmission conditions

#### Jump of Temperature

The equation (6.21) defining the variation of temperature $\Theta^{(i)}$ along the normal direction is integrated along the thickness, and using the trapezoidal rule gives

$$[\![\Theta]\!] = -t\left\langle\frac{q_n}{k^{(i)}}\right\rangle \tag{6.42}$$

The equation above is same as that obtained for the jump in temperature across the thermally conductive interphase (4.23).

#### Jump of Displacement vector

The jump in displacement vector across the imperfect interface is obtained by integrating the derivative of the displacement vector along the normal direction (6.22). Due to the

presence of thermal strain, the jumps in the normal component $u_1^{(i)}$ of the displacement vector is modified to

$$[\![u_1]\!] = t\left\langle \frac{\sigma_{11}^{(i)}}{\lambda^{(i)}+2\mu^{(i)}} + \frac{m^{(i)}\,\Theta^{(i)}}{\lambda^{(i)}+2\,\mu^{(i)}} - \frac{\lambda^{(i)}}{\lambda^{(i)}+2\,\mu^{(i)}}\left(\varepsilon_{22}^{(i)}+\varepsilon_{33}^{(i)}\right)\right\rangle \tag{6.43}$$

and tangential $u_k$ component of $\boldsymbol{u}^{(i)}$, where $k = \{2,3\}$

$$[\![u_k]\!] = t\left\langle \frac{\sigma_{1k}^{(i)}}{\mu^{(i)}} - \frac{1}{h_k}\left(\frac{\partial u_1^{(i)}}{\partial \alpha_k} - u_k\frac{\partial h_k}{\partial \alpha_1}\right)\right\rangle \tag{6.44}$$

This is the same as (5.57).

### Jump of Heat flux

The jump in the thermal flux across the interface is given as

$$[\![q_n]\!] = t\left\langle Q - \mathcal{D}_s\boldsymbol{q} - g\,q_n^{(i)} - m^{(i)}\Theta^{(i)}\dot{\varepsilon}_{kk}^{(i)} + \rho\,c_E\,\frac{\partial\Theta^{(i)}}{\partial t}\right\rangle \tag{6.45}$$

Here, we see that the effect of mechanical coupling term $m\Theta^{(i)}\dot{\boldsymbol{\varepsilon}}$ in the resulting transmission conditions. If no coupling exists due to the mechanical deformation, and the thermal deformation occurs under steady state conditions, then (4.22) is retrieved.

### Jump of Thermoelastic Stress

The jumps in stress vector $\boldsymbol{\sigma}_n^{(i)}$ obtained by integrating (6.34) between the two points. the Normal component $\sigma_{11}$ of stress vector reflects the thermal effect on the mechanical deformation via the presence of the coupling term $m\Theta^{(i)}$

$$[\![\sigma_{11}]\!] = t\left\{\left\langle \rho\ddot{\boldsymbol{u}}^{(i)}\right\rangle - \left\langle \mathcal{B}^{(i)}\right\rangle - \left\langle \mathcal{D}_s\boldsymbol{\sigma}_{n1}^{(i)}\right\rangle - \frac{1-2\,\nu^{(i)}}{1-\nu^{(i)}}\left\langle g\,\sigma_{11}^{(i)}\right\rangle + \left\langle g\,m\,\Theta^{(i)}\right\rangle\right\} \tag{6.46}$$

where $\mathcal{B}$ is the operator defined in (6.40), while the tangential component of stress vector $\sigma_{1k}$ (where $k = \{2,3\}$) is identical to (5.60) and (5.61)

$$[\![\sigma_{1k}]\!] = t\left\{\langle\mathcal{A}_{1k}\rangle - \langle\mathcal{D}_s\boldsymbol{\sigma}_{nk}^{(i)}\rangle - \langle g\sigma_{1k}^{(i)}\rangle\right\} \tag{6.47}$$

## 6.5.2 Three points Integration scheme

The accuracy of the derived transmission conditions is improved by introducing another point of integration within the thickness of the interphase. The thickness $t$ of the interphase is divided into two intervals $t_1$ and $t_2$ and the trapezoidal rule is applied from 0 to $t_1$ between points $A_1$ and $A_3$, and from $t_1$ to $t_2$ between points $A_3$ and $A_2$, as in Fig.2.4a and 2.4b. Therefore,

$$[\![f^{(i)}]\!] = \int_0^{t_1}\frac{\partial f^{(i)}}{\partial\alpha_1} + \int_{t_1}^{t_2}\frac{\partial f^{(i)}}{\partial\alpha_1} = \frac{t_1}{2}\left(\frac{\partial f^{(i)}}{\partial\alpha_1}\bigg|_{A_1} + \frac{\partial f^{(i)}}{\partial\alpha_1}\bigg|_{A_3}\right) + \frac{t_2}{2}\left(\frac{\partial f^{(i)}}{\partial\alpha_1}\bigg|_{A_3} + \frac{\partial f^{(i)}}{\partial\alpha_1}\bigg|_{A_2}\right) \tag{6.48}$$

$$[\![f^{(i)}]\!] = \frac{t_1}{2}\frac{\partial f^{(i)}}{\partial\alpha_1}\bigg|_{A_1} + \frac{t_2}{2}\frac{\partial f^{(i)}}{\partial\alpha_1}\bigg|_{A_3} + \frac{t}{2}\frac{\partial f^{(i)}}{\partial\alpha_1}\bigg|_{A_2} \tag{6.49}$$

Using this, the transmission conditions are defined as for jumps in temperature, heat flux, displacement vector, and normal component of stress as follows.

**Jump of Heat flux**

Eqn.(6.29) is integrated between the three points, between points $A_1$ and $A_3$ as:

$$q_n^{(i)}|_{A_3} - q_n^{(i)}|_{A_1} = \frac{t_1}{2}\left(\left.\frac{\partial q_n^{(i)}}{\partial n}\right|_{A_1} + \left.\frac{\partial q_n^{(i)}}{\partial n}\right|_{A_3}\right) \tag{6.50}$$

and between points $A_3$ and $A_2$ as

$$q_n^{(i)}|_{A_3} - q_n^{(i)}|_{A_2} = -\frac{t_2}{2}\left(\left.\frac{\partial q_n^{(i)}}{\partial n}\right|_{A_2} + \left.\frac{\partial q_n^{(i)}}{\partial n}\right|_{A_3}\right) \tag{6.51}$$

if we add (6.50) and (6.51), we get

$$2\, q_n^{(i)}|_{A_3} = \left(q_n^{(i)}|_{A_1} + q_n^{(i)}|_{A_2}\right) + \frac{t_1}{2}\left(\left.\frac{\partial q_n^{(i)}}{\partial n}\right|_{A_1} + \left.\frac{\partial q_n^{(i)}}{\partial n}\right|_{A_3}\right) - \frac{t_2}{2}\left(\left.\frac{\partial q_n^{(i)}}{\partial n}\right|_{A_2} + \left.\frac{\partial q_n^{(i)}}{\partial n}\right|_{A_3}\right) \tag{6.52}$$

$$= \left(q_n^{(i)}|_{A_1} + q_n^{(i)}|_{A_2}\right) + \frac{t_1}{2}\left.\frac{\partial q_n^{(i)}}{\partial n}\right|_{A_1} + (t_1 - t_2)\left.\frac{\partial q_n^{(i)}}{\partial n}\right|_{A_3} - \frac{t_2}{2}\left.\frac{\partial q_n^{(i)}}{\partial n}\right|_{A_2} \tag{6.53}$$

$$q_n^{(i)}|_{A_3} = \left\langle q_n^{(i)}|_{A_1} + q_n^{(i)}|_{A_2}\right\rangle + \frac{t_1}{4}\left.\frac{\partial q_n^{(i)}}{\partial n}\right|_{A_1} + \left(\frac{t_1 - t_2}{2}\right)\left.\frac{\partial q_n^{(i)}}{\partial n}\right|_{A_3} - \frac{t_2}{4}\left.\frac{\partial q_n^{(i)}}{\partial n}\right|_{A_2} \tag{6.54}$$

and if we subtract (6.50) and (6.51) we get

$$[\![q_n^{(i)}]\!] = \frac{t_1}{2}\left.\frac{\partial q_n^{(i)}}{\partial n}\right|_{A_1} + \frac{t_2}{2}\left.\frac{\partial q_n^{(i)}}{\partial n}\right|_{A_2} + \left(\frac{t_1 + t_2}{2}\right)\left.\frac{\partial q_n^{(i)}}{\partial n}\right|_{A_3} \tag{6.55}$$

Assuming the simplest possible case where $t_1 = t_2 = t/2$, (6.52) and (6.55) simplify to

$$q_n^{(i)}|_{A_3} = \left\langle q_n^{(i)}|_{A_1} + q_n^{(i)}|_{A_2}\right\rangle + \frac{t_1}{4}\left.\frac{\partial q_n^{(i)}}{\partial n}\right|_{A_1} + \left(\frac{t_1 - t_2}{2}\right)\left.\frac{\partial q_n^{(i)}}{\partial n}\right|_{A_3} - \frac{t_2}{4}\left.\frac{\partial q_n^{(i)}}{\partial n}\right|_{A_2} \tag{6.56}$$

$$= \left\langle q_n^{(i)}\right\rangle - \frac{t}{8}\left(\left[\!\left[\frac{\partial q_n^{(i)}}{\partial n}\right]\!\right]\right) \tag{6.57}$$

$$\Longrightarrow \qquad q_n^{(i)}|_{A_3} = \langle q_n\rangle - \frac{t}{8}\left(\left[\!\left[Q - \mathcal{D}_s \boldsymbol{q} - g\, q_n^{(i)} - m\,\Theta^{(i)}\,\mathrm{tr}\,\dot{\boldsymbol{\varepsilon}}^{(i)} + \rho\, c_E\,\frac{\partial \Theta^{(i)}}{\partial t}\right]\!\right]\right) \tag{6.58}$$

and

$$[\![q_n^{(i)}]\!] = \frac{t}{2}\left\langle \frac{\partial q_n^{(i)}}{\partial n}\right\rangle + \left(\frac{t}{2}\right)\left.\frac{\partial q_n^{(i)}}{\partial n}\right|_{A_3} \tag{6.59}$$

$$\Longrightarrow \qquad [\![q_n^{(i)}]\!] = \frac{t}{2}\left\langle Q - 2\,\mathcal{D}_s \boldsymbol{q} - g\, q_n^{(i)} - m\,\Theta^{(i)}\,\mathrm{tr}\,\dot{\boldsymbol{\varepsilon}}^{(i)} + \rho\, c_E\,\frac{\partial \Theta^{(i)}}{\partial t}\right\rangle + \frac{t}{2}\left(Q - g\, q_n^{(i)} - m\,\Theta^{(i)}\,\mathrm{tr}\,\dot{\boldsymbol{\varepsilon}}^{(i)} + \rho\, c_E\,\frac{\partial \Theta^{(i)}}{\partial t}\right)\Bigg|_{A_3} \tag{6.60}$$

Therefore, (6.58) provides the normal component of heat flux values at point $A_3$ inside the interphase, and (6.60) is the jump of the normal component of the heat flux across an imperfect interface.

**Jump of Temperature**

Eqn.(6.21) is integrated between the three points, between points $A_1$ and $A_3$ as:

$$\Theta^{(i)}|_{A_3} - \Theta^{(i)}|_{A_1} = \frac{t_1}{2}\left(\left.\frac{\partial\Theta^{(i)}}{\partial n}\right|_{A_1} + \left.\frac{\partial\Theta^{(i)}}{\partial n}\right|_{A_3}\right) = \frac{-t_1}{2}\left(\left.\frac{\partial q_n^{(i)}}{\partial k^{(i)}}\right|_{A_1} + \left.\frac{\partial q_n^{(i)}}{\partial k^{(i)}}\right|_{A_3}\right) \tag{6.61}$$

and between points $A_3$ and $A_2$ as

$$\Theta^{(i)}|_{A_3} - \Theta^{(i)}|_{A_2} = -\frac{t_2}{2}\left(\left.\frac{\partial\Theta^{(i)}}{\partial n}\right|_{A_2} + \left.\frac{\partial\Theta^{(i)}}{\partial n}\right|_{A_3}\right) = \frac{t_2}{2}\left(\left.\frac{\partial q_n^{(i)}}{\partial k^{(i)}}\right|_{A_2} + \left.\frac{\partial q_n^{(i)}}{\partial k^{(i)}}\right|_{A_3}\right) \tag{6.62}$$

If we add (6.61) and (6.62), we get

$$2\,\Theta^{(i)}|_{A_3} = \left(\Theta^{(i)}|_{A_1} + \Theta^{(i)}|_{A_2}\right) + \frac{t_1}{2}\left(\left.\frac{\partial\Theta^{(i)}}{\partial n}\right|_{A_1} + \left.\frac{\partial\Theta^{(i)}}{\partial n}\right|_{A_3}\right) - \frac{t_2}{2}\left(\left.\frac{\partial\Theta^{(i)}}{\partial n}\right|_{A_2} + \left.\frac{\partial\Theta^{(i)}}{\partial n}\right|_{A_3}\right) \tag{6.63}$$

$$= \left(\Theta^{(i)}|_{A_1} + \Theta^{(i)}|_{A_2}\right) + \frac{t_1}{2}\left.\frac{\partial\Theta^{(i)}}{\partial n}\right|_{A_1} + (t_1 - t_2)\left.\frac{\partial\Theta^{(i)}}{\partial n}\right|_{A_3} - \frac{t_2}{2}\left.\frac{\partial\Theta^{(i)}}{\partial n}\right|_{A_2} \tag{6.64}$$

$$\Theta^{(i)}|_{A_3} = \left\langle\Theta^{(i)}\right\rangle + \frac{t_1}{4}\left.\frac{\partial\Theta^{(i)}}{\partial n}\right|_{A_1} + \left(\frac{t_1 - t_2}{2}\right)\left.\frac{\partial\Theta^{(i)}}{\partial n}\right|_{A_3} - \frac{t_2}{4}\left.\frac{\partial\Theta^{(i)}}{\partial n}\right|_{A_2} \tag{6.65}$$

and if we subtract (6.61) and (6.62) we get

$$[\![\Theta^{(i)}]\!] = \frac{t_1}{2}\left.\frac{\partial\Theta^{(i)}}{\partial n}\right|_{A_1} + \frac{t_2}{2}\left.\frac{\partial\Theta^{(i)}}{\partial n}\right|_{A_2} + \left(\frac{t_1 + t_2}{2}\right)\left.\frac{\partial\Theta^{(i)}}{\partial n}\right|_{A_3} \tag{6.66}$$

Assuming the simplest possible case where $t_1 = t_2 = t/2$, (6.63) and (6.66) simplify to

$$\Theta^{(i)}|_{A_3} = \left\langle\Theta^{(i)}\right\rangle + \frac{t_1}{4}\left.\frac{\partial\Theta^{(i)}}{\partial n}\right|_{A_1} + \left(\frac{t_1 - t_2}{2}\right)\left.\frac{\partial\Theta^{(i)}}{\partial n}\right|_{A_3} - \frac{t_2}{4}\left.\frac{\partial\Theta^{(i)}}{\partial n}\right|_{A_2} \tag{6.67}$$

$$= \left\langle\Theta^{(i)}\right\rangle - \frac{t}{8}\left(\left[\!\left[\frac{\partial\Theta^{(i)}}{\partial n}\right]\!\right]\right) \tag{6.68}$$

$$\Longrightarrow \qquad \Theta^{(i)}|_{A_3} = \langle\Theta\rangle + \frac{t}{8}\left(\left[\!\left[\frac{q_n^{(i)}}{k^{(i)}}\right]\!\right]\right) \tag{6.69}$$

and

$$[\![\Theta^{(i)}]\!] = \frac{t}{2}\left\langle\frac{\partial\Theta^{(i)}}{\partial n}\right\rangle + \left(\frac{t}{2}\right)\left.\frac{\partial\Theta^{(i)}}{\partial n}\right|_{A_3} \tag{6.70}$$

$$\Longrightarrow \qquad [\![\Theta^{(i)}]\!] = -\frac{t}{2}\left\langle\frac{q_n^{(i)}}{k^{(i)}}\right\rangle - \left.\frac{t}{2}\frac{q_n^{(i)}}{k^{(i)}}\right|_{A_3} \tag{6.71}$$

where $q_n^{(i)}|_{A_3}$ is given by (6.58) derived above. Therefore, (6.69) provides temperature values at point $A_3$ inside the interphase, and (6.71) is the jump of the temperature field across an imperfect interface. These equations are similar to (4.38) and (4.35) obtained for the thermally conductive interface.

**Jump of Displacement vector**

Following the same procedure as above, we integrate (6.22) between points $A_1$ and $A_3$, and from $A_3$ to $A_2$. This gives the following set of equations

$$\boldsymbol{u}^{(i)}|_{A_3} - \boldsymbol{u}^{(i)}|_{A_1} = \frac{t_1}{2}\left(\left.\frac{\partial \boldsymbol{u}^{(i)}}{\partial n}\right|_{A_1} + \left.\frac{\partial \boldsymbol{u}^{(i)}}{\partial n}\right|_{A_3}\right) \tag{6.72}$$

$$= \frac{t_1}{2}\left\{\left(2\,\mathbb{C}^{-1}\boldsymbol{\sigma}_n^{(i)} - \mathcal{P}^{(i)}\right)\Big|_{A_1} + \left(2\,\mathbb{C}^{-1}\boldsymbol{\sigma}_n^{(i)} - \mathcal{P}^{(i)}\right)\Big|_{A_3}\right\} \tag{6.73}$$

and between points $A_3$ and $A_2$ as

$$\boldsymbol{u}^{(i)}|_{A_3} - \boldsymbol{u}^{(i)}|_{A_2} = -\frac{t_2}{2}\left(\left.\frac{\partial \boldsymbol{u}^{(i)}}{\partial n}\right|_{A_2} + \left.\frac{\partial \boldsymbol{u}^{(i)}}{\partial n}\right|_{A_3}\right) \tag{6.74}$$

$$= \frac{-t_2}{2}\left\{\left(2\,\mathbb{C}^{-1}\boldsymbol{\sigma}_n^{(i)} - \mathcal{P}^{(i)}\right)\Big|_{A_1} + \left(2\,\mathbb{C}^{-1}\boldsymbol{\sigma}_n^{(i)} - \mathcal{P}^{(i)}\right)\Big|_{A_3}\right\} \tag{6.75}$$

Adding (6.72) and (6.74) provides the values of displacement vector $\boldsymbol{u}^{(i)}$ at point $A_3$ inside the interphase.

$$\boldsymbol{u}^{(i)}|_{A_3} = \left\langle \boldsymbol{u}^{(i)} \right\rangle + \frac{t_1}{4}\left.\frac{\partial \boldsymbol{u}^{(i)}}{\partial n}\right|_{A_1} + \left(\frac{t_1 - t_2}{2}\right)\left.\frac{\partial \boldsymbol{u}^{(i)}}{\partial n}\right|_{A_3} - \frac{t_2}{4}\left.\frac{\partial \boldsymbol{u}^{(i)}}{\partial n}\right|_{A_2} \tag{6.76}$$

and

$$[\![\boldsymbol{u}^{(i)}]\!] = \frac{t_1}{2}\left.\frac{\partial \boldsymbol{u}^{(i)}}{\partial n}\right|_{A_1} + \frac{t_2}{2}\left.\frac{\partial \boldsymbol{u}^{(i)}}{\partial n}\right|_{A_2} + \left(\frac{t_1 + t_2}{2}\right)\left.\frac{\partial \boldsymbol{u}^{(i)}}{\partial n}\right|_{A_3} \tag{6.77}$$

Assuming $t_1 = t_2 = t/2$, the equations can be written in their final form as

$$\boldsymbol{u}^{(i)}|_{A_3} = \left\langle \boldsymbol{u}^{(i)} \right\rangle - \frac{t}{8}\left[\!\!\left[\frac{\partial \boldsymbol{u}^{(i)}}{\partial n}\right]\!\!\right] = \left\langle \boldsymbol{u}^{(i)} \right\rangle - \frac{t}{8}\left[\!\!\left[\left(2\,\mathbb{C}^{-1}\boldsymbol{\sigma}_n^{(i)} - \mathcal{P}^{(i)}\right)\right]\!\!\right] \tag{6.78}$$

and

$$[\![\boldsymbol{u}^{(i)}]\!] = \frac{t}{2}\left\langle \frac{\partial \boldsymbol{u}^{(i)}}{\partial n} \right\rangle + \frac{t_2}{2}\left.\frac{\partial \boldsymbol{u}^{(i)}}{\partial n}\right|_{A_3} \tag{6.79}$$

$$= \frac{t}{2}\left\langle \left(2\,\mathbb{C}^{-1}\boldsymbol{\sigma}_n^{(i)} - \mathcal{P}^{(i)}\right) \right\rangle + \frac{t_2}{2}\left.\left(2\,\mathbb{C}^{-1}\boldsymbol{\sigma}_n^{(i)} - \mathcal{P}^{(i)}\right)\right|_{A_3} \tag{6.80}$$

$\mathcal{P}^{(i)}$ is the surface gradient of the displacement vector defined in (5.29). Along the normal direction, it can be assumed that this gradient along the tangential direction does not vary much, and thus,

$$\mathcal{P}^{(i)}|_{A_3} = \left\langle \mathcal{P}_m^{(i)} \right\rangle \tag{6.81}$$

Therefore,

$$[\![\boldsymbol{u}^{(i)}]\!] = \frac{t}{2}\left\langle \left(2\,\mathbb{C}^{-1}\boldsymbol{\sigma}_n^{(i)} - 2\,\mathcal{P}^{(i)}\right) \right\rangle + \frac{t}{2}\left(2\,\mathbb{C}^{-1}\boldsymbol{\sigma}_n^{(i)}|_{A_3}\right) \tag{6.82}$$

For the normal component of the displacement vector

$$[\![u_1]\!] = \frac{t}{2}\left\{\left\langle \frac{\sigma_{11}^{(i)}}{\lambda^{(i)}+2\mu^{(i)}} + \frac{m^{(i)}\,\Theta^{(i)}}{\lambda^{(i)}+2\,\mu^{(i)}}\right\rangle + \left(\frac{\sigma_{11}^{(i)}}{\lambda^{(i)}+2\mu^{(i)}} + \frac{m^{(i)}\,\Theta^{(i)}}{\lambda^{(i)}+2\,\mu^{(i)}}\right)\Bigg|_{A_3}\right\} - \left\langle 2\,\frac{\lambda^{(i)}}{\lambda^{(i)}+2\,\mu^{(i)}}\left(\varepsilon_{22}^{(i)}+\varepsilon_{33}^{(i)}\right)\right\rangle \tag{6.83}$$

and for the tangential $u_k$ component of $\boldsymbol{u}^{(i)}$, where $k=\{2,3\}$

$$[\![u_k]\!] = \frac{t}{2}\left\{\left\langle \frac{\sigma_{1k}^{(i)}}{\mu^{(i)}}\right\rangle + \frac{\sigma_{1k}^{(i)}}{\mu^{(i)}}\Bigg|_{A_3} - 2\left\langle \frac{1}{h_k}\left(\frac{\partial u_1^{(i)}}{\partial \alpha_k} - u_k\frac{\partial h_k}{\partial \alpha_1}\right)\right\rangle\right\} \tag{6.84}$$

**Jump of Thermoelastic Stress**

Similarly, following the same procedure and under the assumption that $t_1 = t_2 = t/2$, we get the following equations for stress vector at point $A_3$ and for the jump in the normal stress vector by integrating (6.34) between points $A_1$ and $A_3$ and between $A_3$ and $A_2$.

$$\boldsymbol{\sigma}_n^{(i)}|_{A_3} = \left\langle \boldsymbol{\sigma}_n^{(i)}\right\rangle - \frac{t}{8}\left\{[\![\rho\,\ddot{\boldsymbol{u}}^{(i)}]\!] - [\![\mathcal{D}_s\boldsymbol{\sigma}_n^{(i)}]\!] - [\![g\,\boldsymbol{\sigma}_n^{(i)}]\!] - [\![\boldsymbol{A}^{(i)}]\!]\right\} \tag{6.85}$$

$$[\![\boldsymbol{\sigma}_n^{(i)}]\!] = \frac{t}{2}\left\{\left\langle \rho\,\ddot{\boldsymbol{u}}^{(i)}\right\rangle - 2\left\langle \mathcal{D}_s\boldsymbol{\sigma}_n^{(i)}\right\rangle - \left\langle g\,\boldsymbol{\sigma}_n^{(i)}\right\rangle - \left\langle \boldsymbol{A}^{(i)}\right\rangle\right\} + \frac{t}{2}\left\{\rho\,\ddot{\boldsymbol{u}}^{(i)} - g\,\boldsymbol{\sigma}_n^{(i)} - \boldsymbol{A}^{(i)}\right\}\Bigg|_{A_3} \tag{6.86}$$

The jump in normal component $\sigma_{11}$ of $\boldsymbol{\sigma}^{(i)}$ is given as

$$[\![\sigma_{11}^{(i)}]\!] = \frac{t}{2}\left\langle \rho\ddot{\boldsymbol{u}}^{(i)} - \mathcal{B}^{(i)} - 2\,\mathcal{D}_s\boldsymbol{\sigma}^{(i)} - \frac{1-2\,\nu^{(i)}}{1-\nu^{(i)}}g\,\sigma_{11}^{(i)} + g\,m\,\Theta^{(i)}\right\rangle + \frac{t}{2}\left\{\rho\ddot{\boldsymbol{u}}^{(i)} - \mathcal{B}_{11}^{(i)} - \frac{1-2\,\nu^{(i)}}{1-\nu^{(i)}}g\,\sigma_{11}^{(i)} + g\,m\,\Theta^{(i)}\right\}\Bigg|_{A_3} \tag{6.87}$$

while at point $A_3$:

$$\sigma_{11}^{(i)}|_{A_3} = \left\langle \sigma_{11}^{(i)}\right\rangle - \frac{t}{8}\left[\!\!\left[\rho\ddot{\boldsymbol{u}}^{(i)} - \mathcal{B}^{(i)} - \mathcal{D}_s\boldsymbol{\sigma}^{(i)} - \frac{1-2\,\nu^{(i)}}{1-\nu^{(i)}}g\,\sigma_{11}^{(i)} + g\,m\,\Theta^{(i)}\right]\!\!\right] \tag{6.88}$$

The tangential component of the stress vector $\sigma_{1k}$ (where $k=\{2,3\}$) can be obtained at point $A_3$ from the following equation

$$\sigma_{1k}^{(i)}|_{A_3} = \left\langle \sigma_{1k}^{(i)}\right\rangle - \frac{t}{8}\left\{\left[\!\!\left[\rho\ddot{\boldsymbol{u}}^{(i)} - A_{1k} - \mathcal{D}_s\boldsymbol{\sigma}^{(i)} - g\,\sigma_{1k}^{(i)}\right]\!\!\right]\right\} \tag{6.89}$$

while the jump in the tangential component across an imperfect interface is given by:

$$[\![\sigma_{1k}^{(i)}]\!] = \frac{t}{2}\left\{\left\langle \rho\ddot{\boldsymbol{u}}^{(i)} - A_{1k} - 2\,\mathcal{D}_s\boldsymbol{\sigma}^{(i)} - g\,\sigma_{1k}^{(i)}\right\rangle\right\} + \frac{t}{2}\left\{\left\langle \rho\ddot{\boldsymbol{u}}^{(i)} - A_{1k} + g\,\sigma_{1k}\right\rangle^{(i)}\right\}\Bigg|_{A_3} \tag{6.90}$$

## 6.6 Second Integration Scheme

For this scheme, we make use of the first set of eqns, (6.30) and (6.35), instead of (6.29) and (6.34), by integrating them between two or three points within the interphase, as in the previous case. The solution for the integrated solution is obtained by employing the Trapezoidal rule between these points (intervals), and thus arriving at the different form of transmission conditions. The transmission conditions for temperature and displacement vector pertaining to two- and three-points of integration schemes remain the same as derived for the First Integration Scheme.

### 6.6.1 Two points Integration scheme

Similar to 5.5.1, the flux equations (6.30) and (6.35) are integrated between two points $A_1$ and $A_2$.

#### Jump of Heat flux

$$[\![h_2\, h_3\, q_n]\!] = t\Big\langle h_2\, h_3 \left( Q(\xi, \alpha_2, \alpha_3, T) - \mathcal{D}_s \boldsymbol{q}^{(i)} + \rho\, c_E\, \dot{T}^{(i)} + m\, \Theta^{(i)}\, \mathrm{tr}\, \dot{\boldsymbol{\varepsilon}}^{(i)} \right) \Big\rangle \tag{6.91}$$

Making use of identities defined in (2.117) eqn(6.91) can be re-written as

$$\begin{aligned} \langle h_2\, h_3 \rangle \Big[\!\Big[ q_n^{(i)} \Big]\!\Big] + [\![h_2\, h_3]\!] \Big\langle q_n^{(i)} \Big\rangle &= t \left\{ \langle h_2\, h_3 \rangle \left\langle Q - \mathcal{D}_s \boldsymbol{q} - g\, q_n^{(i)} - m\, \Theta^{(i)}\, \mathrm{tr}\, \dot{\boldsymbol{\varepsilon}}^{(i)} + \rho\, c_E\, \frac{\partial \Theta^{(i)}}{\partial t} \right\rangle \right\} \\ &+ \frac{t}{4} \left\{ [\![h_2\, h_3]\!] \left[\!\!\left[ Q - \mathcal{D}_s \boldsymbol{q} - g\, q_n^{(i)} - m\, \Theta^{(i)}\, \mathrm{tr}\, \dot{\boldsymbol{\varepsilon}}^{(i)} + \rho\, c_E\, \frac{\partial \Theta^{(i)}}{\partial t} \right]\!\!\right] \right\} \end{aligned} \tag{6.92}$$

which can be rearranged to give

$$\begin{aligned} \Big[\!\Big[ q_n^{(i)} \Big]\!\Big] + \beta \Big\langle q_n^{(i)} \Big\rangle &= t \left\{ \left\langle Q - \mathcal{D}_s \boldsymbol{q} - g\, q_n^{(i)} - m\, \Theta^{(i)}\, \mathrm{tr}\, \dot{\boldsymbol{\varepsilon}}^{(i)} + \rho\, c_E\, \frac{\partial \Theta^{(i)}}{\partial t} \right\rangle \right\} \\ &+ \frac{t}{4} \beta \left\{ \left[\!\!\left[ Q - \mathcal{D}_s \boldsymbol{q} - g\, q_n^{(i)} - m\, \Theta^{(i)}\, \mathrm{tr}\, \dot{\boldsymbol{\varepsilon}}^{(i)} + \rho\, c_E\, \frac{\partial \Theta^{(i)}}{\partial t} \right]\!\!\right] \right\} \end{aligned} \tag{6.93}$$

where $\beta$ is the parameter given in (2.118).

#### Jump of Thermoelastic Stress

Similarly, the jump in stress for the two-point scheme is obtained by integrating (6.35) between the two points $A_1$ and $A_2$.

$$[\![h_2\, h_3\, \boldsymbol{\sigma}_n^{(i)}]\!] = t\Big\langle h_2\, h_3 \left( \rho\, \ddot{\boldsymbol{u}}^{(i)} - \boldsymbol{A} - \mathcal{D}_s \boldsymbol{\sigma}_n^{(i)} \right) \Big\rangle \tag{6.94}$$

which after implementing the identities in (2.117) and re-arranging gives:

$$\Big[\!\Big[ \boldsymbol{\sigma}_n^{(i)} \Big]\!\Big] + \beta \Big\langle \boldsymbol{\sigma}_n^{(i)} \Big\rangle = t \left\{ \Big\langle \rho\, \ddot{\boldsymbol{u}}^{(i)} - \boldsymbol{A} - \mathcal{D}_s \boldsymbol{\sigma}_n^{(i)} \Big\rangle + \frac{\beta}{4} \Big[\!\Big[ \rho \ddot{\boldsymbol{u}}^{(i)} - \boldsymbol{A} - \mathcal{D}_s \boldsymbol{\sigma}_n^{(i)} \Big]\!\Big] \right\} \tag{6.95}$$

from (6.95), we can get the expression for the jumps in the normal component $\sigma_{11}$ of the stress vector $\boldsymbol{\sigma}^{(i)}$ as:

$$[\![\sigma_{11}]\!] = t\left\{\left\langle \rho\ddot{\boldsymbol{u}}^{(i)} - \mathcal{B}^{(i)} - \mathcal{D}_s\boldsymbol{\sigma}^{(i)} - \frac{\nu^{(i)}}{1-\nu^{(i)}} g\,\sigma_{11}^{(i)} + g\,m\,\Theta^{(i)} \right\rangle\right\} + \frac{\beta}{4}\left\{\left[\!\!\left[\rho\ddot{\boldsymbol{u}}^{(i)} - \mathcal{B}^{(i)} - \mathcal{D}_s\boldsymbol{\sigma}^{(i)} - \frac{\nu^{(i)}}{1-\nu^{(i)}} g\,\sigma_{11}^{(i)} + g\,m\,\Theta^{(i)}\right]\!\!\right]\right\} \tag{6.96}$$

and tangential $\sigma_{1k}$ component of $\boldsymbol{\sigma}^{(i)}$, where $k = \{2, 3\}$

$$[\![\sigma_{1k}^{(i)}]\!] = t\left\langle \rho\,\ddot{\boldsymbol{u}}^{(i)} - A_{1k} - \mathcal{D}_s\boldsymbol{\sigma}_n^{(i)}\right\rangle + \frac{\beta}{4}\left\{\left[\!\!\left[\rho\,\ddot{\boldsymbol{u}}^{(i)} - A_{1k} - \mathcal{D}_s\boldsymbol{\sigma}_n^{(i)}\right]\!\!\right]\right\} \tag{6.97}$$

### 6.6.2 Three points Integration scheme

Similar to three-points method given in First Integration Scheme in 6.5.2, Eqns.(6.30) and (6.35) are inetgrated between three points - from $A_1$ to $A_3$ and then from $A_3$ to $A_2$.

#### Jump of Heat flux

Integrating (6.30) between the points $A_1$ and $A_3$ provides us with the following:

$$\begin{aligned}\left(h_2\,h_3\,q_n^{(i)}\right)\Big|_{A_3} - \left(h_2\,h_3\,q_n^{(i)}\right)\Big|_{A_1} = \\ \frac{t_1}{2}\left\{h_2\,h_3|_{A_3}\left(Q(\xi,\alpha_2,\alpha_3,T) - \mathcal{D}_s\boldsymbol{q}^{(i)} + \rho\,c_E\,\dot{T}^{(i)} + m\,\Theta^{(i)}\,\mathrm{tr}\,\dot{\boldsymbol{\varepsilon}}^{(i)}\right)|_{A_3}\right\} \\ + \frac{t_1}{2}\left\{h_2\,h_3|_{A_1}\left(Q(\xi,\alpha_2,\alpha_3,T) - \mathcal{D}_s\boldsymbol{q}^{(i)} + \rho\,c_E\,\dot{T}^{(i)} + m\,\Theta^{(i)}\,\mathrm{tr}\,\dot{\boldsymbol{\varepsilon}}^{(i)}\right)|_{A_1}\right\}\end{aligned} \tag{6.98}$$

and integrating from $A_2$ to $A_3$ gives

$$\begin{aligned}\left(h_2\,h_3\,q_n^{(i)}\right)\Big|_{A_3} - \left(h_2\,h_3\,q_n^{(i)}\right)\Big|_{A_2} = \\ -\frac{t_2}{2}\left\{h_2\,h_3|_{A_3}\left(Q(\xi,\alpha_2,\alpha_3,T) - \mathcal{D}_s\boldsymbol{q}^{(i)} + \rho\,c_E\,\dot{T}^{(i)} + m\,\Theta^{(i)}\,\mathrm{tr}\,\dot{\boldsymbol{\varepsilon}}^{(i)}\right)|_{A_3}\right\} \\ -\frac{t_2}{2}\left\{h_2\,h_3|_{A_1}\left(Q(\xi,\alpha_2,\alpha_3,T) - \mathcal{D}_s\boldsymbol{q}^{(i)} + \rho\,c_E\,\dot{T}^{(i)} + m\,\Theta^{(i)}\,\mathrm{tr}\,\dot{\boldsymbol{\varepsilon}}^{(i)}\right)|_{A_2}\right\}\end{aligned} \tag{6.99}$$

Adding (6.98) and (6.99)

$$\begin{aligned}\left(h_2\,h_3\,q_n^{(i)}\right)|_{A_3} - \left\langle h_2\,h_3\,q_n^{(i)}\right\rangle = \\ \frac{t_1}{4}\left\{h_2\,h_3|_{A_1}\left(Q(\xi,\alpha_2,\alpha_3,T) - \mathcal{D}_s\boldsymbol{q}^{(i)} + \rho\,c_E\,\dot{T}^{(i)} + m\,\Theta^{(i)}\,\mathrm{tr}\,\dot{\boldsymbol{\varepsilon}}^{(i)}\right)|_{A_1}\right\} \\ -\frac{t_2}{4}\left\{h_2\,h_3|_{A_2}\left(Q(\xi,\alpha_2,\alpha_3,T) - \mathcal{D}_s\boldsymbol{q}^{(i)} + \rho\,c_E\,\dot{T}^{(i)} + m\,\Theta^{(i)}\,\mathrm{tr}\,\dot{\boldsymbol{\varepsilon}}^{(i)}\right)|_{A_2}\right\} \\ +\frac{t_1-t_2}{4}\left\{h_2\,h_3|_{A_1}\left(Q(\xi,\alpha_2,\alpha_3,T) - \mathcal{D}_s\boldsymbol{q}^{(i)} + \rho\,c_E\,\dot{T}^{(i)} + m\,\Theta^{(i)}\,\mathrm{tr}\,\dot{\boldsymbol{\varepsilon}}^{(i)}\right)|_{A_3}\right\}\end{aligned} \tag{6.100}$$

while subtracting the two gives us

$$\begin{aligned}\llbracket h_2\, h_3\, q_n^{(i)} \rrbracket = \frac{t_1}{2} h_2\, h_3|_{A_1} \left( Q(\xi, \alpha_2, \alpha_3, T) - \mathcal{D}_s \boldsymbol{q}^{(i)} + \rho\, c_E\, \dot{T}^{(i)} + m\, \Theta^{(i)}\, \mathrm{tr}\, \dot{\boldsymbol{\varepsilon}}^{(i)} \right) |_{A_1} \\ + \frac{t_2}{2} h_2\, h_3|_{A_2} \left( Q(\xi, \alpha_2, \alpha_3, T) - \mathcal{D}_s \boldsymbol{q}^{(i)} + \rho\, c_E\, \dot{T}^{(i)} + m\, \Theta^{(i)}\, \mathrm{tr}\, \dot{\boldsymbol{\varepsilon}}^{(i)} \right) |_{A_2} \\ + \left( \frac{t_1 + t_2}{2} \right) h_2\, h_3|_{A_3} \left( Q(\xi, \alpha_2, \alpha_3, T) - \mathcal{D}_s \boldsymbol{q}^{(i)} + \rho\, c_E\, \dot{T}^{(i)} + m\, \Theta^{(i)}\, \mathrm{tr}\, \dot{\boldsymbol{\varepsilon}}^{(i)} \right) |_{A_3}\end{aligned} \tag{6.101}$$

Assuming $t_1 = t_2 = t/2$, Eqns.(6.100) and (6.101) can be rewritten as

$$\left( h_2\, h_3\, q_n^{(i)} \right) |_{A_3} = \left\langle h_2\, h_3\, q_n^{(i)} \right\rangle - \frac{t}{8} \left\llbracket h_2\, h_3 \left( Q(\xi, \alpha_2, \alpha_3, T) - \mathcal{D}_s \boldsymbol{q}^{(i)} + \rho\, c_E\, \dot{T}^{(i)} + m\, \Theta^{(i)}\, \mathrm{tr}\, \dot{\boldsymbol{\varepsilon}}^{(i)} \right) \right\rrbracket \tag{6.102}$$

and

$$\begin{aligned}\llbracket h_2\, h_3\, q_n^{(i)} \rrbracket = \frac{t}{2} \left\langle h_2\, h_3|_{A_1} \left( Q(\xi, \alpha_2, \alpha_3, T) - \mathcal{D}_s \boldsymbol{q}^{(i)} + \rho\, c_E\, \dot{T}^{(i)} + m\, \Theta^{(i)}\, \mathrm{tr}\, \dot{\boldsymbol{\varepsilon}}^{(i)} \right) \right\rangle \\ + \frac{t}{2} h_2\, h_3|_{A_3} \left( Q(\xi, \alpha_2, \alpha_3, T) - \mathcal{D}_s \boldsymbol{q}^{(i)} + \rho\, c_E\, \dot{T}^{(i)} + m\, \Theta^{(i)}\, \mathrm{tr}\, \dot{\boldsymbol{\varepsilon}}^{(i)} \right) |_{A_3}\end{aligned} \tag{6.103}$$

Again, implementing the identities (2.117), we get

$$q_n^{(i)}|_{A_3} = \frac{1}{\gamma} \left\{ \left\langle q_n^{(i)} \right\rangle + \beta \left\llbracket q_n^{(i)} \right\rrbracket - \frac{t}{8} \left( \llbracket \mathcal{M} \rrbracket + \beta \langle \mathcal{M} \rangle \right) \right\} \tag{6.104}$$

where

$$\mathcal{M} = Q(\xi, \alpha_2, \alpha_3, T) - \mathcal{D}_s \boldsymbol{q}^{(i)} + \rho\, c_E\, \dot{T}^{(i)} + m\, \Theta^{(i)}\, \mathrm{tr}\, \dot{\boldsymbol{\varepsilon}}^{(i)} \tag{6.105}$$

This is the equation for the normal component of heat flux $q_n^{(i)}|_{A_3}$ at point $A_3$ inside the interphase. Next, employing the same identities and rearranging the terms, we get

$$\left\llbracket q_n^{(i)} \right\rrbracket = \frac{t}{2} \left\{ \langle \mathcal{M} \rangle + \frac{\beta}{4} \llbracket \mathcal{M} \rrbracket + \gamma \mathcal{M}|_{A_3} \right\} - \beta \left\langle q_n^{(i)} \right\rangle \tag{6.106}$$

where

$$\mathcal{M}|_{A_3} = \left( Q(\xi, \alpha_2, \alpha_3, T) + \rho\, c_E\, \dot{T}^{(i)} + m\, \Theta^{(i)}\, \mathrm{tr}\, \dot{\boldsymbol{\varepsilon}}^{(i)} \right) \Big|_{A_3} - \left\langle \mathcal{D}_s \boldsymbol{q}^{(i)} \right\rangle \tag{6.107}$$

Eqn.(6.106) is the jump of the normal component of the heat flux across an imperfect interface reflecting the effect of mechanical coupling via the coupling term $m\, \Theta^{(i)}\, \mathrm{tr}\, \dot{\boldsymbol{\varepsilon}}^{(i)}$.

### Jump of Thermoelastic Stress

Similarly, the procedure can be repeated to obtain the expression for the jumps in stress vector across an imperfect interface and the value of the stress vector at point $A_3$ inside the interphase, by inetgrating (6.35) between the three points - $A_1$ to $A_3$ and $A_3$ to $A_2$. This will result in

$$\boldsymbol{\sigma}_n^{(i)}|_{A_3} = \frac{1}{\gamma} \left\{ \left\langle \boldsymbol{\sigma}_n^{(i)} \right\rangle + \beta \left\llbracket \boldsymbol{\sigma}_n^{(i)} \right\rrbracket - \frac{t}{8} \left( \llbracket \mathcal{R} \rrbracket + \beta \langle \mathcal{R} \rangle \right) \right\} \tag{6.108}$$

and

$$\left[\!\left[\boldsymbol{\sigma}_n^{(i)}\right]\!\right] = \frac{t}{2}\left\{\langle\mathcal{R}\rangle + \frac{\beta}{4}\left[\!\left[\mathcal{R}\right]\!\right] + \gamma\,\mathcal{R}|_{A_3}\right\} - \beta\left\langle\boldsymbol{\sigma}_n^{(i)}\right\rangle \tag{6.109}$$

where

$$\mathcal{R} = \rho\ddot{\boldsymbol{u}}^{(i)} - \boldsymbol{A} - \mathcal{D}_s\boldsymbol{\sigma}_n^{(i)} \quad ; \quad \mathcal{R}|_{A_3} = \left(\rho\ddot{\boldsymbol{u}}^{(i)} - \boldsymbol{A}\right)\Big|_{A_3} - \left\langle\mathcal{D}_s\boldsymbol{\sigma}_n^{(i)}\right\rangle \tag{6.110}$$

Thus, the normal component $\sigma_{11}$ of the stress vector can be expressed as

$$\begin{aligned}\left[\!\left[\sigma_{11}^{(i)}\right]\!\right] = \frac{t}{2}&\left\{\left\langle\rho\ddot{\boldsymbol{u}}^{(i)} - \mathcal{B} - \mathcal{D}_s\boldsymbol{\sigma}^{(i)} - \frac{\nu^{(i)}}{1-\nu^{(i)}}g\,\sigma_{11}^{(i)} - g\,m\Theta^{(i)}\right\rangle\right\} \\ &+ \frac{\beta\,t}{8}\left[\!\left[\rho\ddot{\boldsymbol{u}}^{(i)} - \mathcal{B} - \mathcal{D}_s\boldsymbol{\sigma}^{(i)} - \frac{\nu^{(i)}}{1-\nu^{(i)}}g\,\sigma_{11}^{(i)} - g\,m\Theta^{(i)}\right]\!\right] \\ &+ \frac{\gamma\,t}{2}\left(\rho\ddot{\boldsymbol{u}}^{(i)} - \mathcal{B} - \langle\mathcal{D}_s\boldsymbol{\sigma}^{(i)}\rangle - \frac{\nu^{(i)}}{1-\nu^{(i)}}g\,\sigma_{11}^{(i)} - g\,m\Theta^{(i)}\right)\Big|_{A_3} - \beta\left\langle\boldsymbol{\sigma}_{11}^{(i)}\right\rangle\end{aligned} \tag{6.111}$$

$$\begin{aligned}\sigma_{11}^{(i)}\Big|_{A_3} = \frac{1}{\gamma}&\left\{\left\langle\sigma_{11}^{(i)}\right\rangle + \beta\left[\!\left[\sigma_{11}^{(i)}\right]\!\right] - \frac{t}{8}\left[\!\left[\rho\ddot{\boldsymbol{u}}^{(i)} - \mathcal{B} - \mathcal{D}_s\boldsymbol{\sigma}^{(i)} - \frac{\nu^{(i)}}{1-\nu^{(i)}}g\,\sigma_{11}^{(i)} - g\,m\Theta^{(i)}\right]\!\right]\right\} \\ &+ \frac{\beta\,t}{8\,\gamma}\left\{\rho\ddot{\boldsymbol{u}}^{(i)} - \mathcal{B} - \langle\mathcal{D}_s\boldsymbol{\sigma}^{(i)}\rangle - \frac{\nu^{(i)}}{1-\nu^{(i)}}g\,\sigma_{11}^{(i)} - g\,m\Theta^{(i)}\right\}\end{aligned} \tag{6.112}$$

while the tangential components can be obtained simply by substituting the appropriate values of $\mathcal{R}$ in (6.108) and (6.109).

## 6.7 Numerical Verification

Similar to the previous cases of thermal and elastic interphase, the perturbative effect of a coated circular inclusion of embedded in a matrix is considered. Remote thermal and mechanical loadings are applied. The thickness of the coating is represented by the non-dimensional parameters $\epsilon = t/a \ll 1$, where $a$ is the radius of the inclusion. The geometry is considered to be deforming under plane strain setting.

A simple example of uncoupled, quasi-static case is presented here. Therefore, the thermal subproblem is uncoupled from the mechanical problem, while mechanical deformation takes places due to applied forces and the constrained thermal stress.

The problem is setup in COMSOL Multiphysics, by modeling a square of length $L = 30\,m$, and a circular inclusion of radius $a = 1\,m$. The coating thickness for the perfect interphase problem is taken to be $\epsilon = 0.01$. The geometry is constrained from the right $\boldsymbol{u}_n = 0$ (roller boundary). It can slide along the y-axis, but is constrained to move in the x-direction. The bottom-left point is fully fixed constrained ($\boldsymbol{u} = 0$) while the top left point is partially constrained to move along the tangential direction. This suppresses the rigid body motion and rotation of the geometry. The top, right and the bottom surfaces are subjected to shear surface traction of $\sigma_{xy}^* = 2 * G^{(2)} * \beta_{el}$, where $\beta_{el} = 1$ is the constant shear strain at the remote boundary. This provides three Degrees of Freedom (DoFs) at each node needed to solve the mechanical problem.

For the thermal case, the right side of the domain is kept at $T^*|_{r\to\infty} = T(r,\theta) = -T_0 = -1$, while the left hand side is subjected to uniform heat flux given by $q^*|_{r\to\infty} = -k^{(2)}\,\beta_{th}$, where $\Gamma_{th} = -1(K/m)$ is the constant temperature gradient at the remote boundaries. This produces a temperature gradient across the domain, providing 1 thermal DoF. Therefore, in total, 4 DoFs are defined at each node to solve the thermoelastic problem.

The geometry is meshed with triangular elements producing very fine mesh inside the interphase domain, as shown in Fig.6.1 The interphase is composed of 522502 triangular mesh elements with average element quality of 0.94.

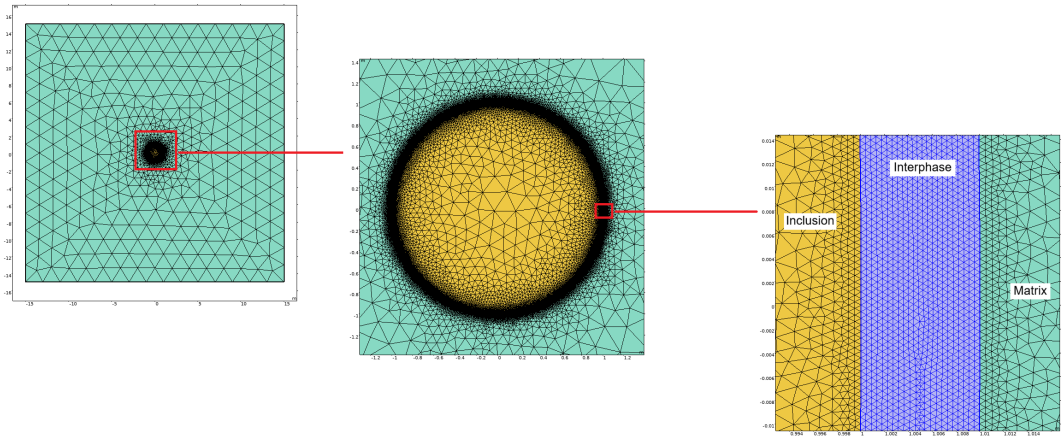


**Fig. 6.1.** Mesh distribution across a thermoelastic circular interphase of thickness $\epsilon = 0.01$.

The material properties are taken as provided in Table.6.1. The material properties are chosen such that the inclusion has higher rigidity as compared to the matrix, as well as highly conductive. It also has the highest expansion coefficient as compared to the matrix, and thus, the matrix will undergo less expansion when subjected to the thermal strain and mechanical loads. The interphase has material properties where it is more compliant or rigid to mechanical deformation and resistive or conductive to the heat conduction.

| | $k$ (W/m.K) | $E$ $(GPa)$ | $\nu$ | $G$ $(GPa)$ | $\alpha$ $(\times 10^{-6}\,m)$ |
|---|---|---|---|---|---|
| Material 1 (inclusion) | 10 | 24 | 0.20 | 10.0 | 10.0 |
| Material 2 (matrix) | 1.0 | 2.7 | 0.35 | 1.0 | 1.0 |
| Material 3 (interphase) | $0.001, 1000$ | $2.5\,G^{(i)}$ | 0.25 | $0.001, 1000$ | $\{0.1, 5, 25\}$ |

**Table 6.1.** Thermoelastic properties of the material in perfect interphase setting.

Three different cases of coefficient of thermal expansion :

- $\alpha^{(i)}/\alpha^{(2)} = 0.1$ : CTE of interphase is lower than that of the adherents, and thus it expands less than the surrounding materials.
- $\alpha^{(i)}/\alpha^{(2)} = 5.0$ : CTE of interphase is lower than that of the inclusion, but higher than the surrounding matrix.

- $\alpha^{(i)}/\alpha^{(2)} = 25.0$ : CTE of interphase is higher than that of the adherents, and thus it expands most than the surrounding materials.

## 6.8 Results and Discussion

We begin by considering the case where tensile mechanical loads are applied on top surface of the geometry. This causes the material to stretch along the y-axis.

Since the thermal effects are independent of the mechanical deformation, the thermal problem becomes equivalent to the thermally conductive problem explored in Chapter 4, and is solved using Segregated Solver in Comsol. The temperature field is first solved, which then serves as the input to the mechanical fields. Fig.6.2 represents the convergence plots for an interphase of CTE $\alpha^{(i)}/\alpha^{(2)} = 0.1$, and the solution converges to error of $10^{-10}$ for both cases of thermally resistive $k^{(i)}/k^{(2)} = 0.001$ and conductive interphase $k^{(i)}/k^{(2)} = 1000$ with soft $G^{(i)}/G^{(2)} = 0.001$ or rigid $G^{(i)}/G^{(2)} = 1000$ shear modulus, and is thus acceptable.

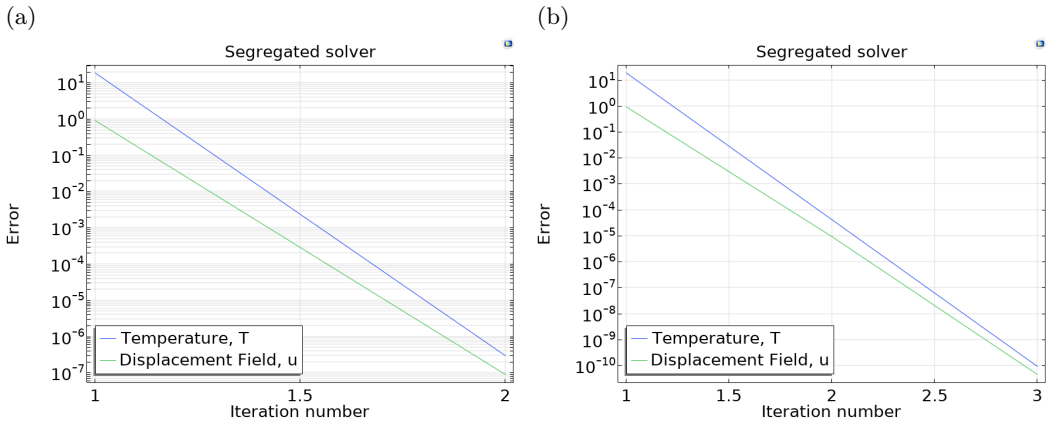


**Fig. 6.2.** Convergence plots for the temperature $T$ and displacement fields,$\boldsymbol{u}$, for both cases of: 6.2a represents thermally resistive $k^{(i)}/k^{(2)} = 0.001$, soft interphase $G^{(i)}/G^{(2)} = 0.001$. 6.2b represents convergence plots for highly conductive $k^{(i)}/k^{(2)} = 1000$ and rigid interphase $G^{(i)}/G^{(2)} = 1000$, for an interphase of thickness $\epsilon = 0.01$ and volumetric heat source of magnitude $Q_0 = 100\,W/m^3$ and shear load of $\sigma^*_{xy} = 2\,G^{(2)}\,\beta_{el}$.

The following graphs highlight the distribution of thermal and mechanical fields and corresponding fluxes across the interphase boundaries, for CTE of $\alpha^{(i)}/\alpha^{(2)} = 0.1$, for an interphase of thickness $\epsilon = 0.01$, accomodating a heat source of $Q_0 = 1.0\,W/m^3$ and computed as per (4.11), rewritten as:

$$Q(r,\theta) = Q_0 \left(\frac{r+\zeta-a-h}{h}\right)^{\alpha} \cos\theta$$

where $a \leq r \leq a+\epsilon$ is the position within the interphase, $\zeta = h/2$, $h = t/2$. Here, $\alpha$ must not be confused with CTE of the materials, that have been represented with appropriate superscript to identify as material properties; $\alpha$ represents the type of heat source which is taken to be linear in this case.

Fig.6.3 illustrates the distribution of temperature and heat flux across the three domains. Since the conductivity of the interphase is low the temperature gradients accumulate within the interphase (6.3a for low conductive $k^{(i)}/k^{(2)} = 0.001$ and soft interphase

$G^{(i)}/G^{(2)} = 0.001$, and 6.3c for high conductive $k^{(i)}/k^{(2)} = 1000$ and rigid interphase $G^{(i)}/G^{(2)} = 1000$) represented by the black contour lines. The given fig presents the distribution (and accumulation) of $\Theta$ which computed as the temperature difference between the temperature $T(r, \theta)$ at a point in the domain and the volume reference temperature $T_{ref}$, which is the temperature beyond which thermal stresses begin to develop. The thermal effects are same as those observed in the previous chapter 4. For the low conductive interphase, the temperature gradients accumulate at the interphase, as is clearly observed in Fig.6.3a, while for a high conductive interphase the temperature is continuous across the domain, as demonstrated by the continuity of the gradients across the domain boundaries.

Fig.6.3b and 6.3d demonstrate the magnitude of the heat flux $q$ in $W/m^2$ computed for low conductive and soft interphase and rigid, highly conductive interphase respectively, for a thickness of $\epsilon = 0.01$.

$$q = \sqrt{q_x^2 + q_y^2}$$

The magnitude of the heat flux highlights the thermal hot spots and the low gradient areas.

Similar to the behaviour observed in Chapter 4, it is seen that the heat flux is continuous across the boundaries for a thermally insulating interphase, As is observable from Fig.6.3b. Higher gradients are observed at $\theta = 90\,\text{deg}$ where temperature accumulates inside the interphase, as depicted in 6.3a. On the contrast, for a high conductive interphase, the heat flux accumulates at the interphase boundaries. From Fig.6.3d, the gradient accumulation is evident at $\theta = 0\,\text{deg}$ . Near the boundaries of the interphase, the heat flux accumulation is higher, due to mismatch of the conductivities at the boundaries of the interphase.

(a) $k^{(i)}/k^{(2)} = 0.001$ and $G^{(i)}/G^{(2)} = 0.001$

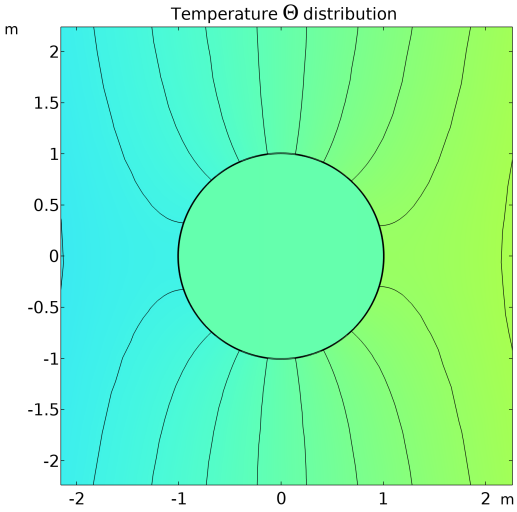


(b)

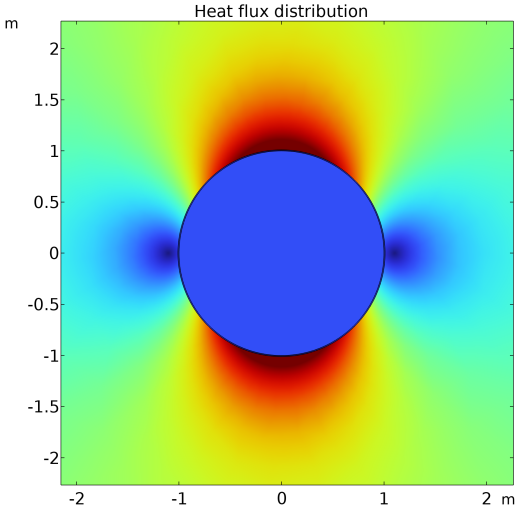


(c) $k^{(i)}/k^{(2)} = 1000$ and $G^{(i)}/G^{(2)} = 1000$

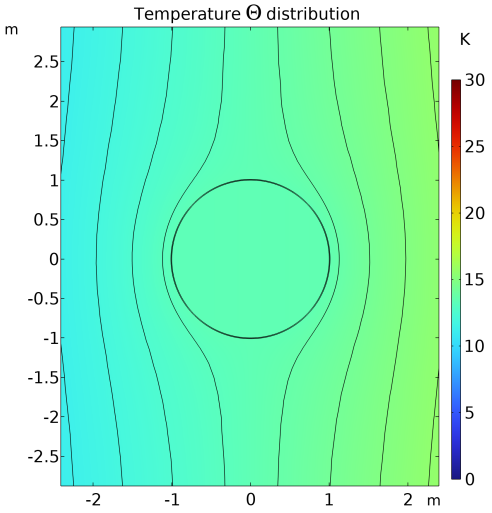


(d)

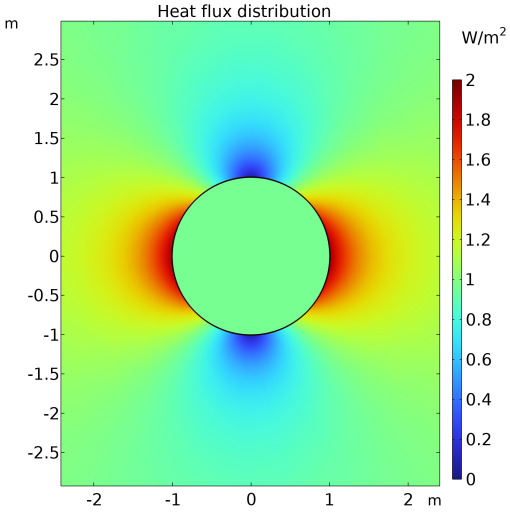


**Fig. 6.3.** Distribution of temperature $\Theta = T - T_{ref}$ (volume reference temperature) and heat flux magnitude $q$ across a thermoelastic circular interphase of thickness $\epsilon = 0.01$, with volumetric heat source $Q_0 = 100\,W/m^3$ and tensile loads of $\sigma^* = 1\,MPa/$. Figs.6.3a and 6.3b illustrate $\Theta$ and $q$ for insulating, soft interphase while Figs.6.3c and 6.3d illustrate $\Theta$ and $q$ for conductive, rigid interphase.

This resulting temperature field then serves as the input to the mechanical subproblem. The distribution of the displacement vectors is represented by the magnitude of the displacement vector, computed as:

$$U = \sqrt{u^2 + v^2}$$

where $(u, v)$ are the components of the displacement vector. From Fig.6.4 it is seen that for a soft, conductive interphase, the displacement gradient is higher, with maximum displacement across the interphase being less than 0.5 mm. This displacement is the result of deformation that occurs due to the presence of thermal strain that develops in the body due to constraints, along with the tensile forces acting at the top surface. Therefore, the mechanical deformation is slightly skewed to the right side, where the heat flux is maximum. The contour lines (in black) represent the accumulation of displacement $U$ across the boundaries of a thermoelastic interphase. However, for a rigid interphase having

high conductivity, the displacement is continuous across the interphase boundaries, as is illustrated by the continuity of the contour lines across the domain.

(a) $k^{(i)}/k^{(2)} = 0.001$ and $G^{(i)}/G^{(2)} = 0.001$

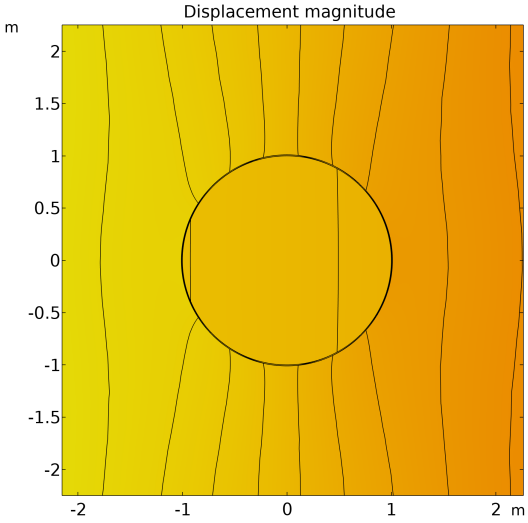


(b) $k^{(i)}/k^{(2)} = 1000$ and $G^{(i)}/G^{(2)} = 1000$

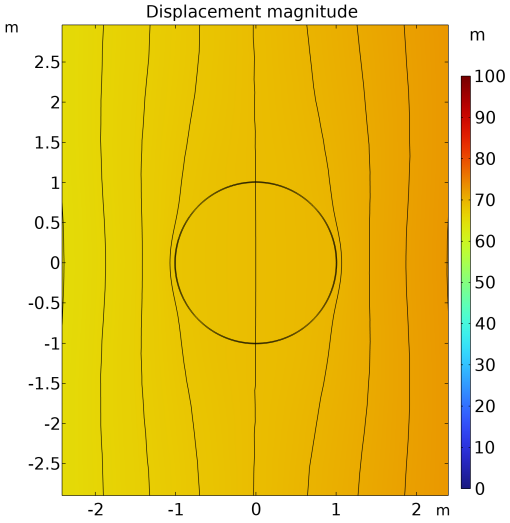


**Fig. 6.4.** Distribution of displacement magnitude $U$ across a thermoelastic circular interphase of thickness $\epsilon = 0.01$.

Shear stresses arise from the interaction between thermally induced expansion and externally applied mechanical loading. In this configuration, the temperature gradient generates predominantly horizontal thermal expansion, while the applied tensile load acts in the vertical direction. The resulting incompatibility between these orthogonal deformation modes produces shear strains along the inclusion–interphase interface. As a consequence, the maximum shear stresses occur at angular locations of approximately $\pm 45$ deg with respect to the principal loading direction, where the combined thermo-mechanical effects lead to peak shear stress concentration. From Figs.6.5c and 6.5f it is seen that the peak stress accumulation are inclined at 45 deg as expected.

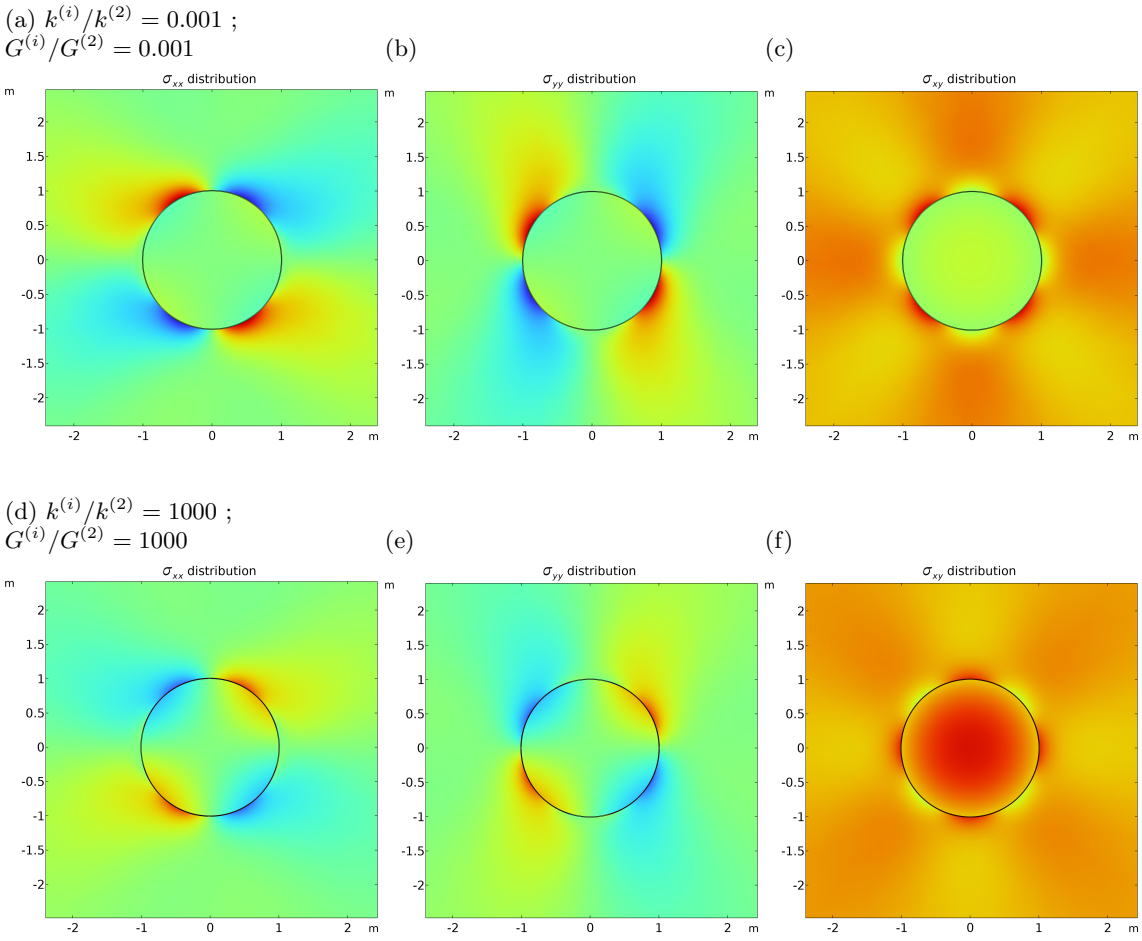


**Fig. 6.5.** Distribution of normal component of stresses $\sigma_{xx}, \sigma_{yy}$ and the shear stress $\sigma_{xy}$ in MPa across a thermoelastic circular interphase of thickness $\epsilon = 0.01$.

Perhaps, the more interesting case is the stress distributions for a highly conductive but rigid interphase, due to thermal and mechanical properties mismatch. The highly conductive interphase allows the heat to be conducted efficiently across the interphase boundaries, but the rigidity of the interphase constrains it from deforming, thus leading to accumulation of stress inside the domain. Coupled with the development of thermal strain due to applied constant heat flux at the remote boundary, the stress profile is intensified near the boundaries of the interphase. In the following graphs, we look at the stress distributions for such an interphase, but for three different values of CTE of the interphase, given as $\alpha^{(i)}/\alpha^{(2)}$. The values considered are: 0.1 least expansion than the surrounding media, 5.0: interphase is more expandable than the matrix but less than the inclusion and lastly, 25.0: interphase is most expandable than the surrounding adherents.

The distribution of stress along the x-direction is presented in Fig.6.6. As the interphase is highly resistive to the expansion as is the case in Fig.6.6a, it is seen that a small peak representing stress accumulation occurs at the boundary between the interphase and the surrounding matrix. This is becuase the matrix expands due to the mismatch of the properties at the boundary, while interphase resists it, developing tensile stress at the boundary, However, at $r = a$ which is the boundary between the interphase and the inclusion, the stress accumulation will be higher, as the inclusion has higher CTE than both

matrix and interphase, and thus, will expand more than the two materials, which becomes constrained, leading to higher stress concentrations. In the second case where $\alpha^{(i)}/\alpha^{(2)} = 5.0$ illustrated in Fig.6.6b, the interphase has a slightly higher expansion coefficient than the surrounding matrix, and thus, small peaks of stress accumulations are observed at the boundary $r = (a+\epsilon)$. However, since the interphase still expands less than the inclusion, the stress accumulation will be higher at the inner boundary $r = a$, between the inclusion and the interphase. For both these cases, the contraction of the inclusion due to compressive stress development is observed. For the last case, where the coating (interphase) has the highest expansion coefficient than the surrounding media, high concentrations of stress is observed at the boundaries. The interphase now expands more than the inclusion, and this deforms or stretches the inclusion, while at the outer boundary the matrix has least expansion than the two enclosing materials, and causes the stress to be more accumulated at the boundaries of the interphase, as it observed from the plots.

(a) $\alpha^{(i)}/\alpha^{(2)} = 0.1$ (b) $\alpha^{(i)}/\alpha^{(2)} = 5.0$ (c) $\alpha^{(i)}/\alpha^{(2)} = 25.0$

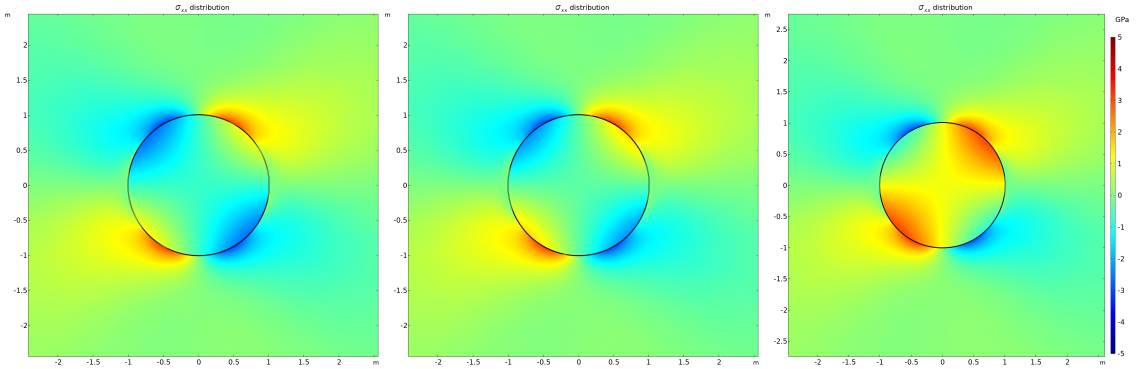

**Fig. 6.6.** Distribution of stress along x-direction $\sigma_{xx}$ in GPa across a thermoelastic circular interphase with three different coefficients of thermal expansions $(\alpha^{(i)}/\alpha^{(2)}$ of thickness $\epsilon = 0.01$, with volumetric heat source $Q_0 = 1\,W/m^3$ and remote shear stress of $\sigma^*_{xy} = 2\,GPa$ for conductive $k^{(i)}/k^{(2)} = 1000$ and rigid interphase $G^{(i)}/G^{(2)} = 1000$.

The distribution of stress along the y-direction is presented in Fig.6.7, which is along the direction of the applied shear loads at the remote boundary. For the first case where the interphase is highly resistive to the expansion demonstrated in Fig.6.7a, it is seen that stress accumulation occurs at the boundary between the interphase and the surrounding matrix. As the matrix undergoes deformation, it stretches along the y-direction, but the coating does not deform much due to high rigidity and low expansion coefficient. This causes tensile stresses to accumulate at the outer boundary of the interphase. At the inner boundary $r = a$ which is the boundary between the interphase and the inclusion, inclusion should deform more due to lower rigidity than the coating and higher expansion coefficient. This is constrained by the resistive interphase, creating pockets of the compressive stress accumulation. In the second case where $\alpha^{(i)}/\alpha^{(2)} = 5.0$ illustrated in Fig.6.6b, the interphase has a slightly higher expansion coefficient than the surrounding matrix, and thus, small peaks of stress accumulations are observed at the boundary $r = (a + \epsilon)$. However, since the interphase still expands less than the inclusion, the stress accumulation will be higher at the inner boundary $r = a$, between the inclusion and the interphase. The inclusion undergoes deformation by compressing along the applied tensile loads. For both these cases, the contraction of the inclusion is observed. For the last case, where the coating (interphase) has the highest expansion coefficient than the surrounding media,

high concentrations of stress is observed at the boundaries. The interphase now expands more than the inclusion, and this deforms or stretches the inclusion, while at the outer boundary the matrix has least expansion than the two enclosing materials, and causes the stress to be more accumulated at the boundaries of the interphase, as it observed from the distinct color of the interphase from the plot. The stress distribution with localization is also observed inside the inclusion, which contracts and expands along with the inclusion, therefore lower gradients are present towards the inner boundary $r = a$ than the outer boundary $r = (a + \epsilon)$.

(a) $\alpha^{(i)}/\alpha^{(2)} = 0.1$ (b) $\alpha^{(i)}/\alpha^{(2)} = 5.0$ (c) $\alpha^{(i)}/\alpha^{(2)} = 25.0$

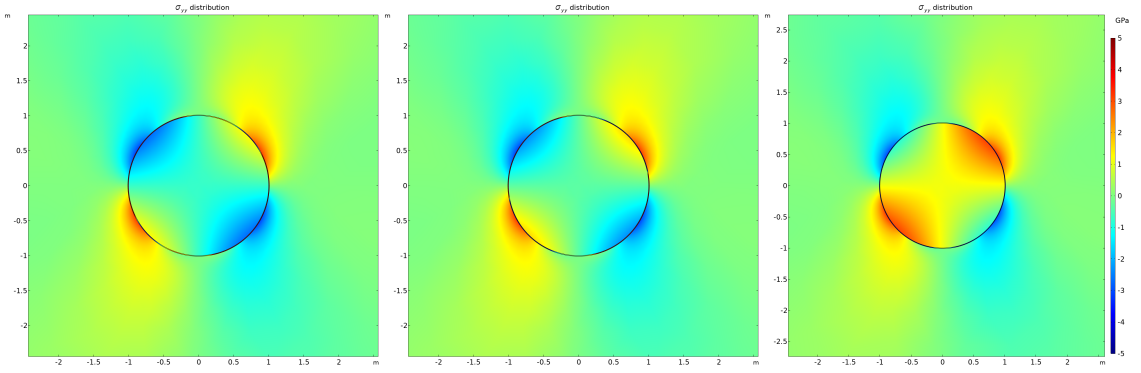


**Fig. 6.7.** Distribution of stress along y-direction $\sigma_{yy}$ in GPa across a thermoelastic circular interphase with three different coefficients of thermal expansions $(\alpha^{(i)}/\alpha^{(2)}$ of thickness $\epsilon = 0.01$, with volumetric heat source $Q_0 = 1\,W/m^3$ and remote shear stress of $\sigma^*_{xy} = 2\,GPa$ for conductive $k^{(i)}/k^{(2)} = 1000$ and rigid interphase $G^{(i)}/G^{(2)} = 1000$.

The shear stress distribution around a coated inclusion is presented in Fig.6.8. In the first case, the interphase is highly resistive to the expansion as illustrated in Fig. 6.8a. It is seen that peak stress accumulation occurs at the boundary between the interphase and the surrounding matrix at an angle of $\pm 45$ deg. The shear loading induces a "stretch" of the matrix along the y-direction, but the thermal gradient due to heat flux at the right side of the geometry creates an additional thermal stress that also brings about the deformation of the geometry. It must also be noted that the peak stress concentrations are strongest towards the right side (applied thermal loads) and along the direction of the applied loads. However, at $r = a$ which is the boundary between the interphase and the inclusion, the accumulation of the stress will be higher, as the inclusion has higher CTE than both matrix and interphase, and thus, will expand more than the two materials, which becomes constrained, leading to higher stress concentrations inside the interphase. In the second case where $\alpha^{(i)}/\alpha^{(2)} = 5.0$ illustrated in Fig.6.6b, the interphase has a higher expansion coefficient than the surrounding matrix, and thus, small peaks of stress accumulations are observed at the boundary $r = (a+\epsilon)$. However, since the interphase still expands less than the inclusion, the stress accumulation will be higher at the inner boundary $r = a$, between the inclusion and the interphase. For both these cases, the contraction of the inclusion is observed. For the last case, where the coating (interphase) has the highest expansion coefficient than the surrounding media, high concentrations of stress is observed at the boundaries. But it can be gleaned from the illustrated figure that the stress concentrations are now more skewed towards the direction of the applied thermomechanical loads as the interphase now expands more than the inclusion along the direction of the applied loads,

and this deforms or stretches the inclusion, while at the outer boundary the matrix has least expansion than the two enclosing materials, and causes the stress to be more accumulated at the boundaries of the interphase, as it observed from the plots.

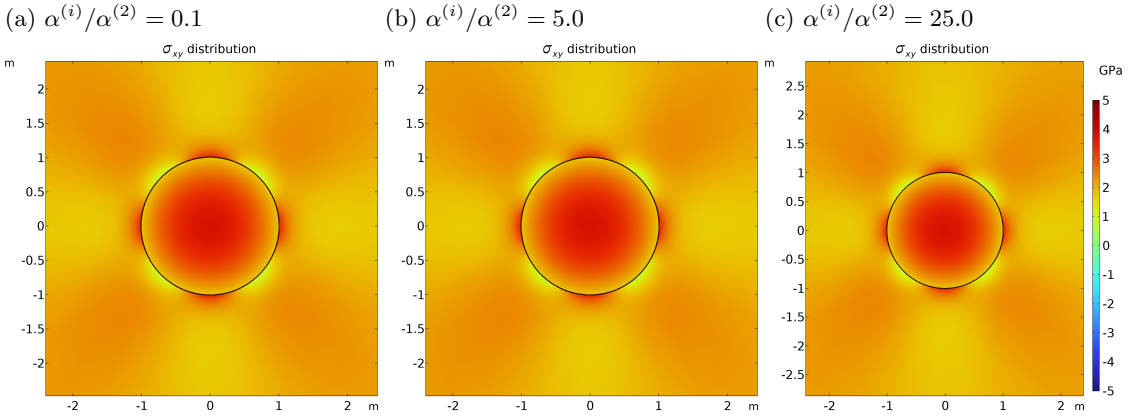


**Fig. 6.8.** Distribution of shear stresses $\sigma_{xy}$ in GPa across a thermoelastic circular interphase with three different coefficients of thermal expansions $(\alpha^{(i)}/\alpha^{(2)}$ of thickness $\epsilon = 0.01$, with volumetric heat source $Q_0 = 1\,W/m^3$ and remote shear load of $\sigma^*_{xy} = 2\,GPa$ for conductive $k^{(i)}/k^{(2)} = 1000$ and rigid interphase $G^{(i)}/G^{(2)} = 1000$.

Table 6.2 provides the values of jumps in temperature $[\![\Theta]\!]$ computed at $\theta = 22.5\,\text{deg}$ for the interphase of thickness $\epsilon = 0.01$ and for the two cases demonstrated above. The table also compares the values of jumps for three different cases of $\alpha^{(i)}/\alpha^{(2)}$, as previously mentioned. Thus, it can be seen that since the thermal effects are uncoupled from the mechanical effects, the coefficient of thermal expansion has no effect on the jumps in temperature or the heat flux, $[\![q_n]\!]$ presented in Table 6.3. Here, the exact solution refers to the jumps in $\Theta$ or $q_n$ computed as the difference between the values obtained at points $A_2$ and $A_1$ inside the interphase. The comparison is made against the approximations computed from First Integrations Schemes (FIS) using two-points (2P) (given by (6.42),(6.45)) or three-points (3P) given by ((6.71),(6.60)) as well as Second Integration Scheme (SIS) using two-points (2P) (given by (6.42),(6.93)) or three-points (3P) of integration, given by ((6.71),(6.106)).

| Jump in Temperature, $\Theta$ | | | | | | |
|---|---|---|---|---|---|---|
| $[\![\Theta]\!]$ | Case A | | | Case B, $(\times 10^{-}5)$ | | |
| | 0.1 | 5.0 | 25.0 | 0.1 | 5.0 | 25.0 |
| Exact Solution | 1.69 | 1.69 | 1.69 | 1.3 | 1.3 | 1.3 |
| FIS 2P | 1.67 | 1.67 | 1.67 | 1.3 | 1.3 | 1.3 |
| FIS 3P | 1.68 | 1.685 | 1.685 | 1.3 | 1.3 | 1.3 |
| SIS 2P | 1.67 | 1.67 | 1.3 | 1.3 | 1.3 | 1.3 |
| SIS 3P | 1.68 | 1.685 | 1.685 | 1.3 | 1.3 | 1.3 |

**Table 6.2.** $[\![\Theta]\!]$ for an uncoupled quasistatic thermoelastic interphase of thickness $\epsilon = 0.01$. with volumetric heat source $Q_0 = 1.0\,W/m^3$, computed for three different value of interphase CTE: $\alpha^{(i)}/\alpha^{(2)} = \{0.1, 5.0, 25.0\}$ . Here, Case A refers to thermally resistive and soft interphase: $k^{(i)}/k^{(2)} = 0.001$ and $G^{(i)}/G^{(2)} = 0.001$ while Case B represents thermally conductive and elastically rigid interphase $k^{(i)}/k^{(2)} = 1000$ and $G^{(i)}/G^{(2)} = 1000$.

From the values provided in the table, it is clear that the three points scheme provides a good estimate of the jumps in temperature and heat flux for high and low conductive interphases.

| Jump in Heat Flux, $q_n$ | | | | | | |
|---|---|---|---|---|---|---|
| $[\![q_n]\!]$ | Case A | | | Case B | | |
| | 0.1 | 5.0 | 25.0 | 0.1 | 5.0 | 25.0 |
| Exact Solution | 0.006 | 0.006 | 0.006 | −0.863 | −0.673 | −0.673 |
| FIS 2P | 0.006 | 0.006 | 0.006 | −0.867 | −0.867 | −0.867 |
| FIS 3P | 0.006 | 00.006 | 0.006 | −0.867 | −0.867 | −0.867 |
| SIS 2P | 0.006 | 0.006 | 0.006 | −0.867 | −0.867 | −0.867 |
| SIS 3P | 0.006 | 0.006 | 0.006 | −0.867 | −0.867 | −0.867 |

**Table 6.3.** $[\![q_n]\!]$ for an uncoupled quasistatic thermoelastic interphase of thickness $\epsilon = 0.01$. with volumetric heat source $Q_0 = 1.0\,W/m^3$, computed for three different value of interphase CTE: $\alpha^{(i)}/\alpha^{(2)} = \{0.1, 5.0, 25.0\}$ . Here, Case A refers to thermally resistive and soft interphase: $k^{(i)}/k^{(2)} = 0.001$ and $G^{(i)}/G^{(2)} = 0.001$ while Case B represents thermally conductive and elastically rigid interphase $k^{(i)}/k^{(2)} = 1000$ and $G^{(i)}/G^{(2)} = 1000$.

The plot below, Fig.6.9 illustrates the heat flux obtained at point $A_3$ inside the interphase, represented by the exact solution (blue dashed line) obtained from the COMSOL solution. The approximation of this value computed for the First Integration Scheme using (6.58) is represented by the green solid line with star markings, and the approximation obtained by (6.104) for the Second Integration Scheme is given by magenta solid line with circle markers. The values are plotted for the three different values of CTEs. It is clear

from the graphs that the values of $q_n|_{A_3}$ from the two equations are in good agreement with the three-phase solution, with the absolute error being $\mathcal{O}(\epsilon^2)$.

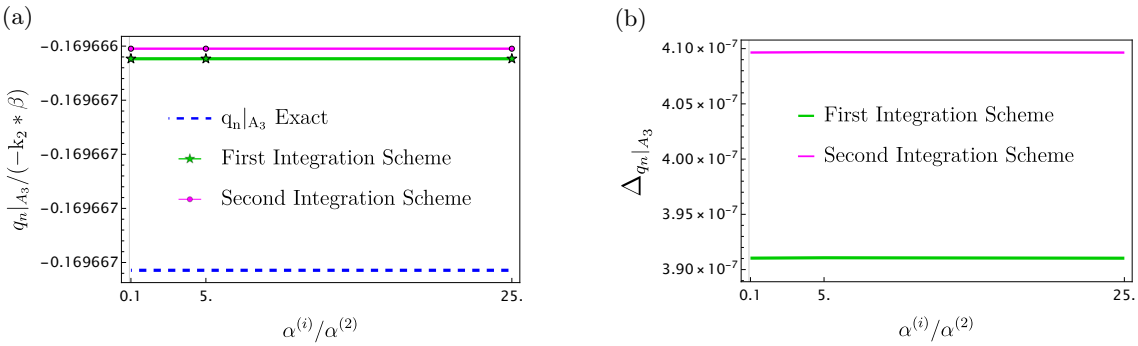


**Fig. 6.9.** Heat flux values $q_n$ at point $A_3$ inside the interphase, computed for First Integration and Second Integration Scheme and compared with the exact solution, for a thermoelastic circular interphase of thickness $\epsilon = 0.01$ for low conductive $k^{(i)}/k^{(2)} = 0.001$ and a soft interphase $G^{(i)}/G^{(2)} = 0.001$.

Further, Fig.6.10 illustrates the comparison and absolute error of the stress along the radial direction $\sigma_{rr}$ at point $A_3$ as computed from the FEM solution (shown in dashed blue lines) and the approximated value computed from (6.88) for the First Integration Scheme is represented by the green solid line with star markings, and the approximation obtained by (6.112) for the Second Integration Scheme is given by magenta solid line with circle markers. The values are plotted for the three different values of CTEs. It is clear from the graphs that the values of $\sigma_{rr}|_{A_3}$ from the two equations are in good agreement with the three-phase solution, with the absolute error being less than $\mathcal{O}(\epsilon^2)$.

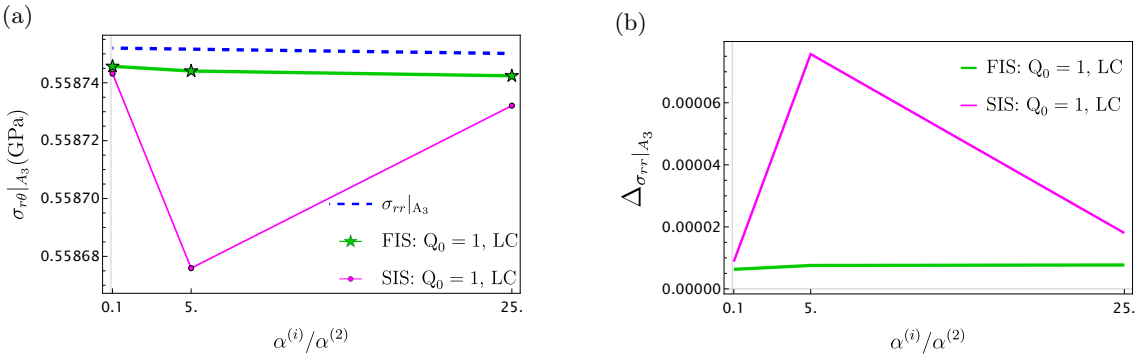


**Fig. 6.10.** Radial stress values $q_n$ at point $A_3$ inside the interphase, computed for First Integration and Second Integration Scheme and compared with the exact solution, for a thermoelastic circular interphase of thickness $\epsilon = 0.01$ for low conductive $k^{(i)}/k^{(2)} = 0.001$ and a soft interphase $G^{(i)}/G^{(2)} = 0.001$.

And similarly, Fig.6.11 illustrates the comparison and absolute error of the stress along the tangential direction $\sigma_{r\theta}$ at point $A_3$ as computed from the FEM solution (shown in dashed blue lines) and the approximated value computed from (6.89) for the First Integration Scheme is represented by the green solid line with star markings, and the approximation obtained by (6.108) for the Second Integration Scheme is given by magenta solid line with circle markers. The values are plotted for the three different values of CTEs. It is clear from the graphs that the values of $\sigma_{rr}|_{A_3}$ from the two equations are in good agreement with the three-phase solution, with the absolute error being less than $\mathcal{O}(\epsilon)$.

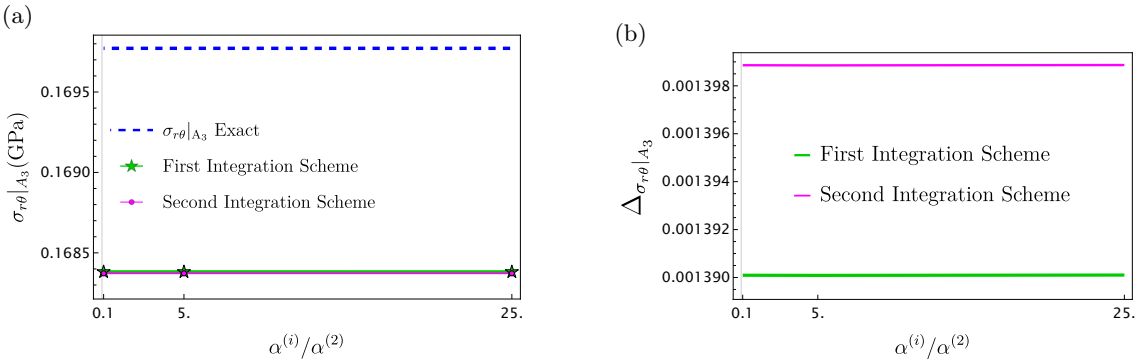


**Fig. 6.11.** Tangential stress values $q_n$ at point $A_3$ inside the interphase, computed for First Integration and Second Integration Scheme and compared with the exact solution, for a thermoelastic circular interphase of thickness $\epsilon = 0.01$ for low conductive $k^{(i)}/k^{(2)} = 0.001$ and a soft interphase $G^{(i)}/G^{(2)} = 0.001$.

The example of a quasistatic coated circular inclusion embedded in a matrix subjected to remote shear and boundray loads is examined here. Different values of coefficients of thermal expansions are observed, and their impact on the expansion and contraction of the interphase is observed, with localizations of stress observed at an angle of $\pm 45$ deg to the flow field. The model proposed here gives a good approximation of the exact solution for the temperature and the displacements fields, as well as the approximations of the surface fluxes inside the interphase.

Although both the schemes have shown good results with respect to exact solution, the First Integration scheme shows better approximation than the Second integration scheme. Thus, it can be concluded that the three-points method using First or Second Integration Scheme provides much better approximation of the jumps across a thermoelastic interface, and the corresponding errors are of the order $\mathcal{O}(\epsilon)$ or less.

# Chapter 7

# Conclusions

In this study, two models Namely First and Second Integration Schemes, have been proposed to study the behaviour of the thermal and elastic transmission conditions across an interphase of arbitrary shape, characterized by conditions and material properties of its neighbours, computed from both sides of the interphase. Each material has a different thermal and mechanical properties, thus providing a sharp contrast to the interphase properties. Two different models, First Integration and Second Integration schemes have been defined, which employ Trapezoidal rule, using two- or three-points of integrations within the interphase thickness to accurately capture the accumulation of temperature and displacements and the fluxes at the boundaries of the interphase along the normal direction of an imperfect interface. The derived conditions respect the continuity of thermal and elastic properties within the interphase, while maintaining the accuracy at the boundaries of the interphase. The derived conditions have the accuracy of $\mathcal{O}(\epsilon^2)$, where $\epsilon = t/R$ is the non-dimensional thickness of the interphase. The proposed conditions are tested in the settings of - firstly, a thermal conduction across three different coated interphase geometries - flat, circular and wavy interphase, embedded in a uniaxial flow field, and secondly in the elastic case for a circular geometry, with remote shear strain loading. The heat source inside the interphase can be linear, quadratic, cubic or constant source, where the continuity is maintained for all types of heat sources. The effect of different parameters, such as heat source magnitude, curvature and surface differential term, on the proposed conditions are also analyzed. The three-points models of the First and Second Integration scheme demonstrates better performance for every case in consideration, and works well for the approximations of interphases from $k_i/k_2 = \{10^{-3}, 10^3\}$, and beyond this range the error grows by $\mathcal{O}(2\epsilon)$ in case of thermally conductive interphase settings. For a rapidly changing curvature, like a wavy interphase, the aforementioned three-points scheme shows good approximation of the jumps in temperature and heat flux for a low conductive interphase and high conductive interphase having a low magnitude of the heat source term ($Q_0 = 1.0\ W/m^3$), for small curvatures, that is, up to $N = 10$ oscillations. For higher curvatures, the boundary normals rapidly change, and the approximations related to second order surface Laplacian $\mathcal{D}_s\boldsymbol{q}$ defined by Eqn.(4.33) as well as the heat flux at point $A_3$ for the First and Second Integration Scheme, given by Eqns.(4.37) and (4.50) respectively, do not hold true, and thus the results obtained from the corresponding solutions would not be accurate.

In the case of elastic interphase, the proposed models were tested in the setting of a coated circular inclusion subjected to far field shear strain loading in the plain strain setting. The proposed schemes show good approximation of the displacement and the stress fields, even for highly rigid interphase and the reported errors are of the order $\mathcal{O}(\epsilon^2)$

which is major achievement.

Again, in the setting of quasistatic linear thermoelastic interphase, the First and Second Integration schemes have provided a good approximation of the exact solution, with error of $\mathcal{O}(\epsilon)$ or less.

Thus, it can be concluded that the First and Second Integration scheme utilizing information from 3 points perform better than the two-points schemes proposed by us as well as those from the literature. In case of temperature and displacement vectors, more accurate schemes are required to approximate the exact solution to increase the accuracy of the corresponding transmission conditions.

# Bibliography


[1] K. Reifsnider. “Modelling of the interphase in polymer-matrix composite material systems”. In: *Composites* 25.7 (1994), pp. 461–469.

[2] M. Comninou. “An overview of interface cracks”. In: *Engineering Fracture Mechanics* 37.1 (1990), pp. 197–208.

[3] N. Research. “Interface Modeling and Asymptotic Analysis in Composites materials”. In: *Nature* (2024).

[4] T. Miloh and Y.Benveniste. “On the effective conductivity of composites with ellipsoidal inhomogeneities and highly conducting interfaces”. In: *Proc. R. Soc. Lond. A.* 455 (1999), pp. 4552687–2706.

[5] Z. Hashin. “Thin interphase/imperfect interface in conduction”. In: *Journal of Applied Physics* 89.4 (2001), pp. 2261–2267.

[6] Y. Benveniste. “A general interface model for a three-dimensional curved thin anisotropic interphase between two anisotropic media”. In: *Journal of the Mechanics and Physics of Solids* (2006).

[7] P. Kapitza. “39 - HEAT TRANSFER AND SUPERFLUIDITY OF HELIUM II”. In: *Collected Papers of P.L. Kapitza*. Pergamon, 1965, pp. 625–639.

[8] Y. Benveniste and T. Miloh. “The effective conductivity of composites with imperfect thermal contact at constituent interfaces”. In: *International Journal of Engineering Science* 24.9 (1986), pp. 1537–1552.

[9] S. e. a. Weng. “Temperature-dependent interphase formation and Li+ transport in lithium metal batteries”. In: *Nature Communications* 14.1 (2023).

[10] S. M. Hatam-Lee, F. Jabbari, and A. Rajabpour. “Interfacial thermal conductance between gold and SiO2: A molecular dynamics study”. In: *Nanoscale and Microscale Thermophysical Engineering* 26.1 (2022), pp. 40–51.

[11] N. Kaur. “Thermal Interface materials for efficient heat management in electronics”. In: *Applied Thermal Engineering* 287 (2026), p. 129415.

[12] Z. Hashin. “Thin interphase/imperfect interface in elasticity with application to coated fiber composites”. In: *Journal of the Mechanics and Physics of Solids* 50.12 (2002), pp. 2509–2537.

[13] Y. Benveniste. “A general interface model for a three-dimensional curved thin anisotropic interphase between two anisotropic media”. In: *Journal of the Mechanics and Physics of Solids* 54.4 (2006), pp. 708–734.

[14] Y. Benveniste and T. Miloh. “Imperfect soft and stiff interfaces in two-dimensional elasticity”. In: *Mechanics of materials* 33.6 (2001), pp. 309–323.

[15] Ville Hirvonen. *The Metric Tensor: A Complete Guide With Examples*. 2025. URL: https://profoundphysics.com/metric-tensor-a-complete-guide-with-examples/.

[16] K. M. G. Borovik A. "Who Gave You the Cauchy–Weierstrass Tale? The Dual History of Rigorous Calculus". In: *Foundations of Science* 17.3 (2012), pp. 254–276.

[17] S. HYDE, B. W. NINHAM, S. ANDERSSON, K. LARSSON, T. LANDH, Z. BLUM, and S. LIDIN. "Chapter 1 - The Mathematics of Curvature". In: *The Language of Shape*. Ed. by S. HYDE, B. W. NINHAM, S. ANDERSSON, K. LARSSON, T. LANDH, Z. BLUM, and S. LIDIN. Amsterdam: Elsevier Science B.V., 1997, pp. 1–42.

[18] H. Rouse and D. Appel. *Advanced Mechanics of Fluids*. Wiley, 1965.

[19] M. H. Sadd. *Elasticity: theory, applications, and numerics*. Academic Press, 2009.

[20] J. R. Barber. *Elasticity*. Springer, 2002.

[21] B. A. Boley and J. H. Weiner. *Theory of thermal stresses*. Courier Corporation, 2012.

[22] G. Cengel. *Heat and Mass Transfer Fundamentals and Applications*. Tata McGraw Hill, 2017.

[23] L. E. Malvern. *Introduction to the Mechanics of a Continuous Medium*. Monograph. 1969.

[24] I.-D. Ghiba. "Linear Thermoelastic Model". In: *Encyclopedia of Thermal Stresses*. Ed. by R. B. Hetnarski. Dordrecht: Springer Netherlands, 2014, pp. 2785–2794.

[25] T. Miloh and Y.Benveniste. "Effective Properties of Interphases". In: *Proc. R. Soc. Lond. A.* 455 (1999), pp. 4552687–2706.

[26] P. BÖvik. "ON THE MODELLING OF THIN INTERFACE LAYERS IN ELASTIC AND ACOUSTIC SCATTERING PROBLEMS". In: *The Quarterly Journal of Mechanics and Applied Mathematics* 47.1 (Feb. 1994), pp. 17–42.

[27] D. Andreeva, W. Miszuris, and A. Zagnetko. "Transmission conditions for thin curvilinear close to circular heat-resistant interphases in composite ceramics". In: *Journal of the European Ceramic Society* 36.9 (2016). CERMODEL 2015 Modelling and simulation meet innovation in Ceramics Technology, pp. 2283–2293.

[28] D. Andreeva and W. Miszuris. "Nonlinear transmission conditions for thin highly conductive interphases of curvilinear shape". In: *Journal of the European Ceramic Society* 38.8 (2018). Cermodel 2017: Modelling and Simulation Meet Innovation in Ceramics Technology, pp. 3012–3019.

[29] Z. Han, S. G. Mogilevskaya, S. Baranova, and D. Schillinger. "BEM-based second-order imperfect interface modeling of potential problems with thin layers". In: *International Journal of Solids and Structures* 230-231 (2021), p. 111155.

[30] S. Baranova, S. Mogilevskaya, T. Nguyen, and D. Schillinger. "Higher-order imperfect interface modeling via complex variables based asymptotic analysis". In: *International Journal of Engineering Science* 157 (2020), p. 103399.

[31] Y. Benveniste. "An O(hN) interface model of a three-dimensional curved interphase in conduction phenomena". In: *Proceedings of the Royal Society A: Mathematical, Physical and Engineering Sciences* (2069 2006).

[32] D. Andreeva and W. Miszuris. "Nonlinear transmission conditions for thin curvilinear low-conductive interphases". In: *Continuum Mechanics and Thermodynamics* 29.1 (2017), pp. 345–358.